Microglial Mechanisms of Cell Death and the Role of the P2X7 Receptor in Relation to Glaucoma

Jack Newman

A THESIS PRESENTED FOR THE DEGREE OF DOCTOR OF PHILOSOPHY AT THE UNIVERSITY OF EAST ANGLIA, NORWICH, UK

SCHOOL OF PHARMACY

2023

Abstract

Purpose: The purpose of this research was to investigate mechanisms of cell death in microglia in the context of neurodegenerative disease including glaucoma. The effects of ATP stimulation on cell membrane disruption and cell death in microglia was investigated and inhibitors used to characterise the pathways involved. The mechanisms and pathways between microglia and macrophages were compared and finally the effects of pathophysiological insults on cell membrane disruption and cell death in microglia were explored using inhibitors again to characterise the pathways involved.

Methods: BV2, P2X7K/O BV2 microglia and J774 macrophages were the cell lines used. Cell membrane disruption was measured using YO-PRO and propidium iodide (PI) dye, while cell death was investigated using cell death assays (LDH and MTS). Cell morphological changes were observed by phase contrast microscopy. Inhibitors for cell death associated proteins were utilised to investigate cell death pathways. Other methods used include SDS-PAGE and Western blot to detect the pyroptotic protein gasdermin D protein and qPCR for measuring mRNA gene expression levels of proteins associated with cell death.

Results: ATP stimulation caused membrane disruption and cell death in BV2 microglia that was P2X7 dependent. However, inhibitors of apoptotic (Z-DEVD-FMK), pyroptotic (MCC950, Ac-YVAD-cmk and Necrosulfonamide) and necroptotic proteins (necrostatin), as well as, other caspase inhibitors (Z-VAD-FMK and Z-IETD-FMK) and calpain inhibitors (PD150606 and CAT811) caused no difference in these changes. The J774 macrophages underwent a pyroptotic cell death, in both LPS and non-LPS primed cells after ATP stimulation, that could be blocked with inhibitors of pyroptosis. LPS priming had no effect on parameters measured in BV2 microglia and cleaved gasdermin D was present in J774 macrophages and not the BV2 microglia after ATP stimulation. The pathophysiological stressors, amyloid-β, oxidative stress, ischaemia and pH, all caused cell death, but the inhibitors predominantly had no effect. Levels of mRNA of activation/pyroptosis-associated proteins levels showed a similar profile between LPS and most of the stressors.

Conclusions: ATP and the pathophysiological stressors all caused damage to the microglia but the pathway this is occurring through is a non-pyroptotic mechanism. This is different to that seen in macrophages. The pathophysiological stressors also caused expression changes indicative of activation. Further elucidation could help in the understanding and development of novel therapies for neurodegenerative disease including Alzheimer's disease and glaucoma.

List of Contents

List of Figures and Tables

Chapter 1

Chapter 2

Chapter 3

Acknowledgements

I would like to thank Dr Julie Sanderson, Dr Leanne Stokes and Dr Matthew Felgate for their support during my time under their supervision.

Cheers Everyone.

Declaration by Candidate

I hereby declare that this thesis is my own work and includes nothing which is the outcome of work done in collaboration. Where other sources of information has been used, they have been acknowledged. This thesis has not be submitted for another degree or qualification in this or any other university or institution and does not exceed the word limit

Signature:

List of Abbreviations

ANOVA	Analysis of Variance
AD	Alzheimer's Disease
ASC	Apoptosis associated speck like protein
ATP	Adenosine triphosphate
APP	Amyloid Precursor Protein
BBB	Blood brain barrier
BBG	Brilliant Blue G
BzATP	Benzoyl-benzoyl adenosine 5'-triphosphate
CNS	Central nervous system
CRISPR	Clustered regular interspaced short palindromic repeats
DAMPs	Damage associated molecular patterns
DISC	Death-inducing signalling complex
DMEM	Dulbecco's Minimum Essential Medium
DMSO	Dimethyl Sulfoxide
DNA	Deoxyribonucleic acid
dNTP	Deoxynucleotide triphosphate
DPBS	Dulbecco's Phosphate Buffered Saline
FBS	Foetal bovine serum
GCL	Ganglion cell layer
GPCR	G protein-coupled receptor
IAP	Influenza A protein
IL	Interleukin
INL	Inner nuclear layer
IOP	Intraocular pressure
IPL	Inner plexiform layer
K/O	Knockout
LDH	Lactate dehydrogenase
LPS	Lipopolysaccharide
MLKL	Mixed lineage kinase domain like pseudokinase
mRNA	Messenger RNA
MTS	3-(4,5-dimethylthiazol-2-yl)-5-(3-carboxymethoxyphenyl)-2-(4-sulphophenyl)-2H-tetrazolium
NF-κB	Nuclear factor kappa B
NLRP3	NLR family pyrin domain containing Protein 3
NS	Necrosulfonamide
OGD	Oxygen glucose deprivation
PACG	Primary angle closure glaucoma
PAMPs	Pathogen associated molecular patterns
PCR	Polymerase chain reaction
PI	Propidium Iodide
POAG	Primary open angle glaucoma
RGC	Retinal ganglion cells
RIPK1/3	Receptor-interacting serine/threonine-protein kinase 1
RNA	Ribose nucleic acid
ROS	Reactive oxygen species
TLR4	Toll-like receptor 4
TUNEL	Terminal deoxynucleotidyl transferase dUTP nick end labelling
WT	Wild-type
ZBP1	Z-DNA binding protein 1

Chapter 1

Introduction

1.1 Microglia

1.1.1 Introduction to Microglia

Microglia are phagocytic, tissue-resident immune cells of the central nervous system (CNS). Microglia were first described and visualised in detail in 1919 (Río-Hortega, 1919) and since then studies into their origins, function and role in disease have revealed new details about this cell type (Mendes and Majewska, 2021). Adult microglia have been shown to be direct descendants of the original embryonic Erythron-Myeloid Progenitors (eEMP) from the embryonic yolk sac by fate mapping studies of mice (Ginhoux et al., 2010, Kierdorf et al., 2013, Schulz et al., 2012). Due to the blood brain barrier (BBB), microglia are separated from the rest of the body, so maintain their unique identity, compared to other immune cells. Their uniqueness is further facilitated by interactions with the other resident CNS cells including neurons, astrocytes and oligodendrocytes (Gosselin et al., 2014, Mass et al., 2016). Microglia were originally thought to have a low turnover rate in the absence of challenge (Lawson et al., 1992), but animal studies have revealed that even when unchallenged, microglia have constant turnover with balanced apoptosis and proliferation (Askew et al., 2017, Tay et al., 2017). They are an abundant cell type in the CNS. For example, in the mouse brain, 10-15% of cells are microglia (Lawson et al., 1992), while studies, on human brain have shown that the numbers in grey matter range between 0.66-11.13% and in white matter from 1.06-8.06% (Dos Santos et al., 2020).

The main role of microglia is to maintain homeostasis in the CNS and they are involved in various physiological processes from development to adulthood (Borst et al., 2021). One of these processes is immune surveillance, in which microglia survey their microenvironment for signs of injury, infection and abnormalities such as protein plaques associated with diseases such as Alzheimer's and Parkinson's disease (Borst et al., 2021). The process that microglia use to clear artifacts found during immune surveillance and any cellular debris and dead or dying neurons, is called phagocytosis, where the cell absorbs the target which is then broken down. Microglia also regulate inflammatory processes within the CNS. They produce both pro-inflammatory and anti-inflammatory signals depending on the context (Tang and Le, 2016). This helps to balance the microenvironment and prevents excessive inflammation, which can be damaging to neurons. Microglia have also been found to release neurotrophic factors which play a role in neuronal survival and function (Chen and Trapp, 2016). During development they have been found to support neurogenesis and can influence the proliferation, differentiation and survival of neural stem cells and progenitor cells in specific regions of the brain (Chen and Trapp, 2016). They also play a key role in myelinogenesis by their association with oligodendrocytes (Borst et al., 2021).

Furthermore, microglia help regulate the integrity of the BBB by interacting with endothelial cells and secreting factors that support barrier function (Gullotta et al., 2023).

More recently, it has been recognised that microglia play an active role in neuronal function. In synaptic pruning they selectively eliminate weak or unnecessary synapses using phagocytosis, which helps refine neural circuits during development and optimises brain function (Cornell et al., 2022). Another way in which microglia influence neurons is releasing signalling molecules, such as chemokines, cytokines and neurotransmitters, which can alter synaptic transmission, neuronal neurotransmitter release and neural network activity (Vidal-Itriago et al., 2022).

The observations detailed by Rio-Hortega (Río-Hortega, 1919) originally led to the belief that microglia existed in two distinctive states, resting and activated. The resting state was characterised as having a highly ramified morphology coupled with limited phagocytic and migratory activity, while the activated state was characterised by its ameboid shape, high motility and high levels of phagocytic and proliferative activity (Vidal-Itriago et al., 2022). However this belief is now seen as outdated. It has been shown that in the “resting” state microglia are extremely mobile with suggestions that this state should be renamed the surveillant state to more accurately describe function. For example, it has been found that “resting” microglia patrol a local area that can be more than 10-fold the area occupied by their cell body (Prinz et al., 2019). An updated model has therefore been proposed, which details that microglial activation and morphology changes are a spectrum from ramified to hyper-ramified to bushy to ameboid (Figure 1.1) (Beynon and Walker, 2012). The surveillant microglia monitor the local environment in the ramified state. Upon activation by detection of stressors, the now activated microglia moves to the hyper-ramified state by retracting some processes from the surrounding tissue while extending other processes towards the threat. The bushy state occurs as the microglia and its remaining processes start to thicken. The cell then further withdraws more processes and moves to a more spherical shape to complete the transition to the ameboid form. These transitions are reversable, responding to threats, then returning to the surveillant state.

Further to this, a more recent model proposes that microglial activation is a process that sits on a multi-spectrum of different morphologies and protein profiles that are activated by different stimuli (Vidal-Itriago et al., 2022). Microglia still take the classic ramified shape while in the surveillant state but transition into a variety of specific morphologies depending on the conditions in which they are activated. For example rod or honeycomb shapes are seen after injury-induced activation and ameboid or jellyfish shapes are seen when a phagocytic activation state is needed (Vidal-Itriago et al., 2022). However Common to all these models is that on detection of a stressor,

the microglial cell undergoes shape and gene expression changes which are described as activation.

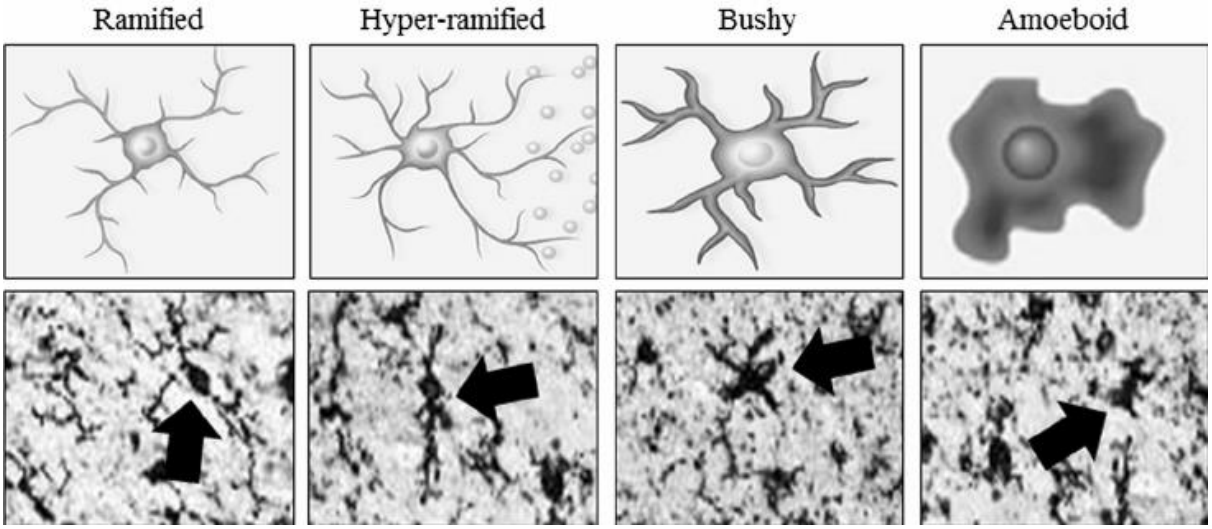

Figure 1.1 Activated Morphology of Microglia. Schematics (Top row) and images (bottom row, black arrow to highlight) of human brain microglia showcasing the morphological stages of the proposed linear spectrum, from ramified to hyper ramified to bushy to ameboid and back. Adapted from: (Crews and Vetreno, 2016)

In terms of defining activation, microglia were classically grouped into 3 different categories M0, M1 and M2 (Tang and Le, 2016). This classification was borrowed from macrophage research in which M1 and M2 corresponded with the differing metabolic and inflammatory reactions of macrophages after activation (Mills et al., 2000).

In Microglia, M0 relates to the surveillant state. It is therefore a highly active phenotype monitoring its local environment to aid in the maintenance of the CNS (Wang et al., 2022). M1, or the classical activation phenotype, is associated with the release of proinflammatory cytokines such as TNFα, IL-1β and reactive oxygen species (ROS) such as superoxide and nitric oxide and leads to an acute immune response (Tang and Le, 2016). The M2 category is regarded as anti-inflammatory and involved in resolution of inflammation. Two states include the “alternative activation phenotype” or the “acquired deactivation phenotype” (Tang and Le, 2016). The alternative activation phenotype is characterised by the production of IL-4 and IL-13 which promote anti-inflammatory responses, tissue repair, debris removal, wound healing and the restoration of brain homeostasis (Colton, 2009, Ponomarev et al., 2007). The acquired deactivation phenotype helps to alleviate acute inflammation and is triggered by the microglia phagocytosing apoptotic cells or being exposed to anti-inflammatory cytokines such as IL-10 and TGF-β (Colton and Wilcock, 2010, Colton, 2009, Sawada et al., 1999). More recent studies looking

at the transcriptome of microglia have helped to support the concept of the M0, M1 and M2 phenotypes, as the studies have revealed a distinct expression signature between the different states (Masuda et al., 2019, Matcovitch-Natan et al., 2016, Varol et al., 2017). However it has also been suggested that the M1/M2 binary is unhelpful and restrictive in understanding expression signatures in relation to their morphology, as studies have found no clear connection between an increased expression of pro- or anti-inflammatory markers and the morphological state of the microglia (Vidal-Itriago et al., 2022). It has also been commented that use of the M1/M2 terms led to the assumption that these different microglial states were either detrimental (M1) or beneficial (M2) (Paolicelli et al., 2022). There has been evidence to show that microglia *in vivo* do not exist in this binary choice often found to co-express both M1 and M2 expression signatures (Ransohoff, 2016).

More recently another attempt to define and understand the roles and processes of microglia is to name specific states of microglia depending on the context in which they are observed (Paolicelli et al., 2022). Examples of these include disease-associated microglia (DAMs), microglial neurodegenerative phenotype (MGnD), human Alzheimer's Disease microglia (HAMs) and lipid-droplet accumulating microglia (LDAMs). While this does take a step closer to understanding the wide array of environments and pathophysiological stressors that microglia have to react too, it misses out other levels of complexity that can define the specific state that a microglial population will transition into. The conditions that dictate the microglial phenotype includes the species, sex or age of the individual, the location of the cells and what stressor the microglia are reacting to. These variables in combination lead to a unique phenomic, metabolomic, proteomic, transcriptomic and epigenomic signature that is thought to lead to a specific morphology and expression profile that deals with the issue at hand (Paolicelli et al., 2022).

1.1.2 Microglia in Disease, Neuroinflammation and Neurodegeneration

A downside to the activities of microglia revolves around chronic activation which leads to neuroinflammation, a state that is normally seen in CNS infections or neurodegenerative conditions, such as Alzheimer's disease (Thakur et al., 2023), multiple sclerosis (Bjelobaba et al., 2017) or glaucoma (Williams et al., 2017). Although neuroinflammation could describe the acute response of immune cells to threats in the CNS, this term is widely used to invoke the concept of chronic inflammation that is thought to have four main concepts: activation of microglia, increased release of cytokines and chemokines, recruitment of peripheral immune cells and local tissue damage (Woodburn et al., 2021). The loss of neurons is a key marker of neurodegenerative disease, and damage to these cells leads to the release of signals, as mentioned above, that lead to the activation of the microglia (Soreq et al., 2017). Persistent inflammation in the CNS leads to

loss of neuronal plasticity, impairs memory and is seen as the main driver of tissue damage in neurodegenerative conditions (Muzio et al., 2021).

As microglia are the main line of defence in the CNS, they are equipped with many receptors involved with the innate immune response. The broad term for these proteins are pattern recognition receptors (PRRs) and are split up into 3 main groups. These groups are known as toll-like receptors (TLRs), retinoic acid-inducible gene-1 like receptors (RLRs) and nucleotide-binding oligomerisation domain like receptors (NLRs). Each of these receptors are able to detect ligands that cause inflammatory stimulation which have been called pathogen-associated molecular patterns (PAMPs) and danger-associated molecular patterns (DAMPs) (ElAli and Rivest, 2016). These insults and pathological conditions cause inflammation and an inflammatory environment that microglia encounter in the CNS. Microglia are activated by, and they themselves cause, inflammation linked states such as oxidative stress and changes in pH. Oxidative stress is caused by the abundance of reactive oxygen species (ROS), which are a family of chemicals formed by O_2 that are highly reactive and include H_2O_2, super oxide and hydroxyl atoms. The presence of low levels of ROS in the cell is an important aspect of cell function (Mittler, 2017). In high concentrations, ROS cause damage to important cell components such as proteins, cell membranes and DNA (Singh et al., 2019). Changes in pH also have significant impacts to the local environment during inflammation with studies showing that pH levels can drop as low as pH5.5 in some instances (Simmen and Blaser, 1993, Simmen et al., 1994). Another inflammatory trigger that can impact microglia in the CNS is ischaemic conditions. This is a state in which a tissue or organ is not being delivered the nutrients, such as oxygen or glucose, needed for survival. This state can also create other issues, as the impaired delivery system is also unable to remove harmful waste products. Ischaemia establishes an environment that creates further pathophysiological stresses. Due to the metabolic disruption of ischaemia, an increase in ROS production occurs and also pH changes, where pH can drop by at least 1 unit, due to the increase in anaerobic glycolysis, ATP hydrolysis and release of other acidic components, such as lactic acid and protons (McQueen, 2010).

As mentioned previously, microglia also have the responsibility of dealing with infections in the CNS. In research that looks at inflammation and microglia activation, lipopolysaccharide (LPS), is used widely as a model (Skrzypczak-Wiercioch and Sałat, 2022). LPS is a structural component found in the outer membrane of Gram-negative bacteria (Lu et al., 2008), The classic pathway for LPS activation starts when LPS binds to Toll-like receptor 4 (TLR4), this is then internalised by the cell, leading to the activation of transcription factors, such as NFκB, which are able to relocate to the nucleus which leads to the upregulation of cytokines (e.g. TNFα, IL1β and IL6), chemokines and inflammatory mediators (e.g. iNOS and COX2) (Skrzypczak-Wiercioch and Sałat, 2022). Initially LPS was used experimentally as a model of sepsis and inflammation in mammals (Pollack and

Young, 1979, From et al., 1979). However the scope of conditions using LPS as a model has grown, including conditions in which neuroinflammation is an important mechanism of the pathology. This can be justified as the innate immune system, through the same TLR4 pathway, is thought to play a role in identifying misfolded proteins, such as those found in Alzheimer's disease (Yang et al., 2020), Huntington's disease (Vuono et al., 2020) and Parkinson's disease (Heidari et al., 2022). When LPS has been used as a model for Alzheimer's disease it has been found to cause amyloidogenesis when injected into mouse brain which then causes neuroinflammation and cognitive impairment (Lee et al., 2008). LPS has also been used as an animal model for Parkinson's disease, where injection into the brain showed evidence of neuroinflammation and loss of dopaminergic neurons (Zhao et al., 2022, Zakaria et al., 2019). There are, however, thought to be limitations to models, using LPS for neurodegenerative disease as the complex nature of each neurodegenerative disease and the conditions that lead to them, cannot be solely recreated using LPS. Furthermore, differences exist in the amount of TLR4 on the surface of microglia when comparing humans and mice (Leitner et al., 2019).

As mentioned above, microglia are also activated by stresses linked to disease states such as Alzheimer's disease, Parkinson's disease and Huntington's disease. In Parkinson's disease microglia are known to respond to α-synuclein aggregates and neuronal damage, while dysfunctional microglia are thought to impair clearance of α-synuclein aggregates which further promotes neurotoxicity (Wang et al., 2023). In Huntington's disease targeting microglia activation has shown promise in animal models (Crapser et al., 2020). For both these conditions, chronic neuroinflammation caused by microglia responding to the misfolded proteins and neuronal damage exacerbates neurodegeneration contributing to disease progression (Gao et al., 2023).

Another of these misfolded proteins that activate microglia is amyloid β in Alzheimer's disease. Amyloid β is the cleaved form of an intrinsic membrane protein called amyloid precursor protein (APP). APP is a cell membrane protein that is expressed in many tissues with a large concentration in neurons. It has roles in anti-microbial action, synapse formation and iron export (Duce et al., 2010, Moir et al., 2018, Priller et al., 2006). Amyloid β is a polypeptide made up of between 36-43 amino acids which are formed when APP is cleaved by β- and γ-secretase. The most common forms are Aβ40 and Aβ42. Experimentally it was discovered that the neurotoxic section of amyloid-β was between the 25-35 residues (Sato et al., 1995). The role of Aβ in healthy brains is not fully understood but there is evidence to show it plays a role in protection against oxidative stress (Baruch-Suchodolsky and Fischer, 2009, Zou et al., 2002) and functions as a transcription factor (Bailey et al., 2011, Maloney and Lahiri, 2011). While the cause of Alzheimer's disease is not fully understood, a key element in the progression is thought to revolve around the β-amyloid protein and aggregation into plaques (Lane et al., 2018). It has been suggested that the progression of Alzheimer's disease happens when production of amyloid β is greater than its

clearance (Mawuenyega et al., 2010, Wildsmith et al., 2013). Microglia have been found to be one of the main clearance pathways through which amyloid β is broken down, with one study finding a loss of this function leads to a promotion of amyloid β aggregation and neurodegeneration (Hickman et al., 2008).

Much like the other neurodegenerative conditions mentioned previously, the misfolded amyloid β is found to activate microglia. Activated microglia have a role in phagocytosis of amyloid β itself and the damaged or dying neurons caused by the misfolded protein (Miao et al., 2023). It has been proposed that the ability of microglia to have many varied phenotypes leads to two peaks of activation in Alzheimer's disease. An early anti-inflammatory peak during the pre-clinical stage and a pro-inflammatory peak during the later stages as the disease progresses (Fan et al., 2017).

Multiple genes associated with microglia have been indicated as having a significant impact on Alzheimer's disease progression (Miao et al., 2023). These include Apolipoprotein E (ApoE), a protein involved in the metabolism of fats and modulating the inflammatory response in microglia (Flowers and Rebeck, 2020). Other proteins include two that are closely linked to each other, called CD33 and Triggering receptor expressed on myeloid cells 2 (TREM2). CD33 is a transmembrane receptor thought to control microglial activation (Eskandari-Sedighi et al., 2023), while TREM2 is a transmembrane receptor that belongs to the immunoglobulin superfamily and binds to several ligands including apoptotic cells, phospholipids, glycolipids and lipoproteins (Song et al., 2017). Evidence shows that CD33 becomes overactive in Alzheimer's Disease, with its expression linked to TREM2 (Griciuc et al., 2019). Mutations in all three of these proteins have been found to significantly increase the chances of someone developing late onset Alzheimer's disease (Sims et al., 2020, Guerreiro et al., 2013, Karch et al., 2012).

Microglia that have been chronically exposed to amyloid β have been found to have an increased expression of TREM2 and ApoE (Krasemann et al., 2017). This phenotype is also associated with an increase in proliferation and production of inflammatory cytokines and a decrease in the cells ability to perform important microglial tasks such as phagocytosis, ramification and synaptic surveillance (Miao et al., 2023). This then leads to an increase inflammatory environment that causes further damage and progression of the disease.

1.1.3 Microglia, Macrophages and cell lines

There are many similarities between macrophages and microglia (Borst et al., 2021, Robinson et al., 2019). They are both myeloid immune cells, which patrol their local surroundings to maintain homeostasis and use phagocytosis to remove threats that might disrupt that homeostasis, such as pathogens or cell debris (Borst et al., 2021, Robinson et al., 2019). They both produce multiple

cytokines and growth factors that can promote pro or anti-inflammatory environments depending on the threat they are dealing with, and both have multiple activation states. They can recruit lymphocytes and other immune cells to help deal with the threat at hand (Borst et al., 2021, Robinson et al., 2019).

There are also differences which exist such as origin and gene expression. Microglia originate from the embryonic yolk sac. Macrophages also originate from the embryonic yolk sac, but different macrophage types are maintained from different sources at different points of development (Ginhoux and Guilliams, 2016). For example the macrophages in the lungs and liver originate from the embryonic yolk sac, but are then propagated by cells from the foetal liver which then maintain the cell during development into adulthood, while macrophages in the heart, pancreas and the gut, originate in the embryonic yolk sac, are propagated by cells from the foetal liver, but are then finally replaced by circulating blood monocytes that are produced in bone marrow (Bain et al., 2014, Tamoutounour et al., 2013). As would be expected due to this differing points of origin, microglia display distinct transcriptomes and epigenomes when compared to other tissue macrophages (Gosselin et al., 2014). Further to this, one study that investigated different tissue-specific macrophages, including Kupffer cells from the liver, gut macrophages and microglia, established that tissue resident macrophages had distinct gene expression profiles and open chromatin regions that could not be explained purely by tissue or lineage specific reasons (Lavin et al., 2014). This shows that while microglia and macrophages are distinct cells, this variety is also true between macrophage cells themselves.

When discussing macrophage biology, most researchers have stuck with the classic M1/M2 definitions. However others have tried to adapt this thinking to a more modern understanding (Murray et al., 2014), while others have suggested abandoning the concept altogether (Nahrendorf and Swirski, 2016). Just like the discussion about terminology for microglia, mentioned above, this is an ever changing and developing field that with each new discovery will allow us to better understand and define terms.

Many cell lines for microglia and macrophages have been created for research purposes, those that are widely used include THP-1, U937 and J774 cell lines for macrophages and HMC3, N9 and BV2 cell lines for microglia.

One cell line used widely as a model for microglial function, is the BV2 cell line. This is an immortalised mouse microglia cell line and has previously been used as a retinal microglia model (Langmann, 2007). The BV2 cell line has been shown to be highly comparable to isolated primary microglia (Henn et al., 2009, Stansley et al., 2012). However, one study comparing expression profiles between primary microglia versus microglia cell lines, including BV2, showed a pronounced difference between key microglia proteins expression such as P2Y12, APOE and TGF-

β1 (Butovsky et al., 2014). While these results should be noted, cell lines are widely used and continue to be a viable option for research.

As mentioned previously, a widely used mouse macrophage cell line is called J774. There have been suggestions that J774 cells do not act in a similar manner to primary macrophages, such as in their response to *M. Tuberculosis* (Andreu et al., 2017). However, one study has found they were closer in activity and other factors to primary macrophages than other macrophage cell lines (Snyderman et al., 1977) . The research described in this thesis is conducted using both the BV2 microglia cells and the J774 macrophages. Furthermore a P2X7 knockout variant of the BV2 cells was also used (Dhuna et al., 2019). One way to investigate the importance of a protein is to create a stable knockout cell line, same as the cell line mentioned above, where the target protein has been inactivated or removed. A popular way of doing this is the clustered regularly interspaced short palindromic repeats (CRISPR) gene editing method. A well-studied form of CRISPR, developed from *Streptococcus pyrogenes,* is Type II CRISPR/Cas9 system (Le Rhun et al., 2019). This process is normally used by bacteria to deal with viral infections and helps maintain the integrity of their genome, however, a simplified version has been utilised by scientists to modify genomes of living organisms such as cell lines and animals including humans. (Bak et al., 2018).

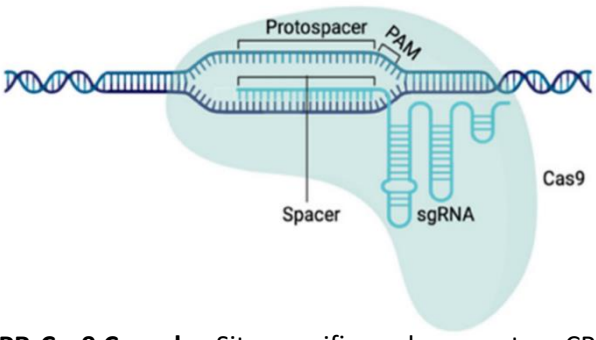

Figure 1.2 CRISPR-Cas9 Complex Site-specific nuclease system CRISPR-Cas9 recognises specific DNA sequence using single guide RNA (sgRNA). The Cas9 recognises the protospacer adjacent motif (PAM) to create a double strand break in the DNA. Adapted from: (Gómez-García et al., 2022)

This involves the Cas9 endonuclease and a single guide RNA (sgRNA) (Fig 1.2). The sgRNA contains a 20bp nucleotide sequence, known as the spacer, that is complimentary to the target sequence, known as the protospacer. The rest of the sgRNA is a scaffold region which allows it to associate with Cas9, which stabilises and activates the endonuclease. Active Cas9 recognises a sequence of three nucleotides next to the protospacer called the protospacer adjacent motif (PAM) which causes a site specific double strand break in the genome (Gómez-García et al., 2022). This break is then repaired using either the non-homologous end joining repair (NHEJ) or the homology directed repair (HDR). NHEJ is a quick way to repair the break but this method is extremely error prone, leading to insertions and deletions within the gene (Cai et al., 2019). The CRISPR Cas9 process relies on these mistakes to knock out the target gene.

1.2 The Retina

The eye is a complex organ used for vision. The human eye contains specialised structures that aid in sight including the cornea, iris, lens, and the retina amongst others (Fig 1.3a). The retina is part of the central nervous system and is instrumental in the transduction of light energy to enable vision. It is situated toward the posterior of the vitreous cavity (Fig 1.3a). The retina contains important regions used in vision. One such region is the optic disc, a pale pink in colour, 1.5mm disc also known as the optic nerve head. This region is important as it is where the axons of the retinal ganglion cells exit the eye. Another region of the retina is the macula, a yellow in colour, 5.5mm disc responsible for high resolution colour vision. At the centre of the macula is the fovea, a 1.5mm disc with a high density of cone cells (Mishra D, 2018)

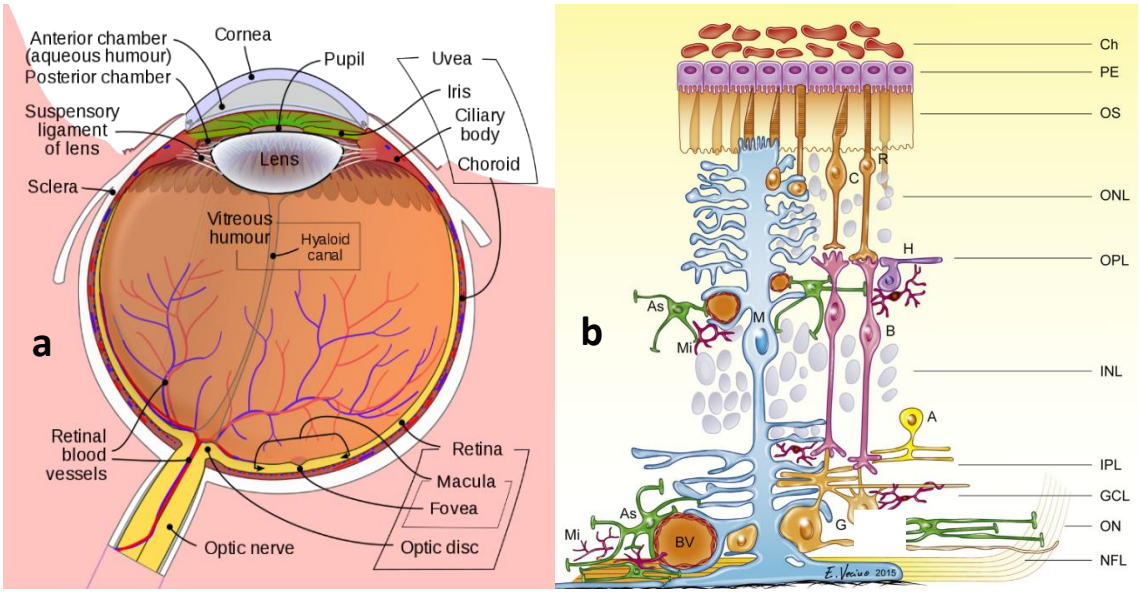

Figure 1.3 Structure of the Eye and Retina (a) Cross section of the Human eye (b) Schematic drawing of the retina. Cells depicted listed alphabetically: Amacrine cells (A), astrocytes (AS), bipolar cells (B), cones (C), ganglion cells (G), horizontal cells (H), microglia (Mi), Müller cells (M) and rods (R). Different layers of the retina from the internal to the outer layers: optic nerve (ON), nerve fibre layer (NFL), ganglion cell layer (GCL), inner plexiform layer (IPL), inner nuclear layer (INL), outer plexiform layer (OPL), outer nuclear layer (ONL), outer segment layer (OS), pigment epithelium (PE), choroid (Ch). Adapted from (a) (Toldi and Thomas, 2020) (b) (Vecino et al., 2016)

The retina is made up of ten layers of specialised cells. Starting from the layer closest to the choroid, the most posterior part, the first layer is the retinal pigment epithelium (Fig 1.3b). This is a pigmented cell layer just outside the neurosensory elements of the retina. The photoreceptor layer follows this which is populated by rods and cones, important for the detection and transduction of light energy. Next is the outer limiting membrane. The next four layers are called the outer nuclear layer, the outer plexiform layer, the inner nuclear layer, and the inner plexiform layer. These layers are populated by support cells such as Müller cells, astrocytes, microglia, and

neurons important in signal processing namely the amacrine, bipolar and horizontal cells. Next is the ganglion cell layer, then the nerve fibre layer and finally the inner limiting membrane.

For light transduction and processing to occur light passes through the transparent nerve layers of the retina until it strikes the rod and cone photoreceptor cells. Light transduction takes place in these cells. The signal is then passed to the bipolar then retinal ganglion cells (RGCs), the axons of which make up the nerve fibre layer. The signal travels to the optic disc, and out of the eye, towards the brain via a mesh like structure called the lamina cribrosa.

1.2.1 Retinal Ganglion Cells

RGCs are the neurons in the retina that collectively transmit image-forming and non-image forming information to several regions of the brain. In terms of structure, RGCs vary significantly in size, the connections they create and their responses to visual stimulation. All RGCs contain a single axon, with this axon forming the nerve fibre layer. These axons, from all RGCs, then meet at the optic disc. In the human retina there are thought to be between 700,000-1.5 million RGCs (Watson, 2014). The optic nerve is formed of RGC axons that, once they have left the eye, become myelinated.

1.2.2 Microglia in the Retina

In terms of the human eye during healthy conditions, microglia are found at varying densities in different layers of the retina including the outer plexiform layer, the inner nuclear layer, the inner plexiform layer, the ganglion cell layer and the nerve fibre layer (Vecino et al., 2016). They are also found close to blood vessels and near the optic nerve head. Interestingly, they have also been found in the iris, ciliary body and choroid (Wang et al., 2016). When the eye is under pathological conditions, microglia are also known to migrate to the ONL, RPE and subretinal space (Fan et al., 2022).

As mentioned previously microglia are known for surveying the local area and interacting with other cell types. This is no different for the retinal microglia, where crosstalk with neurons occurs and plays an important role in synaptic pruning as well as clearance of debris including apoptotic neurons and non-functioning synapses (Borst et al., 2021).

Another cell type that microglia are known to interact with are astrocytes. This connection is responsible for the maintenance of neuronal function and CNS homeostasis. Astrocytes provide trophic support molecules, such as TGF-β and cholesterol, which promotes microglial maturation (Baxter et al., 2021, Zhang et al., 2020, Bohlen et al., 2017). It has also been found that microglia

require cholesterol to maintain a physiological state (Bohlen et al., 2017). The disruption caused during neurodegeneration causes a break in the microglia-astrocyte interaction, which leads to the specific expression signature found in diseased microglia (Borst et al., 2021).

There are also interactions between microglia and Muller cells, where microglia have been found to influence the morphology, function and molecular response during times of inflammation. These interactions have found to be bi-directional and shape the overall injury response within the retina (Wang and Wong, 2014). In one study looking at ocular hypertension as a model for glaucoma, it was found that the microglia-Muller cell interaction leads to an increase in retinal inflammatory response (Hu et al., 2021).

1.3 Glaucoma

Glaucoma is a group of optic neuropathies in which there is progressive degeneration of RGCs (Weinreb et al., 2014). If left untreated total blindness will occur (GBD, 2022).

Glaucoma has been reported to be the cause of 11% of blindness and 2.1% of mild to severe vision impairment worldwide in adults over 50 in 2020 (GBD, 2021) An estimate in 2013 concluded that 64.3 million people suffered from glaucoma caused blindness with this figure projected to increase to 111.8 million by 2040 (Tham et al., 2014). 60% of worldwide glaucoma cases are found on the Asian continent followed by Africa with 13% of cases (Tham et al., 2014). It has been found that people with African ancestry are statistically more likely to get glaucoma (Tham et al., 2014).

Although glaucoma isn't fatal it severely impacts on the quality of a person's day-to-day life or, as it is also known, the disease burden. One way to quantify the disease burden is to look at the disability-adjusted life year (DALY), which is a combinative indicator of the lost healthy years from the disease onset to death. Globally in 2015 just under 550,000 DALYs due to glaucoma were recorded(Wang et al., 2019a). Statistics showed woman carry the heaviest disease burden at all ages over 40, with women over 80 being the worst affected(Wang et al., 2019a)

The same study found substantial health inequality existed in terms of glaucoma. Less developed countries were shown to have the highest DALY figures. This phenomenon has been explained by lower economical and societal development. These include the availability of treatment being lower, high levels of deprivation leading to late presentation by the patient and lower levels of education leading to less adherence of medication regimens (Wang et al., 2019a). While in developed countries treatment is widely available, the demographic changes these countries are seeing could cause issues in the future. A study in the UK found treatment for a glaucoma patient costs the NHS on average £475 per year. The average cost to the NHS over a glaucoma sufferer's

lifetime is around £3000. As the UK's old age population increases, the costs to the NHS are expected to increase substantially (Rahman et al., 2013).

Glaucoma can be grouped by its pathophysiology and cause. Firstly, if there is no underlying condition causing the glaucoma it is referred to as primary glaucoma. If a condition is found that is causing glaucoma such as uveitis (Panek et al., 1990), tumour (Camp et al., 2019), trauma or injury (Girkin et al., 2005) it is classified as secondary glaucoma. Another more important distinction is whether it displays as open angle or closed angle glaucoma (Fig 1.3). This refers to the position of the iris in relation to the lens and the effect this may have on aqueous humour drainage and intraocular pressure (IOP). This is described in more detail in the next section.

1.3.1 Glaucoma and the link to Aqueous Humour and IOP

The biggest risk factor known for cause and progression of glaucoma is elevated IOP. Aqueous humour is the fluid that fills the space in front of the lens. The uvea contains a structure known as the ciliary body (Fig 1.3a). Within the ciliary body there are a series of ridges known as the ciliary processes. It is here where the aqueous humour is produced. The major components of aqueous humour are organic and inorganic ions, carbohydrates, glutathione, urea, amino acids, proteins, oxygen, carbon dioxide and water (Goel et al., 2010). Once produced, the aqueous humour enters the posterior chamber (Fig 1.4a). It then flows through the pupil and into the anterior chamber. For drainage, the aqueous humour mainly flows through the trabecular meshwork and into Schlemm's canal (Fig 1.4a). There is also minor leakage via the muscle bundles close to the ciliary body, also known as the uveoscleral pathway. Both these pathways lead to the episcleral vein which carries the aqueous humour away.

The role of aqueous humour is to deliver nutrients, aid in the actioning of immune responses and keep the eye pressurised to maintain its shape. IOP relates directly to the pressure of the aqueous humour in the eye. The normal range of IOP is between 11 and 21mmHg (Zeppieri and Gurnani, 2023). As discussed above, a healthy eye allows aqueous humour to flow from the posterior chamber into the anterior chamber which is then drained away (Fig 1.4a). These processes allow for equilibrium of the IOP to be maintained. The most prominent forms of glaucoma are primary open-angle glaucoma (POAG) and primary angle-closure glaucoma (PACG). In open-angle glaucoma, the space between the iris and pupil remains open and production of aqueous humour is still as normal, but drainage is affected (Fig 1.4b). In closed angle, the iris is abnormally positioned, thus closing the space between the iris and the pupil. This causes the flow of aqueous humour into the anterior chamber to be impeded (Fig 1.4c). Both forms involve an increase in IOP which is then thought to damage various cells in the retina, notably the retinal ganglion cells. This

damage leads to the symptoms of a reduced visual field and eventually blindness. A form of POAG is normal tension glaucoma (NTG) and what sets this apart from “classic” POAG is that sufferers with NTG have an IOP in the normal range (<21mmHg), but the patient still suffers from glaucoma. As the IOP is in the normal range there must be other underlying causes for NTG.

Another aspect of glaucoma found in animal models is an increase in microglia levels (Wang et al., 2016). There is also evidence of dying RGCs and blood vessels in glaucomatous eyes being surrounded by activated microglia. Activated microglia have also been observed near to choriocapillaris vessels, thought to be due to damage to the blood-retinal barrier (Wang et al., 2016).

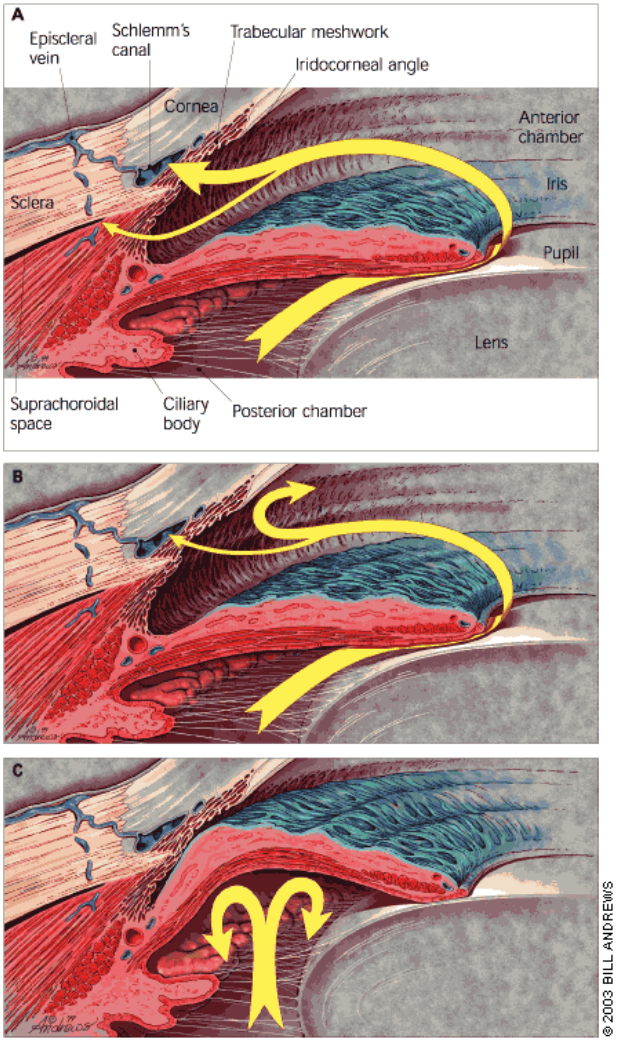

Figure 1.4 Aqueous outflow pathways in glaucoma (a) Normal healthy aqueous flow through the pupil with normal drainage (b) Normal flow through pupil but impeded drainage, as seen in POAG (c) Impeded flow through pupil as seen in PACG. Adapted from. *(Distelhorst and Hughes, 2003)*

1.3.2 Neuroinflammatory stressors in Glaucoma

Glaucoma might seem out of place being coupled with Alzheimer's disease and Parkinson's disease as a neurodegenerative disease but the retina is a part of the CNS and as mentioned above the progression of glaucoma comes from the loss of neuronal cells, RGCs. There is plenty of evidence of inflammatory stressors being present during glaucoma. One such stressor is ROS, which are thought to have a role in the progression of glaucoma (Chrysostomou et al., 2013). For example, the creation of ROS was found to increase in a rat glaucoma model, after the IOP was elevated, which then led to an increase in lipid peroxidation in the retina (Ko et al., 2005). Another study in humans found that ROS led to DNA damage in the trabecular meshwork, which caused a degeneration of the structure (Saccà et al., 2005). Furthermore, use of a free radical scavenger treatment in a glaucoma model in rats found that the RGCs had an increase chance of survival (Ko et al., 2000). Another hypothesis considering the contribution of oxidative stress, suggests that light hitting the retina may be an aggravating event affecting progression of glaucoma. As light reaches the retina, the mitochondria in the RGCs start to produce energy and, therefore, ROS, but due to the lack of blood flow, caused by the early stages of glaucoma, the ROS cannot be cleared fast enough leading to damage being caused to proteins, membranes and DNA (Osborne et al., 2006). A chronic state of oxidative stress, caused by ROS, induces cell damage and neurodegeneration in the CNS (Solleiro-Villavicencio and Rivas-Arancibia, 2018). During this chronic oxidative stress, ROS create an inflammatory state due to constant activation of inflammatory signalling pathways, which promote the deregulation of the inflammatory response (Solleiro-Villavicencio and Rivas-Arancibia, 2018). ROS have been found to create conditions that allow for the constant secretion of pro-inflammatory cytokines and chemokines (Chan, 2001, Hsieh and Yang, 2013) and also have the ability to activate microglia (Pawate et al., 2004).

Ischaemia is thought to play an important role in the cause and progression of glaucoma, as retinal function is very sensitive to changes in haemoglobin oxygen saturation (Brandl and Lachenmayr, 1994). This is thought to mainly be caused by the local blood flow becoming compromised, by either elevated or oscillating IOP, coupled with vascular dysfunction, which leads to repeated hypoperfusion (Flammer et al., 2002, Mozaffarieh et al., 2008, Chan et al., 2017). This ischaemia is detrimental to the cells of the retina, with one study showing that, after a reduction in blood flow, rat RGCs at the optic nerve head start to degrade (Chidlow et al., 2017). Ischaemic damage has also been shown to lead to an increase in an inflammatory environment, as inflammatory cells, such as microglia (Ivacko et al., 1996), infiltrate the damaged tissue and release pro-inflammatory mediators, such as IL-1β and TNF-α (Sivakumar et al., 2011). With inflammatory processes activated, as well as ischaemia, a change in pH might be predicted and it has been shown that an increase in IOP in a rabbit model led to a drop in pH of the vitreous, from 7.3 to 7.0, which caused an increase in retinal cell death (Lu et al., 2001).

Amyloid β has also been implicated in glaucoma. Levels of amyloid β in vitreous fluid were found to significantly change in patients with glaucoma when compared to a healthy control (Yoneda et al., 2005). Another study showed deposition of amyloid β colocalised with RGCs causing an increase in apoptotic cells in a mouse glaucoma model (Guo et al., 2007), while in a mouse model for Alzheimer's disease amyloid β deposits were detected in the RGCs as the mice aged which led to retinal degeneration (Ning et al., 2008). In a study that looked at the retina and optic nerve head of monkeys that had chronic ocular hypertension, amyloid β was found to increase in concentration in the retina in the chronic stages of glaucoma (Ito et al., 2012).

1.3.3 Treatment for Glaucoma

Treatment of any type of glaucoma focuses on the reduction of IOP as the main goal (Weinreb et al., 2014). This has been found to be the only proven method of treating glaucoma (Boland et al., 2013). The aim of the treatment is for a reduction of 20-50% of the patient's IOP at presentation (Weinreb et al., 2014).

For POAG, various treatments exist such as pharmacological options including prostaglandin analogues, reduce IOP by reducing the outflow resistance so the aqueous humour can flow through the uveoscleral pathway (Gaton et al., 2001). Other options are β-adrenergic blockers, α_2-adrenergic agonist or carbonic anhydrase inhibitors (Weinreb et al., 2014). Surgical options include laser or incisional surgeries. A laser trabeculoplasty lowers IOP by changing the configuration of the trabecular meshwork to allow for greater aqueous outflow. The most commonly performed incisional procedure is a trabeculectomy, where a small segment of the trabecular meshwork and adjacent corneoscleral tissue is removed to allow the aqueous humour to drain underneath the conjunctiva where it is absorbed (Weinreb et al., 2014).

For the treatment of PACG, the same pharmacological options as for POAG are available (prostaglandin analogues, β-adrenergic blockers, α-adrenergic agonists, and carbonic anhydrase inhibitors). While the surgical options include a laser iridoplasty, a trabeculectomy can also be performed or a laser peripheral iridotomy, where a hole is created in the iris to allow for flow of aqueous humour (Weinreb et al., 2014).

As with all these treatments, the lowering of IOP is only to slow down the progression of the disease. So, a treatment that can cure or stop the progression of the disease would be very welcome in this field. One option would be to protect important cells in the retina from cell death.

1.4 Purine Nucleosides and Nucleotides and Purinoceptors

1.4.1 Purine Nucleosides and Nucleotides

The involvement of purine nucleosides and nucleotides in producing a potent response was first identified in the cardiovascular system in animal studies in 1929 (Drury and Szent-Györgyi, 1929). The activation was found to arise mainly from the purine nucleoside adenosine and the purine nucleotides ADP and ATP. Further animal studies in 1959 first displayed ATP as a neurotransmitter, with ATP being released when rabbit sensory nerves were electrically stimulated (Holton, 1959).

1.4.2 Purinoceptors

The receptors that these purine nucleosides and nucleotides interact with are called purinoceptors or purinergic receptors. They are cell surface receptors that can be split into adenosine receptors, previously P1 receptors, which bind with adenosine, and P2 receptors that bind ATP or ADP (Ralevic and Burnstock, 1998). Adenosine receptors have been found to have 4 subtypes, A_1, A_{2A}, A_{2B} and A_3 (Fredholm et al., 1994). All these subtypes are classified as G protein-coupled receptors that all feature the classic 7 transmembrane structure (Di Virgilio et al., 2017). P2 receptors are themselves split into two categories. The first is P2X which are ligand-gated ion channels with 7 identified subtypes, P2X1-7. The other is P2Y which are G protein-coupled receptors with 8 identified subtypes, P2Y1-2, P2Y4, P2Y5, P2Y11-14 (Di Virgilio et al., 2017).

P2X receptors are ligand-gated ion channels. The receptors are trimeric as, to form the ion pore, 3 subunits of P2X receptors are involved (Nicke et al., 1998). The N- and C- termini are intracellular and the subunits contains 2 transmembrane domains and an extracellular loop containing the ATP binding site (Hattori and Gouaux, 2012). The P2X receptors are found throughout the body (Table 1.1) and are responsible for various physiological roles including the contraction of various tissues, such as the bladder or vas deferens (Fowler et al., 2008, North, 2002), platelet aggregation (Gachet, 2006), mediation of pain (Chizh and Illes, 2001) and macrophage activation (Wewers and Sarkar, 2009). All P2X receptors are intrinsic cation channels (Table 1.1). One member of the P2X family that differs from the other members is P2X7, firstly, while it still is an intrinsic cation channel, it has also been found to cause large pore formation after prolonged activation (Table 1.1). What also sets it apart from the other P2X receptors is the much longer C-terminus (Di Virgilio et al., 2017) and also that P2X7 requires much higher levels of ATP for activation to occur (Surprenant et al., 1996). These additional elements of P2X7 make it an interesting subject for study which will be covered in the next section.

P2X Subtype	Main Distribution	Transduction Mechanism	Refs
P2X1	**Arteries, urinary bladder and the vas deferens**	**Intrinsic cation channel (Ca^{2+} and Na^{+})**	**(Burnstock, 2012, Mulryan et al., 2000, Vial and Evans, 2000)**
P2X2	**Smooth Muscle, CNS, autonomic, sensory ganglia and the retina**	**Intrinsic cation channel (Particularly (Ca^{2+})**	**(Brändle et al., 1998a, Burnstock, 2012)**
P2X3	**Sensory neurons, some sympathetic neurons and the retina**	**Intrinsic cation channel**	**(Brändle et al., 1998a, Burnstock, 2012)**
P2X4	**CNS, testis, colon and retina**	**Intrinsic cation channel (Especially Ca^{2+})**	**(Brändle et al., 1998a, Burnstock, 2012)**
P2X5	**Skin, gut, bladder, thymus, spinal cord and retina**	**Intrinsic cation channel**	**(Brändle et al., 1998a, Burnstock, 2012)**
P2X6	**CNS, motor neurons in spinal cord**	**Intrinsic cation channel**	**(Burnstock, 2012)**
P2X7	**Central and peripheral nervous system, macrophages, microglia, retina and uterine lining**	**Intrinsic cation channel and a large pore after prolonged activation**	**(Burnstock, 2012) (Brändle et al., 1998b)**

Table 1.1 Overview of P2X Receptors P2X subtypes, their distribution in the body and transduction mechanism

1.4.3 P2X7

As mentioned above, P2X7 is a trimeric ATP-gated cation channel and when ATP binds a pore is formed which allows for the influx of Na^{+} and Ca^{2+} ions and the efflux of K^{+} ions (Di Virgilio et al., 2017). There is evidence that it can create a larger pore, which allows for the passage of large organic ions such as N-methyl-D-glucamine ($NMDG^{+}$), choline and fluorescent dyes (including ethidium bromide, YO-PRO and propidium iodide) to both exit and enter the cell (Alves et al., 2014).

Structural information of P2X7 has been derived from the solved crystal structure of the P2X7 receptor of the giant panda *Ailuropoda melanoleuca* (Karasawa and Kawate, 2016). The shape of the structure has been compared to that of a dolphin (Fig 1.5a) (Di Virgilio et al., 2017). The proposed mechanism of P2X7 opening (Fig 1.5b) is thought to be that when ATP binds to the binding site it causes a large conformational change (Di Virgilio et al., 2017). This causes the "head" domain to move closer to the "dorsal fin" of the adjacent subunit. The transmembrane domains then change mutual orientation thus generating a pore lined by TM2 of each monomer. This then causes a rapid influx of Na^+ and Ca^{2+} and an efflux of K^+ from the cell (Di Virgilio et al., 2017). The P2X7 pore has been found to be inhibited by AZ10606120 (Michel et al., 2007).

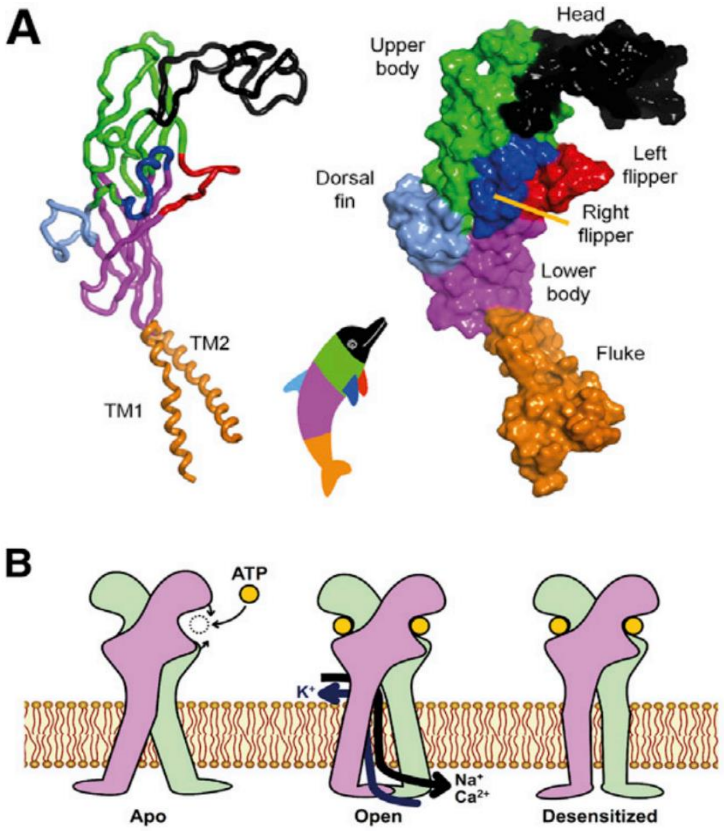

Figure 1.5 Structure of P2X7(a) Skeletal structure of P2X7 (left) next to space filled structure (right) with comparison to dolphin (Centre) (b) Possible conformational change that allows for the pore of P2X7 to open with ATP unbound and bound. Adapted from: (Di Virgilio et al., 2017)

The P2X7 receptor has been found throughout the body in almost all organs but is concentrated in the nervous system, including in the retina (Brändle et al., 1998b, Kaczmarek-Hajek et al., 2018). Expression is high in microglia (Collo et al., 1997, Deuchars et al., 2001, Ishii et al., 2003). It has been described to be involved with multiple processes including mast cell degranulation, inflammation, including the release of cytokines and cell death (He et al., 2017, Jiang et al., 2017, Kawano et al., 2012, Kurashima and Kiyono, 2014, Qu and Dubyak, 2009, Russo and McGavern, 2015, Wareham and Seward, 2016)

1.4.4 P2X7 Pore Formation

For many years ATP has been known to cause larger molecules to both exit and enter the cell. Since the first evidence of this in cancer cells, mast cells and later macrophages (Rozengurt et al., 1977, Cockcroft and Gomperts, 1980, Steinberg et al., 1987), the ATP receptor responsible for this has been of interest. Originally called P2Z, as it was proposed that this receptor would be a different morphology to other P2 receptors (Soltoff et al., 1990). It was later identified as what we now know as P2X7. The mechanism that allows for the permeabilisation of the cell to large molecules via P2X7 has been named large pore formation (Ugur and Ugur, 2019). It was first suggested that this large pore was formed by P2X7 itself (Surprenant et al., 1996), P2X7 was later found to be able to form hexamers which helped this hypothesis (Kim et al., 2001b). However, it was then suggested that the initial opening of the P2X7 receptor led to a signal cascade that then caused the activation of another pore, with pannexin1 the first to be suggested (Pelegrin and Surprenant, 2006). Pannexins are a family of membrane channels of which there are 3 subtypes, Panx1, Panx2 and Panx3. Panx1 has been shown to be needed for the release of ATP and IL1β (Pelegrin and Surprenant, 2006) which made it a prime candidate for P2X7/ATP-mediated large pore formation. However, this was not confirmed by later studies (Alberto et al., 2013, Hanley et al., 2012). More recently, studies have suggested that Gasdermin D is the protein that creates the additional pore (Pronin et al., 2019), as P2X7 has been suggested as a key component in pyroptosis, which leads to the creation of the gasdermin D pore that is needed for the release of cytokines (discussed later in this introduction). The identity of the pore, however, remains the subject of active investigation and others have returned to the idea that the pore is formed by P2X7 itself (Dunning et al., 2021).

1.4.5 Release of ATP in the Eye

ATP is known to be a neurotransmitter in the retina (See before). In addition, Multiple studies concerning the eye have been carried out that show the release of ATP from non-neuronal cells (Ward et al., 2010). One such study showed that hyperosmotic pressure on lens epithelial and human retinal pigment epithelial cells lead to the release of ATP (Eldred et al., 2003) while another study using hyperosmotic pressure on rat lens showed ATP release within the outer cortex (Suzuki-Kerr et al., 2022). Another study involving cultured human and fresh bovine retinal pigment epithelial cells that were subjected to hypotonic stress, indicated that both cell types released ATP (Reigada and Mitchell, 2005). A further study using the cell line ARPE-19 treated cells with sodium cyanide to simulate ischaemia, and also showed a release of ATP (Reigada et al., 2008). Using the same cell line, treatment with ATP led to the release of ATP (Reigada et al., 2005) and UTP, glutamate and NMDA also caused ATP release in various eye models (Mitchell, 2001). Mechanical

stimulation of Müller cells in rat retina also showed release of ATP (Newman, 2001, Newman, 2003), while an increase of IOP in rat eyes *in vivo* showed an increase in the ATP concentration of the vitreous humour (Resta et al., 2007). Human trabecular meshwork cells that underwent hypotonic stress also released ATP (Fleischhauer et al., 2003). Clinically, PACG sufferers have an increased ATP concentration in their aqueous humour (Zhang et al., 2007).

1.4.6 P2X7 in the Retina and Eye

The first evidence of the presence of P2X7 in the retina was detection of the mRNA in whole rat retina (Brändle et al., 1998b). This study also found, using immunostaining of the protein itself, that P2X7 is localized to neuronal cells of the ganglion cell layer, although it was unclear whether they were found in RGCs or displaced amacrine cells. A later study using monkey retina clarified that it was expressed in RGCs (Ishii et al., 2003). In human retina P2X7 has been found in Müller cells (Pannicke et al., 2000) and in the rat retina has also been found in vascular cells of the retina (Kawamura et al., 2003). Another study found that P2X7 is also present in the presynaptic process of rod bipolar cells and other synapses, consistent with the role of ATP as a neurotransmitter within the retina (Puthussery and Fletcher, 2004). A further study using P2X7 knockout mice suggested that P2X7 may play a role in the excitation of photoreceptors or inhibitory cells that regulate rod or cone cell pathways (Vessey and Fletcher, 2012). It has been suggested that activation of P2X7 may affect neurotransmitter uptake from the extracellular space by Müller cells in the retina (Pannicke et al., 2000). Other evidence in human retina showed that P2X7 is found in high levels in the inner plexiform layer and in very low levels in the outer plexiform layer(Niyadurupola et al., 2013) which is consistent with expression in RGCs and/or retinal microglia.

1.4.7 ATP and P2X7 in Microglia

ATP is part of a group of signals released by non-functional and damaged cells that attract microglia (Borst et al., 2021). Glutamate, phosphatidylserine and purine nucleosides and nucleotides activate signalling pathways in which G_i plays an important role and leads to an increase in microglial motility (Li et al., 2020, Merlini et al., 2021, Scott-Hewitt et al., 2020). The pathway that involves ATP starts with ATP being detected by P2Y12, following this the ATP is metabolised to adenosine, which activates a pathway that ends in the upregulation of chemotaxis and actin filament polymerisation genes which allow for faster motility and mobility of the microglia (Badimon et al., 2020, Cserép et al., 2020).

P2X7 was first identified in microglia in a mouse cell line that showed an increase in intracellular Ca^{2+} concentration and an uptake of ethidium bromide after stimulation with ATP (Ferrari et al., 1996). Further research using this same mouse microglia model showed ATP stimulation of the P2X7 receptor led to a release of IL-1β after LPS priming (Ferrari et al., 1997b). Activation of P2X7 has also been shown to lead to the nuclear translocation of transcription factor nuclear factor Kappa-light-chain enhancer of activated B cells (NFκB) which, as a transcription factor, is known to lead to upregulation of gene expression of TNFα, Cox2 and IL-1β (Ferrari et al., 1997b). The genes mentioned above point towards ATP promoted the M1 pro-inflammatory phenotype (Fabbrizio et al., 2017). However, evidence has shown P2X7 activation also leads to an increase in M2 phenotype markers, Arg1 and CD163, when stimulated by the P2X7 agonist Benzoyl-benzoyl adenosine 5'-triphosphate (BzATP) (Fabbrizio et al., 2017).

1.4.8 P2X7 in Cell Death

The link between P2X7 and cell death was first suggested in a study that indicated extracellular ATP stimulation caused the death of a fibroblast cell line and that P2X7 played a primary role (Pizzo et al., 1992). A further study showed that ATP stimulation of P2X7 in macrophages led to spontaneous cell death (Chiozzi et al., 1996).

In another study, cell death was found to occur in microglia cells treated with LPS and ATP (Brough et al., 2002). The same treatment on cells lacking P2X7 did not lead to cell death, while cells lacking IL-1β still died (Brough et al., 2002). Studies have indicated that BzATP has been shown to kill mouse microglia, which was suppressed when treated with the P2X7 antagonist A804598, and also in P2X7 knockout mice (He et al., 2017). Another study has shown that mouse microglia BV2 cells, die when under ischaemic conditions and that this action can be blocked using Brilliant Blue G (BBG), a non-selective P2X7 antagonist (Eyo et al., 2013). In the same study, cell death was reduced in hippocampal slices of P2X7 knockout mice that underwent ischaemic conditions (Eyo et al., 2013).

P2X7 has also been shown to be involved with cell death of RGCs. Studies have indicated that, both *in vivo* and *in vitro*, stimulation of the P2X7 receptor by BzATP leads to the death of RGCs, and this is inhibited by BBG (Hu et al., 2010b, Zhang et al., 2005). Another study showed that an increase in the IOP in rat eyes *in vivo* lead to RGC death, but addition of apyrase, an enzyme that breaks down ATP to AMP, protected the RGCs (Resta et al., 2007). The same study found that, *in vitro,* RGCs showed increased permeability to propidium iodide when ATP was added and this was blocked with the addition of BBG (Resta et al., 2007). P2X7 was found to have an involvement in hypoxia-induced cell death in rat retinal neurons, as this form of cell death could be blocked by

BBG and oxidised ATP (Sugiyama et al., 2010). The role of microglia in P2X7 mediated neurodegeneration in glaucoma has not been specifically investigated, but it has been recognised that mechanisms of RGC death could be either direct or indirect (Niyadurupola et al., 2013). Certainly in relation to neurodegeneration in an age-related macular degeneration model, P2X7 knock-out mice were protected from increased retinopathy and inflammatory gene expression, such as NLP3, IL-1β and IL-6 (Sekar et al., 2023). Finally, in a glaucoma mouse model study that used eyedrops with the P2X7 antagonist, JNJ-47965567, untreated mice showed significant microglia activation and a reduction in RGC number, while the mice treated with the P2X7 antagonist displayed an improved RGC number and reduced activated microglia number (Romano et al., 2020).

1.5 Cell Death

Cell death is the ending of a cell performing biological functions. It can either take the form of programmed cell death, defined as a death that is genetically controlled, or unprogrammed cell death, which is seen as 'accidental' in response to injury.

1.5.1 Necrosis

Unprogrammed cell death mainly takes the form of necrosis, characterized by the swelling of the cell and its organelles leading to rupture. The pathway for necrosis (Fig 1.6) is initiated by external injury where the cell is damaged severely by a sudden shock, for example by radiation, heat, chemicals, hypoxia or mechanical stress (D'Arcy, 2019). This shock then leads to cellular damage which then causes DNA damage, membrane damage and mitochondrial disruption. Cellular damage and membrane damage leads to an increase in intracellular [Ca^{2+}] levels which cause more mitochondrial disruption as well as the activation of calpains and cathespins which then cause protein degradation ending in necrotic cell death. The disruption of mitochondrial processes causes an increase in ROS which then lead to further cellular damage as well as DNA damage. When DNA damage is beyond the repairable limit, PARP activity increases which causes a drop in ATP availability within the cell, leading to necrosis and finally membrane damage past a certain point leads to the loss of the integrity of the cell again leading to necrosis.

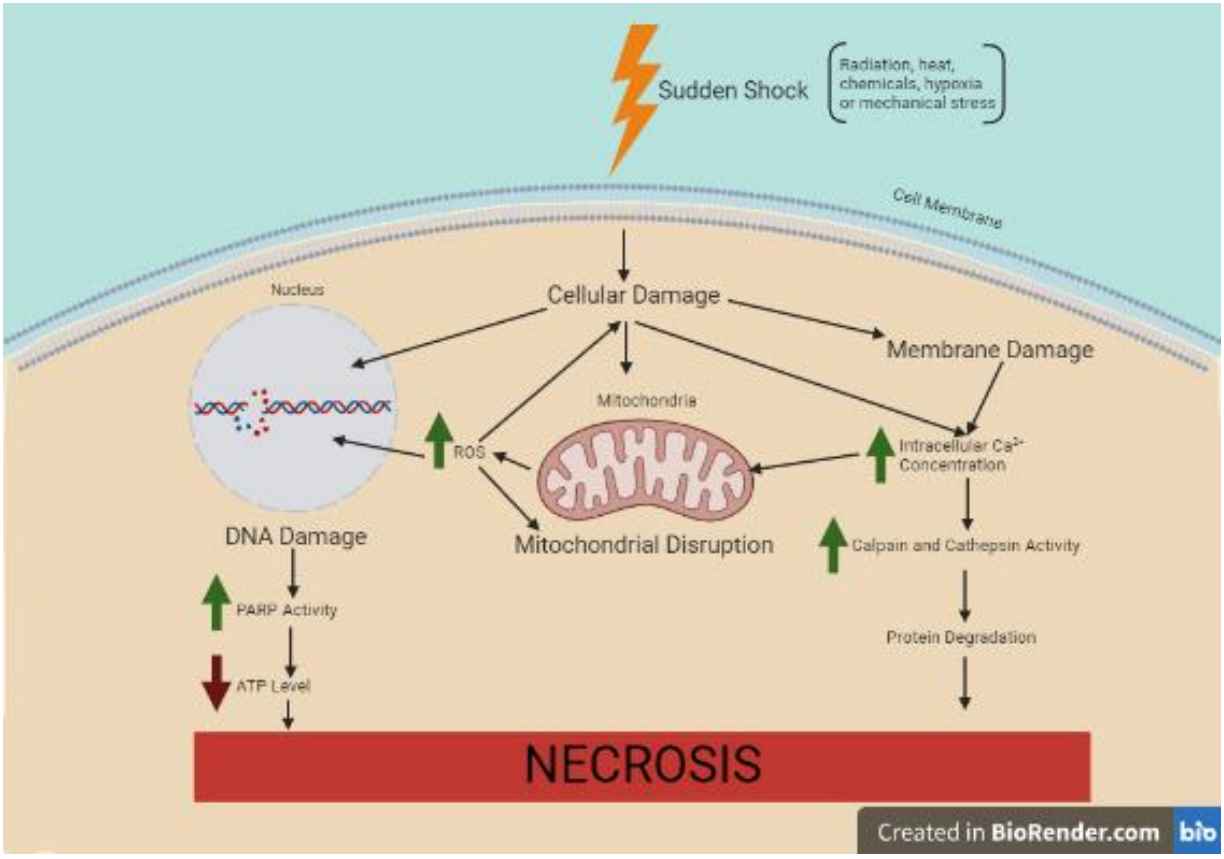

Figure 1.6 Summary of Pathways for Necrosis. A sudden shock leads to cellular damage which causes mitochondrial disruption, membrane and DNA damage. These lead to an increase in ROS production and intracellular Ca^{2+} concentration. Intracellular DNA damage leads to the activation of PARP and the reduction of ATP concentration, while increased Ca^{2+} activates calpain and cathepsins which cause protein degradation. Both of these then cause necrosis. Created with BioRender.com

1.5.2 Apoptosis

Apoptosis, in contrast to necrosis, is a heavily regulated form of cell death in which the cell dies without spillage of its contents into the surrounding environment (D'Arcy, 2019). This form of cell death is known for displaying the morphological features of cell and nuclear shrinkage as well as characteristic apoptotic membrane blebbing (Hotchkiss et al., 2009).

Apoptosis happens via either the intrinsic or extrinsic pathways (Fig 1.7). The intrinsic pathway is initiated by a range of shocks to the cell such as cytokine deprivation, DNA damage or irradiation. This causes membrane disruption of the mitochondria which leads to the release of cytochrome C. This then forms the apoptosome along with Apaf-1 and Pro-caspase 9, which converts caspase 9 into the active form. Caspase 9 then cleaves caspases 3, 6 and 7 as part of the caspase cascade which leads to cleavage of the substrates of these caspases and finally apoptosis.

The extrinsic pathway is caused by a death receptor ligand binding to a death receptor which activates a complex made of TRAF2, TRADD, cIAPs, RIPK1 and FADD. TRADD and FADD then

associate with pro-caspase 8 in another complex called the death-inducing signalling complex (DISC) which converts pro-caspase 8 to the active form. The active form can either, activate bid which causes the later steps of the intrinsic pathway to occur, or it can directly cleave caspases 3, 6 and 7 leading to apoptosis.

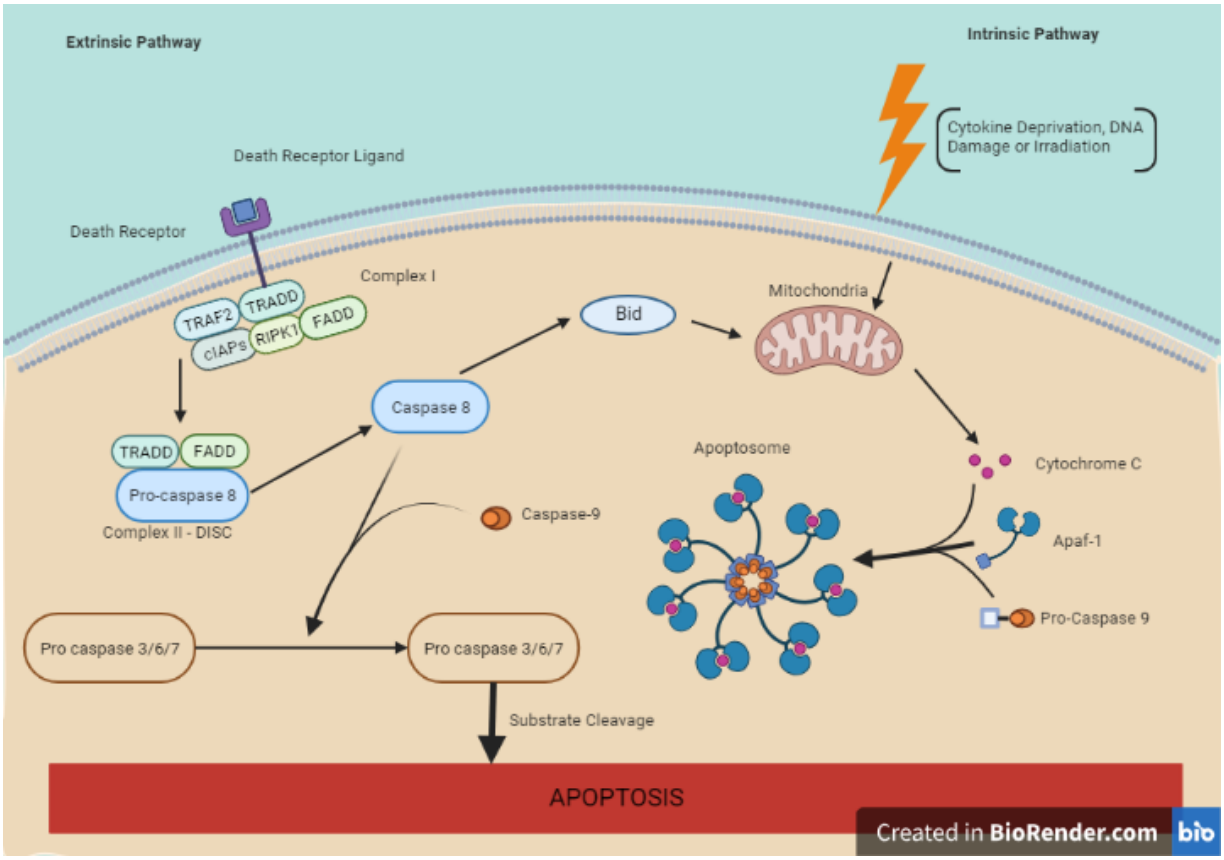

Figure 1.7 Summary of Pathways for Apoptotic cell death. Intrinsic Pathway: a range of shocks to the cell, leads to mitochondrial membrane disruption and the release of cytochrome C. The apoptosome (Cytochrome C, Apaf-1 and Pro-caspase 9) forms and activates caspase 9. Caspase 9 then cleaves caspases 3, 6 and 7, leading to the cleavage of multiple substrates that cause apoptosis. Extrinsic pathway: death receptor ligand binding activates complex I (TRAF2, TRADD, cIAPs, RIPK1 and FADD). TRADD and FADD bind pro-caspase 8 in the death-inducing signalling complex (DISC) which activates pro-caspase 8. This can either activate Bid and the intrinsic pathway, or it can directly cleave caspases 3, 6 and 7 to initiate apoptosis. Created with BioRender.com

Apoptosis has been found to play a major role in an array of diseases, such as neurodegenerative conditions such as Alzheimer's (Cordeiro et al., 2010, Crews et al., 2011, Lee et al., 2010, Nikolaev et al., 2009, Song et al., 2011, Stanga et al., 2010), Parkinson's (Barcia et al., 2011, Berry et al., 2010, da Costa and Checler, 2010), Huntington's disease (Kim et al., 2001c, Richards et al., 2011, Sassone et al., 2010) and glaucoma (Nickells, 1999, Guo et al., 2005)

1.5.3 Necroptosis

A programmed form of necrosis has been termed necroptosis (Fig 1.8). In contrast to apoptosis, a key feature of necroptosis is membrane disruption, leading to cellular swelling and finally cell lysis which causes the release of damage associated molecular patterns (DAMPs) from the cell (Kaczmarek et al., 2013). The pathway is initiated by members of the TNF superfamily, such as TNF Receptor 1 (TNFR1), (Frank and Vince, 2019). This activation would normally lead to apoptosis but for necroptosis to occur, it is thought that certain apoptotic associated proteins need to fail. Cellular inhibitors of apoptotic proteins (cIAP1/2) and caspase 8 have been found to inhibit receptor interacting serine/threonine kinase 1 (RIPK1) and RIPK3 (Fritsch et al., 2019, Oberst et al., 2011, McComb et al., 2012). The lack of inhibition leads RIPK1 recruiting RIPK3 to form the necroptosome. The necroptosome then phosphorylates mixed lineage kinase domain like psdeudokinase (MLKL) which allows MLKL to oligomerise. This oligomer form of MLKL can then insert into the plasma membrane and organelles causing permeabilisation which leads to release of DAMPs and cell death (Duprez et al., 2009). One example of a DAMP is ATP. Recently increasing numbers of conditions have been found to be linked to necroptosis, with some studies suggesting that blocking this form of cell death could lead to new treatments. The conditions found to be associated include stroke (Degterev et al., 2005) and Alzheimer's disease (Ofengeim et al., 2017).

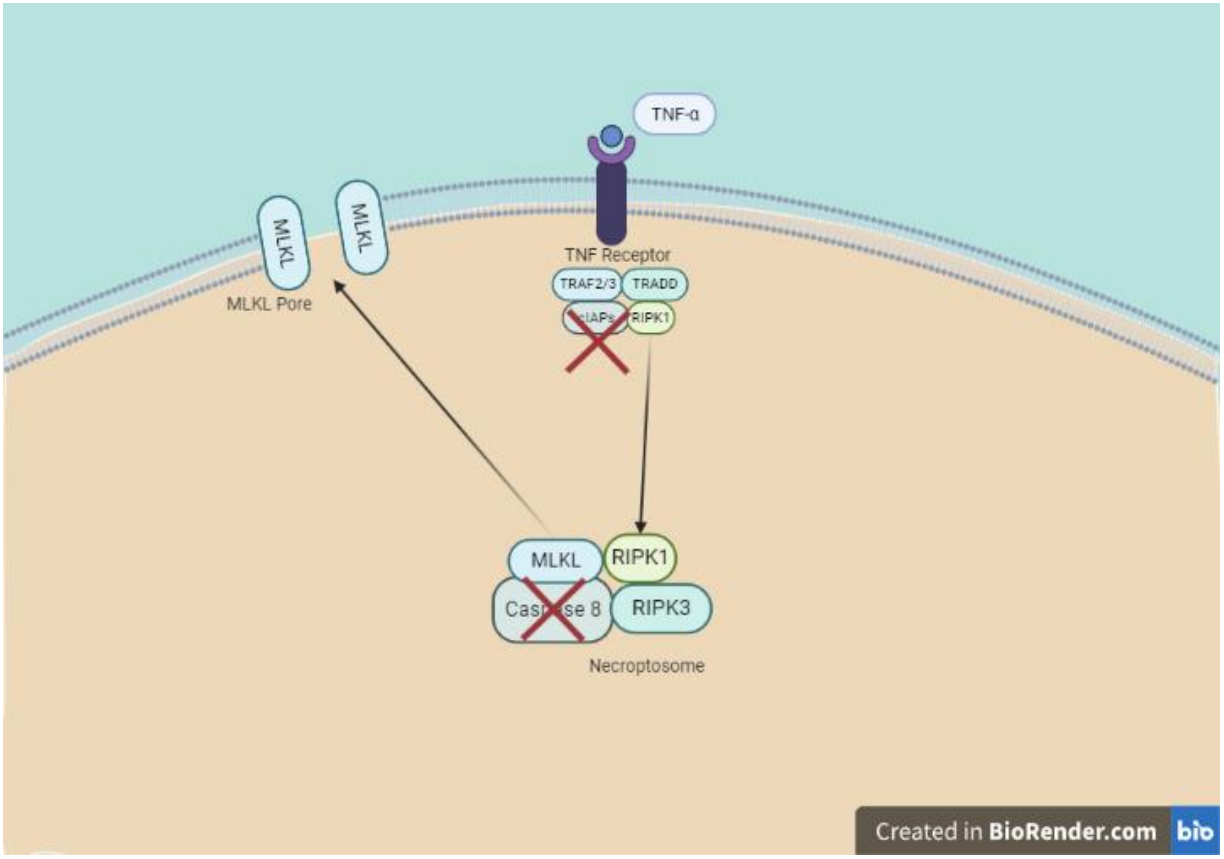

Figure 1.8 Summary of Pathway for Necroptotic cell death. TNF receptor activation leads to the formation of the necroptosome (RIPK1 and RIPK3 with an inhibited Caspase 8) which phosphorylates MLKL causing oligomerisation. Oligomerised MLKL inserts into the plasma membrane causing cell death by necroptosis. Created with BioRender.com

1.5.4 Pyroptosis

Pyroptosis is a non-apoptotic, pro-inflammatory, lytic form of programmed cell death stimulated by a range of infectious and non-infectious stimuli (Bergsbaken et al., 2009).

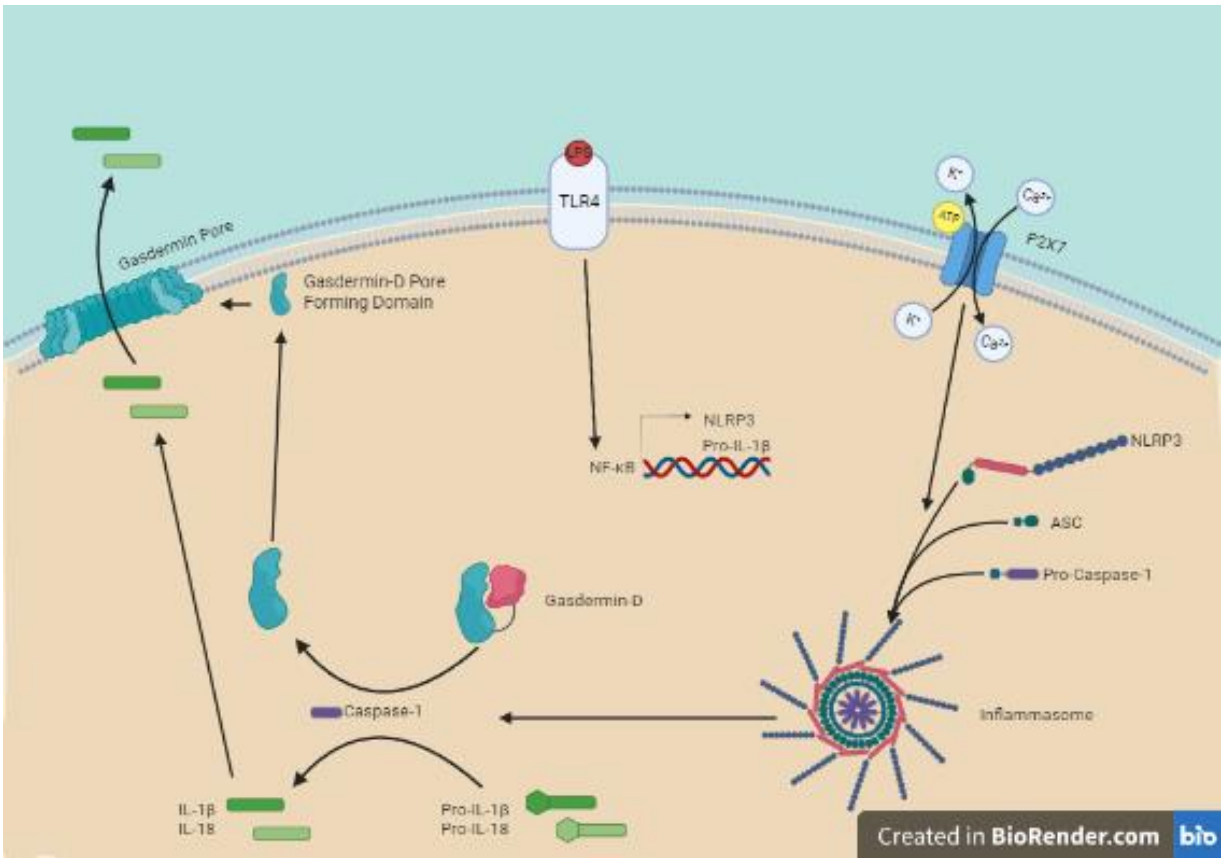

Figure 1.9 Summary of the classical NLRP3 inflammasome Pathway for Pyroptotic Cell Death. The primary signal (LPS) causes the upregulation of pyroptotic associated proteins (NLRP3 and Pro-IL-1β). The secondary signal (ATP via P2X7) leads to the formation of the inflammasome (NLRP3, ASC and Pro-Caspase-1). This leads to the activation of caspase 1 and cleavage of gasdermin D and cytokines (Pro-IL-1β and Pro-IL-18). Gasdermin D inserts into the cellular membrane forming a pore allowing the cytokines to leave the cell and pyroptotic cell death to occur. Created with BioRender.com

A defining feature of pyroptosis is the dependence on caspase 1. The activation of caspase-1 is thought to be conducted by a large signal-induced multiprotein complex, called the inflammasome (Fig 1.9). Five different inflammasomes have been found that activate caspase 1. The most well studied “classical” pyroptotic pathway starts with a primary signal, such as LPS activating TLR4 which upregulates pyroptotic proteins such as NLRP3 and Pro-IL-1β. NLRP3 has been found to be activated by multiple stimuli, including pore-forming toxins, uric acid crystals, virus DNA, RNA, asbestos, UV-B irradiation and extracellular ATP (Swanson et al., 2019). A common response that all these stimuli share is an efflux of potassium. In Fig 1.7 potassium efflux is shown via the P2X7 receptor. Activation of NLRP3 leads to the assembly of the inflammasome, NLRP3 associates with the apoptosis associated speck-like protein containing a CARD (ASC) protein

and pro-caspase 1, leading to the activation of caspase-1. Caspase 1 activation causes the cleavage of proinflammatory cytokines such as IL-1β and IL-18. It also cleaves gasdermin D. Gasdermin D is the final executioner in the pyroptotic pathway, inserting into the membrane to form a pore that mediates cell swelling and membrane rupture. Caspase-1 activation and pyroptosis has been found to be involved in multiple diseases, such as, myocardial infarction, cerebral ischaemia, irritable bowel syndrome, the neurodegenerative diseases Huntingdon's and Alzheimer's disease and endotoxic shock (Frantz et al., 2003, Li et al., 1995, Ona et al., 1999, Schielke et al., 1998, Siegmund et al., 2001).

1.6 Cell Death Pathway Executive Proteins

1.6.1 Calpains

Calpains are a family of Ca^{2+} dependent cysteine proteases(Hosseini et al., 2018). They are thought to be involved in signal transduction, cell death, cell proliferation, migration and differentiation (Sorimachi et al., 2011a, Sorimachi et al., 2011b, Suzuki et al., 2004). More recently there is evidence of calpain involvement in neuronal migration and differentiation, synaptic plasticity and neuroprotection (Baudry and Bi, 2013, Baudry and Bi, 2016). Calpains are found in 15 isoforms, as shown in Figure 1.10, CAPN1 is found in its long (CAPN1) and short CAPNS1 (previously known as CAPN4) form. Calpains are either found ubiquitously or are tissue specific. Ubiquitous calpains include CAPN1, 2, 5, 7, 10, 13 and 15. Tissue specific calpains include CAPN 3 which is found in skeletal muscle and also splice variants of CAPN 3 are found in the retina (Azuma et al., 2000) and the lens (Fukiage et al., 2002). Other tissue specific calpains are CAPN6 which is found in the placenta, CAPN 8 and 9 both found in the gastrointestinal tract, CAPN11 and 16 found in the testes, CAPN12 found in hair follicles and CAPN14 found in the oesophagus (Ono et al., 2016b).

They have been classified into two groups: classic (CAPN1-3, CAPN8-9, CAPN11-14) and non-classic (CAPN5-7, CAPN10, CAPN13, CAPN15-16) calpains. Classic and non-classic are characterised by the presence (classic) or lack of (non-classic) the penta EF (PEF) region, which facilitates Ca^{2+} binding and subsequent activation within the protease.

Inhibitors of calpains have been developed previously including for calpain 1 and 2. An inhibitor for calpain 1 is PD150606 (Low et al., 2014) and for calpain 2 is CAT811 (Abell et al., 2009).

Evidence has been found that calpains are involved in many diseases. Calpains 1 and 2 have been implicated in Alzheimer's (Garwood et al., 2013, Kurbatskaya et al., 2016, Magi et al., 2016), Parkinson's (Diepenbroek et al., 2014), Huntington's (Gafni et al., 2004, Weber et al., 2016) and cataract (Biswas et al., 2004, David and Shearer, 1986). Calpain 3 has been found to be involved

with a form of muscular dystrophy (MD) called Limb girdle MD type 2A (Kramerova et al., 2016, Ono et al., 2016a), while calpain 5 has links to autosomal dominant neovascular inflammatory vitreoretinopathy (Mahajan and Lin, 2013). Calpains 8 and 9 have involvement in gastric ulcers (Ono and Sorimachi, 2012), calpain 10 in diabetes (Pandurangan et al., 2014, Pánico et al., 2014, Sáez et al., 2008) and polycystic ovary syndrome (Shen et al., 2013) and calpain 14 in eosinophilic esophagitis (Litosh et al., 2017).

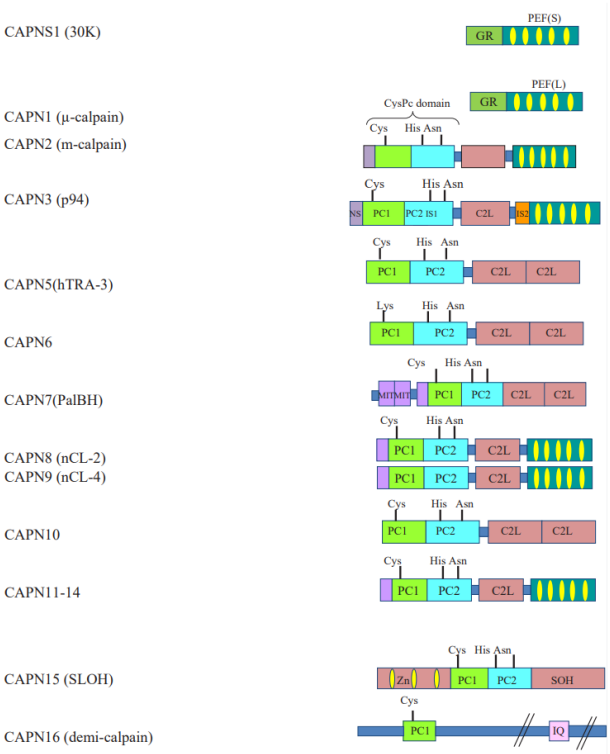

Figure 1.10 The Calpain Family Structure of calpains and their domains. Domains listed are Glycine-Rich (GR), Penta-EF small and large (PEF(S) or PEF(L)), Polycystin-1 and -2 (PC1 and PC2), Insertion Sequence-1 and -2 (IS1 and IS2), C2-Like (C2L), Microtubule-interacting and trafficking (MIT), Small optic lobes homology (SOH) and calmodulin interacting motif (IQ) Adapted from (Hosseini et al., 2018)

Calpains have many substrates with some suggesting that up to 1000 proteins could be modulated by the calpain family (Piatkov et al., 2014). and the kinases protein Kinase C, CaMKII, Bid, Bax23, ERK1/2 and Cdk5/p35 are also substrates of calpains. They are also known to regulate proteolysis of cytoskeletal proteins (Siklos et al., 2015) including spectrin (Ono et al., 2016b, Seinfeld et al., 2016). Spectrin is found to be proteolysed by calpains in neuronal cells and has been found to be associated with neuronal apoptosis (Briz and Baudry, 2017, Czogalla and Sikorski, 2005, Ono et al., 2016b, Siklos et al., 2015). The cytoplasmic tails of actin and integrins are regulated by calpains (Cortesio et al., 2011). Inhibition of calpains has been found to block actin proteolysis and DNA fragmentation during apoptosis of neuronal cells (Rami et al., 2000, Villa et al., 1998).

It has been shown that calpains are the major cause of cell death in photoreceptors expressing misfolded rhodopsin, though the mechanism of cell death in this instance is unknown (Comitato et al., 2020). Calpains have also been shown to play a role in the degeneration and dysfunction of retinal neurons in a rat model of acute ocular hypertension (Suzuki et al., 2014). In addition, monkey retinal explants that underwent hypoxia/reoxygenation saw activation of calpains in the nerve fibre layer that led to the eventual cell death of the connected RGCs (Hirata et al., 2015). One study also showed that activation of calpains 1 and 2 was important in the changes that lead to the degeneration of the retina in WBN/Kob rats, a model for spontaneous retinal degeneration (Azuma et al., 2004) while another study in rats, this time for a glaucoma model, showed that calpains are activated under elevated IOP conditions which lead to the eventual loss of RGCs (Huang et al., 2010).

Calpains have also been shown to be involved in the immune system. One study using rats showed an increased expression in activated glia and other inflammatory cells in experimental allergic encephalomyelitis, a model for multiple sclerosis (MS) (Shields et al., 1998). Calpain activity and expression has also been found to increase in activated glia and other inflammatory cells using a rat model for penumbra spinal injury lesions (Shields et al., 2000). A calpain inhibitor, calpeptin, has been used to treat optic neuritis in rats, an inflammatory auto immune disease that often occurs in humans that suffer from multiple sclerosis (MS). With treatment there was a decrease in inflammation, reactive astroglia and activated microglia. The results of this treatment led to a decrease in axonal damage and promoted intracellular neuroprotective pathways in the optic nerve (Das et al., 2013). Another study has also found that calpains have a vital role in human macrophages. It has been found to be essential for protein secretion that is ATP driven and also activation of the inflammasome (Välimäki et al., 2016).

1.6.2 Caspases

Caspases are a family of cysteine-dependent proteases. They are known for cleaving their substrates on the C-Terminal side of an aspartate although they can also cleave after glutamate and phosphoserine residues.

There have been found to be 3 groups of caspases (Van Opdenbosch and Lamkanfi, 2019). Group 1 are the inflammatory caspases which share a long caspase recruitment domain and a preference for a large aromatic or hydrophobic residue in the P4 position of their substrates (Julien and Wells, 2017). This group contains Caspases 1, 4, 5 and 11 (Van Opdenbosch and Lamkanfi, 2019). Group 2 is made up of effector or executioner caspases that share a short pro-domain This group is made up of caspase 3, caspase 6 and caspase 7. Finally group 3 are the initiator caspases which share a

long pro-domain and prefer leucine and valine in the P4 position of their substrates This group consists of caspase 8, caspase 9 and caspase 10 (Van Opdenbosch and Lamkanfi, 2019).

There are also caspases that do not neatly fit into these groups. Caspase 2 has the long pro-domain of group 3 but the substrate specificity of group 2 and is thought to be involved in the cell cycle (Fava et al., 2017). Caspase 12 is only found in some small subsets of the human population (Kachapati et al., 2006) and caspase 14 is thought to have a highly specific role in the differentiation process of keratinocytes (Eckhart et al., 2000).

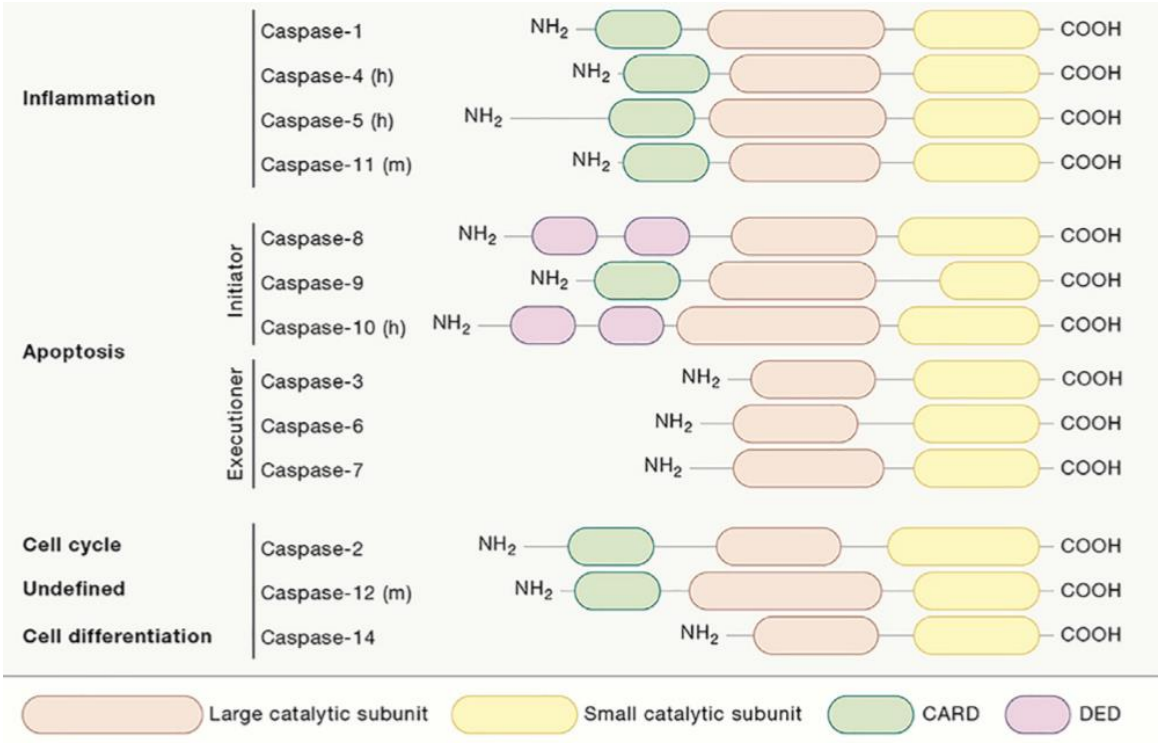

Figure 1.11 The Caspase Family Classification and basic structure of human and murine caspases. Adapted from: (Van Opdenbosch and Lamkanfi, 2019)

Many inhibitors have been found for various caspases including a pan caspase which is found to block caspases 1, 3, 7 and 8 (Cain et al., 1996). Specific caspase inhibitors include a caspase 1 inhibitor, that also has some inhibition of caspase 4 (Ac-YVAD-cmk) (Cain et al., 1996), a caspase 3 inhibitor (Z-DEVD-FMK) (Masuda et al., 1997) and a caspase 8 inhibitor (Z-IETD-FMK) (Concha and Abdel-Meguid, 2002, Thornberry et al., 1997)

1.6.2.1 Inflammatory Caspases

1.6.2.1.1 Caspase 1

The first of the inflammatory caspases is caspase 1. As shown on Figure 1.11 caspase 1 contains large and small catalytic subunits with a linker region and also a caspase recruitment domain

(CARD). The preferred substrate motifs for peptides is WEHD and for proteins is either YVHD or FESD (Julien and Wells, 2017).

As mentioned previously, caspase 1 plays a vital part in pyroptosis where it is a key component of the canonical inflammasome. A sensor protein becomes activated which binds and activates the ASC protein which then recruits procaspase 1 by its corresponding CARD domains. This allows the associated procaspase 1 to become dimerised which leads to autocatalytic cleavage into active caspase 1. Active caspase 1 then converts the cytokines, IL1β and IL18, as well as the pyroptotic executioner protein gasdermin D, into their active forms.

Caspase 1 has also been found to have non-pyroptotic actions including possible roles in apoptosis. A recent study using a hypoxia and ischaemia-induced neuronal cell death model found caspase 1 was able to cleave the BID protein (Zhang et al., 2003), while another study showed it could activate caspase 6 apoptotic human neurons (Guo et al., 2006).

Caspase 1 has also been found to play multiple roles in phagocytosis. One study showed caspase 1 promoted the lysosomal degradation of *legionella* in macrophages (Amer et al., 2006). Other studies have shown that caspase 1 is able to cause the acidification of lysosomes in the degradation of bacteria or apoptotic debris (Monteith et al., 2018, Sokolovska et al., 2013). Caspase 1 has also been found to cause lysosomal exocytosis due to its downstream effects that cause an increase in intracellular calcium levels (Bergsbaken et al., 2011) and a further study found that caspase 1 upregulated mitochondrial autophagy in hepatocyte cell death in a haemorrhagic shock model (Sun et al., 2013).

Knockout studies for caspase 1 in mice show normal growth and development (Kuida et al., 1995) however there is evidence that they are more susceptible to viral infection (Thomas et al., 2009) and also that there is an increased risk of tumour formation (Hu et al., 2010a). Caspase 1 has also been associated with HIV, where it is thought to be involved in the mechanism of CD4 T-cell depletion (Zhang et al., 2021, Monroe et al., 2014, Doitsh et al., 2014).

Although not directly associated with caspase 1, an increase in the levels of the caspase 1 cytokine substrate, IL-1β, have been shown to be a risk factor for type 2 diabetes and also add to insulin resistance (Spranger et al., 2003, Maedler et al., 2009). IL-1β has also been implicated in many other diseases including neurodegenerative conditions such as Alzheimer's disease, Parkinson's disease and glaucoma (Oliveira et al., 2018, Piancone et al., 2021).

1.6.2.1.2 Caspase 4, 5 and 11

The function of Caspases 4 and 5 are not fully known. However, they are known to have a murine homologue known as caspase 11, which has a role in the non-canonical activation of the inflammasome and contains a LPS detecting section within its structure (Van Opdenbosch and Lamkanfi, 2019).

1.6.2.2 Executioner Caspases

1.6.2.2.1 Caspase 3

The first of the executioner caspases is caspase 3. As shown in Figure 1.11 caspase 3 is made up of both a large and small catalytic subunit, with a linker region. The procaspase form is a stable dimer and is activated by cleavage of this linker region to create a tetrameric formation. The preferred substrate motifs in both peptides and proteins for caspase 3 is DEVD (Julien and Wells, 2017).

As mentioned previously caspase 3 is a vital component of the apoptotic machinery, playing a role in both the intrinsic pathway, where is it cleaved and activated by caspase 9, and the extrinsic pathway, where it is cleaved and activated by caspase 8. There is also evidence of interaction between caspase 3 and members of the gasdermin family. One study showed that caspase 3 is able to activate pyroptosis by cleaving gasdermin E (Zeng et al., 2019), while another study showed it can block pyroptosis by inactivating gasdermin D through cleavage at an alternate site (Taabazuing et al., 2017).

Caspase 3 has also been found to have roles outside of cell death including, tissue differentiation (erythrocytes, monocytes and neurons), tissue regeneration and neural development, synaptic plasticity and axon guidance. Knockout experiments in mice show that most die perinatally and those that do survive have abnormal neural structures and behaviour deficits (Kuida et al., 1996) although this was shown to possibly be strain dependent (Leonard et al., 2002). It was also shown that caspase 3 knockout mice exhibited marked cataracts at the anterior lens pole (Zandy et al., 2005).

Caspase 3 has been shown to be involved in many diseases including cancer, Huntington's disease and Alzheimer's disease (Asadi et al., 2022).

1.6.2.2.2 Caspase 6

The next executioner caspase is caspase 6 and again if we look at Figure 1.11 the structure is made up of large and small catalytic subunits with a linker region. The preferred substrate motifs for peptides is VQVD and for proteins it is VEVD(Julien and Wells, 2017).

Caspase 6 plays a central role in apoptosis. It has been found to be processed and activated by caspases 3, 7, 8 and 10, while evidence has also shown the ability to undergo self-processing (Wang et al., 2010). Another vital role for caspase 6 is host defence and cell death during an influenza A Virus infection where it has been found to activate the NLRP3 inflammasome (Zheng et al., 2020).

Like caspase 3, caspase 6 is involved in many of the same conditions, including cancer, Huntington's disease, and Alzheimer's disease (Graham et al., 2011).

1.6.2.2.3 Caspase 7

The last of the executioner caspases is caspase 7. Shown in Figure 1.11, as with the other executioner caspases, we see a large and small catalytic subunit with a linker region. The pro caspase form is a stable heterodimer which is cleaved to make a tetramer formation (Lamkanfi and Kanneganti, 2010). Identical to caspase 3, caspase 7 has DEVD as a preferred substrate motif in both peptides and proteins (Julien and Wells, 2017).

Caspase 7 plays a central role in apoptosis. It has been found to be processed and activated by caspases 3, 8, 9 and 10.

Caspase 7 knockout mice develop normally with a normal appearance and organ morphology (Lakhani et al., 2006). It is thought, due to the similar structure, caspase 3 compensates for the lack of Caspase 7. However, studies have shown that there are differences between caspase 3 and 7 when it comes to protein processing, with caspase 7 being more selective. This is also true for the substrates as some proteins are more selective towards caspase 7 than caspase 3 (Walsh et al., 2008). These differences are also highlighted in knockout studies using different cell death stimuli. Caspase 7 knockout mouse embryonic fibroblasts stimulated with UV or ligands for the Fas receptor showed a higher resistance to apoptosis than the caspase 3 knockouts (Lakhani et al., 2006).

Caspase 7 has also been found to have a role in inflammation. In macrophages stimulated with LPS and ATP or infected with *Salmonella typhymurium* and *Legionella pneumophila* it has been shown that inflammasomes containing caspase 1 process and activate caspase 7 but not caspase 3. Caspase 7 knockout macrophages are also less able to restrict intracellular *Legionella pneumophila*

replication (Akhter et al., 2009) and caspase 7 knockout mice display a resistance to death triggered by injection of intraperitoneal LPS, a common model for human shock syndrome (Lamkanfi et al., 2009).

Caspase 7 is involved with a number of conditions including Huntington's disease and Alzheimer's disease, where an increased presence of caspase 7 expression is indicative of higher neuronal cell death (Hermel et al., 2004, Ramasamy et al., 2006) and sepsis, where caspase 7 is thought to play a role in extensive leukocyte apoptosis (Hotchkiss and Nicholson, 2006). Also it has been found that single nucleotide polymorphisms in caspase 7 have been linked with rheumatoid arthritis (Teixeira et al., 2008) and insulin dependent diabetes mellitus (Babu et al., 2003).

1.6.2.3 Initiator Caspases

1.6.2.3.1 Caspase 8

The first of the initiator caspases is caspase 8. As seen in Figure 1.11 caspase 8 has a large and a small catalytic subunit, along with 2 death effector domain (DED) regions. The preferred substrate motif for peptides is LETD and for proteins is XEXD, where X is any residue (Julien and Wells, 2017).

Caspase 8 plays a role in multiple cell death pathways (Orning and Lien, 2021). Firstly, in the extrinsic apoptotic pathway, as mentioned previously, caspase 8 is an important component of the DISC (Kischkel et al., 1995). Activation of death receptors, such as Fas, leads to the recruitment of TRADD, FADD and RIPK1 which along with caspase 8 form the DISC allowing caspase 8 dimerisation and autocleavage of caspase 8 (Orning and Lien, 2021). This then activates caspase 3 and 7 leading to apoptosis. It has been found that in certain cells the intrinsic apoptotic pathway can be triggered through cleavage of BID by activated caspase 8 (Li et al., 1998).

Another component of the DISC is cellular FLICE inhibitory protein (cFLIP). This protein has been found to block apoptosis. There are 3 isoforms of cFLIP, 2 short ($cFLIP_R$ and $cFLIP_S$) and 1 long ($cFLIP_L$). Caspase 8 can dimerise with $cFLIP_L$ which leads to the inhibition of the autocleavage ability of caspase 8 (Orning and Lien, 2021).

Caspase 8 also plays an inhibitory role in necroptosis. Active caspase 8 cleaves RIPK1 that has bound to RIPK3 blocking the necroptotic pathway (Feng et al., 2007, Lin et al., 1999, Oberst et al., 2011). Therefore, necroptosis can only occur with the inhibition of caspase 8.

In pyroptosis, caspase 8 has been found to have the ability to regulate different parts of the inflammasome. Firstly it can trigger inflammasome activity in response to β-glucans and *C. Albicans* downstream of dectin-1 (Ganesan et al., 2014), it has also been found to associate with the ASC protein through its DED region (Vajjhala et al., 2015). It has also been found to be involved

in the activation of caspase 1 (Philip et al., 2014) and can cleave IL-1β (Antonopoulos et al., 2013, Gringhuis et al., 2012, Maelfait et al., 2008) and finally it has been shown to be able to also cleave gasdermin D directly (Orning et al., 2018, Sarhan et al., 2018).

Knockout experiments in mice show that loss of caspase 8 is embryonically lethal, thought to be linked to the inhibitory role caspase 8 plays in necroptosis (Newton et al., 2019, Varfolomeev et al., 1998). Loss of caspase 8 in humans is not embryonically lethal, which is thought to be down to the presence of caspase 10.

Caspase 8 has been found to be involved in human disease such as early onset inflammatory bowel disease (Lehle et al., 2019).

1.6.2.3.2 Caspase 9

The next initiator caspase is caspase 9. As seen on Figure 1.11, caspase 9 contains a small and large catalytic subunit, with a linker domain that is much longer when compared to the other caspases, also caspase 9 is the only CARD containing caspase in the executioner and initiator groups. The preferred substrate motifs for peptides is (W/L)EHD while the motif for proteins is still to be determined (Julien and Wells, 2017).

As mentioned previously caspase 9 has an important role in the intrinsic apoptotic pathway, where it acts as the main initiator caspase. Caspase 9 is a key component of the apoptosome but as procaspase 9. The role of the apoptosome is thought to provide a location for the dimerisation of procaspase 9, which then leads to the rapid autocatalytic cleavage producing the active caspase 9 (Renatus et al., 2001).

Caspase 9 has been found to be involved with an array of conditions such as Huntington's disease (Kiechle et al., 2002), Alzheimer's disease (Zhao et al., 2016) and a possible role in the progression of sepsis (Miliaraki et al., 2021).

1.6.2.3.3 Caspase 10

The last of the initiator caspases is caspase 10. As seen on Figure 1.11, caspase 10 has a similar structure to caspase 8, with 2 DED regions and a large and small catalytic subunit. The preferred substrate motifs in both peptide and protein is LEHD (Julien and Wells, 2017).

Caspase 10, which is known to activate caspases 3 and 7 and is processed by caspase 8, is thought to have an important role in the extrinsic apoptotic pathway though this role is not fully understood.

A recent study suggested that caspase 10 is a negative regulator of caspase 8 mediated cell death and supports FasL induced gene induction. They showed that caspase 10 rewires the DISC signalling to NFκB activation/cell survival (Horn et al., 2017).

There is no mouse homologue known, so knockout studies have been unable to be conducted which has limited the ability to investigate function.

Mutations in caspase 10 have been found to cause autoimmune lymphoproliferative syndrome (ALPS) type II, caused by defective lymphocyte homeostasis leading to excess lymphocytes and then autoimmunity (Wang et al., 1999).

1.6.3 Necroptotic Proteins

1.6.3.1 Receptor interacting protein kinase 1 (RIPK1)

Receptor interacting protein kinase 1 (RIPK1) was the first of the RIPK family to be discovered (Stanger et al., 1995). The structure of RIPK1 is made up of a kinase domain, an intermediate domain containing a RIP homotypic interaction motif (RHIM) and finally a death domain (Zhang et al., 2010). With this death domain it is thought to interact with the death domains of death receptors such as Fas and TNF1-R1 as well as adaptor proteins such as FADD and TRADD. The intermediate domain and death domain allow RIPK1 to associate with various other kinases including RIPK3, MEKK1 and MEKK3 (Yu et al., 1999, Yang et al., 2001, Sun et al., 1999, Kim et al., 2001a).

As mentioned previously RIPK1 plays a vital role in multiple cell death pathways including being a component of the DISC of extrinsic apoptosis, the necroptosome in necroptosis and an initiator in necrosis. RIPK1 has been found to be inhibited by necrostatin (Degterev et al., 2005).

Knockout studies for RIPK1 result in the mice dying up to 3 days after birth (Kelliher et al., 1998).

1.6.3.2 Receptor interacting protein kinase 3 (RIPK3)

RIPK3 was the third member of the RIPK family to be discovered. The structure of RIPK3 is made up of a kinase domain and a further domain that contains a RHIM (Zhang et al., 2010). As mentioned before RIPK3 plays a vital role in necroptosis after forming the necroptosome alongside RIPK1, while caspase 8 is inhibited, RIPK3 cleaves MLKL leading to cell death.

Both RIPK1 and RIPK3 have been found to have roles outside of necroptosis and apoptosis. A recent study has shown both RIPK1 and RIPK3 are involved in cytokine production in myeloid cells to help regulate myeloid homeostasis (Wong et al., 2014) while a further study show that both

proteins are able to activate the inflammasome after RNA virus stimulation (Wang et al., 2014). There is further evidence of other roles for RIPK3. A study has shown that RIPK3 is able to generate a bioactive form of IL1β (Vince et al., 2012) while another study showed that RIPK3 is able to promote injury induced cytokine expression and tissue repair in dendritic cells (Moriwaki et al., 2014).

1.6.3.3 Mixed Lineage Kinase Domain Like Psdeudokinase (MLKL)

MLKL is a 54Kda protein from the kinase superfamily. This protein is made up of a C-Terminal pseudo kinase domain, a linker region and an N-Terminal 4 helix bundle (4HB) (Su et al., 2014, Murphy et al., 2013). As mentioned previously MLKL is activated by phosphorylation carried out by the necrosome. The location of this phosphorylation site is in the pseudo kinase domain which causes a conformational change which causes the 4HB to become exposed (Tanzer et al., 2016, Petrie et al., 2018, Czabotar and Murphy, 2015). With the 4HB now exposed MLKL-p is able to form disulphide bond dependent oligomers (Liu et al., 2017, Tanzer et al., 2016, Petrie et al., 2018) which are able to form pores, thought to be 4nm in diameter (Ros et al., 2017).

The antibiotic necrosulfonamide has been found to block MLKL pore formation (Sun et al., 2012).

MLKL has been found to play a role in a variety of diseases such as diabetes (Xu et al., 2019) and cancer (Dong et al., 2019)

1.6.4 Pyroptotic Proteins

1.6.4.1 NLR Family Pyrin Domain Containing Protein 3 (NLRP3)

NLRP3 is a member of a family of sensor proteins involved in the inflammasome. The structure of NLRP3 consists of a PYD, a NACHT and an LRR (Kelley et al., 2019). NLRP3 activation occurs due to PAMPS such as viral RNA, microbial toxins and bacterial surface components (Allen et al., 2009, Duncan et al., 2009) and DAMPS such as uric acid crystals, ATP and β amyloid peptide (Halle et al., 2008, Mariathasan et al., 2006, Martinon et al., 2006). Other signals and stimuli thought to be involved with the activation of the NLRP3 inflammasome include ion flux, mitochondrial dysfunction, ROS, lysosomal disruption and mtDNA (Kelley et al., 2019). After activation NLRP3 oligomerises which allows it to bind to ASC using the corresponding PYD domains and as mentioned before this then results in the pyroptotic cell death pathway (Sharma and de Alba, 2021). NLRP3 has been found to be inhibited by MCC950 (Coll et al., 2015).

NLRP3 has been linked to a number of conditions such as Alzheimer's disease, type 2 diabetes and cancer (Menu and Vince, 2011).

1.6.4.2 Apoptosis Associated Speck-like Protein Containing a CARD (ASC)

Apoptosis associated speck like protein with a caspase recruitment domain (ASC) is a small 22kDa protein made up of a N-terminal PYD and a C-terminal CARD with a linker region in between (Masumoto et al., 1999, Sahillioglu et al., 2014). ASC works as a linker for the inflammasome structure, as it is able to bind NLRP3, as well as other inflammasome sensor proteins, by binding the corresponding PYD domains while also binding to procaspase 1 using the corresponding CARD domains (Srinivasula et al., 2002, Stehlik et al., 2003, Masumoto et al., 1999).

The ASC protein has been found to be involved in an array of conditions and diseases such as Alzheimer's disease (Couturier et al., 2016), arthritis (Ippagunta et al., 2010), stroke (Denes et al., 2015) and autoimmune encephalomyelitis (Shaw et al., 2010, Martin et al., 2016)

1.6.4.3 Gasdermins

Gasdermins are pore-forming cytosolic proteins that are extremely hazardous to the cell. Unwanted activation of this family of proteins has been associated with deafness, alopecia, and exacerbation of sepsis in animal models (Kayagaki et al., 2015, Kovacs and Miao, 2017). The structure is thought to be made up of a pore forming domain (PFD), a linker domain and a repressor domain (RD) that auto inhibits the pore forming activity of the gasdermin. When the linker domain is cleaved the PFD oligomerises with other cleaved PFDs in the cell membrane to create a pore 10-15nm in diameter (Aglietti et al., 2016, Ding et al., 2016, Liu et al., 2016), though one group suggests 21nm (Sborgi et al., 2016). If a small number of gasdermin pores exist, the IL-1β and IL-18 can pass through the pore without the need for rupture (Brough and Rothwell, 2007, Martín-Sánchez et al., 2016, Russo et al., 2016). The cell can then compensate any volume increases using swelling-activated K^+, Cl^-, and organic osmolyte (e.g. taurine) channels that export these solutes and any accompanying water (Hoffmann et al., 2009). If the level of active gasdermin pores goes over the critical threshold the cell swells extensively. This leads to the separation of the plasma membrane and the cortical cytoskeleton in large fluid-filled balloons, which are distinct from the characteristic apoptotic blebs (Shi et al., 2015).
The gasdermin family of proteins has 6 members, gasdermin A, B, C, D and E.

1.6.4.3.1 Gasdermin A

Gasdermin A is expressed in epithelial cells of the skin, tongue, oesophagus, stomach, mammary gland and umbilical cord (Kovacs and Miao, 2017). It is involved with inflammation of the skin and asthma, thought to be through the autophagy pathway (Shi et al., 2015, Yu et al., 2011). Humans are found to have one variant of gasdermin A, but mice have been found to have 3, Gasdermins A1, A2 and A3. Gasdermin A3 mutations in mice were found to cause alopecia, hyperkeratosis and inflammation (Tanaka et al., 2013). Gasdermin A has also been found to be able to damage the mitochondria and induce mitophagy (Shi et al., 2015).

1.6.4.3.2 Gasdermin B

Gasdermin B is expressed in lymphocytes, oesophagus, stomach, liver and colon (Kovacs and Miao, 2017, Wu et al., 2009). Like gasdermin A it is thought to be involved in asthma (Moffatt et al., 2010, Moffatt et al., 2007, Wu et al., 2009, Yu et al., 2011). It has been found to be cleaved by caspases 3, 6 and 7 (Chao et al., 2017) and is inactivated during apoptosis.

1.6.4.3.3 Gasdermin C

Gasdermin C has been found to be expressed in the oesophagus, stomach, trachea, spleen, intestine, bladder and skin (Kovacs and Miao, 2017, Wu et al., 2009). There is also evidence of increased expression in metastatic melanoma (Watabe et al., 2001) and decreased in oesophageal and gastric cancer (Saeki et al., 2009).

1.6.4.3.4 Gasdermin D

Gasdermin D is expressed in the placenta, B and T lymphocytes, oesophagus, stomach and all 21 gastric cancer cell lines (Saeki et al., 2009). It is thought to be cleaved by caspases 1, 4, 5 or 11 and is described as the main player in pyroptosis (Kovacs and Miao, 2017). Activity of gasdermin D was first thought to only be terminal (Lieberman et al., 2019). However, subsequent research has shown that gasdermin D activation does not always lead to cell death (Evavold et al., 2018, Heilig et al., 2018). The cell death after gasdermin D pore formation is regulated and can be delayed and even avoided (Lieberman et al., 2019). Gasdermin D has been found to have its pore forming ability blocked by necrosulfonamide (Rathkey et al., 2018).

1.6.4.3.5 Gasdermin E

Gasdermin E is expressed in the placenta, brain, heart, kidney, cochlea, intestines and IgE-primed mast cells (Kovacs and Miao, 2017, Wu et al., 2009). Gasdermin E has been found to play a role in both apoptosis, where it is thought to insert into the mitochondria leading to the release of cytochrome C, and pyroptosis, where it replaces gasdermin D as the pore protein (Liao et al.,

2022). Gasdermin E has been found to be associated with many conditions including cancers, hearing loss and kidney disease (Liao et al., 2022).

1.7 Aims

Taking all that has been covered previously into consideration, it is important to look at microglia, cell death, ATP and P2X7, with a view to try to understand how these aspects could play a role in neuroinflammation and the progression of neurodegenerative conditions, such as glaucoma and Alzheimer's disease. Therefore the aims of this thesis are, firstly to investigate the effects of ATP stimulation on cell membrane disruption and cell death in microglia, and to use pharmacological inhibitors to try to characterise this pathway. Secondly, for a wider understanding of the cell death mechanism happening following ATP stimulation in microglia, a comparison between this pathway and the cell death pathway happening in macrophages after ATP stimulation with and without LPS priming will be performed. Finally, for a deeper look into other pathophysiological stressors microglia may come into contact within the CNS, the effects of pathophysiological insults on cell membrane disruption and cell death in microglia will be investigated and pharmacological inhibitors used to try and characterise these pathways.

1.8 Hypothesis

The hypothesis that drove the research presented in this thesis is that cell death in microglia stimulated by ATP occurs via the cell death mechanism pyroptosis, with increased permeability mediated by gasdermin D. This mechanism will be similar to the response seen in macrophages. Other pathophysiological stressors found in neurodegenerative conditions, including glaucoma, will cause cell death via the pyroptotic mechanism.

Chapter 2

Materials and Methods

2.1 Cell Culture

Cells used were BV2 (Blasi et al., 1990) and a P2X7K/O variant of BV2 cells, produced by Dr Leanne Stokes using the CRISPR-Cas9 gene editing technique to remove the P2X7 gene from the wild type BV2 cells (Dhuna et al., 2019). BV-2 cells were transfected with endotoxin free 1 mg EditR-Cas9 plasmid with blasticidin resistance (GE Healthcare Dharmacon, Lafayette, CO) plus 25 nM target RNA and 25 nM complementary RNA for P2RX7 using Dharmafect DUO reagent. After this, antibiotic selection was performed using blasticidin. The treated cells underwent flow cytometry testing for the presence of P2X7 and cells lacking P2X7 underwent a single-cell cloning procedure. DNA was extracted from successful clones and sent for sequencing to verify mutations were present. All cells were cultured under aseptic conditions. BV2 cells were cultured in Dulbecco's Modified Eagle Medium: F12 Nutrient Mixture F-12 (DMEM/F12) (Fisher. Loughborough), supplemented with 10% heat-inactivated FBS (Pan-Biotech, Wimborne), 1% of a 200mM L-Glutamine solution (Life Technologies, Fisher, Loughborough) and 100 U/ml Penicillin plus 100µg/ml Streptomycin (Life Technologies, Fisher, Loughborough) at 37^{o}C and 5% CO_2 in a Nunc^{tm} EasYFlask^{tm} 75cm^3 Nunclon^{tm} Delta Surface flask (Fisher, Loughborough). J774 mouse macrophage cells (obtained from The European Collection of Authenticated Cell Cultures (ECACC) General Cell Culture Collection, UK) were cultured in Roswell Park Memorial Institute (RPMI) 1640 medium (Fisher, Loughborough), supplemented with 10% heat-inactivated FBS (Pan-Biotech, Wimborne), 1% of a 200mM L-Glutamine solution (Life Technologies, Fisher, Loughborough) and 100 U/ml Penicillin plus 100µg/ml Streptomycin (Life Technologies, Fisher, Loughborough) at 37^{o}C and 5% CO_2 in a Nunc^{tm} EasYFlask^{tm} 75cm^3 Nunclon^{tm} Delta Surface flask (Fisher, Loughborough). When the cells reached 80-90% confluency they were passaged.

BV2 and P2X7K/O variant of BV2 cells were passaged as follows: The medium in the flask containing the cells was removed and 5ml 0.25% Trypsin-EDTA (1x) (Life Technologies, Fisher, Loughborough) was added, and the flask returned to the incubator for 5 minutes. The flask was removed from the incubator and lightly tapped to dislodge any cells still attached. An equal volume of 10% FBS DMEM/F12 was added and the contents of the flask placed into a 14ml Falcon tube. This cell suspension was spun for 5 minutes at 4000rpm. The medium was aspirated with care not to disturb the pellet of cells. The pellet was resuspended in 10 ml of 10% FBS DMEM/F12. The resuspended cells could now be plated for use in experiments (see below) or were used to seed a fresh flask at a 1:20 dilution and cultured until the next passage was required (3-4 Days).

For J774 cells, the cells were removed using a cell scraper and then the contents of the flask placed into a 14ml Falcon tube. This cell suspension was spun for 5 minutes at 4000rpm. The media was aspirated with care not to disturb the pellet of cells. The pellet was resuspended in 10 ml of 10% FBS RPMI. The resuspended cells could now be plated for use in experiments (see below) or were used to seed a fresh flask at a 1:10 dilution and cultured until the next passage was required (4-5 Days).

For plating, the resuspended cells were counted using a haemocytometer. A density of 20,000 cells per well (BV2 and a P2X7K/O variant of BV2) or 40,000 cells per well (J774) was used for 96 well plates and 680,000 cells per well (BV2 and a P2X7K/O variant of BV2) and 1,360,000 cells per well (J774) for the 6 well plates. From previous use of these cells in the group, it was observed that the BV2 and P2X7K/O variant of BV2 had a growth rate double that of the J774 cells. To even this out, so that a similar level of cells would be present for testing, the seeding density of J774 cells was double that of the BV2 and a P2X7K/O variant of BV2. The 96 well plates were coated with poly-D-lysine (see below). The plated cells were then incubated until use (approximately for 24 hours) at 37^{o}C and 5% CO_2.

2.2 PDL Plate preparation

A Nunclon^{TM} Delta Surface 96 well plate (Thermo Scientific, Fisher, Loughborough) was coated with a 50µg/ml solution of poly-D-Lysine (PDL) (Merck-Millipore, Watford) per well. After 30 minutes the PDL solution was removed with a multichannel pipette and sterile water was used to wash the well. The plate was now ready for use or was wrapped in Parafilm and stored at 4^{o}C.

2.3 Cell Stimulation solutions

For cell stimulations, stock solutions were made prior to the experiment. For ATP (Sigma Aldrich, Poole) a stock solution of 100 mM was made in distilled water and pH was corrected to 7.4 with 5M NaOH. Aliquots were frozen at −20 °C and used once. Dilution to the experimental concentration was in phenol red free DMEM/F12 (Fisher, Loughborough) with L-glutamine and buffered with 15mM HEPES. This will now be referred to as HEPES medium. Stock LPS (Sigma-Aldrich, Poole) was prepared in solution of 100mg/ml in PBS (Invitrogen, Fisher, Loughborough) and aliquots frozen at -20^{o}C and refrozen after use. Stock nigericin (Sigma-Aldrich, Poole) was prepared as a solution of 10mM in DMSO and aliquots frozen at -20^{o}C. Experimentally it has been shown that the neurotoxic section of amyloid-β was the 25-35 residues (Sato et al., 1995). Stock 25-35 amyloid-β (Genscript, Oxford) was prepared as a solution of 200µM in water and aliquots frozen at -20^{o}C and used once. It was diluted further to the experimental concentration needed in

the HEPES media. For oxidative stress experiments, H_2O_2 solutions were made immediately before use on cells from a 9.98M stock (Fisher, Loughborough), diluted to a 10mM working solution in HEPES media, which was diluted further to the experimental concentration needed. For experiments looking at pH changes, the pH of the HEPES media was adjusted to alkaline conditions using 5M NaOH and acidic conditions using 3M HCl acid. pH was read using a pH meter (Fisher, Loughborough), and then passed through a 0.2µM filter to sterilise.

2.4 Cell Image Capture

Images were captured using phase-contrast microscopy with an EVOS XL Core microscope (Thermo Scientific, Loughborough) at 10x magnification. All images were captured of cells grown in a 96 well plate.

2.5 Cell Death Assays

2.5.1 LDH Assay

Lactate dehydrogenase (LDH) detection was performed using the cytotoxicity detection kit (LDH) (Roche Diagnostic GmbH, Mannheim, Germany). LDH from cells is released during forms of lytic cell death, due to cell membrane disruption, so can be used as a measure of death in cell populations. LDH converts lactate to pyruvate. The reaction reduces NAD^+ to NADH and NADH in turn reduces iodonitrotetrazolium (INT) to a formazan dye (present in the assay solution) which can then be colourimetrically detected. All LDH assays were performed in a 96 well plate.

In order to measure cell death, 100µl of each sample (cell bathing medium) was placed into a 96-well plate. A ratio of 1:45 Diaphorase/NAD^+ catalyst solution to Sodium Lactate/INT dye solution was prepared according to the manufacturer's instructions. An equal volume of catalyst/dye solution was added to each sample. Three wells of 2% Triton X (Merck-Millipore, Watford) lysed cells were used as a positive control. Triton X is a non-ionic surfactant that fully disrupts the membrane of cells, so 100% of LDH should be released upon treatment, and is used to represent total LDH release. Three wells of the HEPES medium were used to determine the background. The 96 well plate was then placed in the Flexstation 3 microplate reader at 37^{o}C and was read at wavelengths 490nm and 660nm every 45 seconds. Two wavelengths are used as the 490nm wavelength is the test wavelength, so detects the substrate colour absorption maximally, where the 660nm wavelength is an "offpeak" reference wavelength, there to detect any imperfections such as smudges or bubbles in the well. The reference wavelength (600nm) is subtracted from the test wavelength (490nm) to provide improved precision and accuracy. The corrected background is then subtracted from this value. The LDH release was calculated using the following calculation:

$$\%\ \boldsymbol{LDH\ release} = \left(\frac{\boldsymbol{Average\ Sample\ LDH\ Absorbance}}{\boldsymbol{Average\ Total\ LDH\ Absorbance}}\right)\boldsymbol{x100}$$

2.5.2 MTS Assay

Viability of cells was detected using the CellTiter 96 AQueous One Solution Cell Proliferation Assay (MTS assay) (Promega, Southampton, UK). The assay is made up of 2 components, (3-(4,5dimethylthiazol-2-yl)-5-(3-carboxymethoxyphenyl)- 2-(4-sulphophenyl)-2H-tetra-zolium) (MTS) and an electron coupling agent, phenazine ethosulfate (PES). Viable cells reduce NAD^+ to NADH, NADH in turn reduces MTS to a formazan dye, using PES as a co-factor and electron donor, which can then be colourimetrically detected. All MTS assays were performed in a 96 well plate.

In order to measure the viability of the cells, the MTS solution was added to the cell bathing medium in the 96 well plates in the well at a ratio of 1:10. HEPES medium with added MTS, was used as background. The plate was incubated at 37°C for one hour. The plate was then placed in the Flexstation 3 microplate reader and absorbance at 490nm was measured.

Control/Sample MTS Absorbance = (Sample 490nm reading – Background 490nm reading)

$$\%\ \boldsymbol{Cell\ Viability} = \left(\frac{\boldsymbol{Average\ Sample\ MTS\ Absorbance}}{\boldsymbol{Average\ Control\ MTS\ Absorbance}}\right)\boldsymbol{x100}$$

2.6 Dye Uptake Experiments

Dye uptake experiments were used to look at membrane permeability. YO-PRO and propidium iodide (PI) were the two dyes used. As the structures show (Fig 2.1) both these dyes are large molecules. YO-PRO has a molecular weight of 375.5 and PI has a molecular weight of 668.4. This means these dyes will only be able to access the cell once a large enough pore has allowed entry. On entry, the dye is inserted between the bases of DNA (intercalation), this causes a chemical change, which causes fluorescence that can be detected using a plate reader. Therefore, dye outside the cell will not fluoresce but dye inside the cell, with access to DNA, is able to. This shows that cell pore formation or membrane disruption has occurred. All dye uptake experiments were performed in a 96 well plate.

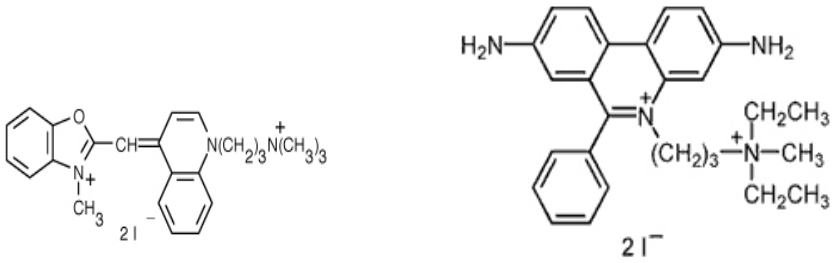

YO-PRO Iodide Dye Propidium Iodide Dye

Figure 2.1: Structure of YO-PRO and Propidium Iodide Dyes Chemical structures of fluorescent dyes used in dye uptake experiments

In order to measure dye uptake, medium was removed from the cells and replaced with either a 0.2% YO-PRO (HelloBio, Bristol) solution or a 0.2% PI (Sigma-Aldrich, Poole) solution. Both solutions were made up in the HEPES medium. The Flexstation 3 microplate reader (Molecular Devices, Wokingham) was set up to read from the bottom of the well at an excitation wavelength of 490nm and emission wavelength of 520nm for YO-PRO or an excitation wavelength of 533nm and emission wavelength of 617nm for PI. An initial reading was taken as a baseline. For cell stimulation, ATP solutions were made using the HEPES media to 10x the final concentration (e.g. for cells stimulated with a final concentration of 1mM ATP, a 10mM ATP solution was made). The plate was removed from the plate reader and the 10x ATP solutions were injected into the correct wells using a multichannel pipette, and placed back into the reader. Readings were taken every 5 minutes for the duration of the experiment using SoftMax Pro v5.4.6 software. In experiments using inhibitors, the dye solution was mixed with the inhibitor of choice. All Inhibitor stocks, apart from AZ10606120, were made using DMSO as the vehicle, and all experimental conditions were made to the highest DMSO concentration used in that experiment (Table 1). The cells were incubated for 30 minutes with the inhibitors (Table 1) prior to the experiment.

Inhibitor	Protein Target	References	Cell Death Mechanism	DMSO Conc (%)	Inhibitor Conc (μM)	Source
PD150606	Calpain 1 and 2	(Low et al., 2014)	Necrosis	0.1	50	Bio-Techne (Tocris) Abingdon
CAT811	Calpain 2	(Abell et al., 2009)	Necrosis	0.5	14	
AZ10606120	P2X7	(Michel et al., 2007)	Various	0.0	10	Bio-Techne (Tocris) Abingdon
MCC950	NLRP3	(Coll et al., 2015)	Pyroptosis	0.1	10	Bio-Techne (Tocris) Abingdon
Necrostatin	RIPK1	(Degterev et al., 2005)	Necroptosis	0.2	10	Bio-Techne (Tocris) Abingdon
Necrosulfonamide	MLKL and Gasdermin D	(Sun et al., 2012, Rathkey et al., 2018)	Necroptosis and pyroptosis	0.1	20	Bio-Techne (Tocris) Abingdon
Ac-YVAD-cmk	Caspase 1 some caspase 4	(Cain et al., 1996)	Pyroptosis	0.1	25	Bio-Techne (Tocris) Abingdon
Z-VAD-FMK	Caspase 1, 3, 7 and 8	(Cain et al., 1996)	Pyroptosis and Apoptosis	0.1	10	Bio-Techne (Tocris) Abingdon
Z-DEVD-FMK	Caspase 3	(Masuda et al., 1997)	Apoptosis	0.1	10	Bio-Techne (Tocris) Abingdon
Z-IETD-FMK	Caspase 8	(Concha and Abdel-Meguid, 2002, Thornberry et al., 1997)	Apoptosis	0.1	10	Bio-Techne (Tocris) Abingdon

Table 2.1: **Overview of Cell Death Associated Inhibitors Used** List of inhibitors used, the protein they target, which cell death mechanism they are involved with and important experimental information

2.7 Real time Ca^{2+} Response Measurements

Fura-2-acetoxymethyl ester (Fura-2AM) (HelloBio, Bristol) is a ratiometric Ca^{2+} indicator. It is membrane permeant due to the hydrophilic AM group, which is cleaved by esterases once inside the cell. Both bound and unbound dye fluoresces which is why a ratio is used. Ratio is proportional to the intracellular calcium concentration ($[Ca^{2+}]_i$). All real time Ca^{2+} response measurements were performed in a 96 well plate.

In order to measure the real time Ca^{2+} response, the medium was removed from cells in the 96-well plate and replaced with a loading buffer consisting of 2µM FURA-2AM and 250µM sulfinpyrazone (Sigma-Aldrich, Poole) which prevents dye extrusion from cells. This was made up in Hank's balanced Salt Solution (HPSS) (Fisher. Loughborough) and incubated at 37°C for 45 minutes. Inhibitors were made up in Etotal running buffer (147mM NaCl, 2mM KCl, 13mM D-Glucose, 10mM HEPES, 2mM $CaCl_2$ and 1mM $MgCl_2$ (All Sigma-Aldrich, Poole)). The buffer pH was corrected to 7.4 using 5M NaOH and the osmolarity was measured with an acceptable range of 300-310. The inhibitor solutions, or corresponding vehicle control solution, replaced the loading buffer and cells were incubated at 37°C for a further 30 minutes.

For cell stimulation, ATP solutions were made using the Etotal running buffer, made at 10x the final concentration. The 10x ATP solutions were placed in a deep-well drug plate with V-bottom (Greiner, UK) in the Flexstation. The Flexstation 3 microplate reader was set up to read from the bottom of the well at excitation wavelengths of 340nm and 380nm and an emission wavelength of 510nm every 3.5 seconds for 300 seconds. A baseline fluorescent reading was taken for 30 seconds before injection of the agonist solutions. Upon Ca^{2+} binding to Fura-2, a shift in optimum absorption wavelength intensity occurs, from 380nm (without Ca^{2+}) to 340nm (With Ca^{2+}) with emission measured at 510nm. The data is then shown as a ratio of fluorescent excitation/emission (340nm/380nm).

2.8 Protein Detection

2.8.1 Protein Preparation

In order to prepare protein for use in a Western blot, BV2 and J774 cells in a 6 well plate were stimulated with 3mM ATP and harvested at 2, 4 and 6 hours timepoints with 2 unstimulated controls harvested at timepoints 0 and 6 hours. Cells were harvested using a cell scraper and then transferred to a 15ml centrifuge tube and centrifuged at 7000rpm for 8 minutes to form a pellet. The supernatant was removed, and the pellet kept on ice. To lyse the cells, 50µl of RIPA lysis buffer (Thermo Scientific, Loughborough) was added and left on ice for one hour. The cells were then centrifuged at 10000g for 10 minutes at 4^{o}C. The supernatant was placed in a separate Eppendorf and the pellet discarded.

2.8.2 Total Protein Quantification

A bicinchoninic assay (BCA) was then performed to calculate the quantity of protein in each sample. The supernatant for each sample was diluted 1 in 50 using Milli-Q (MQ) Water. Protein standards in MQ water were prepared using bovine serum albumin (BSA) (Sigma-Aldrich, Poole) ranging from 0-1000µg/ml. Duplicates of the samples and standards were added to a 96 well plate along with the BCA reagents A and B (Thermo Scientific, Loughborough) according to manufacturer's instructions. The plate was then incubated at 37^{o}C for 30 minutes and read using the Flexstation 3 microplate reader (Molecular Devices, Wokingham, UK) at an absorbance of 550nm. The protein concentration of each sample was then calculated from the standard curve.

2.8.3 SDS-PAGE Gel

SDS-PAGE was carried out on a Bolt™ Bis-Tris Plus Mini Protein Gels, 4-12%, 1.0 mm, WedgeWell™ format (Invitrogen, UK) according to the Bolt™ Mini Gel protocol provided. A loading solution was made for each of the cell protein extracts using 25µg of protein, worked out using the total protein quantification results (See above), along with 5µl Bolt^{TM} LDS Sample Buffer (4x), 2µl Bolt^{TM} Reducing Agent (10x) and made up to 20µl using MQ water. These samples were then heated to 70^{o}C for 10 minutes. The gel was placed into an Invitrogen Mini Gel Tank (Thermo Scientific, Loughborough) along with 1xMES running buffer (Thermo Scientific, Loughborough). The samples were loaded into separate wells of the gel alongside a biotinylated protein ladder (Cell Signalling Technologies, Leiden, NL). The gel was run for 30 minutes at 200V.

2.8.4 Western Blot

To transfer the protein from the gel to a hydrophobic PVDF transfer membrane, the Immobilon P Transfer membrane (Bio-Rad, Hemel Hempstead) was soaked in methanol while 12 pieces of chromatographic paper were soaked in the transfer buffer (48nM Tris, 39nM glycine, 20% methanol and 0.04% SDS). A Fisher Brand Semi Dry Blotter (Bio-Rad, Hemel Hempstead) was then packed with 6 layers of chromatographic paper, the membrane, the gel and then a further 6 layers of chromatographic paper and run at 350mA for 30 minutes. The membrane was removed and blocked with 5% skimmed milk at 4^{o}C overnight. The next day the membrane was washed on a rocker for 10 minutes in TRIS buffered saline (Fisher, Loughborough) with 0.1% Tween 20 (Fisher, Loughborough), (TBST), which was then drained, and the wash repeated 2 more times. A 1:1000 solution of primary gasdermin D rabbit antibody [EPR19828] (Abcam, Cambridge) in 5% skimmed milk was added to the membrane and placed on a rocker for 2 hours before being washed 3 more times in TBST. A solution for the secondary antibodies was made using 5% skimmed milk with 1:1000 anti-rabbit antibody (GE Healthcare, Buckinghamshire) and 1:1000 biotinylated ladder antibody (Cell Signalling Technologies, Leiden, NL). This was added to the membrane and placed on a rocker for one hour after which the membrane was washed a further 3 times in TBST. Finally, 3ml of Immobilon Crescendo Western HRP Substrate (Bio-Rad, Hemel Hempstead) was added for 5 minutes and the membrane imaged using a Chemidoc Imager (Bio-Rad, Hemel Hempstead).

2.9 Quantification of mRNA Expression

2.9.1 Pathophysiological stressors

In order to prepare mRNA for use in RNA extraction and eventually a qPCR, BV2 cells in a 6 well plate were stimulated with pathophysiological stressors and harvested after 4 hours. These stressors were 2µg/ml LPS, 50µM Amyloid-β, 500µM H_2O_2, pH5.5 and OGD, as described below.

2.10 OGD

For experiments simulating ischaemic conditions an oxygen glucose deprivation (OGD) model previously described (Niyadurupola et al., 2013) was used. Control cells were placed in DMEM with glucose (Fisher, Loughborough) and the OGD cells were placed in glucose free DMEM (Fisher, Loughborough). The OGD cells were then placed in a sealed modular incubator container (Billups-Rothenburg, Del March, California) with a moisture reservoir and then a 1% O_2, 94% N_2, 5% CO_2 gas mixture was passed through the container to displace the oxygen. After 10 minutes the valves were sealed, and the container was placed in a 37^{o}C incubator for the duration of the experiment.

2.9.2 RNA Extraction

BV2 cells that had undergone the pathophysiological stresses, see above, were harvested using a cell scraper and then transferred to a 15ml centrifuge tube and centrifuged at 7000rpm for 8 minutes to form a pellet. RNA extraction was performed using the RNeasy Mini Kit (Qiagen, Manchester) as per manufacturer's instructions. This kit is used in combination with the RNase-Free DNase set (Qiagen, Manchester) which was used as per manufacturers instructions. RNA concentration was measured using a Nanodrop NS-1000 Spectrophotometer. The RNA was stored at -80°C.

2.9.3 PCR

RNA was converted to double stranded DNA (dsDNA) using PCR. PCR was performed using the Tetro cDNA Synthesis Kit (Meridian Biosciences, London) as per manufacturer's instructions . The PCR reaction mix (1µl 10mM dNTP mix, 1µl Primer Oligo (dT), 1µl Ribosafe RNase Inhibitor, 1µl Tetro Reverse Transcriptase (200u/l) and 4µl 5x RT Buffer) used 1µg of total RNA, worked out using the data from the nanodrop (see above) and made up to 20µl using DEPC-treated water. This mix was made up in a 0.2ml 8-strip non-flex PCR tube with a flat cap (Starlab, Hamburg). PCR performed on a LifeECO PCR machine (Bioer, Hangzhou, China) with the programme set to run at 45°C for 30 minutes and then 85°C for 5 minutes, with a hold on 4°C until removal.

2.9.4 qPCR

The qPCR was performed using a reaction mix that consisted of 5µl SensiFAST SYBR No-ROX Kit (Meridian Biosciences, London), 0.5µl 5µM reverse and forward primer stocks using the primers for each of the genes shown in Table 5, 1µl dsDNA sample (From PCR, see above) and 3µl RNA free water. This was made in a 0.1ml Strip tube and cap (Starlab, Hamburg). This was placed in a Rotor-gene Q (Qiagen, Manchester) and the qPCR was performed using the following programme: hold at 95°C for 2 minutes, then cycle through 95°C for 5 seconds, 60°C for 10 seconds and 72°C for 20 seconds. This was repeated 40 times and ending with a melt stage which rises from 72°C to 95°C before finishing. The results were analysed in the Rotor-Gene Q series Software and the Ct for each duplicate noted. Relevant mRNA levels were then calculated using the $2^{-\Delta\Delta Ct}$ method (calculation shown below).

$$Target\ gene\ Raw\ Ct - \beta Actin\ gene\ Ct = Target\ gene\ Ct$$

$$Target\ Gene\ Ct\ (Condition) - Target\ Gene\ Ct\ (Control) = X$$

$$2^{-x} = mRNA\ Level$$

Protein	Forward Primer	Reverse Primer
P2X7	GAACACGGATGAGTCCTTCGTC	CAGTGCCGAAAACCAGGATGTC
Gasdermin A3	GGTCTGTCACAAAGCAGCACAC	GTTCAGGAACGAGTGGTCTGCT
Gasdermin D	GGTGCTTGACTCTGGAGAACTG	GCTGCTTTGACAGCACCGTTGT
Gasdermin E	ACGGACACCAATGTAGTGCTGG	CTCTCATGCTCGAAGCCACCAT
IL-1β	TGGACCTTCCAGGATGAGGACA	GTTCATCTCGGAGCCTGTAGTG
NLRP3	TCACAACTCGCCCAAGGAGGAA	AAGAGACCACGGCAGAAGCTAG
Caspase 1	GGCACATTTCCAGGACTGACTG	GCAAGACGTGTACGAGTGGTTG
Calpain 1	CCTTGTTCAGCAAGTTGGCAGG	TCCAGGCTGAAGCCATTAGTGC
Calpain 2	AGGGAGCGGTCAGATACCTT	CTCCGAGAAGACTCGGATGC
Calpain 3	ACCTGGACGGTGTCTGTAAACG	GGTCATCGTCTTCCTCCCAGAAG
B-Actin	CATTGCTGACAGGATGCAGAAGG	TGCTGGAAGGTGGACAGTGAGG

Table 2.2 Primers used in qPCR experiments. Forward and reverse primers used in the qPCR experiments in Chapter 5 (Sigma-Aldrich, Poole)

Chapter 3

The role of P2X7 and downstream cell death associated proteins in ATP mediated cell death.

3.1 Introduction

Neurodegenerative conditions involve the progressive loss of neurons. Whether because of, for example, amyloid- β protein plaques in Alzheimer's disease, the Lewy bodies of Parkinson's disease or ischaemia during strokes, neuropathologies have major effects on cellular function leading to neuronal cell death. As neurons are rarely replaced this death leads to irreversible damage to the local area affected. For glaucoma this loss occurs mainly in the RGCs which leads to a loss of the visual field and blindness (Almasieh et al., 2012). The death of RGCs is thought to occur due to loss of nutrients, activation of apoptosis, mitochondrial dysfunction or reactive glia such as astrocytes or microglia (Almasieh et al., 2012). Microglia are the resident immune cells of the CNS and so deal with the aftermath of the loss of these neuronal cells (See section 1.1.2). They are also the cause of neuroinflammation which can contribute to neurodegeneration. Neuronal death leads to cellular content leakage of damage associated molecular patterns (DAMPs), such as high mobility group box 1 (HMGB1) and ATP. ATP is an important part of the metabolic process of the cell, but also acts as a signal ligand for a group of receptors that are activated by this purine nucleotide (See Section 1.3). Due to the high levels of intracellular ATP, cell death leads to high levels of ATP release into the extracellular space, activating purinergic receptors, including P2X7 (See section 1.3.3) on surrounding cells. Activation of the P2X7 receptor causes inflammation, due to cytokine release and death of the microglial cell. The precise mechanisms of cell death following P2X7 activation in microglia are unclear.

Cell death can occur via many different multiprotein pathways (See Section 1.4) including apoptosis, a programmed non-lytic form of cell death, necrosis, a unprogrammed lytic form of cell death, and the programmed lytic forms of cell death, necroptosis and pyroptosis. Each cell death type has its own unique selection of proteins that play key roles in the pathways of these types of cell death (See Section 1.5). In apoptosis the pathway utilises a caspase cascade including caspase 3 and 7. For necroptosis, RIPK1, RIPK3 and the pore forming protein MLKL form the basis of the pathway and finally for pyroptosis the inflammasome proteins, NLRP3, ASC and caspase 1 associate and activate the executioner protein of pyroptosis, gasdermin D. Another family of proteins involved in cell death is the calcium-activated proteases, the calpains. These proteins have been found to be involved with different aspects of different cell death mechanisms including necrosis, where calpains play an important role.

Cell death associated proteins have been pharmacologically targeted in order to prevent cell death as possible therapeutic agents. For the caspase family, multiple inhibitors have been developed

that are able to target different members of this family. Firstly, caspase 1 has been found to be inhibited by Ac-YVAD-cmk (Cain et al., 1996). This inhibitor has also been shown to block microglial IL-1β production in mice injected with LPS (Zhu et al., 2017). An inhibitor for Caspase 3 has also been developed (Z-DEVD-FMK) (Masuda et al., 1997). This inhibitor has also been shown to suppress apoptosis in microglia (Nishioku et al., 2000). Caspase 8 activity has been found to be blocked by Z-IETD-FMK (Concha and Abdel-Meguid, 2002, Thornberry et al., 1997) and finally a pan caspase inhibitor, that blocks caspase 1, 3, 7 and 8 called Z-VAD-FMK (Cain et al., 1996). For the calpains, inhibitors that block calpain 1 and 2, at different affinities, called PD150606 and CAT811. For the necroptotic protein RIPK1 there is an inhibitor called necrostatin (Degterev et al., 2005). This inhibitor has been found to reduce necroptotic cell death in microglia (Huang et al., 2018). The inhibitors of pyroptotic proteins include MCC950 that blocks NLRP3 (Coll et al., 2015) and necrosulfonamide which blocks gasdermin D (Rathkey et al., 2018). There are also a selective inhibitor for the P2X7 pore called AZ10606120 (Michel et al., 2007).

Using the inhibitors described above, the research presented in this chapter investigates ATP associated cell death mechanisms in microglia cells. The aim was to determine the involvement of the P2X7 receptor and investigate pore formation by assessment of membrane permeability to large cations. Determining the mechanism of cell death caused by ATP was also an aim with pyroptosis the most likely candidate, as stated in the hypothesis.

3.2 Results

3.2.1 ATP Causes P2X7 mediated cell death in BV2 microglia after 24 hours

To determine whether ATP stimulation causes cell death in microglia and the role of P2X7 in this process, BV2 cells and the P2X7K/O variant of BV2 cells were stimulated with 3mM ATP for 24 hours and the level of cell death (LDH) and cell viability (MTS) measured (Fig 3.1).

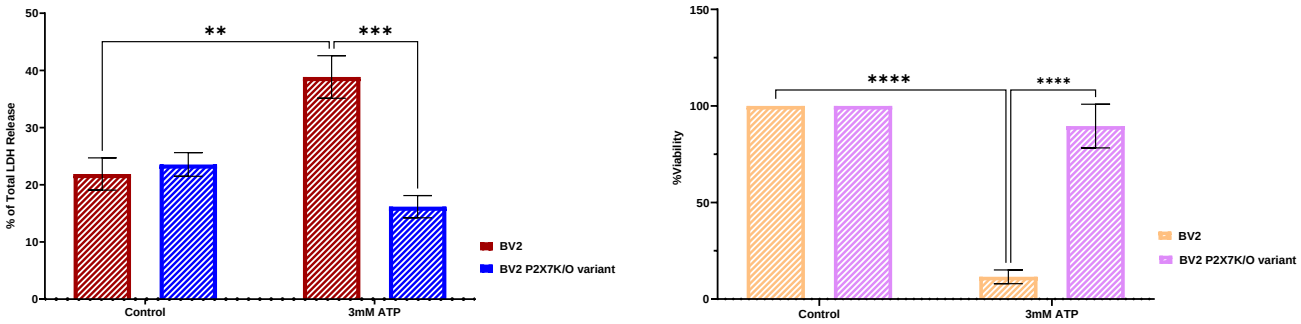

Figure 3.1 Stimulation of BV2 Microglia with ATP causes Cell Death that is blocked in the P2X7K/O BV2 microglial cells (a) Mean % LDH release after 24 Hours in BV2 and P2X7K/O BV2 microglial cells stimulated with 3mM ATP (b) Mean % Viability release after 24 Hours in BV2 and P2X7K/O BV2 microglial cells stimulated with 3mM ATP (mean +SEM, n=3) * Indicates significance compared to control (P<0.05) using one-way ANOVA with Dunnett's post hoc test.

ATP stimulation (Fig 3.1a) caused an increase in cell death (LDH release) when comparing the control BV2 cells with those stimulated with 3mM ATP. In P2X7K/O BV2 cells, the level of cell death is comparable to that seen in the control populations. The cell viability results (Fig 3.1b) indicate a statistically significant reduction in cell viability in the 3mM ATP stimulated BV2 cells while the 3mM ATP stimulated P2X7K/O variant of BV2 cells maintain cell viability after 24 hours. These results indicate that6 ATP mediated cell death was via the P2X7R. To confirm this, BV2 cells were stimulated with 3mM ATP in the presence of the P2X7 inhibitor, AZ10606120.

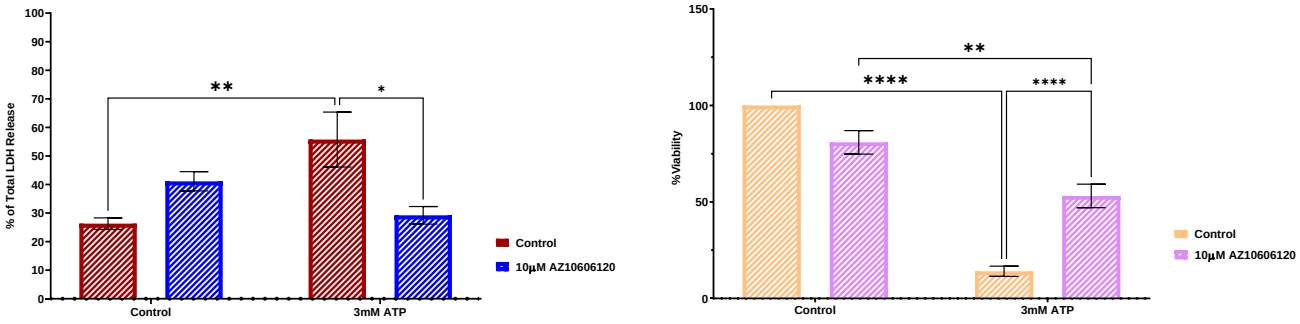

Figure 3.2 Stimulation of BV2 Microglia with ATP causes Cell Death that is blocked by inhibition of P2X7 (a) Mean % LDH release after 24 Hours in BV2 and microglial cells stimulated with 3mM ATP ± AZ10606120 10µM (b) Mean % Viability release after 24 Hours in BV2 microglial cells stimulated with 3mM ATP ± AZ10606120 10µM (mean +SEM, n=3) * Indicates significance compared to control (P<0.05) using one-way ANOVA with Dunnett's post hoc test.

Stimulation with 3mM ATP caused a significant increase in cell death, which was almost totally blocked by incubation with AZ10606120 (10µM) (Fig 3.2a). The AZ10606120 alone did not cause any significant change.

Consistent with this, the cell viability data (Fig 3.2b) showed that 3mM ATP stimulated cells have a statistically significant drop in cell viability but this loss is reduced in the presence of AZ10606120. Again, no significant difference in cell viability was seen with AZ10606120 alone. These data confirm that ATP stimulated cell death occurs 24 hours after stimulation and that this is P2X7 dependent. However, this only shows the cell death at the 24 hour time point and gives no indication of what is happening earlier in the process, so a time course of the earlier stages will need to be investigated.

3.2.2 ATP causes P2X7 mediated cell death and morphology changes after 8 hours in BV2 microglia

P2X7K/O and WT BV2 cells were stimulated with 3mM ATP and the level of cell death (LDH release) was monitored over an 8-Hour time course. Samples were taken at the 1-, 2-, 4- and 8-Hour time points (Fig 3.3). There was little change over the course initial time points, although the WT BV2 cells stimulated with 3mM ATP did show a slight increase at the 2- and 4-hour time points. At the 8-hour time point a significant amount of cell death was shown for the WT BV2 cells stimulated with 3mM ATP, which was statistically significant when compared to both the WT BV2 control and the 3mM ATP stimulated P2X7K/O variant of BV2 cells.

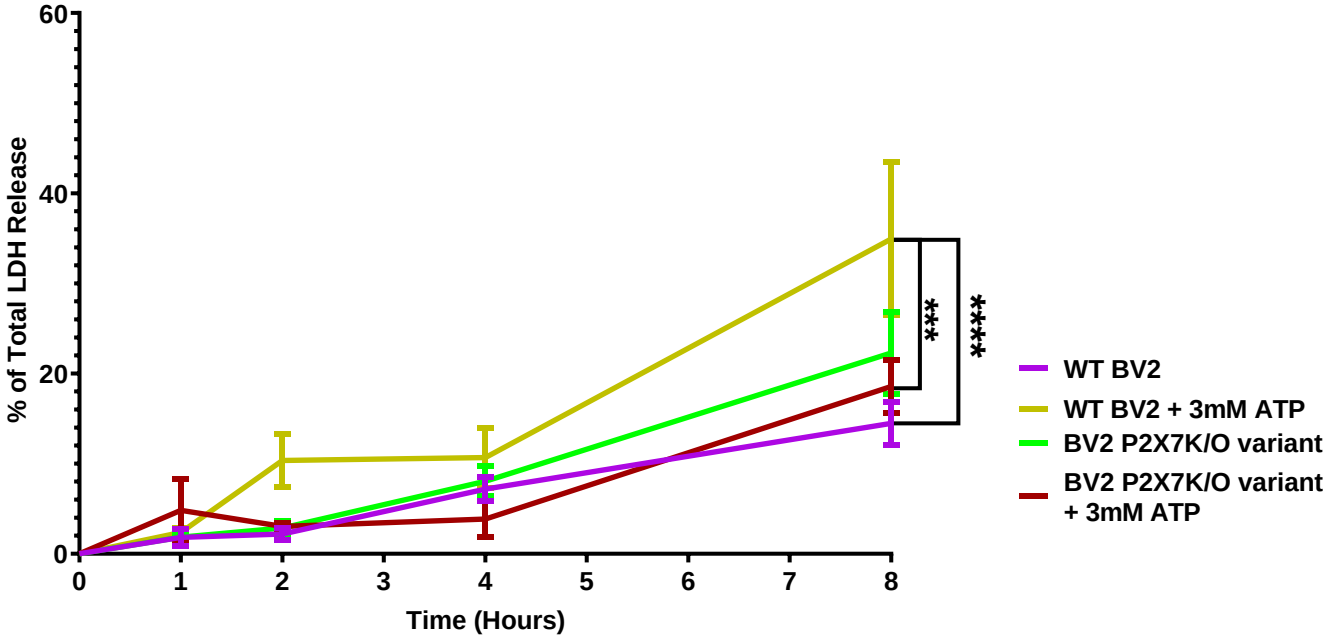

Figure 3.3 Stimulation of BV2 Microglia with ATP causes P2X7 mediated cell death Mean values for % of total LDH release over a time course of 8 hours in P2X7K/O variant of the BV2 microglial cells and WT BV2 microglia cells stimulated with 3mM ATP (mean +SEM, n=3) * Indicates significance ($P<0.05$) using two-way ANOVA with Tukey post hoc test.

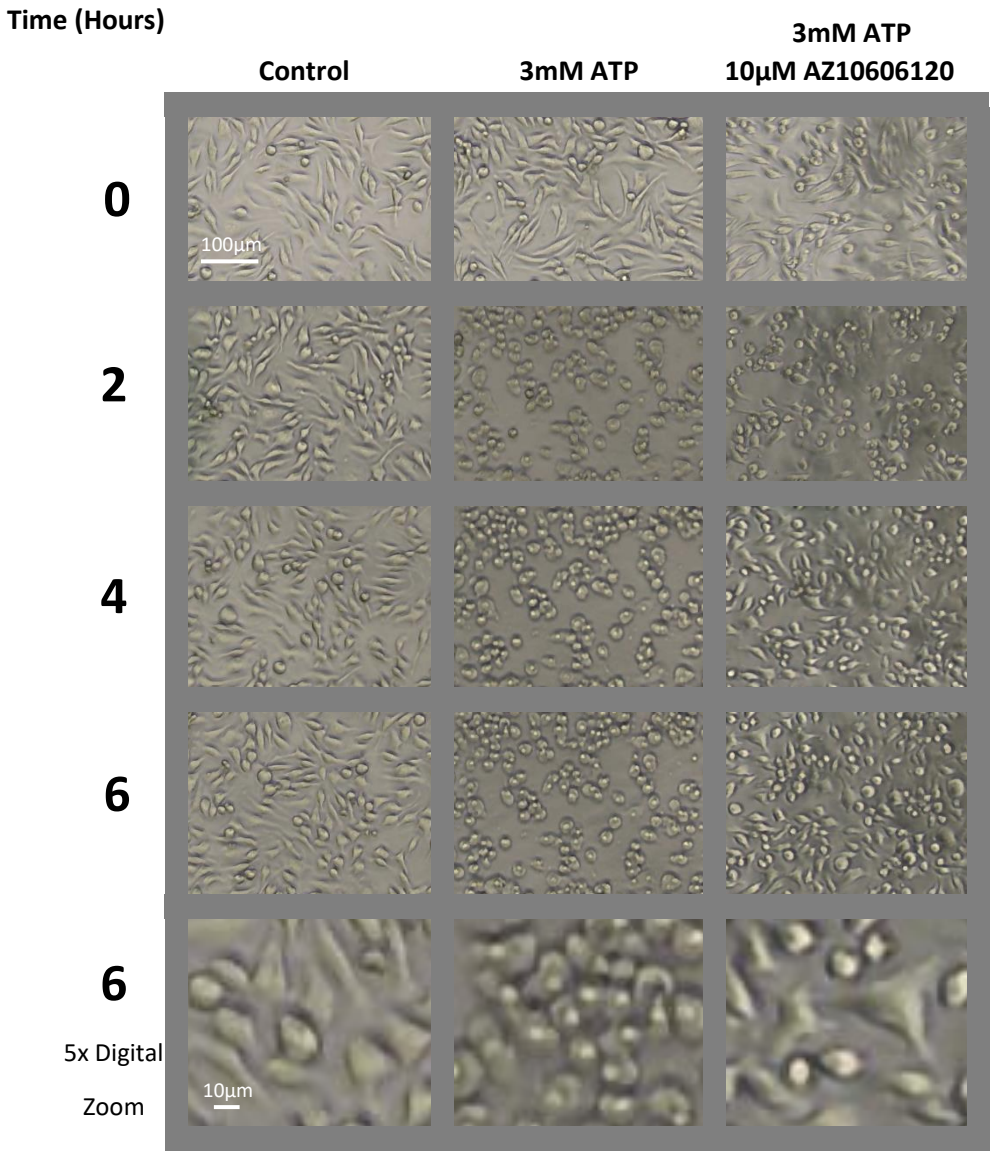

Figure 3.4 Stimulation of BV2 Microglia with ATP causes P2X7 mediated cell morphological changes
Effect of 3mM ATP and 10µM AZ10606120 on BV2 cells over the course of 6 hours. Final row shows representative cell morphology at 6 hours (5x digital zoom)

As different forms of cell death lead to different changes in morphology, the BV2 cells were also imaged over a 6-hour time course. The unstimulated population of cells maintained the same morphology over the experiment most cells having an elongated morphology. With ATP stimulation (3mM), even after 2 hours, every cell had changed morphology, becoming swollen and rounded. When incubated in the P2X7 inhibitor, AZ10606120 (10µM) together with 3mM ATP, the cells largely maintained their morphology across the 6 hours, with cell morphology comparable to control.

3.2.3 ATP causes P2X7 mediated dye uptake in BV2 microglia

The fluorescent dye, YO-PRO, can be used to look at changes in membrane permeability in real time. YO-PRO is a large cation (375.5g/mol) and therefore such changes in membrane permeability occur due to pore formation or membrane disruption allowing the molecule to pass into the cell. YO-PRO uptake was therefore used to investigate the time course of changes in membrane permeability caused by exposure to a range of concentrations (50µM-5mM) of ATP over an 8-hour time period. This allows cell death associated changes in the membrane permeability to be investigated in real time. Membrane permeability changes are important events of the cell death process.

The lower ATP concentrations (50µM-500µM) show little to no YO-PRO uptake when compared to the control (Fig 3.5a). However, the higher ATP concentrations (1mM, 3mM and 5 mM) do show an increase in YO-PRO permeability. When stimulated with 1mM ATP, the dye uptake plot takes the shape of a sigmoidal curve, with a significant change in rate just after the hour mark. The dye uptake plots for the 3mM and 5mM ATP concentrations are linear, then start to plateau around the 6 hour mark. This data can also be presented as area under the curve (AUC) (Fig 3.5b) which shows that the 3 highest ATP concentrations(1mM, 3mM and 5mM) have a statistically significant increase when compared to the control, with the 3mM ATP causing the largest increase.

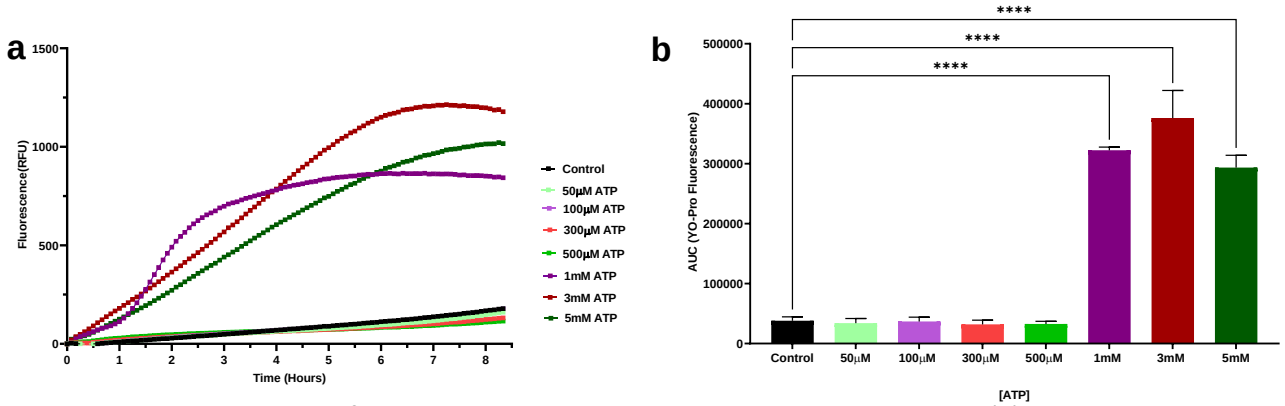

Figure 3.5 Stimulation of BV2 Microglia with ATP causes YO-PRO dye uptake (a) Mean YO-PRO uptake in BV2 microglial cells in response to increasing concentrations of ATP (0-5mM) (n=4) (b) YO-PRO uptake (AUC 0-500mins) (mean +SEM, n=4) * Indicates significance compared to control ($P<0.05$) using one-way ANOVA with Dunnett's post hoc test.

To determine if ATP-induced YO-PRO uptake was P2X7 dependent, the ATP dose response was performed with the P2X7K/O variant of BV2 cells (Fig 3.6a). As was seen in the previous experiment WT BV2 cells stimulated with ATP (1-5mM) showed YO-PRO uptake. Using the P2X7K/O variant of BV2 cells (Fig 3.6b), none of the ATP concentrations (300µM-5mM) led to any uptake of the YO-PRO dye. Comparison of the AUC data (Fig 3.6c) showed there was a statistically significant difference between the 1mM and 3mM ATP stimulated BV2 and P2X7K/O variant of BV2 cells which indicates that P2X7 does play a role in YO-PRO dye uptake.

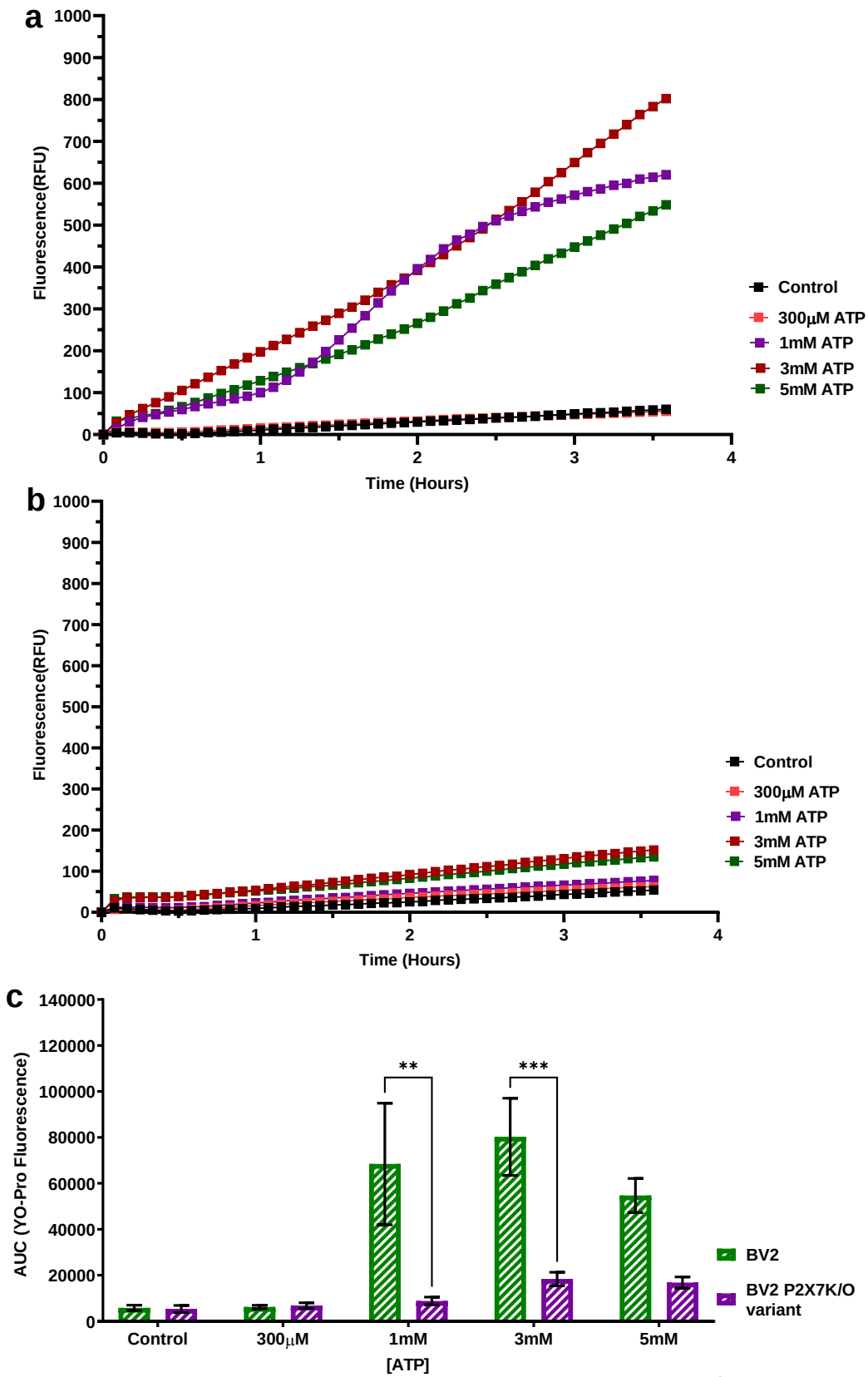

Figure 3.6 ATP-induced YO-PRO uptake in BV2 Microglia is blocked in the P2X7K/O BV2 microglial cells (a) Mean YO-PRO uptake in BV2 microglial cells in response to increasing concentrations of ATP (n=4) (b) Mean YO-PRO uptake in P2X7K/O BV2 microglial cells in response to increasing concentrations of ATP (n=4) (c) YO-PRO (AUC 0-220 Mins) (Mean+SEM; n=4) * Indicates significance ($P<0.05$) using two-way ANOVA with Sidak's post hoc test.

3.2.4 Cell death associated protein inhibitors do not alter dye uptake in ATP stimulated BV2 microglia

Inhibitors of key components of cell death pathways were then investigated to see if YO-PRO uptake could be modified (Fig 3.7) and give an indication of the cell death pathways that were occurring. The inhibitors used were, the P2X7 inhibitor, AZ10606120, and an inhibitor for the apoptotic protein caspase 3, Z-DEVD-FMK. A range of inhibitors that block the pyroptotic proteins NLRP3 (the inflammasome sensor protein), caspase 1 (the pyroptotic caspase that cleaves important pyroptosis proteins like IL-1β and IL-18), and gasdermin D (the executioner pore protein of pyroptosis) were also used: MCC950, Ac-YVAD-cmk and necrosulfonamide (NS) respectively. An inhibitor for the necroptosis-linked protein RIPK1 was also used (necrostatin), as well as, caspase inhibitors for caspases involved in multiple forms of cell: an inhibitor for caspase 8 (Z-IETD-FMK) and a pan caspase inhibitor (Z-VAD-FMK). A calpain 1 and 2 inhibitor (PD150606) was also used.

The P2X7 inhibitor, AZ10606120, totally inhibited ATP-mediated YO-PRO uptake, the uptake plot returning to that of the control (Fig 3.7a and g). The apoptotic (Fig 3.7b and h), pyroptotic (Fig 3.7c and i), necroptotic (Fig 3.7d and j) and pan caspase and caspase 8 inhibitors (Fig 3.7e and k) had no effect on YO-PRO uptake with 3mM ATP. Both the YO-PRO uptake plots and the accompanying AUC data maintain a similar profile to that of the 3mM ATP stimulated cells. There was, however, a change in ATP-induced YO-PRO dye uptake with the calpain inhibitor, PD150606. This is also clear in the AUC data, where a statistically significant reduction in the YO-PRO uptake can be seen (Fig 3.7f and l) indicating an involvement of calpain in P2X7-mediated microglial cell death.

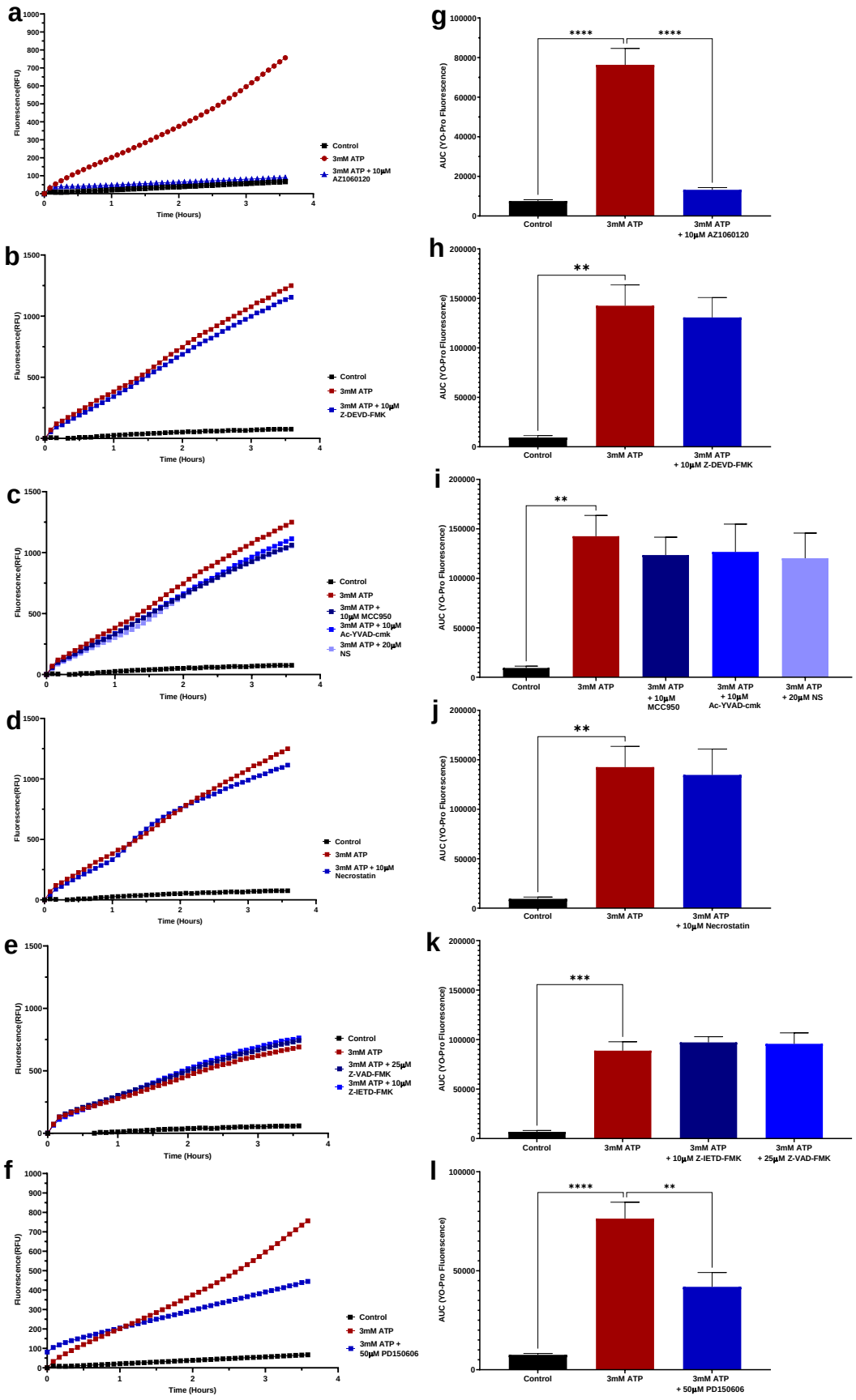

Figure 3.7 ATP-induced YO-PRO uptake in BV2 Microglia is altered by inhibition of P2X7 or calpain
(a-f) Mean YO-PRO uptake in BV2 microglial cells in response to (a) 3mM ATP ± P2X7 inhibitor (b) 3mM ATP ± apoptotic inhibitor (c) 3mM ATP ± pyroptotic inhibitors (d) 3mM ATP ± necroptotic inhibitors (e) 3mM ATP ± other caspase inhibitors (f) 3mM ATP ± calpain inhibitors (g-l) Associated YO-PRO AUC (0-220 Mins) (Mean+SEN; n=5) * Indicates significance ($P<0.05$) using one-way ANOVA with Dunnett's post-hoc test.

3.2.5 Different Calpain inhibitors show different effects following ATP stimulation in BV2 microglia

The PD150606 inhibitor was then investigated in the context of cell death. LDH release was measured over the course of 8 hours after stimulation with 3 mM ATP (Fig 3.8). There was little change in the cell death over the first 6 hours for all conditions. However, the cells stimulated with 3mM ATP showed an increase at the last two time points, that was not seen in the control and 3mM ATP stimulated cells incubated in PD150606.

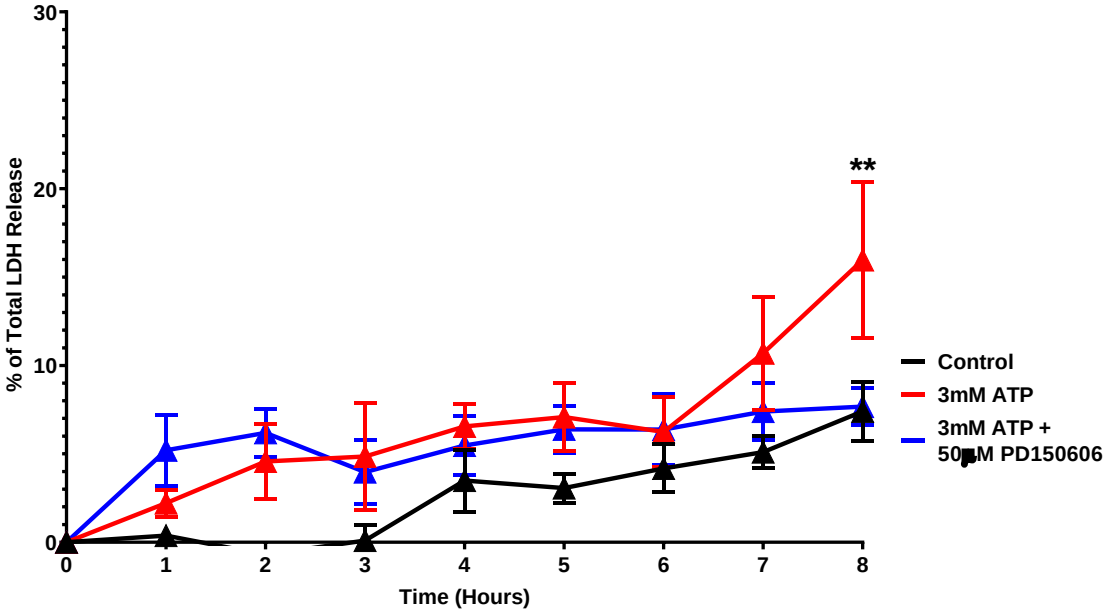

Figure 3.8 ATP- induced cell death of BV2 Microglia is altered by inhibition of calpain
Mean values for % of total LDH release over a time course of 8 hours in BV2 microglia cells stimulated with 3mM ATP ± PD150606 (Mean+SEN; n=4) * Indicates significance ($P<0.05$) using two-way ANOVA with Tukey post hoc test.

Morphological changes in BV2 cells stimulated with 3mM ATP with and without the calpain inhibitor were then investigated. At the 2- and 8-hour time points (Fig 3.9) cells stimulated with 3mM ATP have morphological changes when compared to the control group, with cells becoming rounded and swollen. ATP stimulated cells that were also treated with PD150606 appeared less swollen and, in fact, appeared to be more shrunken in appearance, although, were still rounded and had clear signs of ATP-induced changes.

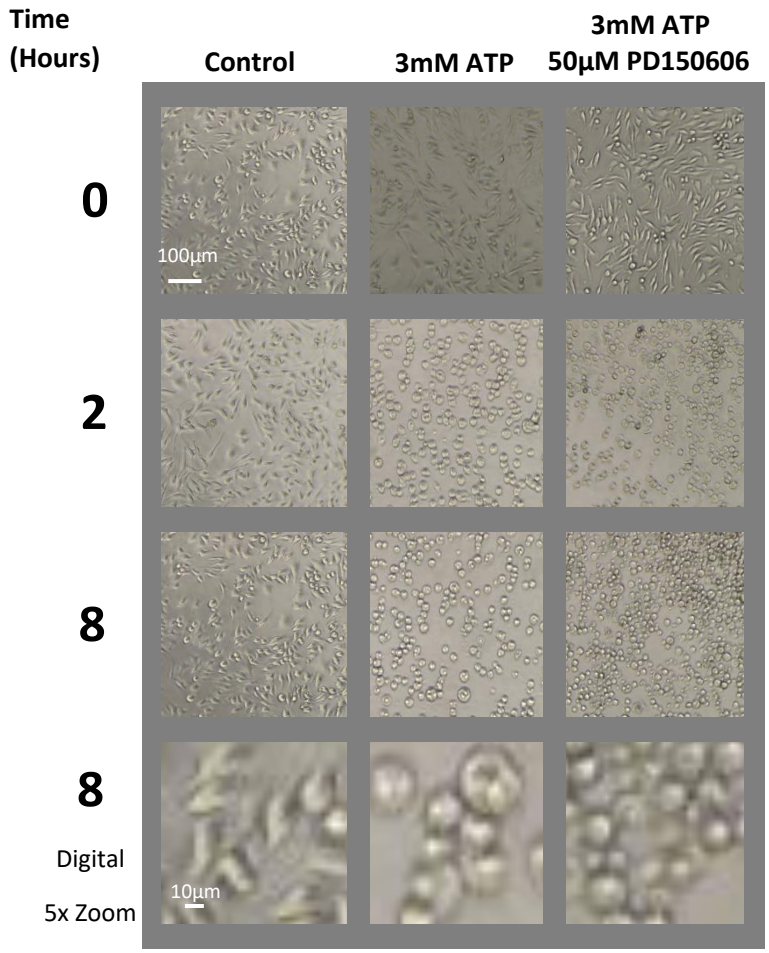

Figure 3.9 ATP-induced morphological changes of BV2 Microglia are altered by inhibition of calpain Effect of 3mM ATP and 50µM PD150606 on BV2 cells over the course of 8 hours. Final row shows representative cell morphology at 8 hours (5x digital zoom)

Results, therefore, showed that PD150606 inhibited ATP-induced cell death and ATP-induced membrane permeability changes. ATP-induced morphological changes were also affected by the calpain inhibitor. This could indicate the involvement of calpain in the cell death process triggered by ATP. However, there was also the possibility that PD150606 was able to block the P2X7R directly as an "off target" effect. The P2X7 receptor is inhibited by many different drugs of different chemical classes, so it was important to investigate whether this was the case (Stokes, 2021). Direct inhibition of the receptor was investigated by measuring P2X7-mediated increases in intracellular Ca^{2+}. BV2 cells were stimulated with 300µM, 1mM and 3mM ATP and their fluorescence was measured over the course of 300 seconds, in the presence and absence of the P2X7 inhibitor, AZ10606120, and the calpain inhibitor, PD150606 (Fig 3.10).

At the lowest concentration of ATP (300µM) (Fig 3.10a), all three treatments shared a rapid increase in Ca^{2+} influx just after stimulation by the ATP which drops after 15 seconds. In ATP alone, this is followed by a slow sustained increase. This sustained increase was blocked by both inhibitors. At higher ATP concentrations (1mM and 3mM ATP) the sustained Ca^{2+} influx was much larger than that of the 300µM ATP stimulated cells and while AZ10606120 maintained total inhibition of the sustained Ca^{2+} influx, the PD150606 only slightly reduces this sustained element of the plot. This is highlighted by the AUC data from 30-300 seconds (Fig 3.10d) which showed the complete loss of Ca^{2+} influx between the stimulated cells and the ATP stimulated cells with and without AZ10606120. This data indicates that this sustained influx is due to the P2X7 receptor. PD150606 clearly affected the Ca^{2+} influx. At the lower ATP concentration there was total inhibition, but at the higher ATP concentrations Ca^{2+} influx still occurs. It does appear therefore that PD150606 may have some P2X7R antagonist activity, although not at the same level as AZ10606120. However, firm conclusions could not be drawn.

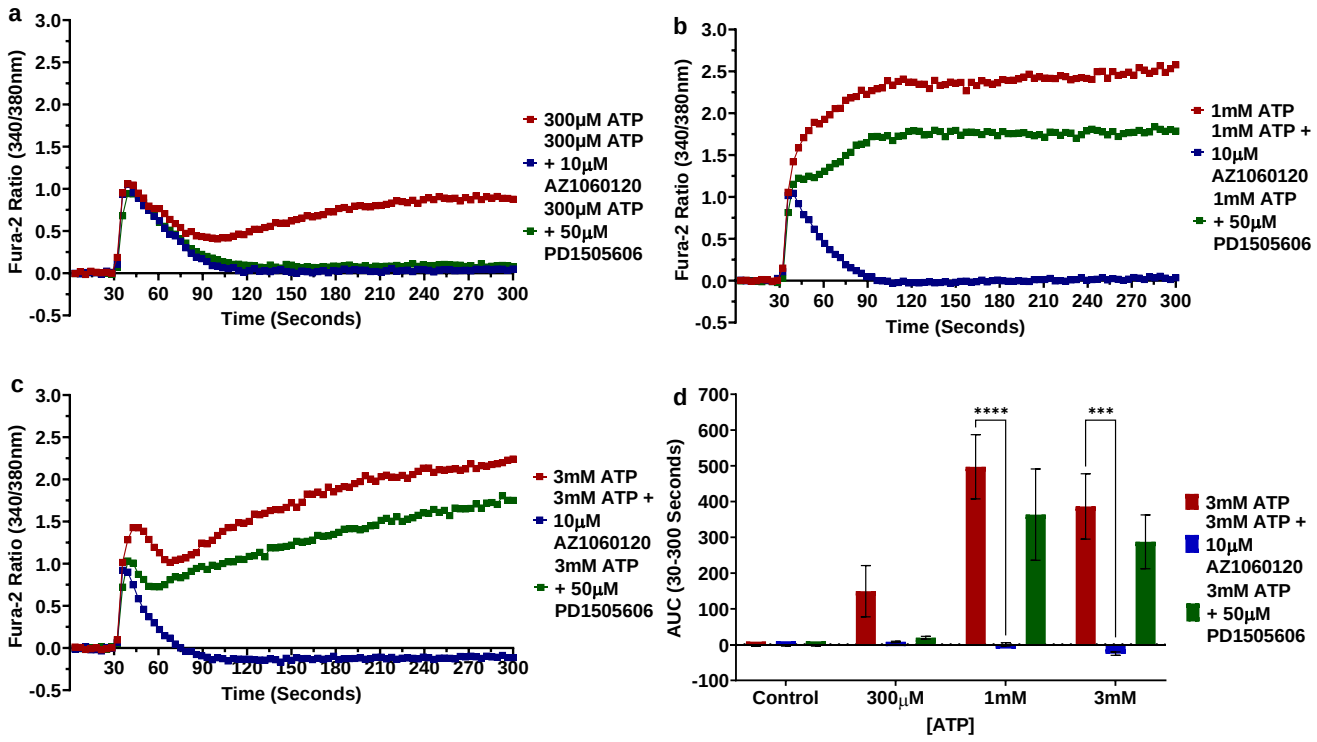

Figure 3.10 Calpain inhibitor, PD150606, alters ATP-induced Ca^{2+} influx in BV2 Microglia (a-c) Mean values for intracellular Ca^{2+} concentration (340/380nm FURA-2 ratio) in BV2 microglial cells in response to 300µM, 1mM and 3mM ATP and ± AZ10606120 (10µM) or PD150606 (50µM) (n=3) (d) Intracellular Ca^{2+} Concentration (AUC 90-300 Mins) (Mean+SEN; n=3) * Indicates significance ($P<0.05$) using two-way ANOVA with Sidak's post hoc test.

ATP-induced YO-PRO uptake was therefore investigated using a different calpain inhibitor, CAT811, that is chemically different to PD150606 (Fig 3.11). CAT811 did not block ATP-induced YO-PRO uptake, indicating an off-target effect of PD150606.

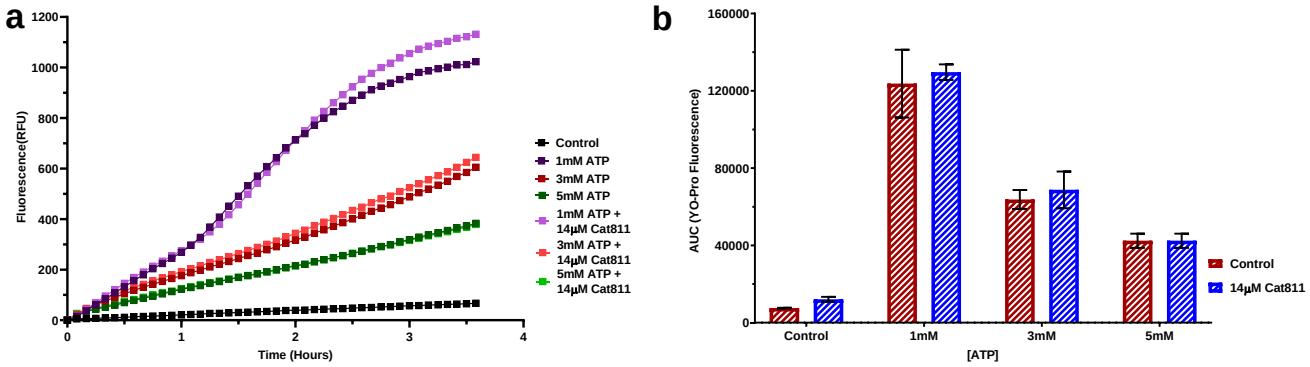

Figure 3.11 Calpain inhibitor, CAT811, does not alter ATP-induced YO-PRO uptake in BV2 Microglia (a) Mean YO-PRO uptake in BV2 microglial cells in response to 1mM, 3mM and 5mM ATP concentrations ± CAT811 14μM (b) YO-PRO (AUC 0-220 Mins) (Mean+SEN; n=3) * Indicates significance (P<0.05) using one-way ANOVA with Dunnett's post-hoc test

3.2.6 Cell death associated protein Inhibitors do not change cell death levels or viability after ATP stimulation in BV2 microglia

To complete the data using the inhibitors of cell death pathways, experiments were carried out using the other remaining inhibitors to investigate the effect on ATP (3mM) induced cell death (Fig 3.12).

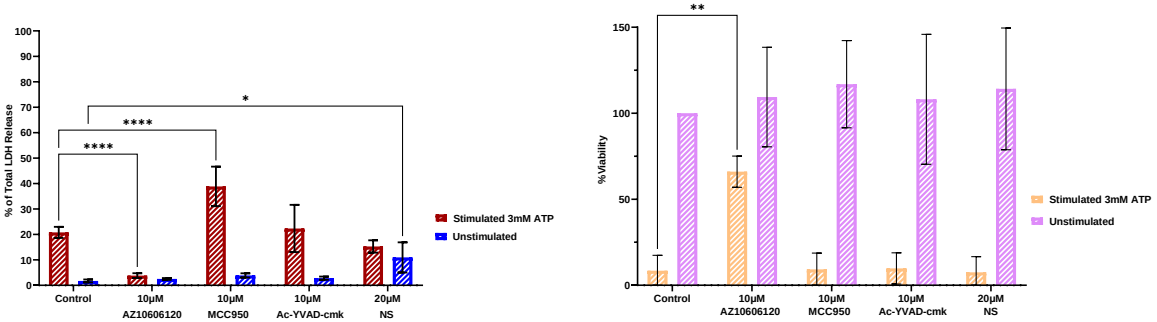

Figure 3.12 Cell death associated protein Inhibitors do not alter ATP-induced cell death in BV2 microglia (a) Mean % LDH release after 6 Hours in BV2 microglial cells ± AZ10606120 10μM, MCC950 10μM, Ac-YVAD-cmk 10μM or Necrosulfonamide 20μM (b) Mean % Viability release after 6 Hours in BV2 microglial cells ± AZ10606120 10μM, MCC950 10μM, Ac-YVAD-cmk 10μM or Necrosulfonamide 20μM * Indicates significance compared to control (P<0.05) using one-way ANOVA with Dunnett's post hoc test.

As expected, ATP-induced increase in cell death returned to control levels when incubated in the P2X7 inhibitor AZ10606120 (Fig 3.12a). There is no change in the level of ATP-induced cell death when incubated in the caspase 1 inhibitor, Ac-YVAD-cmk.

There was, however, a statistically significant increase in cell death when incubated with the NLRP3 inhibitor, MCC950, in the presence of ATP. In addition, there was a statistically significant increase in cell death with the gasdermin D inhibitor, necrosulfonamide, in the absence of ATP possibly indicating a level of toxicity by this drug under control conditions.

The MTS assay (Fig 3.12b) as expected showed a significant reduction in viability by ATP (3mM) which is rescued when incubated in the P2X7 inhibitor, AZ10606120. No differences between the viability of the ATP-stimulated cells with any of the other inhibitors was observed.

3.3 Discussion

Microglia play a very important role in neurodegeneration (Subhramanyam et al., 2019, Wei et al., 2019). The death of neuronal cells in the CNS is thought to create an inflammatory environment caused by the release of cellular contents such as ATP. The ATP-activated P2X7 receptor has previously been shown to be widely expressed in adult rat microglia (Lord et al., 2015), and have downstream effects that affect neuronal survival (Miras-Portugal et al., 2017). The P2X7R also plays a substantial role in retinal ganglion cell death relating to glaucoma (Niyadurupola et al., 2013). Microglial viability is influenced by the P2X7R (Monif et al., 2010) and in turn will affect neuronal survival. The aim of the research presented in this chapter was to investigate ATP-linked cell death in microglia with the hope of identifying which cell death pathway is occurring.

Stimulation of a mouse microglia cell line, BV2, with 3mM ATP caused a significant increase in cell death and decrease in cell viability (Fig 3.1, 3.2 and 3.3). The central role of the P2X7 receptor was confirmed by protection when P2X7 receptor activation is prevented, either by knockout (Fig 3.1 and 3.3) or by inhibiting with AZ10606120 (Fig 3.2). In addition the effects of ATP stimulation on cell morphology were observed. A change in morphology towards a swollen and rounded shape could be seen when compared to the control and this morphological change could be blocked by the presence of the P2X7 inhibitor, AZ10606120.

P2X7 therefore, plays a vital role in cell death in BV2 cells stimulated with high concentrations of ATP. P2X7 has previously been linked to cell death in various cell types (Sluyter, 2017) including microglia (Bartlett et al., 2013, Brough et al., 2002, He et al., 2017). The drop in viability can also be interpreted as a loss of mitochondrial function and P2X7 has been shown to be involved with mitochondrial fission and decrease in function in microglia due to the P2X7 dependent increased intracellular Ca^{2+} levels (Tao et al., 2022).

P2X7 has historically shown to lead to the forming of a large pore opening (Chessell et al., 1997). In addition P2X7 could also mediate the opening of separate pore forming proteins or cause loss of cell membrane integrity. All of these would lead to an increase in membrane permeability. A technique that is widespread in the literature to investigate membrane permeability uses large fluorescent dyes that fluoresce on contact with nucleic material such as DNA or mtDNA. One such dye is YO-PRO that has been used extensively with regards to pore formation associated with P2X7 (Chessell et al., 1998, Dhuna et al., 2019, Virginio et al., 1997). After stimulation with a wide range of ATP concentrations while in the presence of YO-PRO (Fig 3.5), the higher concentrations (1mM, 3mM and 5mM ATP) cause a significant increase in YO-PRO to the cell over the time course investigated. The comparisons between the BV2 cells and the P2X7K/O variant of BV2 cells (Fig 3.6) plus the effect of the P2X7 inhibitor, AZ10606120 (Fig 3.7a and g) shows that the P2X7 receptor is vital in the mechanism that leads to dye uptake of YO-PRO in ATP-stimulated BV2 cells.

This suggests that the cell death, morphological changes and the dye uptake were all linked and are P2X7 dependent.

When comparing the protocols for the dye uptake and the LDH experiments, a difference in timings can be seen. The dye uptake experiments look at membrane permeability, where YO-PRO is able to make its way into the cell from the media. The LDH assay looks at membrane disruption, where the intracellular protein, LDH, is released from the cell into the media. The processes, therefore, require differing levels of changes in the membrane to occur, with YO-PRO measuring lesser changes in the membrane permeability compared to LDH which shows a lytic response. Therefore, dye uptake experiment would not take as much time to start to show changes compared to the LDH assay. Accordingly, YO-PRO started to show uptake within the first hour and reached a plateau after 5 hours (Fig 3.5). LDH release only starts to show significant increases after 7 or 8 hours (Fig 3.3 & 3.8). Other studies that have used both these techniques but in mouse macrophages stimulated with ATP, also have a much shorter time course for dye uptake then they did the LDH assay (Bidula et al., 2019).

The data suggests a lytic form of cell death and the morphological changes seen with ATP stimulation (Fig 3.4) make pyroptosis a plausible mechanism, with swollen and rounded cell morphology being characteristic of pyroptotic cell death (Zheng et al., 2021). However, the images taken during the experiments reported here were not able to reveal the intricacies of the morphological changes as they were low magnification phase microscope images. Therefore, in any further investigation, an increased magnification would be used. This could be improved further by using fluorescent microscopy and different stains to highlight specific cellular structures, such as the nucleus or mitochondria which change according to the mechanism of cell death. Specific structures such as the inflammasome or cytoskeletal changes could also be investigated using immunohistochemistry. Timelapse microscopy would give a detailed look at the different stages of the cell death process in real time and even use of an electron microscope for ultrastructural analysis could reveal detailed morphological changes associated with different forms of cell death.

In support of a pyroptotic mechanism, there have also been numerous connections reported between P2X7 and pyroptosis (Yang et al., 2015) and P2X7 has been linked to the production and release of IL-1β and IL-18, cytokines released during pyroptosis (He et al., 2017). A pyroptotic form of cell death would suggest gasdermin D is the possible secondary large pore that forms, with gasdermin D forming a pore up to 21nm in size (Sborgi et al, 2016). This could explain the cell membrane disruption that occurs to allow the YO-PRO into the cell and the subsequent LDH release evident of a lytic form of cell death occurring. The next step of the research was therefore to use inhibitors of pyroptosis, and other cell death pathways, to delve into the specific

mechanisms of cell death. The apoptotic, pyroptotic, necroptotic and the caspase inhibitors showed no effect on YO-PRO uptake. This would suggest that none of the cell death mechanisms, including the promising pyroptotic pathway, had any involvement in the uptake of YO-PRO. It was also surprising since other studies have shown ATP stimulation in immune cells causes pyroptotic cell death (Rathkey et al., 2018).

Interestingly, however, the calpain inhibitor, PD150606, did show a significant reduction in YO-PRO uptake (Fig 3.7) while also showing a significant reduction in cell death after stimulation with ATP (Fig 3.8). The calpain inhibitor also affected the morphological changes of the cells (Fig 3.9). Although they did not appear the same as control cells, looking more rounded and shrunken. This could point to a different type of cell death occurring, possibly a non-lytic form of cell death. As non-lytic forms of cell death, such as apoptosis, are known for the containing of the cellular contents this could possibly explain why ATP-induced LDH release is decreased.

Investigating the relationship between PD150606 and P2X7 was important to investigate whether it affected the P2X7 receptor directly. P2X7-induced Ca^{2+} increases was chosen as the manner to test this as Ca^{2+} influx is directly caused by the opening of the P2X7 channel. The calcium data (Fig 3.10) did show a slight reduction of calcium movement across all ATP concentrations tested, when incubated with the calpain inhibitor, however this reduction was not statistically significant. The P2X7 inhibitor, AZ10606120, however, stopped all P2X7 related calcium movement to a statistically significant degree, which shows that the calcium movement is P2X7 dependent. This was not enough evidence for whether P2X7 was affected by PD150606. To further investigate whether calpains do have a hand in the reduction of YO-PRO permeability and cell death, the use of another calpain inhibitor, CAT811, was used. As there were no differences in the YO-PRO uptake data (Fig 3.11) between any of the ATP alone and ATP in the presence of CAT811, suggesting that calpains play no role in the cell death or YO-PRO uptake pathways. However, differences could also be explained by differing selectivities of the calpain inhibitors used. PD150606 is able to inhibit the protease core of calpain 1 and the full length calpain 2 (Low et al., 2014), while CAT811 is found to be a potent and selective calpain 2 inhibitor (Abell et al., 2009). It is possible that calpain 1 is involved in the pathway but not calpain 2. This would require further investigation. However, it was clear from these experiments that inhibition of calpain could not prevent the ATP-induced microglia cell death.

Other studies that have investigated the mechanism of cell death in microglia after ATP stimulation have found mixed results. An early investigation found evidence that pointed to apoptosis as the mechanism, due to the morphological and biochemical changes that occurred in mouse microglial cell lines, N9 and N13 (Ferrari et al., 1997a), while a later study that used BV2 cells, also found that apoptosis was the likely mechanism when cell death occurred after ATP

stimulation (Hao et al., 2013). However, more recent studies have found evidence that ATP-induced cell death is via pyroptosis. One study using a rat model found after LPS/ATP stimulation microglia cells die via the pyroptotic pathway (Liu et al., 2023a) and another showed that after ATP stimulation, pyroptosis occurs via the activation of caspase-7 and -3 (McKenzie et al., 2020). This was not replicated in the current experiments.

The experiments used in this chapter go some way to determining the mechanisms involved in this process, but it remains that none of the selective inhibitors of cell death pathways had any effect on membrane permeability or cell death, so further study is needed. Some of the experiments themselves have limitations, for example, the cell death experiments could be closer aligned to each other and if repeated the different cell death assays would be performed over the same timepoints. The LDH and MTS assays used are suitable for detection of a lytic form of cell death, but do not give any further insight into the specific mechanism that is occurring after ATP stimulation. Other techniques that could be carried out to examine this more closely include apoptosis detecting assays such as the Terminal deoxynucleotidyl transferase dUTP nick end labelling (TUNEL) assay, which detects DNA fragmentation characteristic of apoptotic cells. A caspase-3/7 activity assay would measure the activity of the effector caspases of apoptosis, where higher levels of activation would suggest an apoptotic form of cell death occurring. Finally, the JC1 assay could be used, which measures mitochondrial membrane potential and would be able to indicate whether mitochondrial dysfunction was occurring. If there was evidence of this the mitochondrial role in this process could be investigated further. Pyroptosis could be further investigated by detecting cleavage of caspase 1 or gasdermin D using immunoblotting or immunofluorescence staining, while an ELISA could be used to test for the secretion of IL-1β and IL-18, cytokines released during pyroptosis. Finally, annexin V staining, which binds to phosphatidylserine exposed on the surface of the plasma membrane during apoptosis and pyroptosis, can be detected using flow cytometry or fluorescent microscopy.

The results presented in this chapter therefore indicate that microglia were dying in response to ATP, but not via pyroptosis. This was an unexpected finding as it was hypothesised based on previous literature (Rathkey et al., 2018), that pyroptosis was the most likely mechanism of cell death. The data presented further implies that the mechanisms in microglia and different to those seen in macrophages. The next experiments therefore compared ATP-induced cell death in microglia and macrophages.

Chapter 4

Comparisons Between Macrophage and Microglia Cell Death Mechanisms after ATP stimulation

4.1 Introduction

In 2018, Rathkey et al published research linking pyroptosis and ATP in macrophages. The experiments clearly showed that macrophages primed with LPS and stimulated with ATP, or nigericin, were undergoing pyroptosis that could be blocked using necrosulfonamide, a gasdermin D inhibitor (Rathkey et al., 2018). Results presented in the previous chapter indicate that BV2 microglia, stimulated with ATP, do not die via the pyroptosis cell death mechanism. It was hypothesised that this would be the case, largely based on a comprehensive study in macrophages that showed dye uptake and cell death in LPS primed human macrophages, THP1 or iBMDMs, stimulated with ATP and nigericin, which could be blocked using the gasdermin D inhibitor, necrosulfonamide (Rathkey et al., 2018). It may be that differences with this original study, not LPS priming the cells, using a different fluorescent dye and using microglial cells rather than macrophages, is the cause of the results in the previous chapter. It was therefore important to create conditions that more closely replicated those seen in the Rathkey paper.

Further evidence has shown that macrophages are able to die by the cell death pathway of pyroptosis. Early papers describing pyroptotic activation in macrophages initiated the process using proteins of bacterial origins which cause the cells to lyse (Fink and Cookson, 2006, Fink and Cookson, 2007). Later research has also shown that high levels of ROS can also lead to the activation of the pyroptotic pathway (Wang et al., 2019b) and high levels of glucose, with and without priming with LPS, also caused cell death that used the pyroptotic pathway (Aki et al., 2020, Zhao et al., 2021).

There are many similarities between macrophages and microglia (See 1.1.3). Both are myeloid immune cells, patrol their local surroundings and use phagocytosis to remove threats. (Borst et al., 2021, Robinson et al., 2019). There are also differences which exist such as origin and gene expression (Ginhoux and Guilliams, 2016).

This research investigates macrophage ATP-associated cell death mechanisms to validate the results published by Rathkey (Rathkey et al., 2018), and the effectiveness of the pyroptotic inhibitors being used and to compare this mechanism in macrophages with the findings in microglia presented in the previous chapter to help understand similarities and differences in the pathways occurring in both cell types.

4.2 Results

4.2.1 LPS-priming and stimulation with ATP and nigericin on J774 macrophages causes dye uptake

Initial experiments replicated conditions from the Rathkey paper (Rathkey et al., 2018) using mouse macrophage cell line, J774. The aim was to show that results could be reproduced. Particularly important was that the inhibitor necrosulfonamide was active as this had no effect on ATP-induced YO-PRO influx in microglia (Fig 3.7c and i). These experiments also used the J774 cell line rather than the THP1 and iBMDMs, so reproduction of results with this cell line was also important. J774 cells were primed with LPS (2µg/ml) for 4 hours before being stimulated by either 10µM nigericin or 5mM ATP and PI uptake measured for an hour and a half in the presence and absence of the gasdermin D inhibitor, necrosulfonamide.

The LPS primed cells stimulated with nigericin (Fig 4.1a) showed PI uptake after the 30-minute mark. When incubated with necrosulfonamide the dye uptake returned to that of the control. The AUC for these plots (Fig 4.1b) display a significant difference between the LPS-primed nigericin-stimulated cells when compared to both the control and the LPS-primed nigericin stimulated cells that were incubated in necrosulfonamide. The ATP stimulated cells showed PI uptake in the LPS-

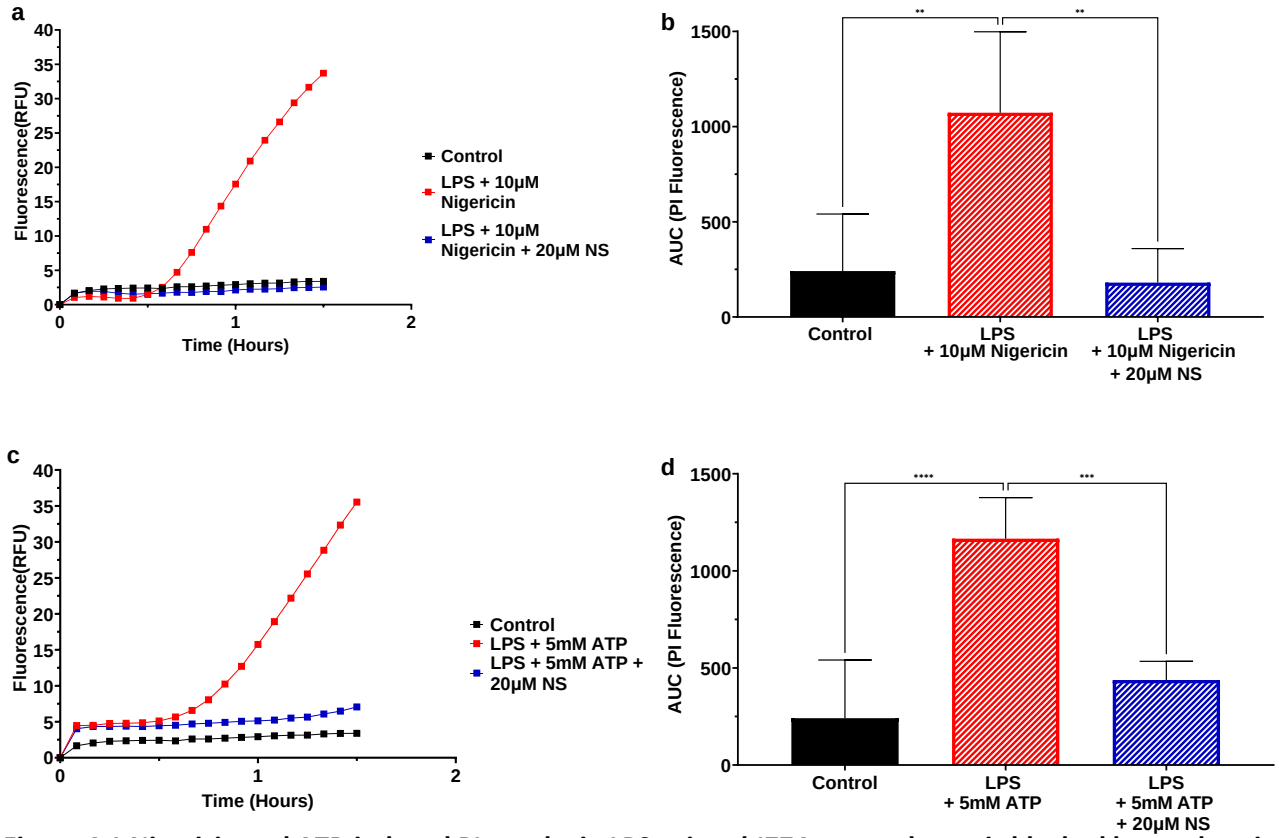

Figure 4.1 Nigericin and ATP-induced PI uptake in LPS-primed J774 macrophages is blocked by gasdermin D inhibition (a) Mean PI uptake in J774 macrophage cells in response to 4-hour LPS (2µg/ml) priming and stimulation with 10µM nigericin (b) PI uptake (AUC 0-90mins) (c) Mean PI uptake in J774 macrophage cells in response to 4-hour LPS (2µg/ml) priming and stimulation with 5mM ATP (d) PI uptake (AUC 0-90mins) (mean +SEM, n=4) * Indicates significance (P<0.05) using one-way ANOVA with Dunnett's post-hoc test.

primed 5mM ATP stimulated cells. No increase was seen under control conditions or when incubated with ATP and necrosulfonamide (Fig 4.1c and d). The results of the Rathkey paper were therefore replicated and clearly showed that in the macrophage cell line, J774, there is gasdermin D dependent mechanism involved in the dye uptake that is stimulated by either nigericin or ATP and indicates the activation of pyroptotic pathways.

In order to be able to compare these experiments with the previous experiments in the microglial cell line, BV2 (Chapter 4) YO-PRO (rather than PI) was used as the dye to investigate membrane permeability over the course of 3 and a half hours, in the presence and absence of LPS priming and using different concentrations of ATP (Fig 4.2 and 4.3).

The YO-PRO dye uptake experiment showed that LPS primed J774 cells stimulated with nigericin had dye uptake around the 30 minute mark, but if the cells are non-LPS primed then no uptake occurs. When stimulating with ATP, 1mM ATP was similar to nigericin as it also needed the LPS priming to allow any YO-PRO uptake. The higher ATP concentrations, 3mM and 5mM ATP, exhibit equivalent dye uptake in both the non-LPS and LPS primed cells with dye uptake being almost identical under both conditions. The AUC data showed the significant difference between the LPS primed cells stimulated with nigericin and the control as well as the non-LPS primed cells stimulated with nigericin. For the 1mM ATP stimulated cells, there was no significant difference between the LPS primed and non-LPS primed or control cells. The highest concentrations of ATP, 3mM and 5mM, showed an increase that was statistically significant compared to the control, whether they were LPS primed or not. However when the LPS and non-LPS primed cells stimulated with 3mM or 5mM were compared they did not show a significant difference.

The same experiment was repeated, but this time using PI as the fluorescent dye. A similar story can be seen. Nigericin needed LPS priming before dye uptake occurs and the higher concentrations of ATP, 3mM and 5mM ATP, caused dye uptake in both the non-LPS and LPS primed cells. The 1mM ATP caused an increase in PI uptake which was enhanced by LPS priming. Dye uptake occurred at around the 30-minute mark for all cells that exhibit dye uptake. This confirms that PI uptake in the J774 cell line is comparable to YO-PRO uptake. The uptake is dependent on LPS priming when the cells are stimulated with nigericin (10μM) but suggests that it is not required for ATP-induced changes but although the cells appear more sensitive to ATP stimulation.

Gross morphological changes in the J774 cell line were also monitored. Those stimulated with nigericin and 1mM ATP in the non-LPS primed cells show little change and appeared no different to the control cells (Fig 4.4a). When the cells are LPS primed (Fig 4.4b), nigericin and 1mM ATP caused morphological changes after 2 hours, displaying a loss of defined cell structure, although they did not appear to be swollen. 3mM and 5mM ATP causes some cells to swell, but it was not possible to say definitely if there was change using these microscopic techniques.

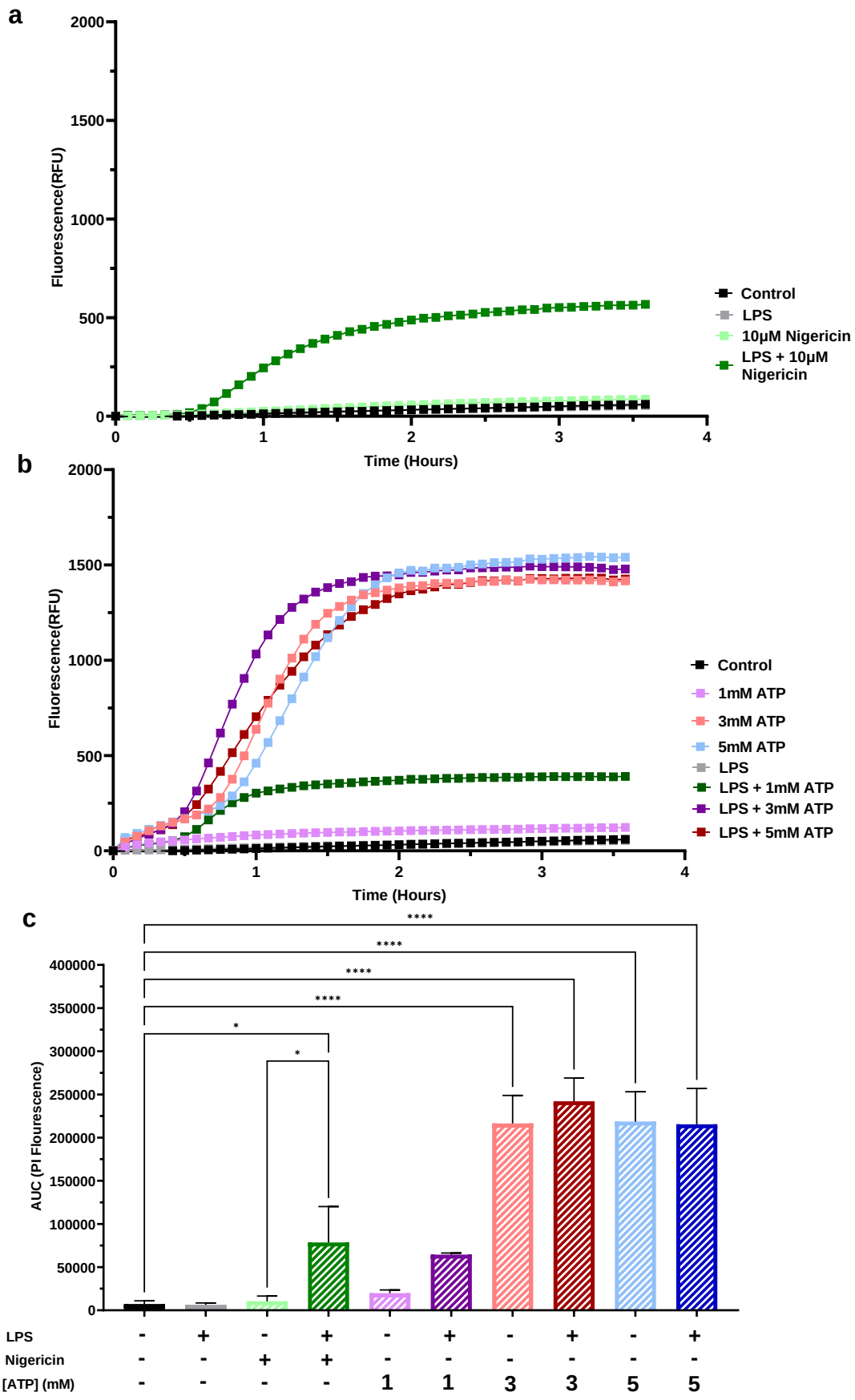

Figure 4.2 Nigericin and ATP cause YO-PRO uptake in LPS-primed J774 macrophages (a) Mean YO-PRO uptake in J774 macrophage cells in response to ±4-hour LPS (2µg/ml) priming and ±nigericin 10µM (b) Mean YO-PRO uptake in J774 macrophage cells in response to ±4-hour LPS (2µg/ml) priming and ±ATP 1mM, 3mM and 5mM (c) YO-PRO uptake (AUC 0-210mins) (mean +SEM, n=4) * indicates significance compared to control (P<0.05) using a one-way ANOVA with Tukey post hoc test

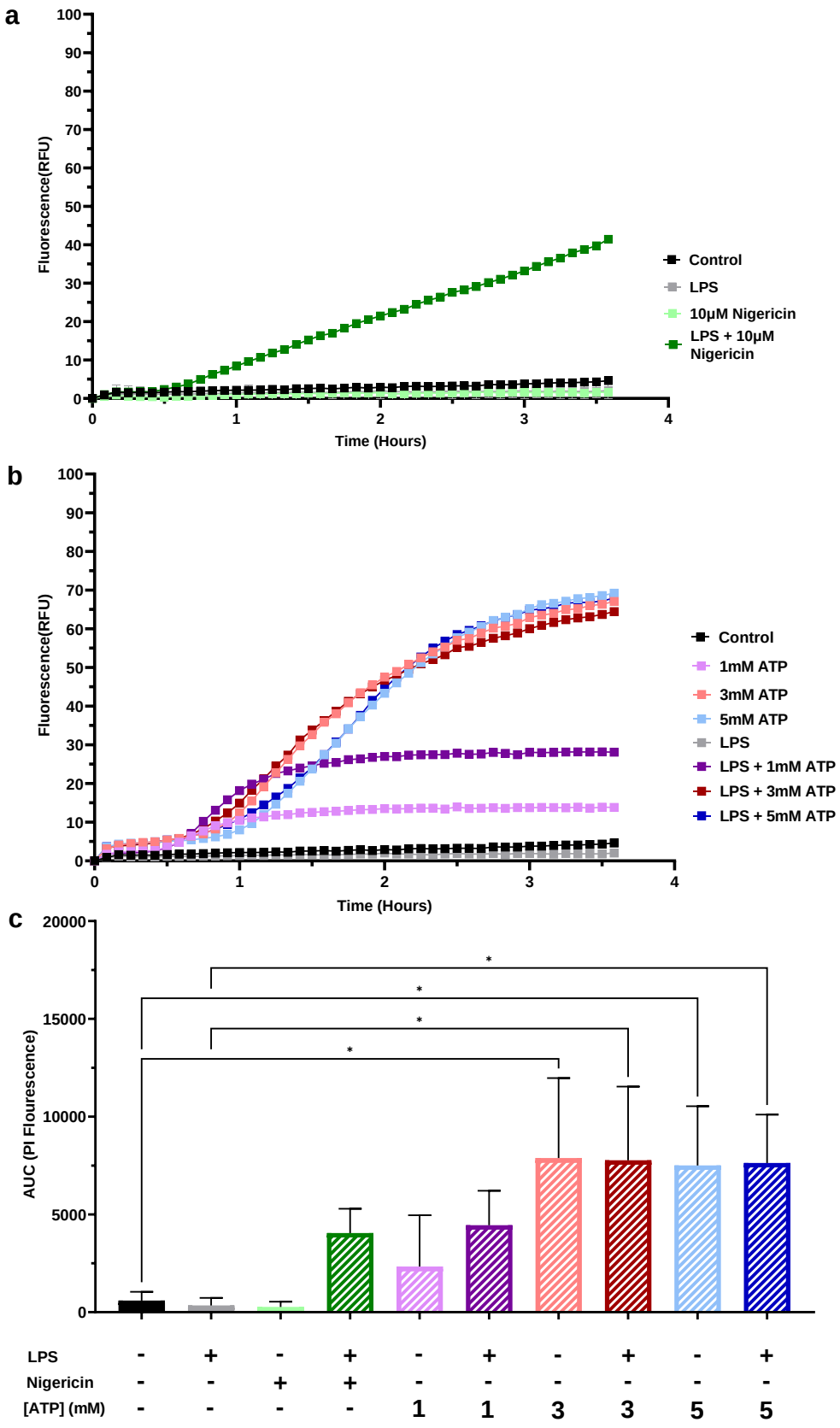

Figure 4.3 (a) Nigericin and ATP cause PI uptake in LPS-primed J774 macrophages Mean PI uptake in J774 macrophage cells in response to ±4-hour LPS (2µg/ml) priming and ±nigericin 10µM (b) Mean PI uptake in J774 macrophage cells in response to ±4-hour LPS (2µg/ml) priming and ±ATP 1mM, 3mM and 5mM (c) PI uptake (AUC 0-210mins) (mean +SEM, n=4) * indicates significance compared to control (P<0.05) using a one-way ANOVA with Tukey post hoc test

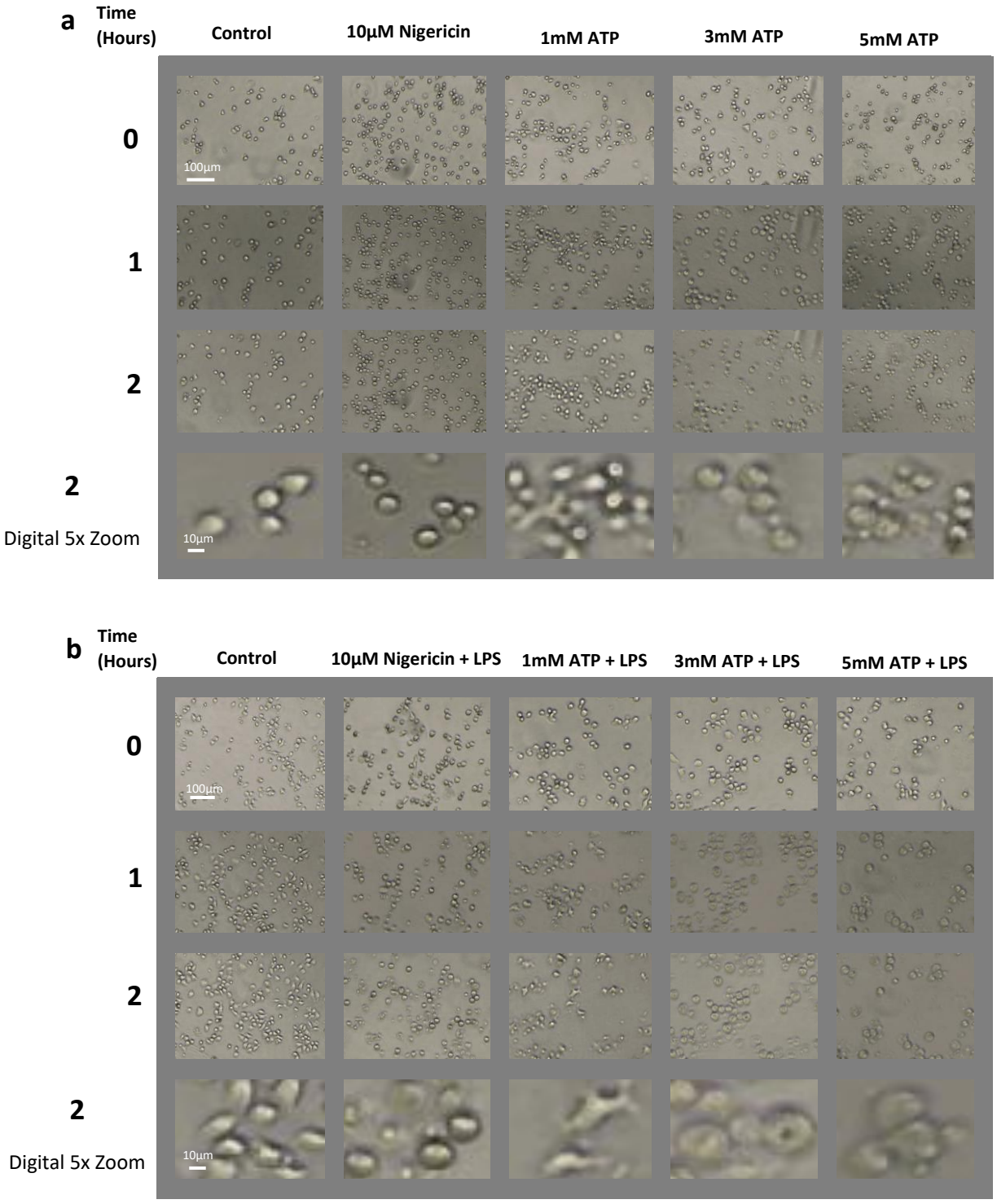

Figure 4.4 LPS priming causes cell morphological changes in J774 macrophages after stimulation with ATP and Nigericin (a) Time course images of mouse macrophage cells (J774) in response to stimulation by nigericin 10µM and ATP 1mM, 3mM and 5mM (b) Time course images of J774 macrophage cells in response to 4-hour LPS (2µg/ml) priming and stimulation by nigericin 10µM and ATP 1mM, 3mM and 5mM. Final rows shows representative cell morphology at 2 hours (5x digital zoom)

4.2.2 Pyroptotic associated protein inhibitors alter dye uptake in LPS-primed J774 macrophages stimulated with ATP and Nigericin

To investigate the mechanism of PI uptake in the macrophages, and specifically whether this was due to a pyroptotic pathway, the J774 cells were again primed for 4 hours with LPS and then stimulated with either 10µM nigericin or various concentrations of ATP. This was carried out in the presence and absence of inhibitors used in the experiment in the previous chapter (Chapter 3) that block parts of the pyroptotic pathway, specifically the NLRP3 inhibitor, MCC950, caspase 1 inhibitor, Ac-YVAD-cmk, and the gasdermin D, necrosulfonamide (NS) the P2X7 inhibitor, AZ10606120.

PI uptake in the LPS primed cells stimulated by nigericin(Fig 4.5a) occurred from around 30 minutes and when also incubated with MCC950 (10µM), an inhibitor of the inflammasome sensor protein, NLRP3, there is a complete inhibition of this uptake and a return to the level of PI uptake in the control. The AUC data (Fig 4.5c) shows a significant difference between the LPS primed cell stimulated with nigericin and the LPS primed cell stimulated with nigericin incubated with MCC950. The LPS primed cells stimulated with a range of ATP concentrations (Fig 4.5b and c) showed that at 1mM ATP, dye uptake was seen over the time course of the experiment which was also totally inhibited by MCC950. At 3mM and 5mM ATP there was a much higher dye uptake and MCC950 showed a delay in the onset of the response increasing just over an hour after stimulation rather than the usual 30 minutes, there was also a significant decrease in total dye uptake (Fig 4.5c)

This data suggests that pyroptotic pathways, specifically the NLRP3 inflammasome, is involved in the loss of permeability of the J774 cells after LPS priming and stimulation with either nigericin or ATP (1mM-5mM). These results also showed that under these conditions MCC950, at 10µM, is a viable inhibitor for the use in investigating this pathway.

The next inhibitor used was the caspase 1 inhibitor, Ac-YVAD-CMK (Fig 4.6) Caspase 1 is central to the pyroptotic pathway and cleaves important pyroptosis proteins including IL-1β, IL-18 and gasdermin D. The LPS primed macrophages that were nigericin stimulated (Fig 4.6a) showed PI uptake across the time course that was inhibited by Ac-YVAD-CMK. With 1mM ATP (Fig 3.5b) showed the expected uptake of PI over the time course and when these cells were also incubated with the Ac-YVAD-CMK there was a slight reduction in uptake of the dye. With 3mM and 5mM ATP, Ac-YVAD-CMK caused a large reduction in uptake compared to ATP alone (Fig 4.5b and c).

This data indicates that caspase 1 plays a role in ATP-induced disruption of cell permeability after LPS priming in J774 cells and shows that Ac-YVAD-CMK can be used for investigating this pathway.

The next inhibitor used was necrosulfonamide, an inhibitor of the pyroptosis executioner protein, gasdermin D (Fig 4.7). The PI uptake stimulated with nigericin after LPS priming was reduced by necrosulfonamide. This was also the case for ATP (1, 3 and 5mM)

This indicates that gasdermin D plays a role in the disruption of cell permeability under these conditions and confirms that the use of necrosulfonamide as a pharmacological tool in investigating pyroptosis is appropriate and effective.

Finally, the last inhibitor used was the P2X7 inhibitor AZ10606120 (Fig 4.8). AZ10606120 did not affect dye uptake due to nigericin but fully inhibited the ATP-stimulated increase, dye uptake remaining at control levels (Fig 4.8b and c).

This indicates that the disruption of cell permeability in the LPS-primed J774 cells stimulated with ATP is P2X7 dependent and together with the previous experiments using the pyroptotic pathway inhibitors that this stimulation of P2X7 leads to activation of the pyroptotic pathway in the J774 cells.

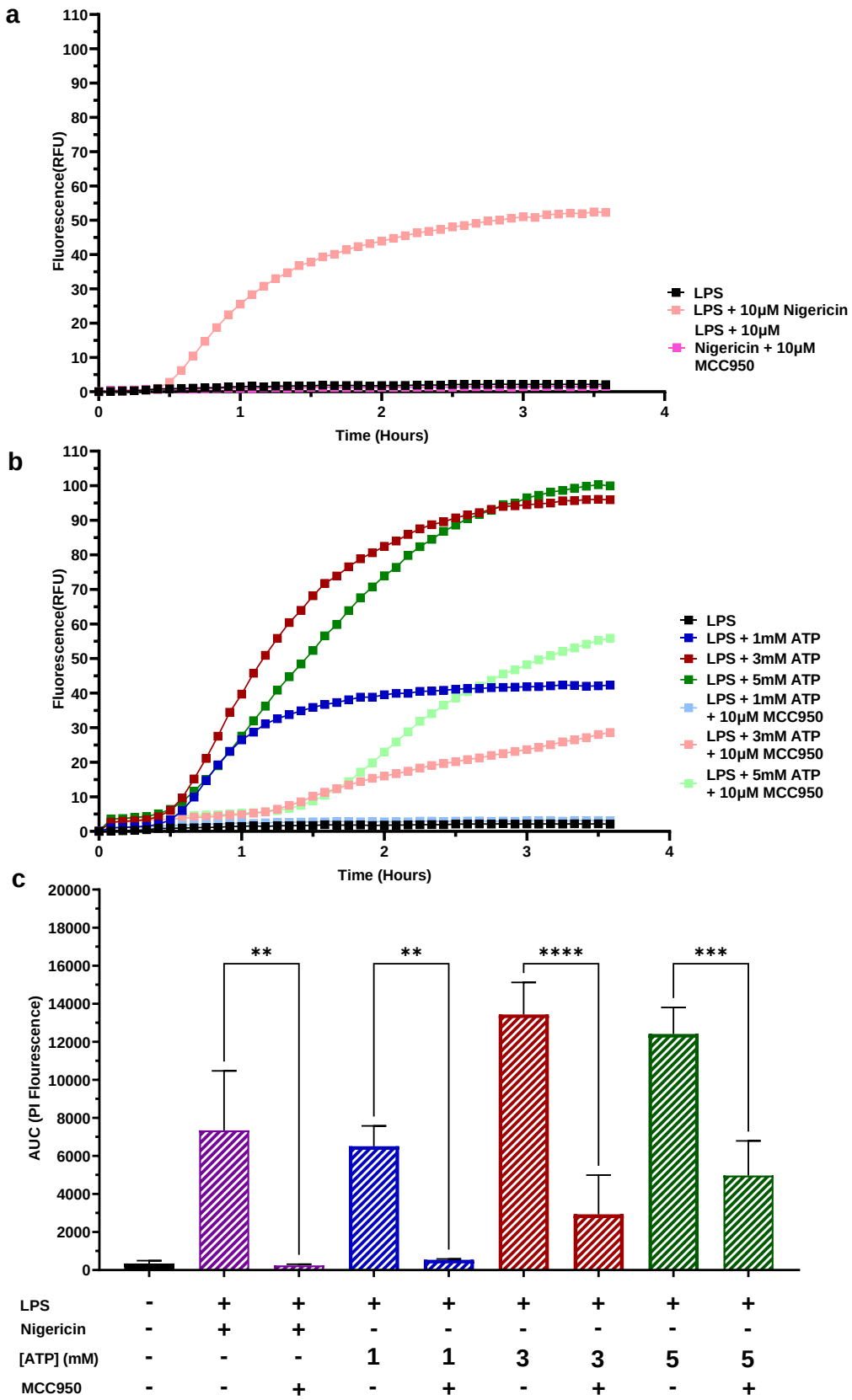

Figure 4.5 Nigericin and ATP-induced PI uptake in LPS-primed J774 macrophages is blocked by NLRP3 inhibition (a) Mean PI uptake in J774 macrophage cells in response to 4-hour LPS (2µg/ml) priming and nigericin 10µM ± MCC950 10µM (b) Mean PI uptake in J774 macrophage cells in response to ±4-hour LPS (2µg/ml) priming and ATP (1mM, 3mM and 5mM) ± MCC950 10µM (c) PI uptake (AUC 0-210mins) (mean +SEM, n=4) * indicates significance compared to control (P<0.05) using a one-way ANOVA with Tukey post hoc test

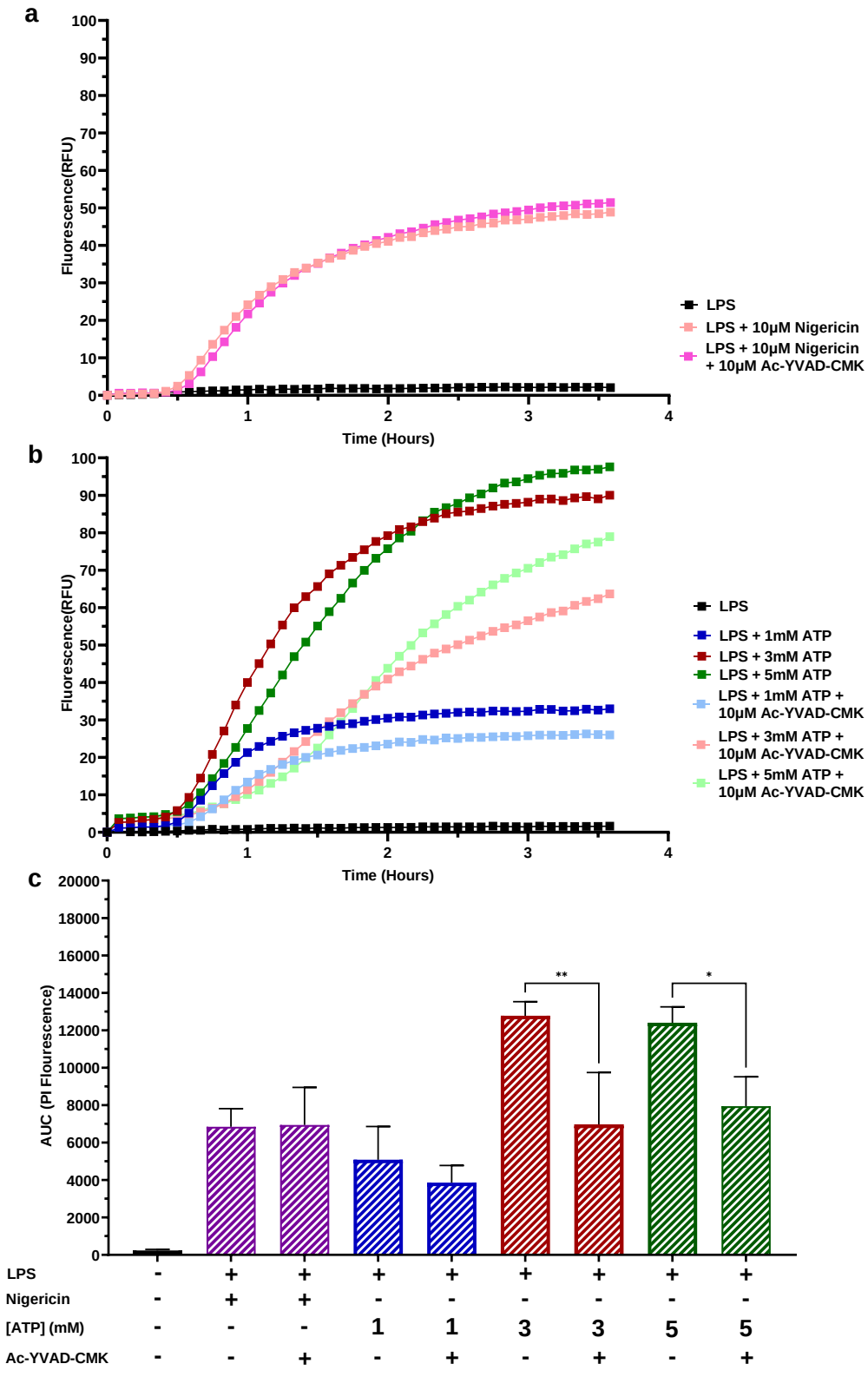

Figure 4.6 ATP-induced PI uptake in LPS-primed J774 macrophages is blocked by Caspase 1 inhibition (a) Mean PI uptake in J774 macrophage cells in response to 4-hour LPS (2µg/ml) priming and nigericin 10µM ± Ac-YVAD-CMK 10µM (b) Mean PI uptake in J774 macrophage cells in response to 4-hour LPS (2µg/ml) priming and ATP (1mM, 3mM and 5mM) ± Ac-YVAD-CMK 10µM (c) PI uptake (AUC 0-210mins) (mean +SEM, n=4) * indicates significance compared to control (P<0.05) using a one-way ANOVA with Tukey post hoc test

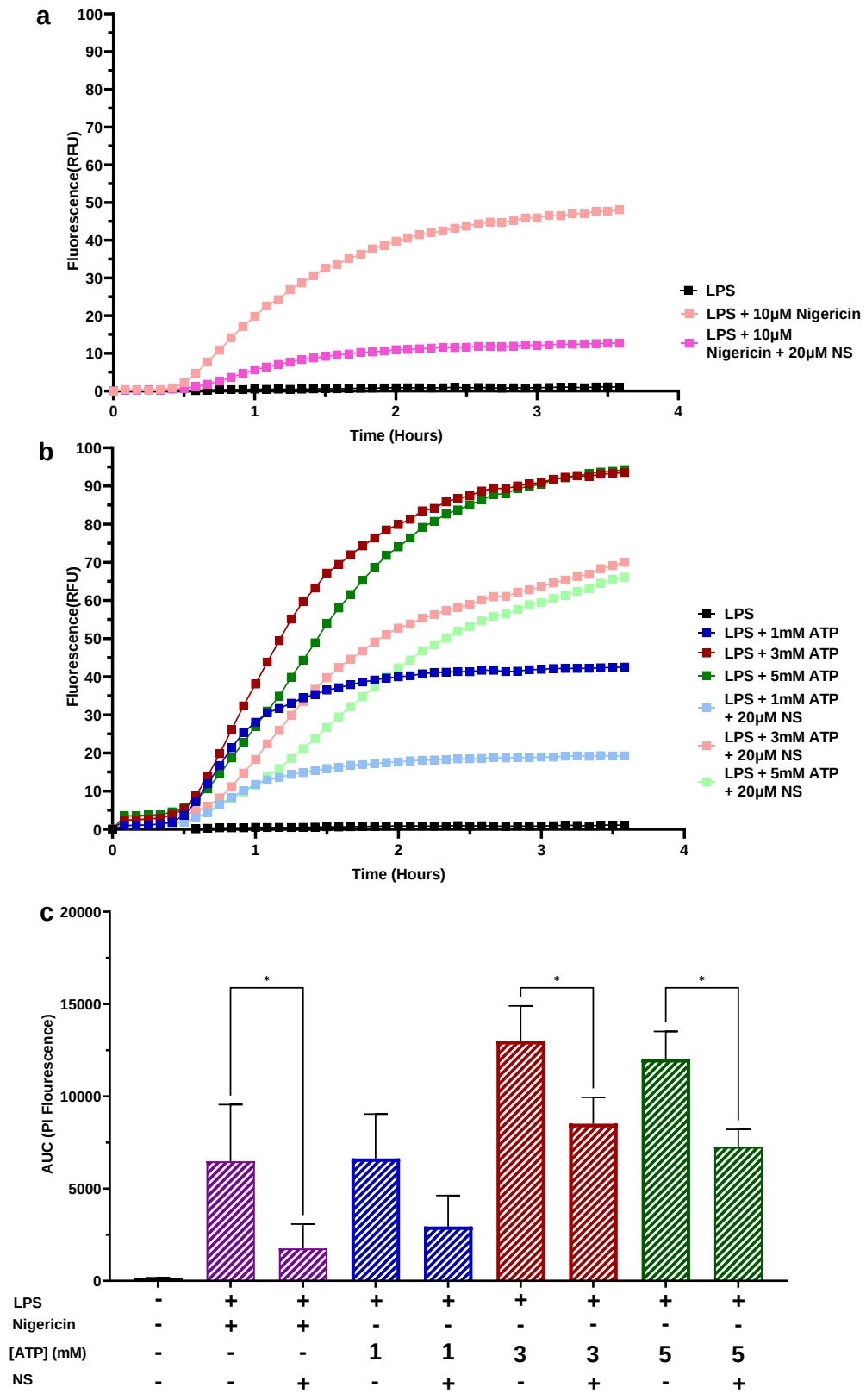

Figure 4.7 Nigericin and ATP-induced PI uptake in LPS-primed J774 macrophages is blocked by gasdermin D inhibition (a) Mean PI uptake in J774 macrophage cells in response to 4-hour LPS (2µg/ml) priming and nigericin 10µM ± Necrosulfonamide 20µM (b) Mean PI uptake in J774 macrophage cells in response to 4-hour LPS (2µg/ml) priming and ATP (1mM, 3mM and 5mM) ± Necrosulfonamide 20µM (c) PI uptake (AUC 0-210mins) (mean +SEM, n=4) * indicates significance compared to control (P<0.05) using a one-way ANOVA with Tukey post hoc test

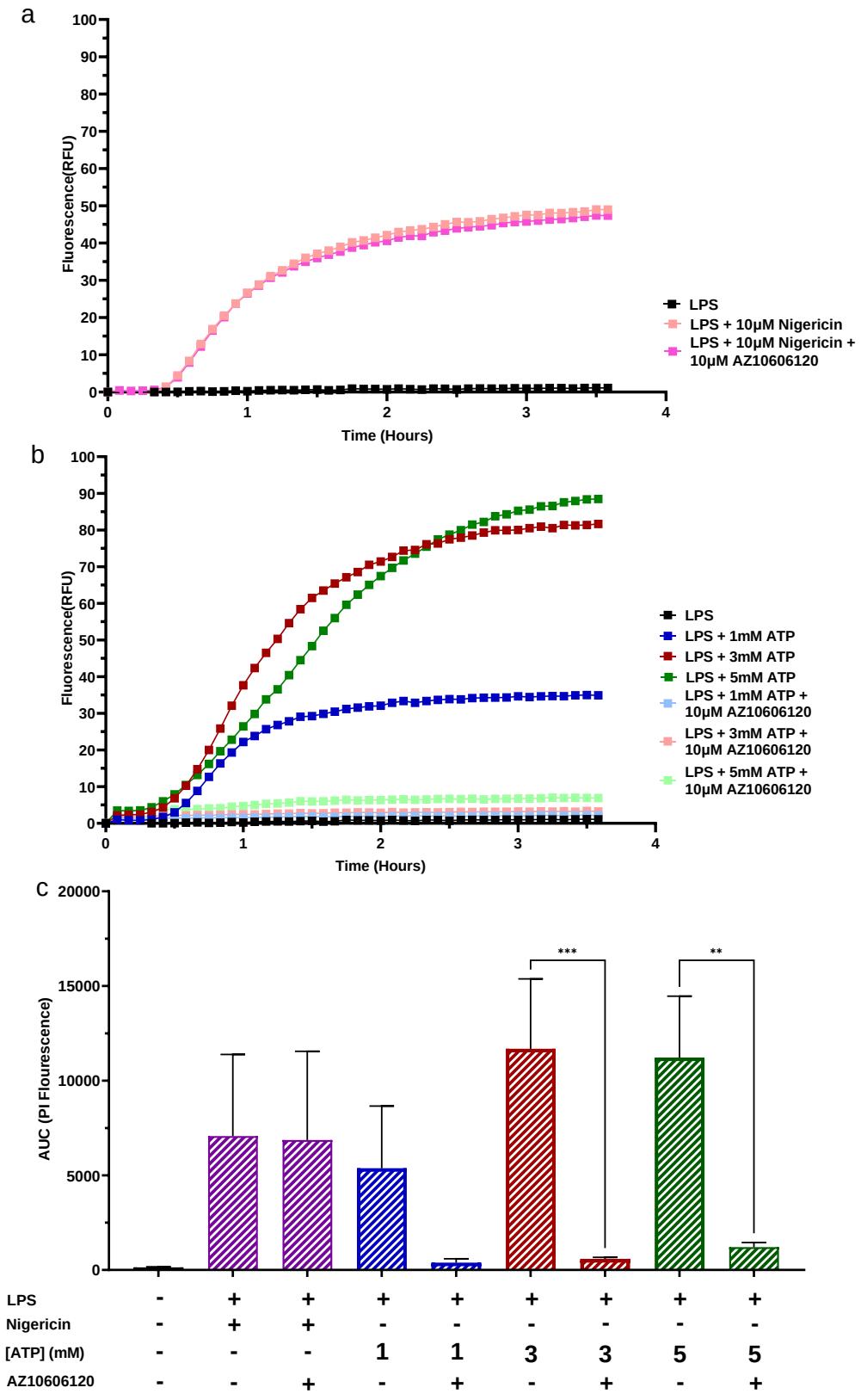

Figure 4.8 ATP-induced PI uptake in LPS-primed J774 macrophages is blocked by P2X7 inhibition (a) Mean PI uptake in J774 macrophage cells in response to 4-hour LPS (2µg/ml) priming and nigericin 10µM ± AZ10606120 10µM (b) Mean PI uptake in J774 macrophage cells in response to 4-hour LPS (2µg/ml) priming and ATP (1mM, 3mM and 5mM) ± AZ10606120 10µM (c) PI uptake (AUC 0-210mins) (mean +SEM, n=4) * indicates significance compared to control (P<0.05) using a one-way ANOVA with Tukey post hoc test

4.2.3 Pyroptotic associated protein inhibitors alter dye uptake in Non-LPS-primed J774 macrophages stimulated with ATP

It was then investigated whether LPS priming was required for the activation of the pyroptotic pathway, by using the inhibitors used previously, MCC950, Ac-YVAD-cmk, necrosulfonamide or AZ10606120, and measuring the PI uptake in response to ATP in non-primed J774 cells, 1mM ATP has little to no PI uptake but stimulation with 3mM and 5mM ATP caused a large PI uptake over the time course which was attenuated by all of the inhibitors (Fig 4.9a-h).

These results indicate that the J774 cells do not need LPS priming for the higher concentrations of ATP (3mM and 5mM) to cause a disruption in cell permeability and that the pathway that is a P2X7-mediated pyroptotic pathway. It was important to confirm this data as these are the same conditions that were used in the previous chapter but using the macrophage rather than the microglial cell line.

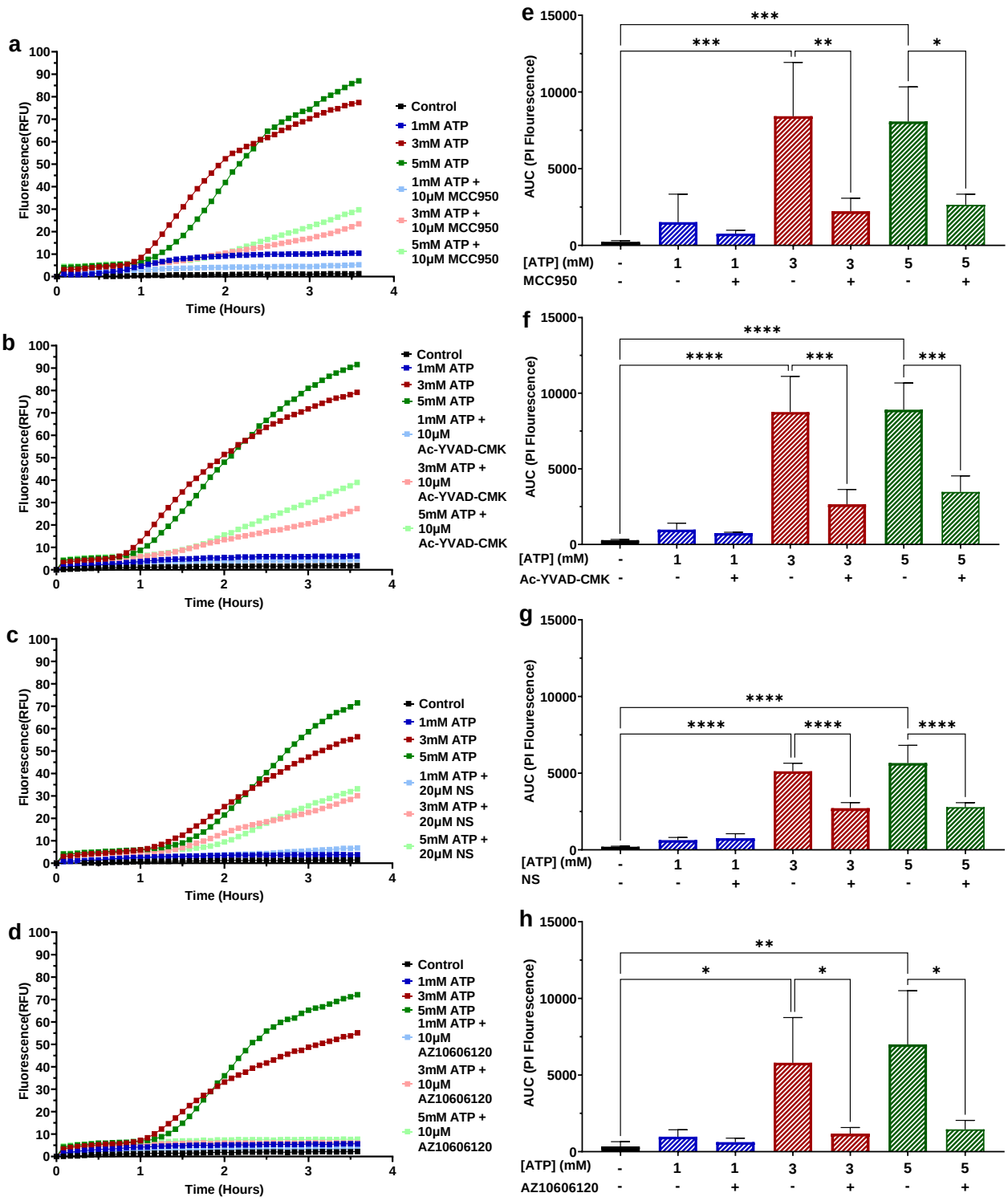

Figure 4.9 ATP-induced PI uptake in non-LPS-primed J774 macrophages is blocked by Inhibition of pyroptotic proteins and P2X7 (a) Mean PI uptake in J774 macrophage cells in response to stimulation by ATP (1mM, 3mM and 5mM) ± MCC950 10µM (b) Mean PI uptake in J774 macrophage cells in response to stimulation by ATP (1mM, 3mM and 5mM) ± Ac-YVAD-CMK 10µM (c) Mean PI uptake in J774 macrophage cells in response to stimulation by ATP (1mM, 3mM and 5mM) ± Necrosulfonamide 20µM (d) Mean PI uptake in J774 macrophage cells in response to stimulation by ATP (1mM, 3mM and 5mM) ± AZ10606120 20µM (e-h) Corresponding PI uptake (AUC 0-210mins) (mean +SEM, n=4) * indicates significance compared to control (P<0.05) using a one-way ANOVA with Sidak's post hoc test

4.2.4 Pyroptotic associated protein inhibitors alter levels of cell death in Non-LPS-primed J774 macrophages stimulated with ATP

The level of cell death was also measured after stimulation with 3mM ATP for 4 hours in the presence or absence of the pyroptotic pathway inhibitors (Fig 4.10). Cell death was fully inhibited by the P2X7 inhibitor. Necrosulfonamide also decreased ATP-induced cell death. The inflammasome and caspase 1 inhibitor had no effect. This indicates a disconnect between permeability changes seen and cell death as MCC950 and Ac-YVAD-cmk both inhibit dye uptake but did not prevent lytic cell death.

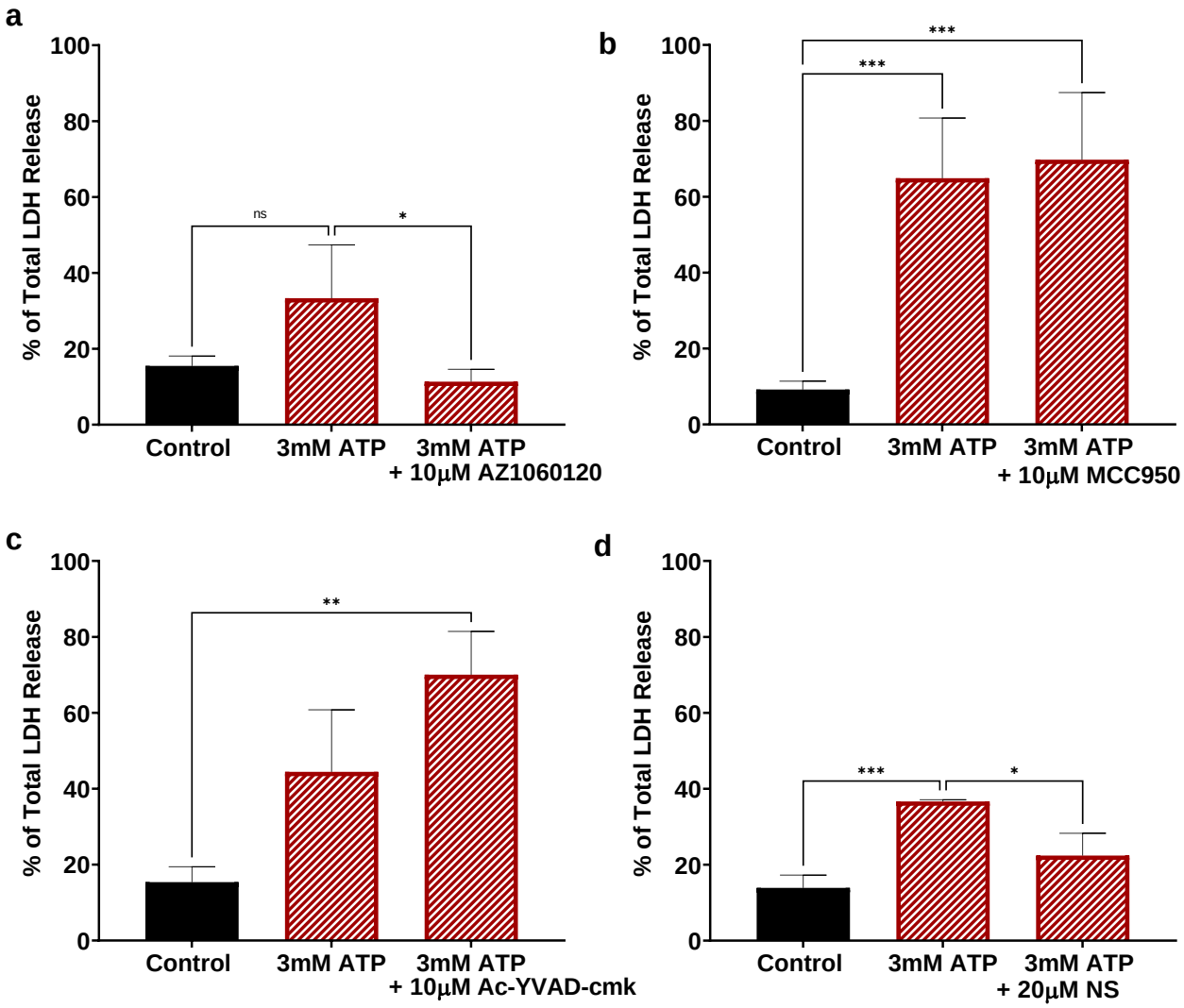

Figure 4.10 ATP-induced LDH release in non-LPS-primed J774 macrophages is blocked by Inhibition of P2X7 and gasdermin D (a) Mean % LDH release after 4 Hours in J774 macrophage cells ± AZ10606120 10µM, , or (b) Mean % LDH release after 4 Hours in J774 macrophage cells ± MCC950 10µM (c)) Mean % LDH release after 4 Hours in J774 macrophage cells ± Ac-YVAD-cmk 10µM (d) Mean % LDH release after 4 Hours in J774 macrophage cells ± Necrosulfonamide 20µM * Indicates significance compared to control ($P<0.05$) using one-way ANOVA with Dunnett's post hoc test.

Changes in cell morphology are a key indicator of the possible form of cell death that is occurring, Blocking of the pyroptotic pathway may be able to stop these morphological changes from happening and therefore save the cells from cell death.

To investigate the effects of ATP on the J774 cell line in the context of cell morphology changes, and how this might link with cell death, the J774 cells were stimulated with 3mM ATP in the presence and absence of the pyroptotic inhibitors and then imaged over a time course of 4-hours to review their morphology.

The J774 cells were imaged (Fig 4.11) but it was not possible to detect any major differences.

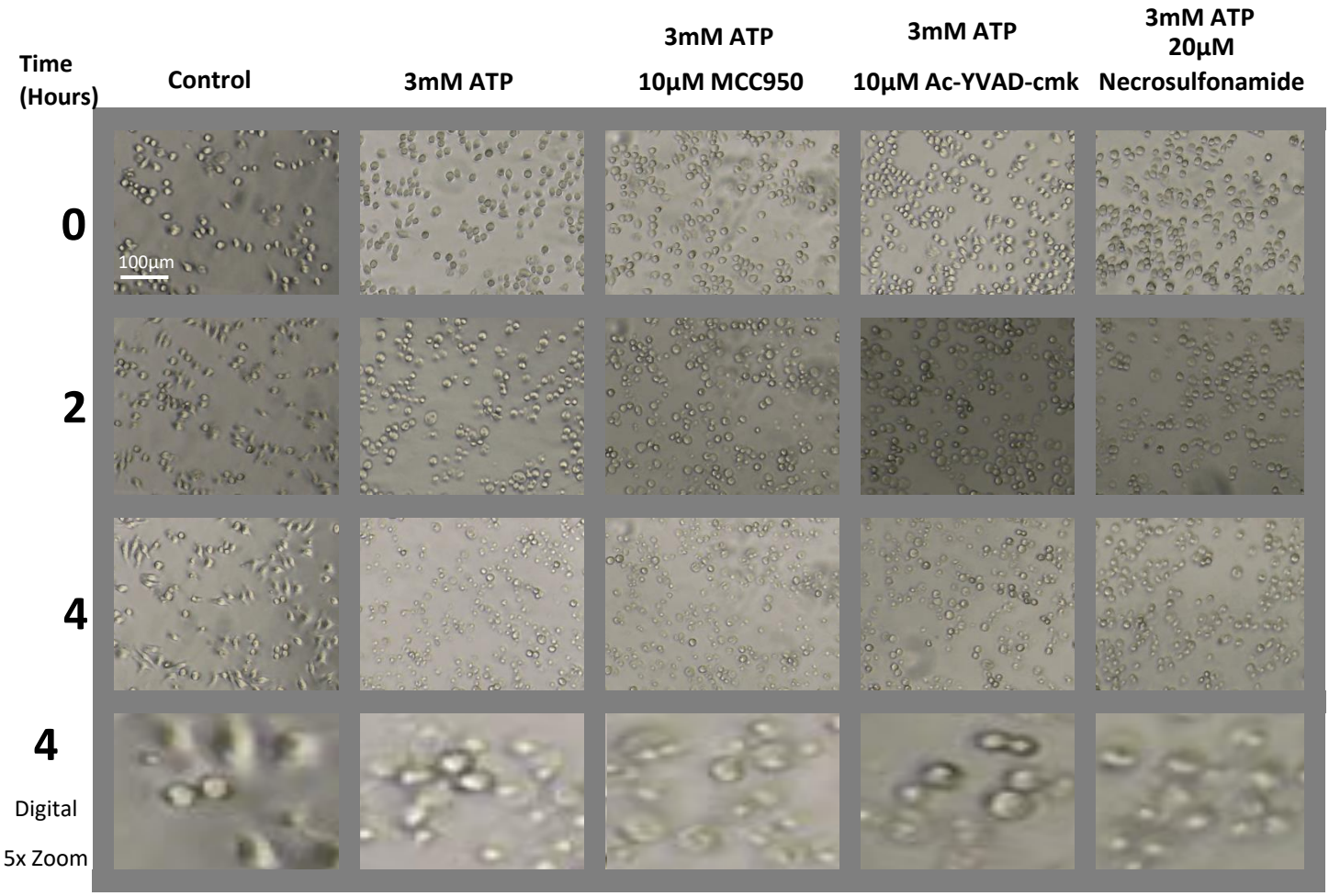

Figure 4.11 Pyroptotic inhibitors have no effect on cell morphological changes in ATP stimulated J774 macrophages Time course images of J774 macrophage cells in response to stimulation by ATP 3mM ± Necrosulfonamide 20µM, Ac-YVAD-CMK 10µM or MCC950 10µM. Final row shows representative cell morphology at 4 hours (5x digital zoom)

4.2.5 Pyroptotic associated protein inhibitors do not alter dye uptake in LPS-Primed BV2 microglia stimulated with ATP. No Dye uptake occurs after LPS primed BV2 cells are stimulated with Nigericin

As the experiments so far have shown that in the presence and the absence of LPS priming, there is ATP-induced dye uptake in the J774 cells. The pyroptotic inhibitors were also shown to block this dye uptake in both conditions. The data suggest that microglial (BV2) cells are responding differently to macrophage (J774) cells, but a final experiment in BV2 cells that were LPS-primed would confirm this. PI and YO-PRO were used as the fluorescent dyes.

BV2 cells, were primed with LPS for 4 hours and then stimulated with nigericin and a range of ATP concentrations (1mM, 3mM and 5mM). Using PI (Fig 4.12) the nigericin did not cause PI uptake with or without LPS priming (Fig 4.12a). All concentrations of ATP showed an uptake of PI with no difference between the primed and non-primed cells (Fig 4.12b and c). Similar results were found when using YO-PRO to monitor membrane permeability (Fig 4.13).

Morphological changes were also observed (Fig 4.14). No differences were seen between LPS and non-LPS primed BV2 cells. Nigericin did not change morphology, whereas ATP caused the cells to become rounded.

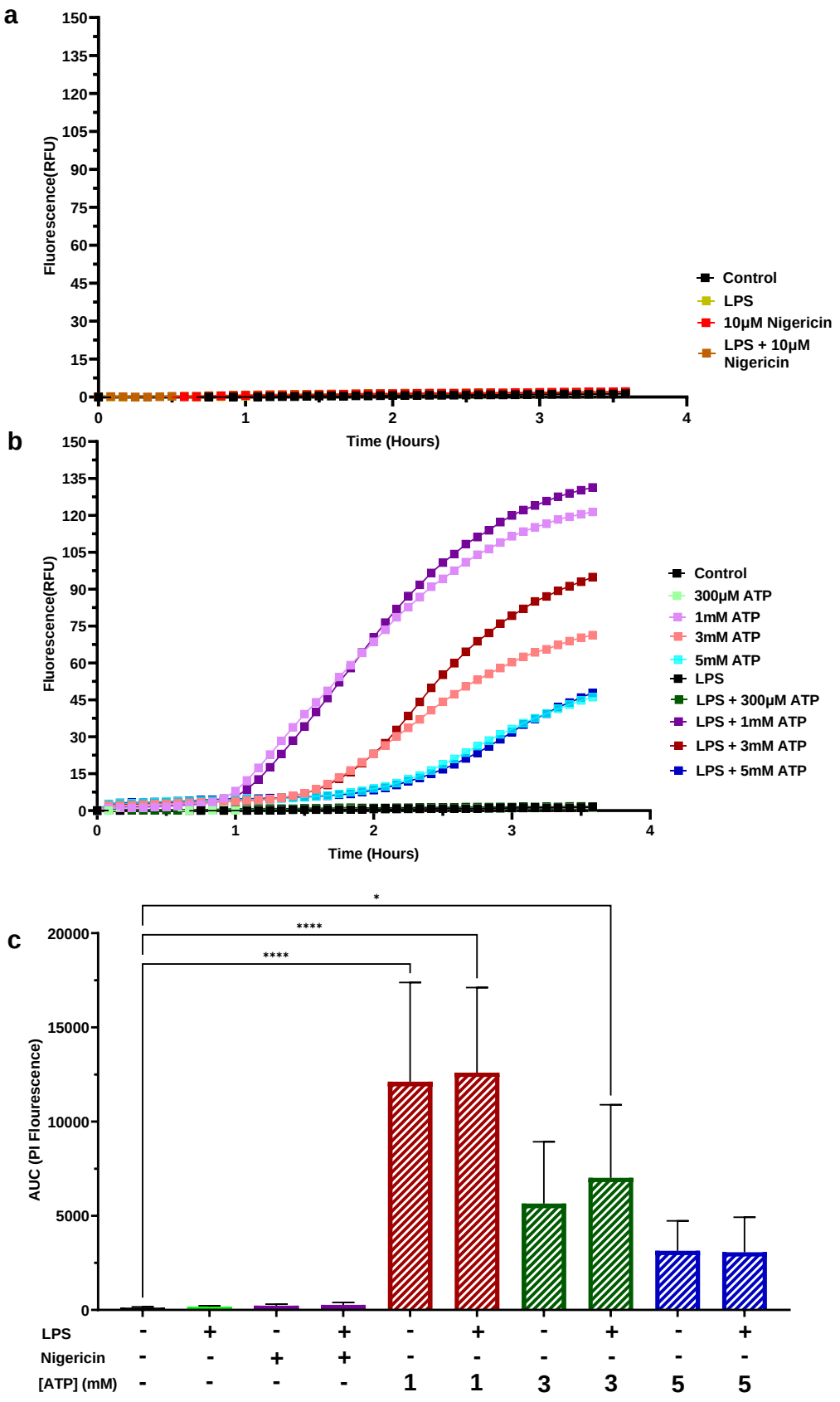

Figure 4.12 LPS priming has no effect on PI uptake in ATP stimulated BV2 microglia (a) Mean PI uptake in BV2 microglia cells in response to ±4-hour LPS (2µg/ml) priming and ±nigericin 10µM (b) Mean YO-PRO uptake in BV2 microglia cells in response to ±4 hour LPS (2µg/ml) priming and ±ATP 1mM, 3mM and 5mM (c) YO-PRO uptake (AUC 0-210mins) (mean +SEM, n=4) * indicates significance compared to control ($P<0.05$) using a one-way ANOVA with Tukey post hoc test

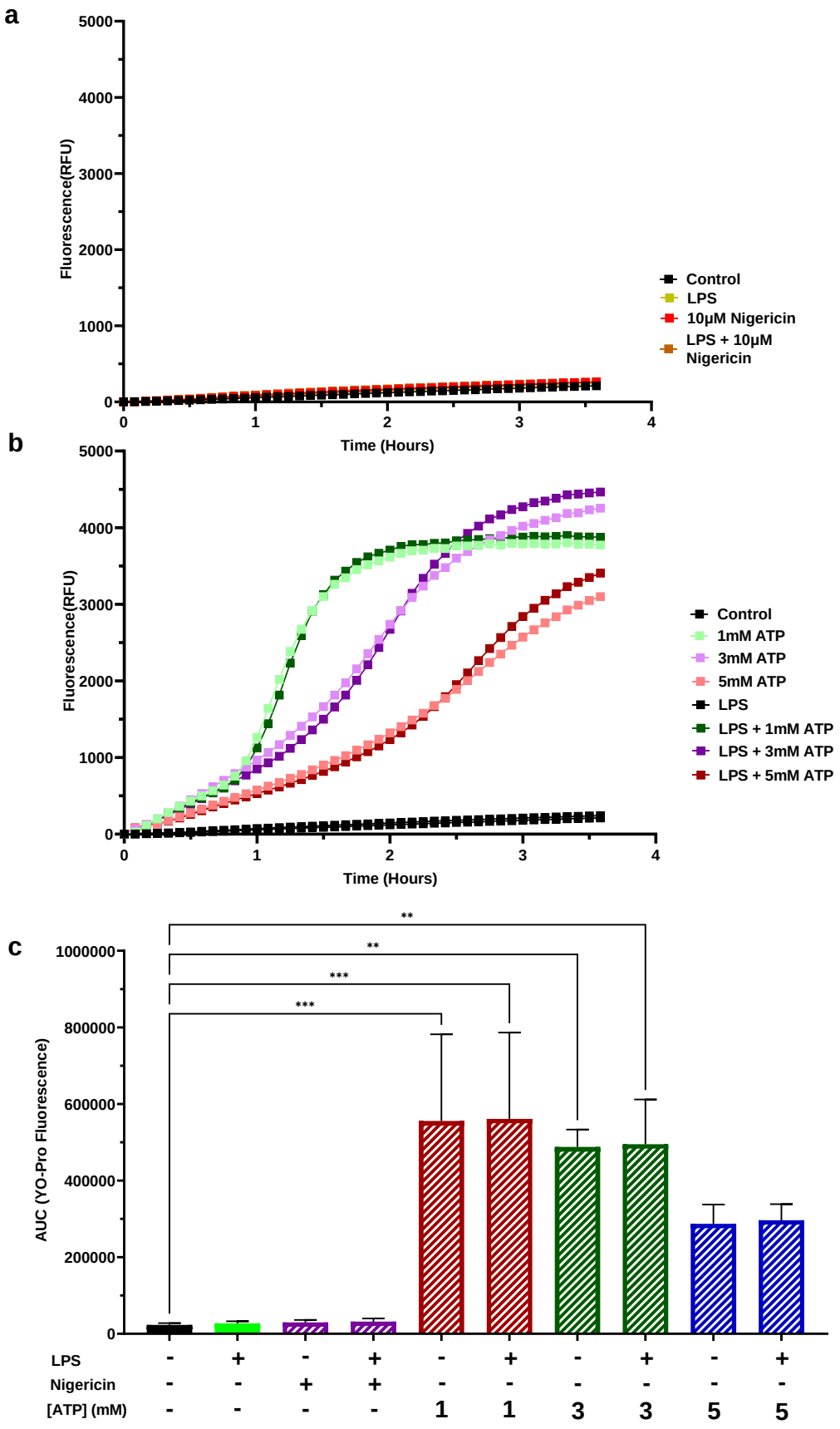

Figure 4.13 LPS priming has no effect on YO-PRO uptake in ATP stimulated BV2 microglia (a) Mean YO-PRO uptake in BV2 microglia cells in response to ±4-hour LPS (2µg/ml) priming and ±nigericin 10µM (b) Mean YO-PRO uptake in BV2 microglia cells in response to ±4 hour LPS (2µg/ml) priming and ±ATP 1mM, 3mM and 5mM (C) YO-PRO uptake (AUC 0-210mins) (mean +SEM, n=4) * indicates significance compared to control (P<0.05) using a one-way ANOVA with Tukey post hoc test

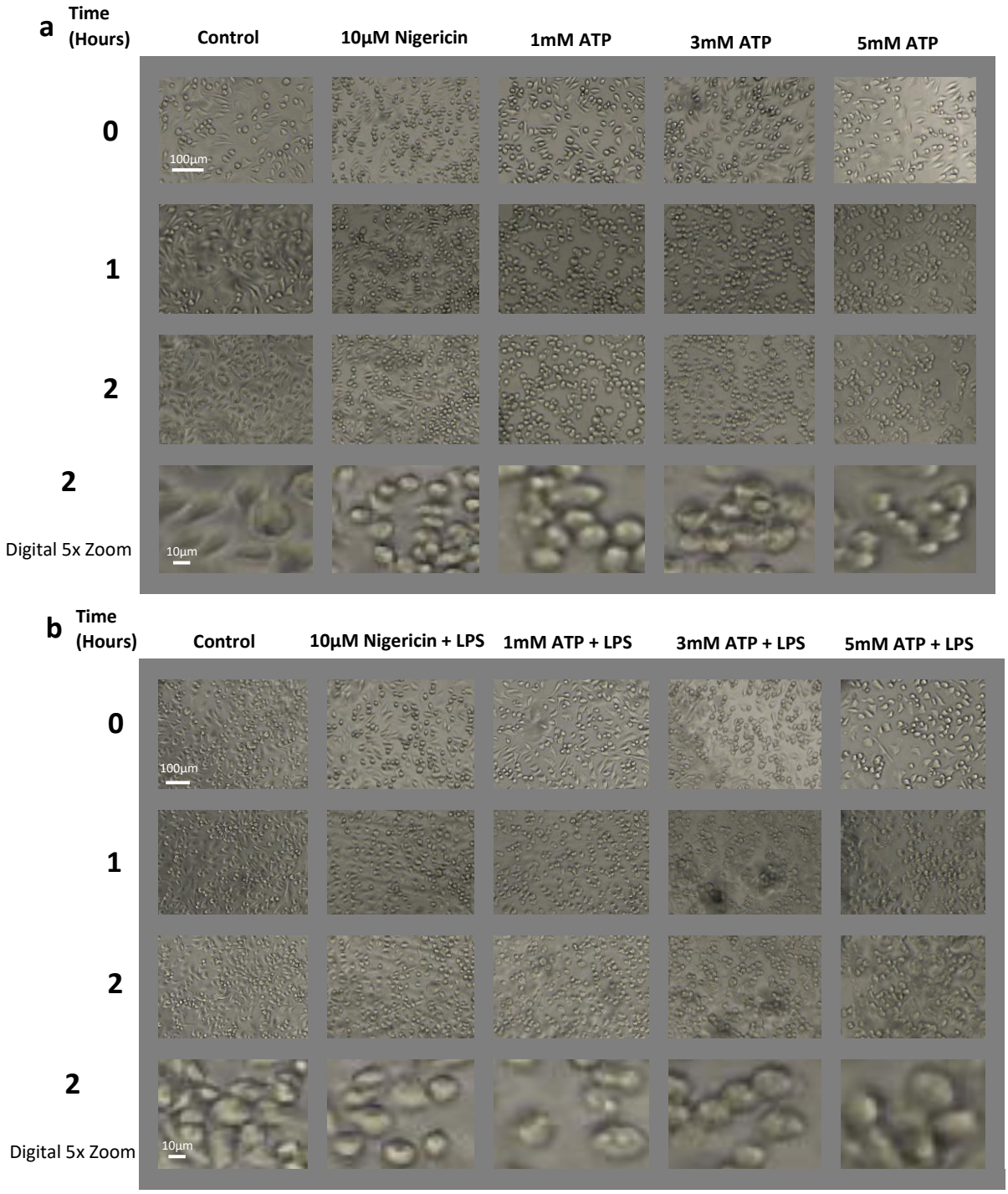

Figure 4.14 LPS priming has no effect on cell morphological changes in ATP stimulated BV2 microglia (a) Time course images of mouse microglia cells (BV2) in response to stimulation by nigericin 10µM and ATP 1mM, 3mM and 5mM (b) Time course images of J774 macrophage cells in response to 4-hour LPS (2µg/ml) priming and stimulation by nigericin 10µM and ATP 1mM, 3mM and 5mM. Final rows shows representative cell morphology at 6 hours (5x digital zoom)

It is clear from these experiments that the BV2 and J774 cells have different responses to ATP stimulation. Importantly, in J774 cells ATP-induced increase in membrane permeability were affected by the pyroptotic inhibitors but this was not the case in BV2 cells. This indicates that the J774 cells are utilising the pyroptotic pathway but the BV2 cells are not.

4.2.6 Gasdermin D is expressed in J774 Macrophages after ATP stimulation but not in BV2 Microglia

Finally, a comparison was made of gasdermin D cleavage between J774 and BV2 cells stimulated with 3mM ATP. Gasdermin D is the executioner protein of pyroptosis and is cleaved to create a pore in the cell membrane that allow the mature IL-1β and IL-18 to exit the cell. This, also, leads to loss of cell membrane integrity which leads to cell swelling and eventually death.

To compare the presence of gasdermin D in the BV2 and J774 cells, a gasdermin D detecting Western blot was performed. The cells were stimulated with 3mM ATP and samples taken at 2, 4 or 6 hours, along with an unstimulated 6-hour control (Fig 4.15).

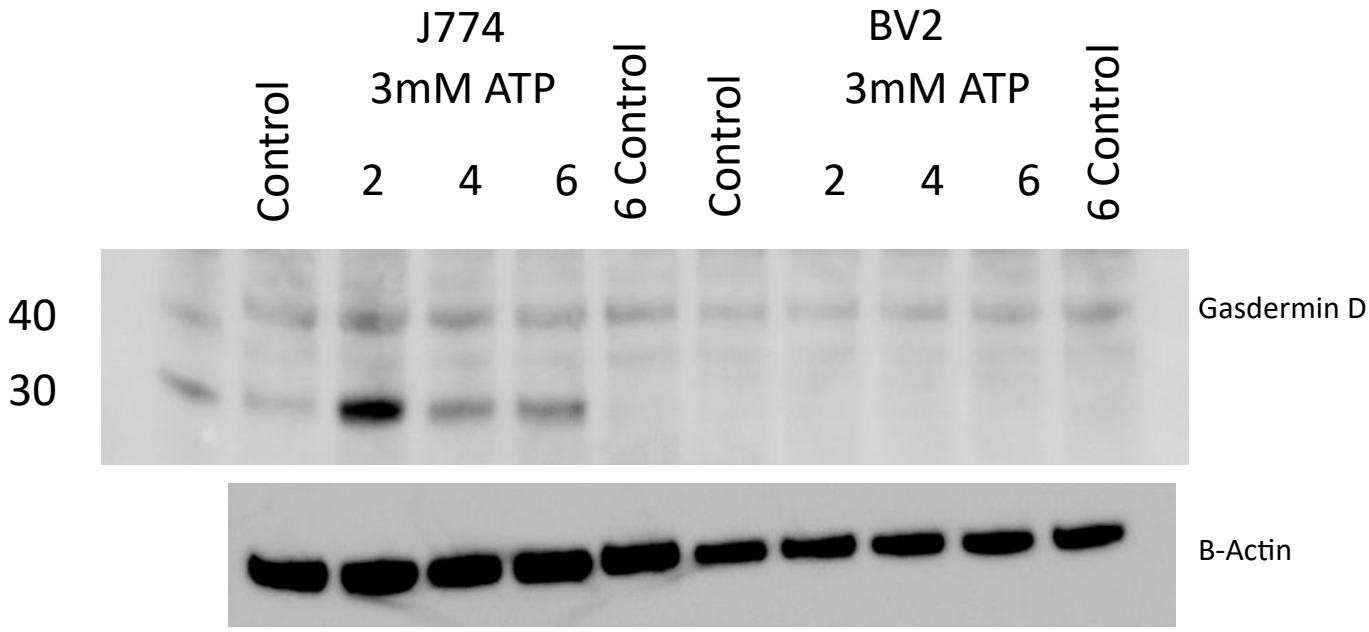

Figure 4.15 Cleaved Gasdermin D is present in J774 cells after ATP stimulation Western blot analysis of anti-gasdermin D antibody with J774 and Bv2 cells 2-, 4- and 6-hours after stimulation with 3mM ATP and controls at beginning and end time points. B-actin used as loading control (n=3).

In macrophages, the gasdermin D antibody identified two distinct bands. The first one was at 40kDa and the second at 30kDa. In microglia there was only one band at 40kDa. In J774 cells, the 2-hour timepoint 40kDa band appeared to increase in intensity before decreasing again at the 4-hour timepoint. The band at 30kDa, only present in the J774 cells, showed a stronger increase in signal at the 2-hour timepoint, which then decreased at the 4 and 6-hour time points but

remained stronger than control. In BV2 cells the band at 40kDa remains a consistent signal over the time course and no other bands are visible. The β-actin shows a consistent level of protein across the J774 and BV2 cells.

This Indicates that gasdermin D is present in both cell types but only the J774 cells show a change after ATP stimulation. This ties into the J774 and BV2 dye uptake results that in J774 cells ATP activates the pyroptotic pathway and that BV2 cells do not.

4.3 Discussion

Pyroptotic cell death has been shown to be a defined cell death mechanism in many macrophages (Fink and Cookson, 2006, Fink and Cookson, 2007). A standard technique to stimulate pyroptosis experimentally has been by LPS priming cells and then stimulating with a second stimulus such as ATP or nigericin. The aim of the research of this chapter was to characterise pyroptotic cell death in J774 cells, a macrophage cell line, to compare to the BV2 (microglia) cells used previously.

The J774 cell line was selected because, firstly, this is a mouse cell line, so the results could be compared to the BV2 cells. Also, the J774 cell line has been used extensively in research and has been involved in multiple studies looking at pyroptosis including stimulation with bacterial components (Wellington et al., 2014, Hu et al., 2014). The basis of the experimental methods used in this research, were taken from a study that looked at dye uptake and cell death in LPS primed macrophages that were stimulated with nigericin and ATP, and were pharmacologically blocked using necrosulfonamide (Rathkey et al., 2018).

Priming with LPS followed by stimulation of the mouse macrophage cell line showed an uptake of PI when stimulated with ATP or nigericin (Fig 4.1). This could be blocked using the gasdermin D inhibitor, necrosulfonamide. This replicated data from Rathkey indicating that the mouse macrophage behaves in the same way as human macrophages that pyroptosis could be a possible cause of this membrane disruption. This experiment was then performed using a wider array of ATP concentrations using YO-PRO and PI as the dye and for a longer time period reusing the same conditions as those used in the previous chapter when investigating microglia (Fig 4.2 and Fig 4.3). An ATP-dependent increase in membrane permeability was confirmed in the J774 cells, therefore, inhibitors for proteins linked to pyroptosis were used to help prove whether a pyroptotic process was involved in the dye uptake in the J774 cells.

The inflammasome sensor protein, NLRP3, seems to have a vital role in PI uptake in LPS primed J774 cells, whether the cells were stimulated with nigericin or ATP, as PI uptake was significantly reduced when the cells were incubated in the NLRP3 inhibitor, MCC950. When incubated in the caspase 1 inhibitor, Ac-YVAD-cmk, there was a significant drop in PI uptake for the cells stimulated with the higher concentrations of ATP, 3mM and 5mM, further suggesting a pyroptotic pathway involved in this mechanism. Finally, when the gasdermin D inhibitor, necrosulfonamide, was used a significant reduction in the higher concentrations of ATP and nigericin were seen. The cells incubated with AZ10606120 showed that there was no effect on PI uptake in the nigericin treated cells. This would be as expected as nigericin acts as an antiporter of H^+ and K^+ (Shavit et al., 1968) essentially bypassing the P2X7 receptor. For the highest concentrations of ATP, necrosulfonamide and AZ10606120 both caused a significant reduction in PI uptake, which is proof of the importance of P2X7 in this process alongside the importance of the pyroptosis proteins. This has

been shown previously in the J774 cell line with one paper showing that stimulation of P2X7 leads to widespread cell death in J774 cells (Coutinho-Silva et al., 2001). It identified this cell death mechanism as apoptosis, although no evidence was given to prove it was specifically apoptosis, only that the cells are allowing uptake of PI, which is also true for other mechanisms of cell death. Another paper showed blocking caspase 1 after ATP stimulation reduced pyroptotic cell death (Jin et al., 2013). Two other papers have also shown proof of pyroptotic mechanisms downstream from LPS priming and stimulation by ATP in J774 cells. One shows the presence of cleaved caspase 1 and IL-1β processing (Li et al., 2017), while the other revealed the presence of the cleaved pore forming section of gasdermin D (Shen et al., 2021).

All previous experiments used LPS priming before exposure to ATP. The experiments described in this chapter shows that LPS-priming is not a pre-requisite for ATP-induced pyroptosis in macrophages (Fig 4.9). All inhibitors were able to decrease PI uptake for the highest ATP concentrations. This shows solid proof that this is a pyroptotic process that is started by the activation of P2X7 by ATP. An important feature to notice in all the dye uptake experiments with the J774 cells when they are LPS primed (Fig 4.1-4.3, 4.5-4.8) but not in the presence of inhibitors, is that dye uptake occurs at around the 30-minute timepoint, a time point much sooner than seen in the BV2 cells in the previous chapter. This would suggest that the mechanism that is allowing the dye to enter the cell is the same for all stimulations, indicating that this time is needed for the production of the inflammasome and the cleavage of the gasdermin D pore. In the non-LPS primed cells this time is delayed to around the 1 hour timepoint. This is around the same as the BV2 cells in the previous chapter, although the pyroptotic inhibitors were unable to block the mechanism in the BV2 cells. This extra time in the J774 cells could be needed for the upregulation and creation of certain elements of the pyroptotic pathway. These elements could be upregulated already by LPS priming before stimulation in the LPS primed cells. The DAMP, ATP, alone is therefore capable of activating all the elements in the pathway.

An aspect of the stimulated cells with inhibitors is that most of the inhibitors reduced dye uptake but did not block it completely, with the exception of AZ10606120. After an initial blocking of the dye uptake the MCC950, AC-YVAD-cmk and necrosulfonamide, dye uptake started to occur sometime later over the time course. This would suggest that the dye had found a different route into the cell. This could have been through P2X7 itself (Ugur and Ugur, 2019) or it could be another pathway of cell membrane disruption, such as the non-canonical inflammasome pathway or another gasdermin protein, such as gasdermin E.

Therefore, the dye uptake data suggests that the mechanism by which the macrophages operate once they are stimulated with high levels of ATP, whether they are LPS primed or not, is pyroptotic. The cell death data for the J774 cells, however, have a more mixed outcome. The

inhibitors at the beginning of the pathway and the end of the pathway (AZ10606120 and necrosulfonamide) were able to show a significant reduction in the release of LDH. The inhibitors for the middle of the pathway, however, did not show statistical significance, which means MCC950 and Ac-YVAD-cmk are unable to block ATP induced cell death in the J774 cells. This could suggest that the inflammasome is bypassed allowing cell death to occur via P2X7 via a different route. This could possibly occur by either the non-canonical pyroptotic pathway or another form of cross talk that is found in cell death mechanisms. For example caspase 3 has been shown to cleave gasdermin E (Zeng et al., 2019) which would still lead to a lytic form of cell death, having bypassed the inhibited part of the pathway.

The results in the previous chapter, using BV2 microglia cells, showed that after stimulation with 3mM ATP, there was dye uptake, a loss of viability and the BV2 cells had a cell morphology that was swollen, rounded and had a clear loss of defined cell structure, a phenotype that is associated with pyroptotic cell death. However, the pyroptotic inhibitors had no impact, suggesting that pyroptosis does not play a role in ATP-mediated cell membrane disruption or cell death in the BV2 cells. However, in the previous chapter, the BV2 cells were not primed with LPS. As mentioned previously, LPS priming is a standard technique to experimentally stimulate pyroptosis. LPS priming was therefore investigated to see what effect this had and if this could prompt a pyroptotic mechanism (Fig 4.12 and 4.13). Unlike in macrophages no uptake of either YO-PRO or PI was seen when stimulated with LPS and nigericin, and there was no difference in the LPS and non-LPS primed cells when stimulated with any ATP concentration, suggesting that pyroptosis does not play a role in the dye uptake in the BV2 cells.

Comparing the J774 cell line and the BV2 cell line, and their respective mechanisms, the macrophage data suggests cell death and dye uptake are most likely occurring via the pyroptotic pathway whereas in microglia it is not.

Gasdermin D Western blot was used to further investigate this difference (Fig 4.15). A 50kDa gasdermin D signal present in both cell types, with this signal most likely being the full length gasdermin D protein. A protein at around 30kDa, which could be the cleavage product of gasdermin D, is only present in the macrophages and peaks 2 hours after ATP stimulation again suggesting that pyroptosis is occurring in this cell type. This was not seen in the BV2 cells, adding to the evidence that ATP does not activate pyroptotic mechanisms in microglial cells.

Contrary to this, other studies were able to induce pyroptosis in the BV2 cell line. Two separate studies have been able to cause a pyroptotic phenotype, with cleavage of both caspase 1 and gasdermin D with LPS priming of the cells alone (Xu et al., 2021, Yao et al., 2021). Another was able to show evidence of pyroptosis in BV2 cells caused by stimulation of the cells with the widely used anaesthetic, sevoflurane (Tian et al., 2021). Cleavage of caspase 1, gasdermin D and also

gasdermin E was seen after 6 hour incubation (Tian et al., 2021). Finally, another paper was able to stimulate PI dye uptake in the BV2 cells using LPS and nigericin as well as ATP, which was then blocked using mafenide, an antibiotic, that is thought to be a possible inhibitor for gasdermin D (Han et al., 2020). This was also alongside a Western blot that showed evidence of gasdermin D and its cleavage (Han et al., 2020). It is difficult to reconcile the data in both the previous chapter and this chapter with the published BV2 data that shows evidence of pyroptosis. One possible reason for the differing results could be down to the differences in cell culture techniques, specifically the serum used. One study found that different brands of FBS have different effects on cell protein production, namely IL-8, in human epithelial cell lines(Liu et al., 2023b). This study concluded that FBS has the biggest impact on immune related experiments. Another aspect that is difficult to control is the differences between the same cell line in different laboratories. Research previously that looked at HeLa cell lines and the cancer cell line MCF7 both showed that there was a massive diversity between the cells from one laboratory to the next (Ben-David et al., 2018, Liu et al., 2019). Clearly this can cause an issue in the pursuit of reproducibility. It could also be mentioned here that it is difficult to prove a negative and many negative results do not get published.

The data presented in this chapter show that upon ATP stimulation, macrophages follow a pyroptotic pathway, but that microglia cells do not. To further investigate and compare the cell death pathways of macrophages or microglia, techniques mentioned previously, such as the IL-1β and IL-18 ELISA, Annexin V staining or immunostaining for pyroptotic proteins, could be used. The results for these would be able to add more evidence to the differences between the two cell types. Another avenue to explore is gene expression analysis, such as qPCR. This would reveal which genes are being upregulated in macrophages and microglia after stimulation with ATP and the results compared.

A further finding was that LPS priming is not a necessary step despite most research including this in protocols investigating macrophage and microglial function. The question needs to be asked whether it is appropriate to use LPS in experiments investigating neuroinflammation as microglia will rarely encounter this molecule. There are, however, a broad range of different stressors microglia can come into contact with in the CNS. Therefore, it seems important to investigate other insults to see if the mechanism of changes in cell membrane disruption, cell death or cell morphology could be characterised. This will be explored in the next chapter.

Chapter 5

The Effects of Pathophysiological Insults on microglia

5.1 Introduction

The use of the bacterial cell wall component, LPS, for activation of immune cells raises the question of the challenges that microglia are likely to encounter in the CNS. Due to the blood-brain barrier (BBB), entry to the CNS is highly regulated, so the presence of pathogens in the CNS would only happen in rare occurrences. To put this in perspective, data shows that during the years 1990-2016 there were only around half a million CNS infection cases globally (Robertson et al., 2018) while in the year 2019 alone 55 million people are living with Alzheimer's disease, a neurodegenerative condition (GBD, 2022) and in 2013, it was believed 64.3 million people suffered from glaucoma caused blindness with this figure projected to increase to 111.8 million by 2040 (Tham et al., 2014). In the year 2020 alone, it was thought 3.6 million people over the age of 50 received a glaucoma diagnosis (GBD, 2021). The pathophysiological insults that microglia encounter in the CNS, including the retina, include loss of nutrient supply, such as during an ischaemic episode, and inflammation linked states such as oxidative stress and pH changes. There are also stresses linked specifically to disease states for example amyloid β that is found in Alzheimer's disease and has been found to be present in the retina during glaucoma. These physiological stressors are discussed in more detail below.

5.1.1 Amyloid β

Alzheimer's disease is a neurodegenerative condition that affects memory, cognitive function and mood which eventually leads to death. It is thought to be responsible for 60-70% of dementia cases with the number of people suffering from the condition projected to increase to 170 million by 2050 (GBD, 2022). While the cause of Alzheimer's disease is not fully understood, a key element in the progression is thought to revolve around the amyloid protein (Discussed previously in Section 1.1.2).

Amyloid β has also been implicated in glaucoma. Levels of amyloid β in vitreous fluid was found to significantly change in patients with glaucoma when compared to a healthy control (Yoneda et al., 2005). Another study showed deposition of amyloid β in the RGC layer caused apoptosis in a mouse glaucoma model (Guo et al., 2007), while in a mouse model for Alzheimer's disease amyloid β deposits were detected in the RGC layer as the mice aged which led to retinal degeneration (Ning et al., 2008). In a study that looked at the retina and optic nerve head of monkeys that had chronic ocular hypertension, amyloid β was found to increase in concentration in the retina in the chronic stages of glaucoma (Ito et al., 2012).

5.1.2 Oxidative stress

Oxidative stress is caused by the abundance of reactive oxygen species (ROS). ROS are a family of chemicals formed by O_2 that are highly reactive and include H_2O_2, super oxide and hydroxyl atoms. ROS production is both enzymatic and non-enzymatic and is generated endogenously from processes inside the cell and exogenously by exposure to environmental factors. Endogenous ROS production is caused by a number of natural processes and disease states such as immune cell activation, the respiratory process, inflammation, cancer, infection, ischaemia and aging (Liguori et al., 2018). Exogenous causes of ROS production occur due to the presence of airborne pollutants, heavy metals, drugs, cooking, smoking, alcohol and ionising radiation (Liguori et al., 2018).

ROS play key roles in a range of cell processes such as host defence, proliferation, cell signalling and cell death (Abdal Dayem et al., 2017). In high concentrations, ROS cause damage to important cell components such as proteins, cell membranes and DNA (Singh et al., 2019). For example, ROS are known to damage the membrane and DNA of mitochondria which leads to mitochondrial disruption which itself creates more ROS (Singh et al., 2019). Another action of ROS, is that they may prevent immune responses and lead to immunosuppression (Mittler, 2017).

Not surprisingly, oxidative stress has also been found to play an important role in various diseases, such as cancers, cardiovascular disease, glaucoma and neurodegenerative diseases such as Parkinson's disease and Alzheimer's disease (Liguori et al., 2018). Evidence of the presence of oxidative stress in Alzheimer's disease was first shown in human brain sections of people who suffered from the condition (Pappolla et al., 1992). It is now thought that oxidative stress plays a role in both causing Alzheimer's disease and also its progression. Oxidative stress is thought to influence amyloid β aggregation and plaque formation (Bai et al., 2022). In addition, ROS lead to the activation of microglia and astrocytes, creating an inflammatory environment which itself facilitates the assembly of amyloid β plaques (Bai et al., 2022). The presence of plaques has been found to lead to the creation of further ROS which in turn leads to further oxidative stress. This then causes neuronal cell death leading to the progressive deterioration of brain function (Bai et al., 2022).

ROS are also thought to have a role in the progression of glaucoma (Chrysostomou et al., 2013). For example, the creation of ROS was found to increase in a rat glaucoma model which then led to an increase in lipid peroxidation in the retina (Ko et al., 2005). Another study in humans found that ROS led to DNA damage in the trabecular meshwork, which caused a degeneration of the structure (Saccà et al., 2005). Furthermore, use of a free radical scavenger treatment in a glaucoma model in rats found that the RGCs had an increase chance of survival (Ko et al., 2000). Another hypothesis considering the contribution of oxidative stress, suggests that light hitting the retina may be an aggravating event affecting progression of glaucoma. As light reaches the retina,

the mitochondria in the RGCs start to produce energy and therefore ROS, but due to the lack of blood flow, caused by the early stages of glaucoma, the ROS cannot be cleared fast enough leading to damage being caused to proteins, membranes and DNA (Osborne et al., 2006).

A chronic state of oxidative stress, caused by ROS, induces cell damage and neurodegeneration in the CNS (Solleiro-Villavicencio and Rivas-Arancibia, 2018). During this chronic oxidative stress, ROS create an inflammatory state due to constant activation of inflammatory signalling pathways, which promote the deregulation of the inflammatory response (Solleiro-Villavicencio and Rivas-Arancibia, 2018). ROS has been found to create conditions that allow for the constant secretion of pro-inflammatory cytokines and chemokines (Chan, 2001, Hsieh and Yang, 2013) and also have the ability to activate microglia (Pawate et al., 2004).

5.1.3 pH

Another aspect of inflammation that could impact local cells is pH changes, with studies showing that pH levels can drop as low as pH5.5 in some instances (Simmen and Blaser, 1993, Simmen et al., 1994). Acidosis of the local area can occur by conditions including an accumulation of bacteria (Rotstein et al., 1987, Rotstein et al., 1989), a build-up of lactic acid due to certain metabolic changes (Menkin and Warner, 1937) or autoimmune and other inflammatory conditions such as rheumatoid arthritis (Ward and Steigbigel, 1978, Geborek et al., 1989, Månsson et al., 1990). A drop in pH to pH6.5-6.0 have been found in the brain following ischaemia during a stroke (Gebert et al., 1971, Nedergaard et al., 1991).

There has been evidence to show that cells are able to detect pH changes by various classes of proteins. These proteins include GPCRs (Ishii et al., 2005, Radu et al., 2005, Liu et al., 2010), acid-sensing ion channels (ASICs) (Wemmie et al., 2013) and the transient receptor potential channel vanilloid subfamily 1 (TRPV1) (Aneiros et al., 2011). All of these proteins have been found to be expressed on immune cells including microglia (Zha et al., 2022).

The role of pH in disease has had little investigation. For glaucoma, however, one study found that an increase in IOP in a rabbit model led to a drop in pH of the vitreous, from 7.3 to 7.0, which caused an increase in retinal cell death (Lu et al., 2001). In Alzheimer's disease a study that used an organotypic brain slice model found a drop in pH, down to pH 6.6, which damaged the capillary endothelial cells and cholinergic neurons. This indicates that low pH would have severe negative effects on the cerebral microenvironment (Pirchl et al., 2006).

5.1.4 Ischaemia

Another inflammatory trigger that can occur in the body is ischaemia. This is a state in which a tissue or organ is not being delivered essential nutrients, such as oxygen or glucose, needed for

survival. This state can also create other issues, as the impaired delivery system is also unable to remove harmful waste products.

Ischaemia, a lot like the other pathophysiological insults discussed in this section, establishes an environment that creates further pathophysiological stresses. Due to the metabolic disruption of ischaemia, an increase in ROS production occurs and also pH changes, where pH can drop by at least 1 unit, for example, due to the increase in anaerobic glycolysis, ATP hydrolysis causing the release of acidic components, such as lactic acid and protons (McQueen, 2010).

The link between Alzheimer's disease and ischaemia has been suggested, in numerous investigations, that both conditions are a factor that contributes to the other (Pluta, 2022). Deposition of Amyloid-β in the walls of arteries in the brain have been found to create lesions and brain bleed, in a condition termed cerebral amyloid angiopathy (Rost et al., 2022). Ischaemia has been found to help in the creation of Alzheimer's by upregulating certain proteins linked to the disease (Pluta, 2022).

Ischaemia is also thought to play an important role in the cause and progression of glaucoma, as retinal function is very sensitive to changes in haemoglobin oxygen saturation (Brandl and Lachenmayr, 1994). This is thought to mainly be caused by the local blood flow becoming compromised, by either elevated or oscillating IOP, coupled with vascular dysfunction, which leads to repeated hypoperfusion (Flammer et al., 2002, Mozaffarieh et al., 2008, Chan et al., 2017). This ischaemia is detrimental to the cells of the retina, with one study showing that, after a reduction in blood flow, rat RGCs at the optic nerve head start to degrade (Chidlow et al., 2017). Ischaemic damage has also been shown to lead to an increase in an inflammatory environment, as inflammatory cells, such as microglia (Ivacko et al., 1996), infiltrate the damaged tissue and release pro-inflammatory mediators, such as IL-1β and TNF-α (Sivakumar et al., 2011).

The aims of the research in this chapter were to investigate known pathophysiological stressors occurring in the CNS, including the retina, specifically looking at their effects on BV2 microglial cell death and also activation. These pathophysiological stressors include amyloid-β, oxidative stress, pH change and ischaemia all of which are found in various neurodegenerative diseases. The amyloid-β used in this research was the 25-35 residue peptide, oxidative stress was created using H_2O_2, ischaemic conditions were created using OGD and pH was tested by exposing the cells to a range of acidic and alkaline pHs. These were compared with the "standard" neuroinflammatory stress, LPS. Due to the role P2X7 has been found to play in the inflammation process and cell death, the role of P2X7 receptor in the response to the pathophysiological stressors was also considered by investigating the stress in P2X7K/O variant of BV2 microglia cells. All of the experiments were carried out for 12 hours as it was hypothesised that changes would occur over a longer time period than had previously investigated.

5.2 Results

5.2.1 LPS has no effect on cell death or cell morphology in BV2 Microglia

The effect on cell viability and cell death of LPS, on both the WT and the P2X7K/O variant BV2 cells, was investigated. In research, LPS is the most widely used stimulant for activation of immune cells as a model for bacterial infection. In this chapter LPS will be used as the basis for comparison with the other pathophysiological insults investigated.

The cells were incubated with a range of LPS concentrations (0-5µg/ml) for 12 hours and then the levels of cell death (LDH) and viability (MTS) measured. For both measures (Fig 5.1) very little change was observed. There was a trend of increasing levels of LDH release, although with no corresponding change in cell viability, in both the WT and the P2X7K/O variant BV2 cells as the concentration of LPS increased, no significant difference was seen. Either with concentration or between the WT or the P2X7K/O variant BV2 cells. Images of the cells were taken at the end of the experiment to see what effect LPS had on the cell morphology (Fig 5.2). When comparing all the cells stimulated with LPS (0.1µg/ml-5µg/ml) against the control, cell morphologies had not been changed after 12 hours.

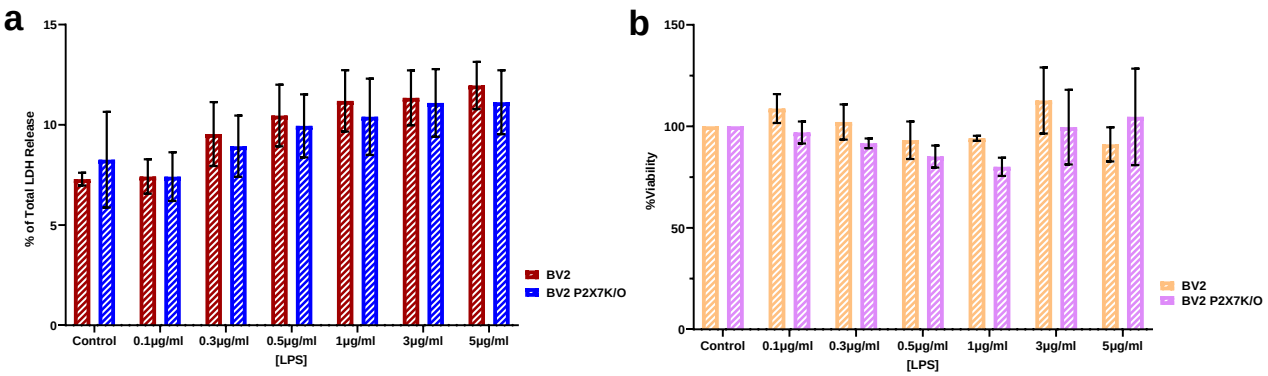

Figure 5.1 LPS does not cause cell death changes in BV2 Microglia (a) Mean % LDH release after 12 Hours in BV2 and P2X7K/O BV2 microglial cells in response to increasing concentrations of LPS (0-5µg/ml) (n=3) (b) Mean % Viability release after 12 Hours in BV2 and P2X7K/O BV2 cells in response to increasing concentrations of LPS (0-5µg/ml) (n=3) * Indicates significance compared to control ($P<0.05$) using one-way ANOVA with Dunnett's post hoc test.

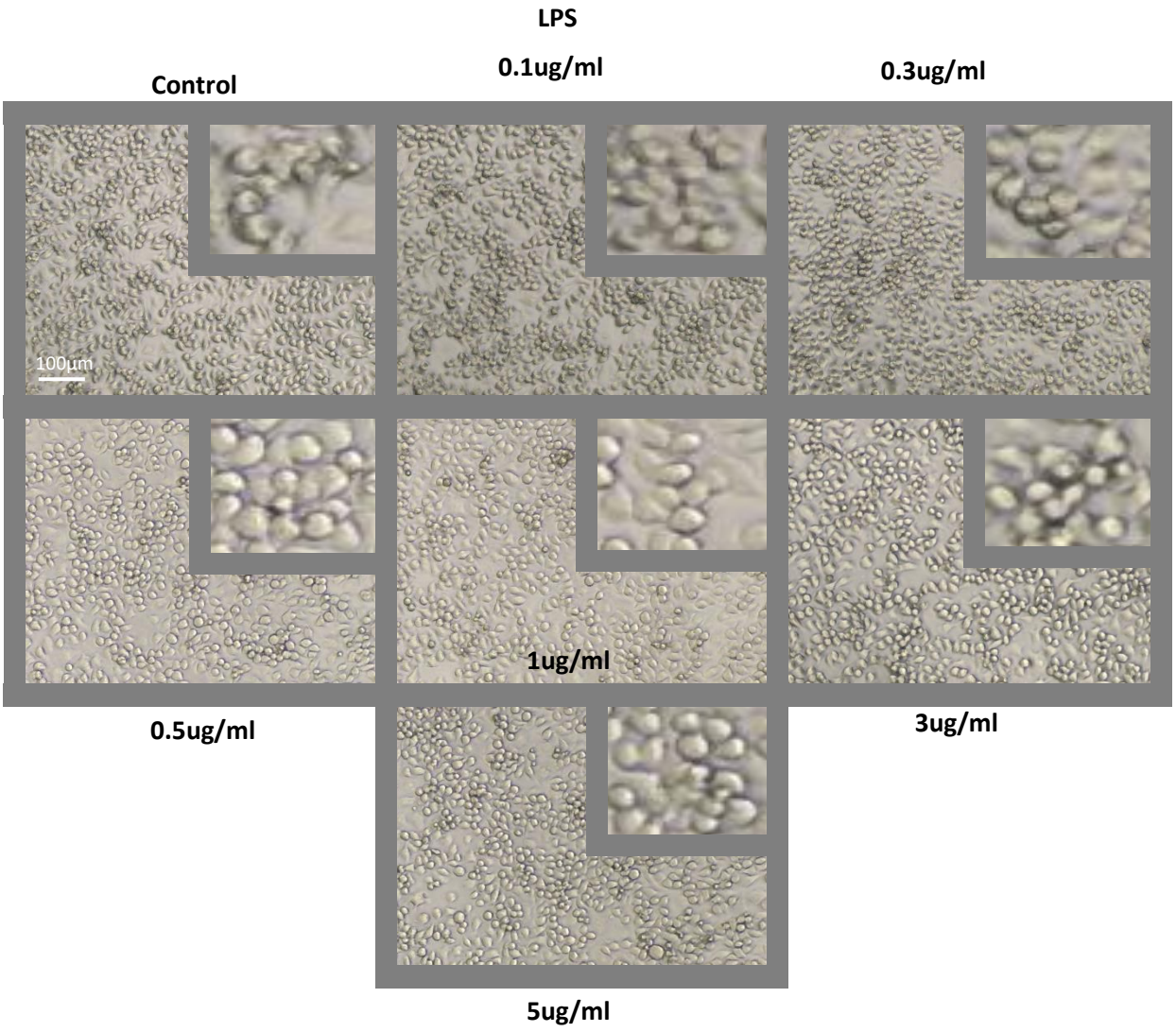

Figure 5.2 LPS does not cause changes in cell morphology Effect of a range concentrations of LPS (0-5µg/ml) on BV2 cells after 12 hours. Inset shows representative cell morphology at 12 hours (5x digital zoom)

5.2.4 Amyloid β causes cell death, dye uptake and morphological changes in BV2 Microglia

The next pathophysiological condition to be investigated was amyloid-β, an important protein involved in the progression of Alzheimer's Disease. To explore this, the BV2 and the P2X7K/O BV2 cells were incubated in a range of amyloid-β (25-35) concentrations (0-100µM) over the course of 12 hours and then the levels of cell death and cell viability were measured. The levels of cell death (Fig 5.3a) showed that there was a trend of increasing cell death as the concentration of amyloid-β increased from 30µM and above. This reached statistical significance after stimulation with 100µM amyloid-β. This was true for both the BV2 and the P2X7K/O variant BV2 cells. The viability assay (Fig 5.3b), show a comparative story to that of the cell death data. At lower concentrations (5µM and 10µM amyloid-β) there was no change in viability. Exposure of the cells to 30µM amyloid-β showed a decrease in viability, with larger reductions seen at both 50µM and 100µM amyloid-β. Again, no difference was seen between the WT and P2X7K/O cells.

Comparing the WT BV2 and the P2X7K/O variant BV2 cells, the WT BV2 cells had a consistently larger reduction in viability when compared to the P2X7K/O variant BV2 cells stimulated with the same concentration of amyloid-β, but no statistical significance was reached.

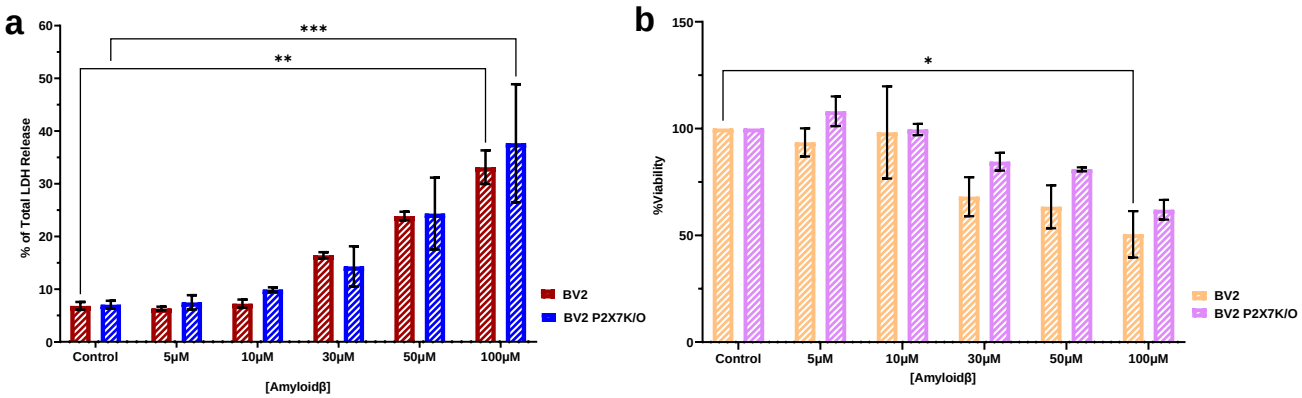

Figure 5.3 Amyloid β causes cell death and loss of cell viability in BV2 microglia (a) Mean % LDH release after 12 Hours in BV2 and P2X7K/O BV2 microglial cells in response to increasing concentrations of amyloidβ (0-100µM) (n=3) (b) Mean % Viability release after 12 Hours in BV2 and P2X7K/O BV2 microglial cells in response to increasing concentrations amyloidβ (0-100µM) (n=3) * Indicates significance compared to control ($P<0.05$) using one-way ANOVA with Dunnett's post hoc test.

At the end of cell death assay experiments, the cells were imaged to see if any changes in cell morphology had occurred (Fig 5.4). For the lower concentrations (5µM and 10µM) the cells appeared very similar to the control, with no changes seen in cell morphology. From 30µM amyloid-β and above, there was some evidence of the cells starting to cluster. This became more pronounced as the concentration of amyloid-β was increased, with decreased density, increased spaces and clusters becoming apparent.

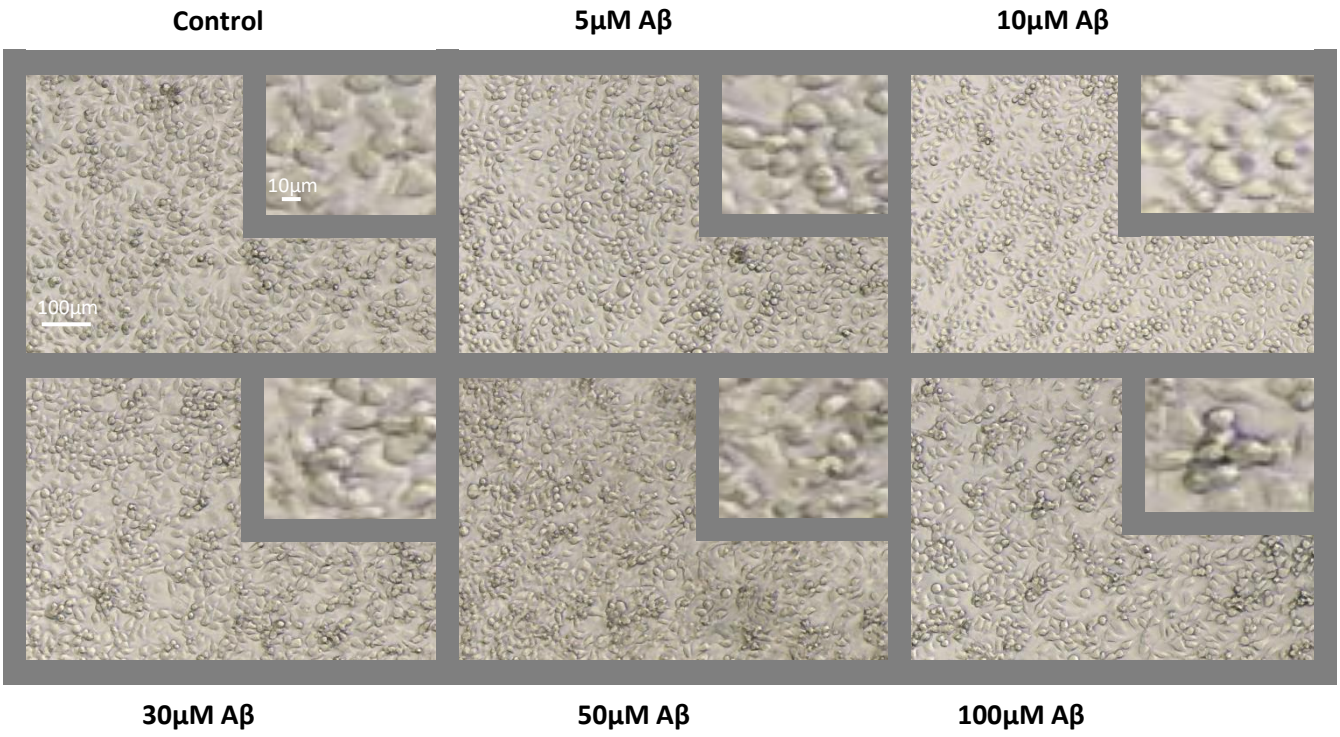

Figure 5.4 Amyloid β exposure causes BV2 microglia to cluster Effect of a range concentrations of amyloidβ (0-100µM) on BV2 cells after 12 hours. Inset shows representative cell morphology at 12 hours (5x digital zoom).

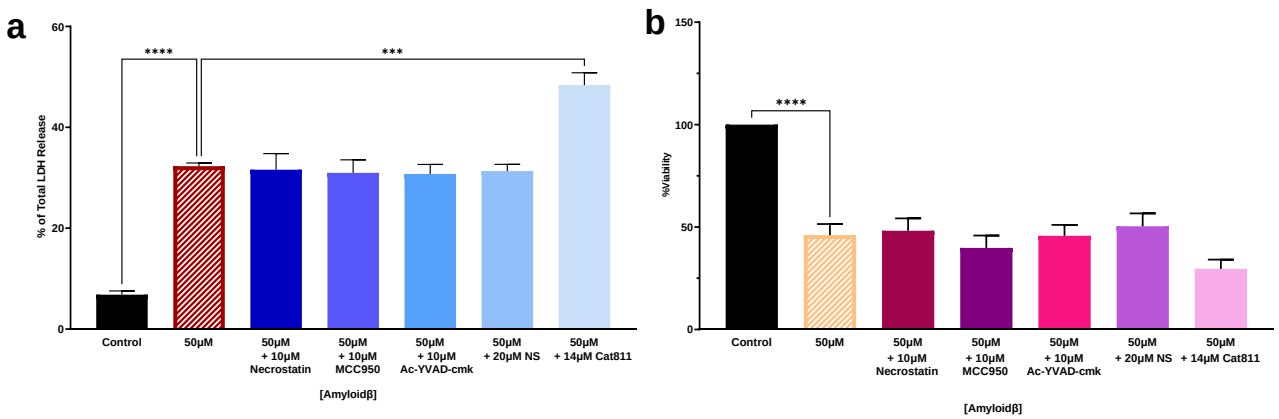

Figure 5.5 Amyloid β-induced cell death in BV2 microglia is altered by inhibition of calpain (a) Mean % LDH release after 12 Hours in BV2 microglial in response to increasing concentrations of amyloid-β (0-100µM) (n=3) ± Necrostatin 10µM, MCC950 10µM, Ac-YVAD-cmk 10µM and Necrosulfonamide 20µM, Cat811 14µM (b) Mean % Viability release after 12 Hours in BV2 microglial cells in response to increasing concentrations of amyloid-β (0-100µM) (n=3) ± Necrostatin 10µM, MCC950 10µM, Ac-YVAD-cmk 10µM and Necrosulfonamide 20µM, Cat811 14µM * Indicates significance compared to control (P<0.05) using one-way ANOVA with Dunnett's post hoc test.

Since cell death increased and viability decreased with amyloid-β, the possible mechanisms involved in the cell death process were investigated. The cells were stimulated with 50µM amyloid-β while also incubated with various inhibitors, then cell death and cell viability were measured after 12 hours (Fig 5.5). The inhibitors used in this experiment were MCC950 (inflammasome sensor protein inhibitor), Ac-YVAD-cmk (caspase 1 inhibitor), necrosulfonamide (gasdermin D inhibitor), necrostatin (RIPK1 inhibitor), and CAT811 (calpain 2 inhibitor). None of the inhibitors used reduced amyloid-β-induced cell death, but CAT811 caused a statistically significant increase in cell death over the 12 hours. Corresponding decreases in cell viability were seen (Fig 5.5b) although the further decreased cell viability with CAT811 was not significant.

To investigate the effects of amyloid-β on cell permeability, dye uptake experiments using either PI (Fig 5.6) or YO-PRO (Fig 5.14) were performed. The BV2 cells and the P2X7K/O variant, were stimulated with a range of amyloid-β concentrations (0-100μM) over the course of 6 hours. In WT BV2 cells (Fig 5.6a). There was a dose dependent increase in PI uptake in response to amyloid-β. The time course showed a relatively linear increase in concentrations 10μM -50μM amyloid-β. However, 100μM amyloid-β showed a rapid uptake between 10-50 minutes.

In the P2X7K/O variant BV2 cells (Fig 5.6b) the uptake followed the same trends as the WT BV2 cells, however, the PI uptake with 100μM amyloid-β did not show the rapid initial stage as that seen in the WT BV2 cells. This is reflected in the AUC data although decreased dye uptake at 100μM amyloid-β was not significantly different between the two variants.

When this was repeated with YO-PRO (Fig 5.7), there is a similar story to that seen with PI. Amyloid-β increased influx in a dose dependant manner but without any observable differences between the WT and P2X7K/O cells (Fig 5.7a and b).

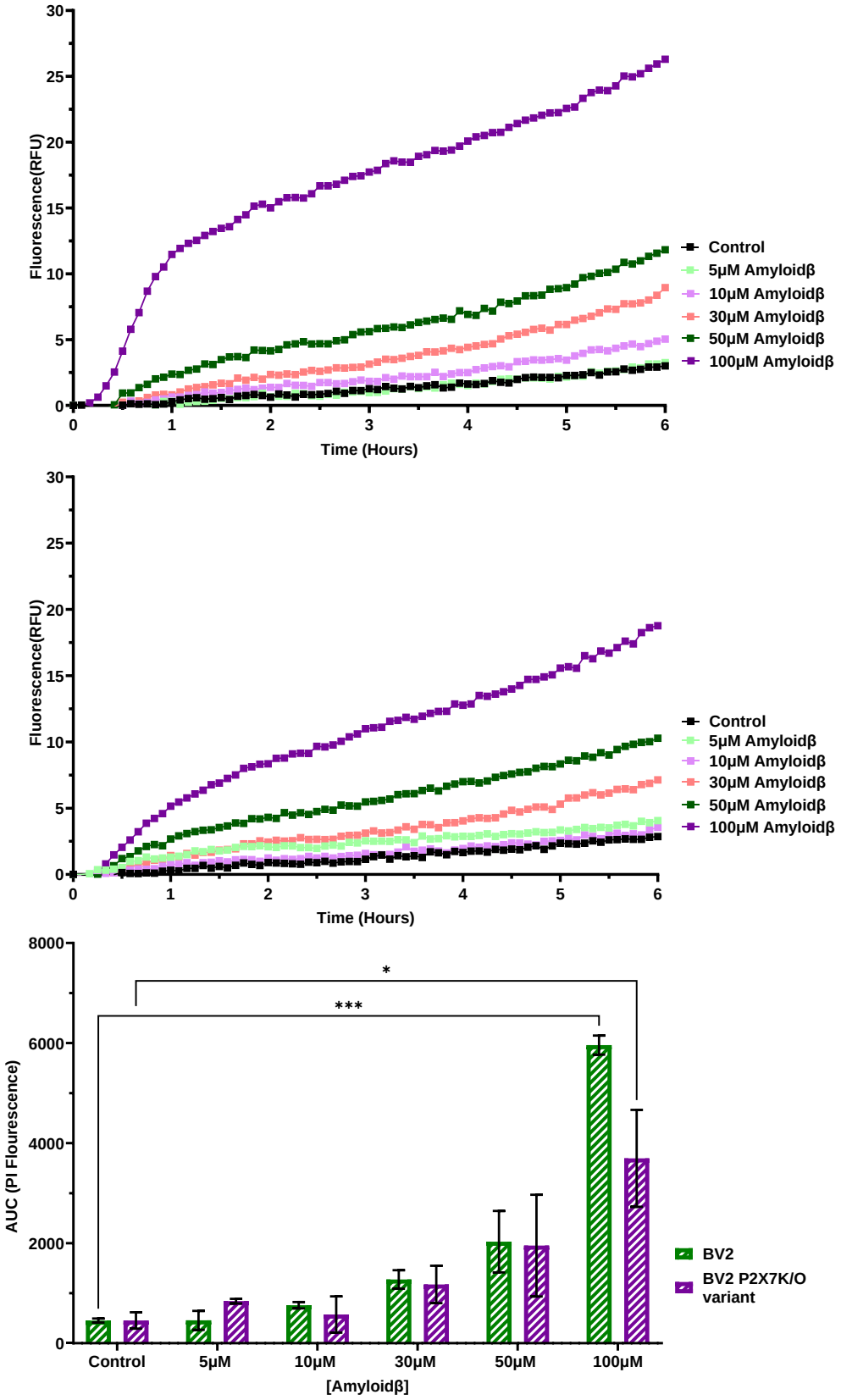

Figure 5.6 Exposure of BV2 and the P2X7K/O BV2 microglial cells to Amyloid β causes PI uptake (a) Mean PI uptake in BV2 microglial cells in response to increasing concentrations of amyloidβ (0-100μM) (n=2) (b) Mean PI uptake in P2X7K/O BV2 microglial cells in response to increasing concentrations of amyloidβ (0-100μM) (n=2) (c) PI (AUC 0-360 Mins) (Mean+SEN; n=2) * Indicates significance (P<0.05) using two-way ANOVA with Sidak's post hoc test.

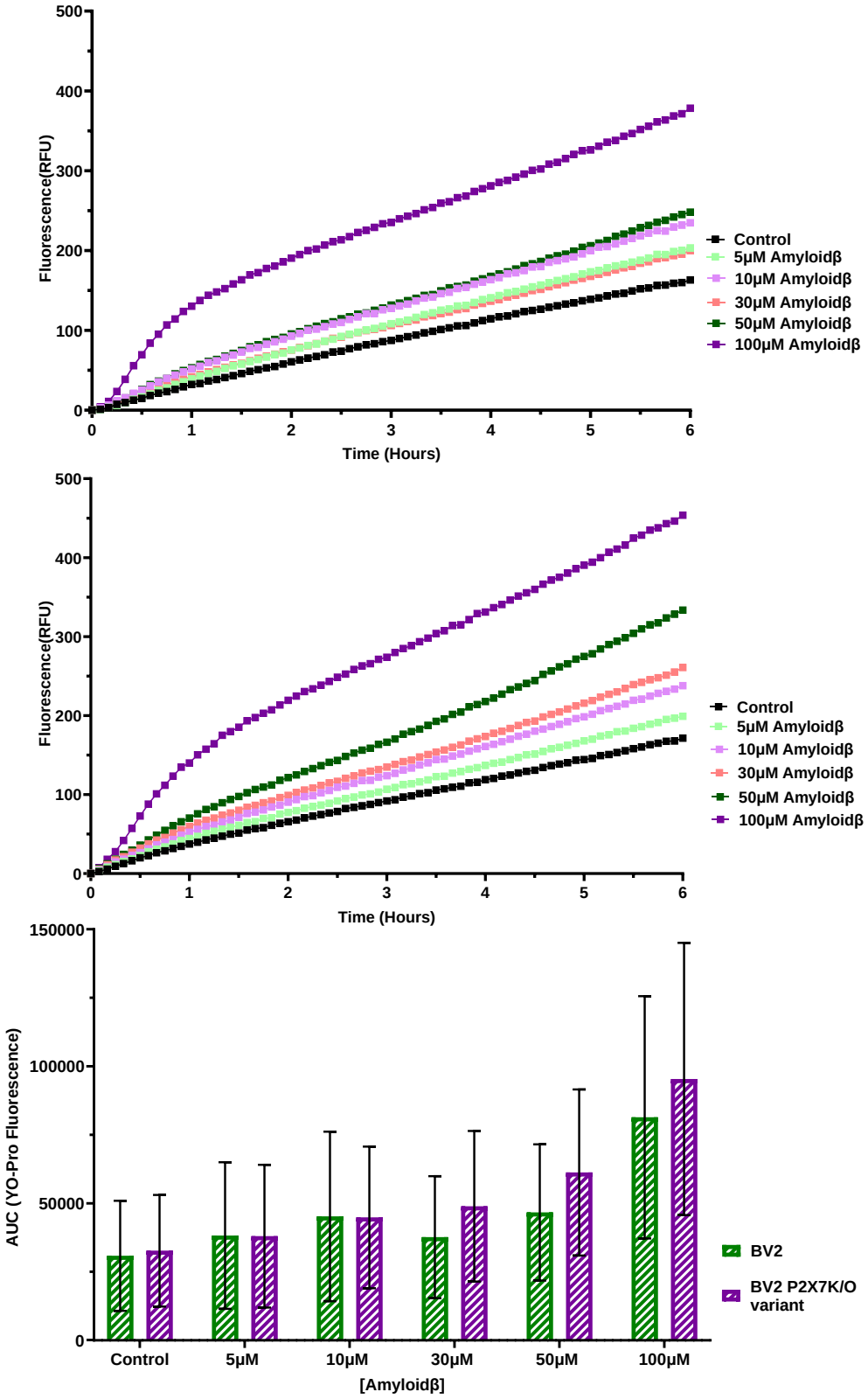

Figure 5.7 Exposure of BV2 and the P2X7K/O BV2 microglial cells to Amyloid β causes YO-PRO uptake (a) Mean YO-PRO uptake in BV2 microglial cells in response to increasing concentrations of amyloidβ (0-100μM) (n=3) (b) Mean YO-PRO uptake in P2X7K/O BV2 microglial cells in response to increasing concentrations of amyloidβ (0-100μM) (n=3) (c) PI (AUC 0-360 Mins) (Mean+SEN; n=3) * Indicates significance (P<0.05) using two-way ANOVA with Sidak's post hoc test.

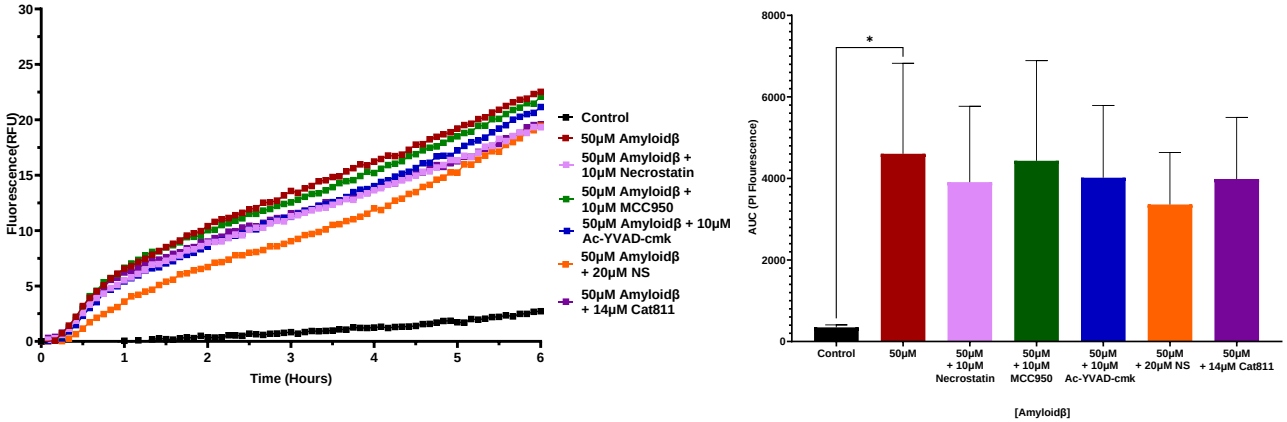

Figure 5.8 Cell death associated protein Inhibitors do not alter Amyloid β-induced PI uptake in BV2 microglia (a) Mean PI uptake in BV2 microglia cells in response to 50μM amyloidβ ± Necrostatin 10μM, MCC950 10μM, Ac-YVAD-cmk 10μM and Necrosulfonamide 20μM, Cat811 14μM (b) PI uptake (AUC 0-360mins) (mean +SEM, n=3) * indicates significance compared to control (P<0.05) using a one-way ANOVA with Dunnett's post hoc test.

Next the dye uptake experiments were repeated, with both PI and YO-PRO, to look at whether the amount of dye uptake with 50μM amyloid-β could be changed when incubated with the inhibitors used previously (Fig 5.8 and 5.9). The PI uptake (Fig 5.8a) and their associated AUC graphs (Fig 5.8b) showed that the inhibitors had no effect on dye uptake. The YO-PRO dye uptake (Fig 5.9a) showed a slight decrease in the uptake with all the inhibitors when compared to the cells stimulated with 50μM amyloid-β alone. The gasdermin D inhibitors, necrosulfonamide, caused the biggest drop. The AUC data, however, revealed that these reductions were not statistically significant.

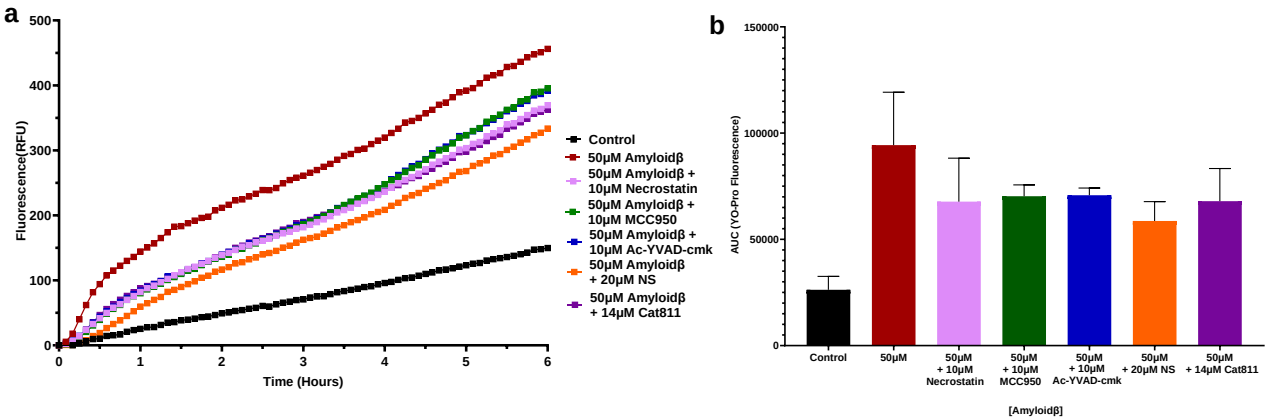

Figure 5.9 Cell death associated protein Inhibitors do not alter Amyloid β-induced YO-PRO uptake in BV2 microglia (a) Mean YO-PRO uptake in BV2 microglia cells in response to 50μM amyloidβ ± Necrostatin 10μM, MCC950 10μM, Ac-YVAD-cmk 10μM and Necrosulfonamide 20μM, Cat811 14μM (b) YO-PRO uptake (AUC 0-360mins) (mean +SEM, n=2) * indicates significance compared to control (P<0.05) using a one-way ANOVA with Dunnett's post hoc test.

5.2.3 Oxidative stress causes cell death, dye uptake and morphological changes in BV2 Microglia

The next condition investigated that microglia are likely to experience in the nervous system was oxidative stress. The oxidising agent H_2O_2 was used as the oxidative stress.

First cell death (LDH) and viability assays (MTS) were performed to investigate the effect of oxidative stress on both the WT BV2 and the P2X7K/O variant BV2 cells. The cells were stimulated with a range of H_2O_2 concentrations (100µM-5mM) for 12 hours after which the level of cell death and cell viability was measured and the morphology of the cells observed. All concentrations of H_2O_2 caused an increase in cell death for both the WT BV2 and the P2X7K/O variant BV2 cells when compared to the relevant controls (Fig 5.10a).

In the comparison between the WT BV2 and the P2X7K/O variant BV2 cells there was a slight increase in LDH release at the higher concentrations that stimulated the P2X7K/O variant BV2 cells (3mM and 5mM H_2O_2) but this increase is not statistically significant when compared with the WT BV2 cells. The cell viability assay (Fig 5.10b) showed that all concentrations caused a large reduction in viability. There was no difference between the stimulated WT BV2 cells and stimulated P2X7K/O variant BV2 cells.

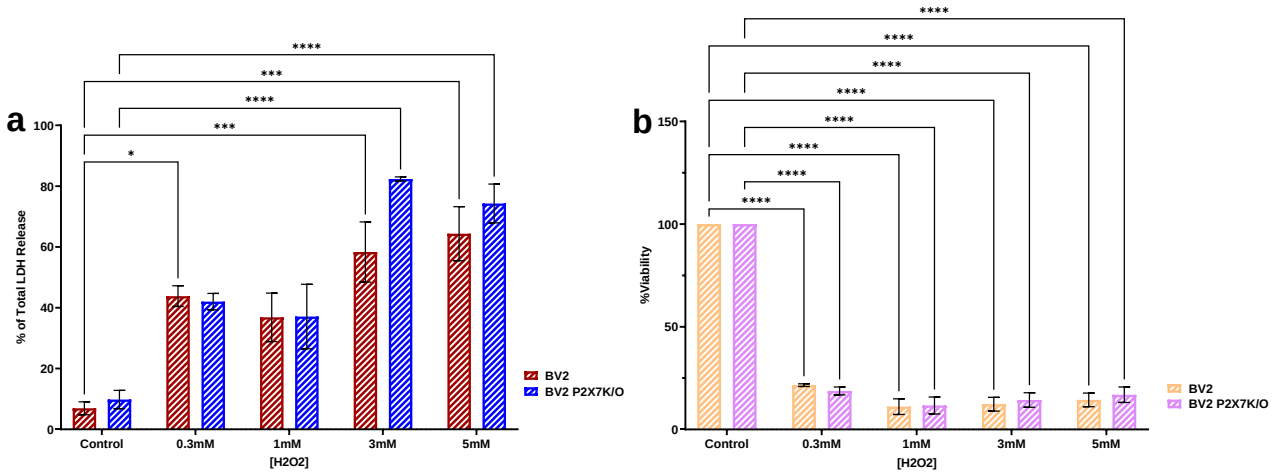

Figure 5.10 Oxidative stress causes cell death and loss of cell viability in BV2 microglia
(a) Mean % LDH release after 12 Hours in BV2 and P2X7K/O BV2 microglial cells in response to increasing concentrations of H_2O_2 (0-5mM) (n=3) (b) Mean % Viability release after 12 Hours in BV2 and P2X7K/O BV2 microglial cells in response to increasing concentrations of H_2O_2 (0-5mM) (n=3) * Indicates significance compared to control ($P<0.05$) using one-way ANOVA with Dunnett's post hoc test.

The cells were imaged at the 12 hour time point (Fig 5.11). Firstly, the control is what would be expected, the plate looks fully covered, packed with cells and no spaces between them. Moving up to the 300µM H_2O_2 stimulated cells, there appears to be more gaps between the cells and some of the cells have a more myeloid shape. This is even more apparent in the cells stimulated with 500µM and 1mM H_2O_2, which have a drastically reduced cell presence and all the cells that are left are in a myeloid configuration. For the highest concentrations, 3mM and 5mM H_2O_2, there are more cells visible when compared to the other stimulated cells but compared to the control these cells are clearly shrunken and not viable.

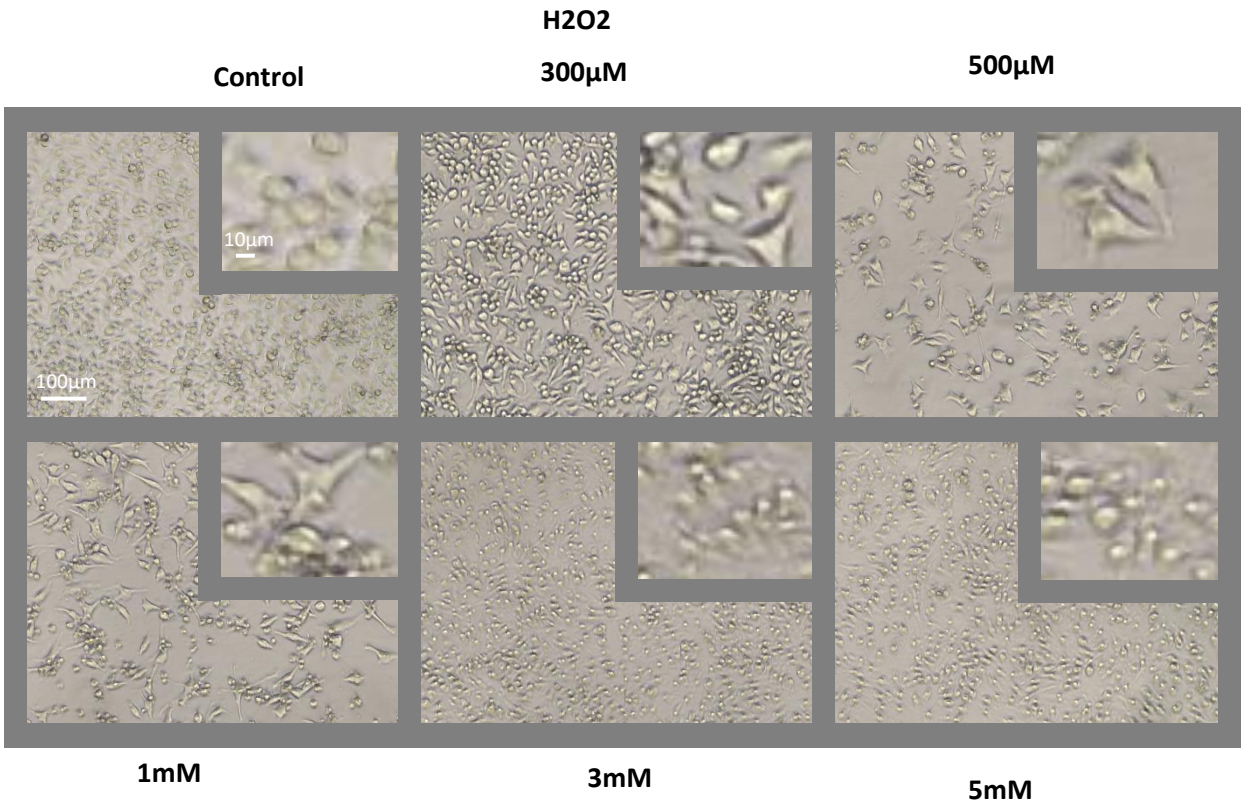

Figure 5.11 Oxidative stress causes cell morphology changes in BV2 microglia Effect of a range concentrations of H_2O_2 (0-5mM) on BV2 cells after 12 hours. Inset shows representative cell morphology at 12 hours (5x digital zoom)

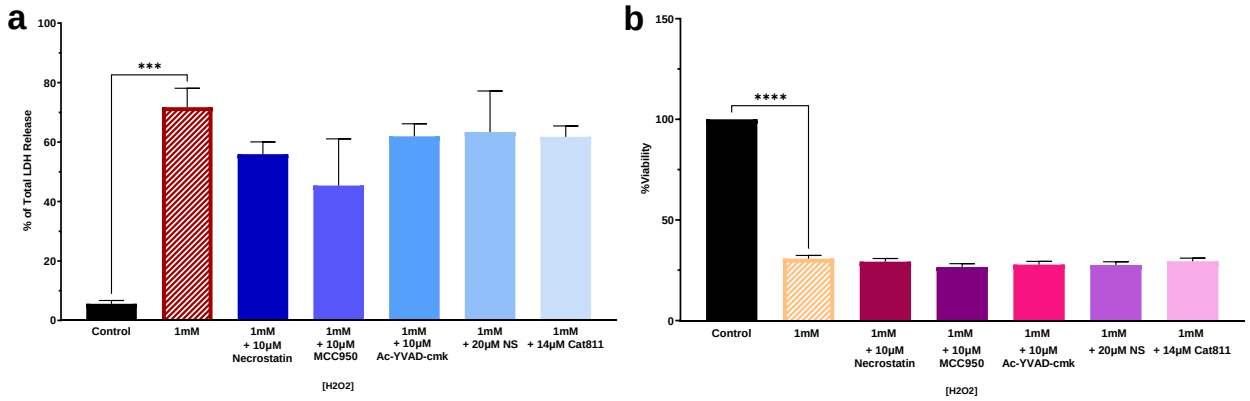

Figure 5.12 Cell death associated protein Inhibitors do not alter Oxidative stress-induced cell death and loss of cell viability in BV2 microglia (a)) Mean % LDH release after 12 Hours in BV2 microglial in response to 1mM H_2O_2 (n=3) ± Necrostatin 10µM, MCC950 10µM, Ac-YVAD-cmk 10µM and Necrosulfonamide 20µM, Cat811 14µM (b) Mean % Viability release after 12 Hours in BV2 microglial cells in response to 1mM H_2O_2 (n=3) ± Necrostatin 10µM, MCC950 10µM, Ac-YVAD-cmk 10µM and Necrosulfonamide 20µM, Cat811 14µM * Indicates significance compared to control (P<0.05) using one-way ANOVA with Dunnett's post hoc test.

Next, cell death and viability change in response to 1mM H_2O_2 was measured in the presence and absence of the inhibitors of cell death pathways (Fig 5.12). First, levels of cell death (Fig 5.12a), showed a statistically significant increase in LDH release after stimulation with 1mM H_2O_2, as seen before in the previous LDH release data (Fig 5.10a). The only inhibitor that caused a notable decrease was the NLRP3 antagonist, MCC950, however this was not statistically significant. The viability data (Fig 5.12b), showed the expected statistically significant drop in viability after stimulation with 1mM H_2O_2. In this case no effect could be seen with any of the inhibitors.

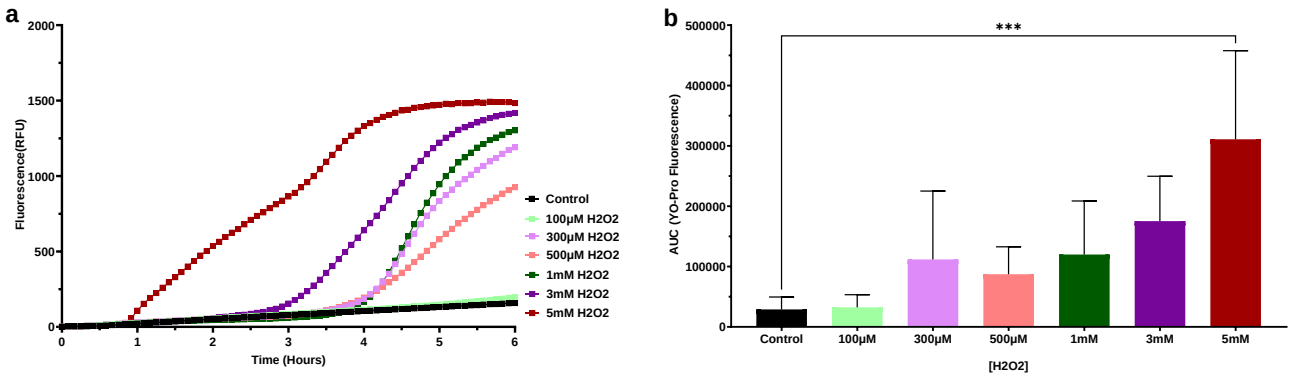

Figure 5.13 Oxidative stress causes YO-PRO uptake in BV2 microglia (a) Mean YO-PRO uptake in BV2 macrophage cells in response to increasing concentrations of H_2O_2 (0-5mM) (b) YO-PRO uptake (AUC 0-360mins) (mean +SEM, n=4) * indicates significance compared to control (P<0.05) using a one-way ANOVA with Dunnett's post hoc test.

The cell permeability was then investigated using dye uptake experiments. The cells were stimulated with a range of H_2O_2 concentrations (100µM-5mM) over the course of 6 hours while in the presence of either YO-PRO (Fig 5.13) or PI (Fig 5.14). The YO-PRO uptake data (Fig 5.13a) showed that for the lowest concentration (100µM H_2O_2) the uptake seen was similar with that seen in the control. H_2O_2 at 300µM, 500µM and 1mM, uptake of YO-PRO was measured from around the 4 hour timepoint. For the highest concentrations (3mM H_2O_2) uptake occurred earlier starting at around the 3 hour time point. At 5mM H_2O_2, the uptake starts extremely early, compared to the other concentrations, occurring at around the 1 hour timepoint. The maximum uptake increased with concentration of H_2O_2 which is reflected in the AUC data (Fig 5.13b).

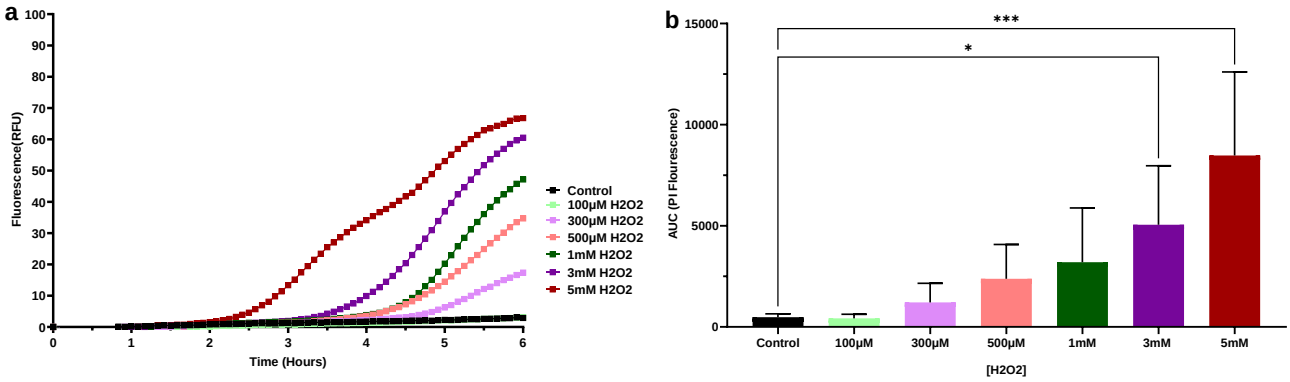

Figure 5.14 Oxidative stress causes PI uptake in BV2 microglia (a) Mean PI uptake in BV2 microglia cells in response to increasing concentrations of H_2O_2 (0-5mM) (b) PI uptake (AUC 0-360mins) (mean +SEM, n=4) * indicates significance compared to control ($P<0.05$) using a one-way ANOVA with Dunnett's post hoc test.

The PI uptake (Fig 5.14a) when stimulated with the H_2O_2 concentrations (100µM-5mM) showed the same trends as that seen in the YO-PRO uptake experiment, although timepoints were later. The AUC data (Fig5.14b) showed statistically significant increases at 3mM and 5mM H_2O_2 concentrations when compared to the control. The P2X7K/O variant BV2 cells uptake showed very similar PI uptake to the WT BV2 cells (Fig 5.15a-c)

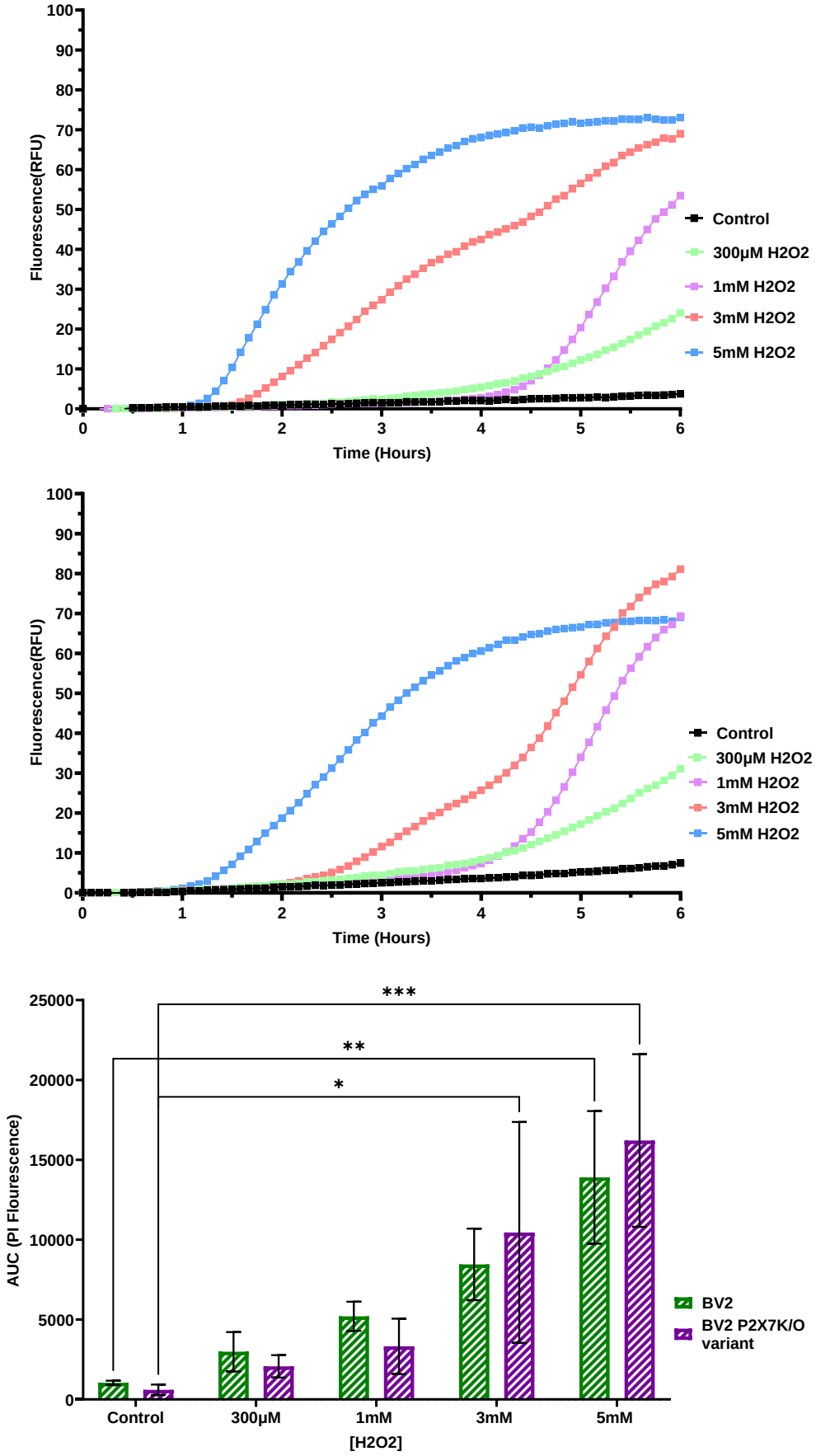

Figure 5.15 Exposure of BV2 and the P2X7K/O BV2 microglial cells to Oxidative stress causes PI uptake (a) Mean PI uptake in BV2 microglial cells in response to increasing concentrations of H_2O_2 (0-5mM) (n=3) (b) Mean PI uptake in P2X7K/O BV2 microglial cells in response to increasing concentrations of H_2O_2 (0-5mM) (n=3) (c) PI (AUC 0-220 Mins) (Mean+SEN; n=3) * Indicates significance (P<0.05) using two-way ANOVA with Sidak's post hoc test.

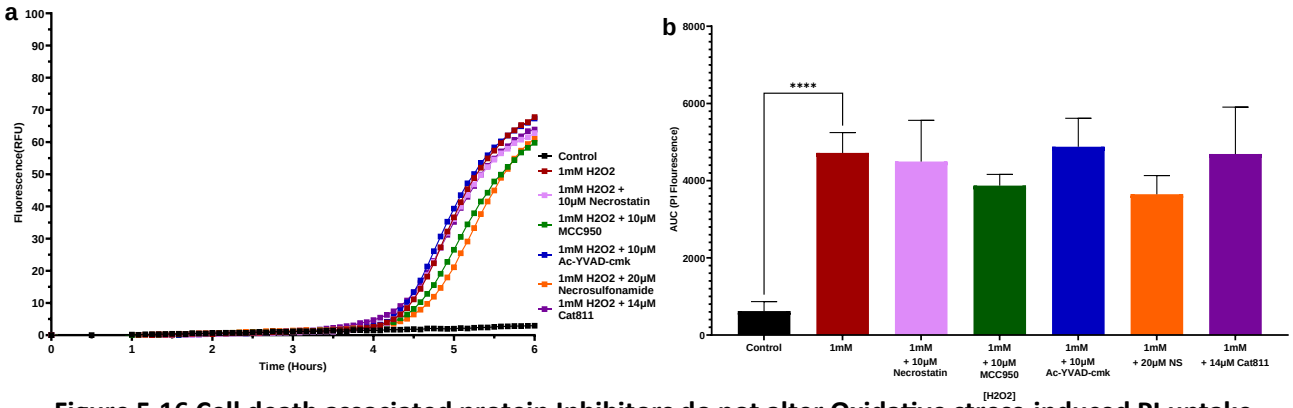

Figure 5.16 Cell death associated protein Inhibitors do not alter Oxidative stress-induced PI uptake in BV2 microglia (a) Mean PI uptake in BV2 microglia cells in response to 1mM H_2O_2 ± Necrostatin 10µM, MCC950 10µM, Ac-YVAD-cmk 10µM and Necrosulfonamide 20µM, Cat811 14µM (b) PI uptake (AUC 0-360mins) (mean +SEM, n=3) * indicates significance compared to control (P<0.05) using a one-way ANOVA with Dunnett's post hoc test.

PI and YO-PRO uptake were also measured in response to 1mM H_2O_2 and the cell death pathways inhibitors. The PI uptake (Fig 5.16a) showed that the inhibitors necrostatin, Ac-YVAD-cmk and CAT811 caused no change in the uptake of PI with 1mM H_2O_2. However, the cells incubated with necrosulfonamide and the MCC950 saw a noticeable, but not significant reduction in the PI uptake when compared to the 1mM H_2O_2 stimulated cells. This was further explored by looking at PI influx at specific time points. At around the 5 hour mark, 2 time points (290- and 295-minute) for the cells stimulated with 1mM H_2O_2 ±20µM necrosulfonamide, showed a significant decrease in PI influx (Fig 5.16b) despite the overall AUC graphs showing no statistical significance across the entire 6 hour time course.

Using YO-PRO (Fig 5.17a) none of the inhibitors had any significant effect when compared to 1mM H_2O_2 alone. Necrosulfonamide caused a slight reduction in the dye uptake, but this wasn't significant. The same trend was seen when AUC (Fig 5.17b) was measured.

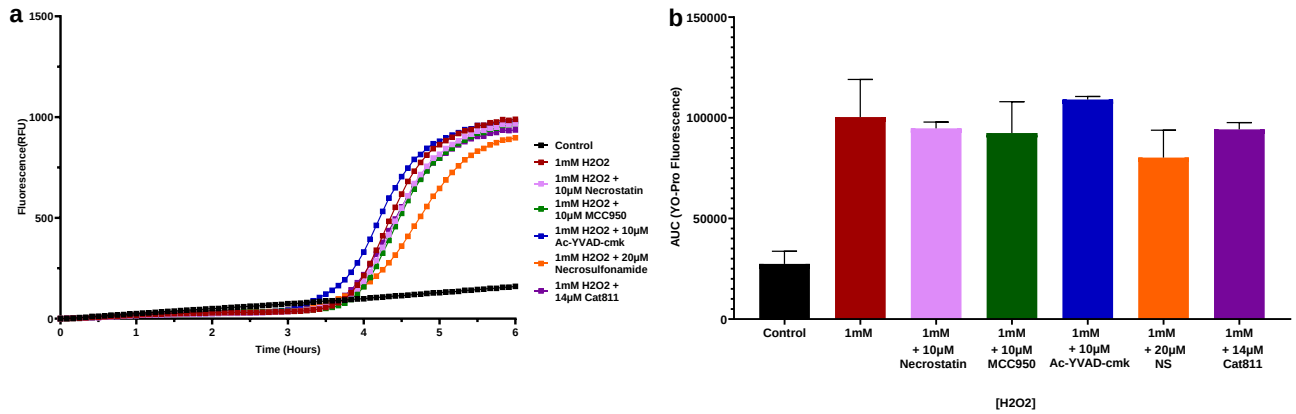

Figure 5.17 Cell death associated protein Inhibitors do not alter Oxidative stress-induced YOPRO uptake in BV2 microglia (a) Mean YO-PRO uptake in BV2 macrophage cells in response to 1mM H_2O_2 ± Necrostatin 10µM, MCC950 10µM, Ac-YVAD-cmk 10µM and Necrosulfonamide 20µM, Cat811 14µM (b) PI uptake (AUC 0-360mins) (mean +SEM, n=2)

5.2.2 Acidic pH causes cell death and morphological changes in BV2 Microglia

To further investigate the effects of conditions that microglia are likely to experience in the nervous system, the BV2 cells were subjected to a broad range of pH values (pH 5.0-9.0) to investigate the effect this has on levels of cell death, viability and cell morphology. The use of inhibitors was not able to be implemented, as pH can impact the ability of inhibitors to bind to their targets (Milne, 1965).

The extremes of the pH spectrum caused a higher level of cell death(Fig 5.18a), with pH 5.0-6.0 and pH8.5-9.0 all causing an increased cell death in both the BV2 WT and the P2X7K/O variant BV2 cells compared to the control (pH7.3). The acidic side of the scale (pH5.0) caused the highest increase in cell death although the increase in level of cell death was only statistically significant in the P2X7K/O variant BV2 cells. Cell viability (Fig 5.18b) at basic pHs (pH8.0-9.0) showed similar levels of cell viability compared to the control. The acidic pHs (pH5.0-7.0) revealed a large statistically significant drop in cell viability in both WT BV2 cells and P2X7K/O variant BV2 cells when compared to the control. When comparing the WT BV2 cells and stimulated P2X7K/O variant BV2 cells the results are consistent with the changes seen in the cell death results, in that cell viability decreased, but no changes were significant.

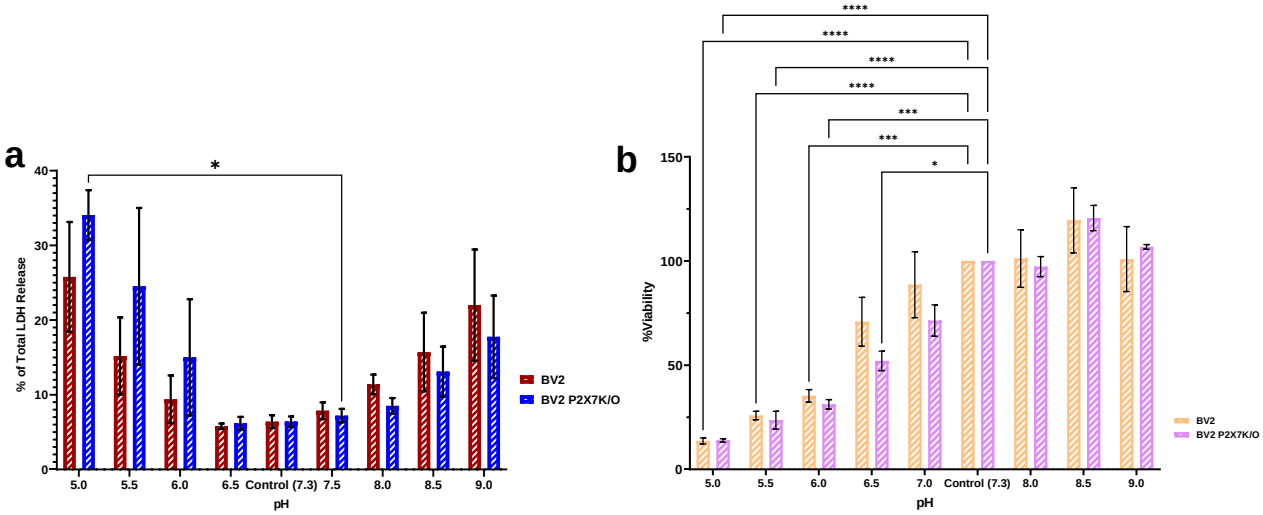

Figure 5.18 Acidic pH causes cell death and loss of cell viability in BV2 microglia (a) Mean % LDH release after 12 Hours in BV2 and P2X7K/O BV2 microglial cells in response to a range of pH values (5.0-9.0) (n=3) (b) Mean % Viability release after 12 Hours in BV2 and P2X7K/O BV2 microglial cells in response to a range of pH values (5.0-9.0) (n=3) * Indicates significance compared to control (P<0.05) using one-way ANOVA with Dunnett's post hoc test.

As expected from the cell death and viability data, more acidic conditions caused a reduction in the number of cells, and the remaining cells appeared rounded in shape (Fig 5.19). In more alkali conditions, however, there appeared to be an increase in cell number. An increase in cell number was supported by the cell viability data, but no changes were significant. However, increased cell death was also suggested by the LDH release data, which could suggest increased cell turnover. Interestingly there appears to be clustering in the cells at alkaline pH (Fig 5.19)

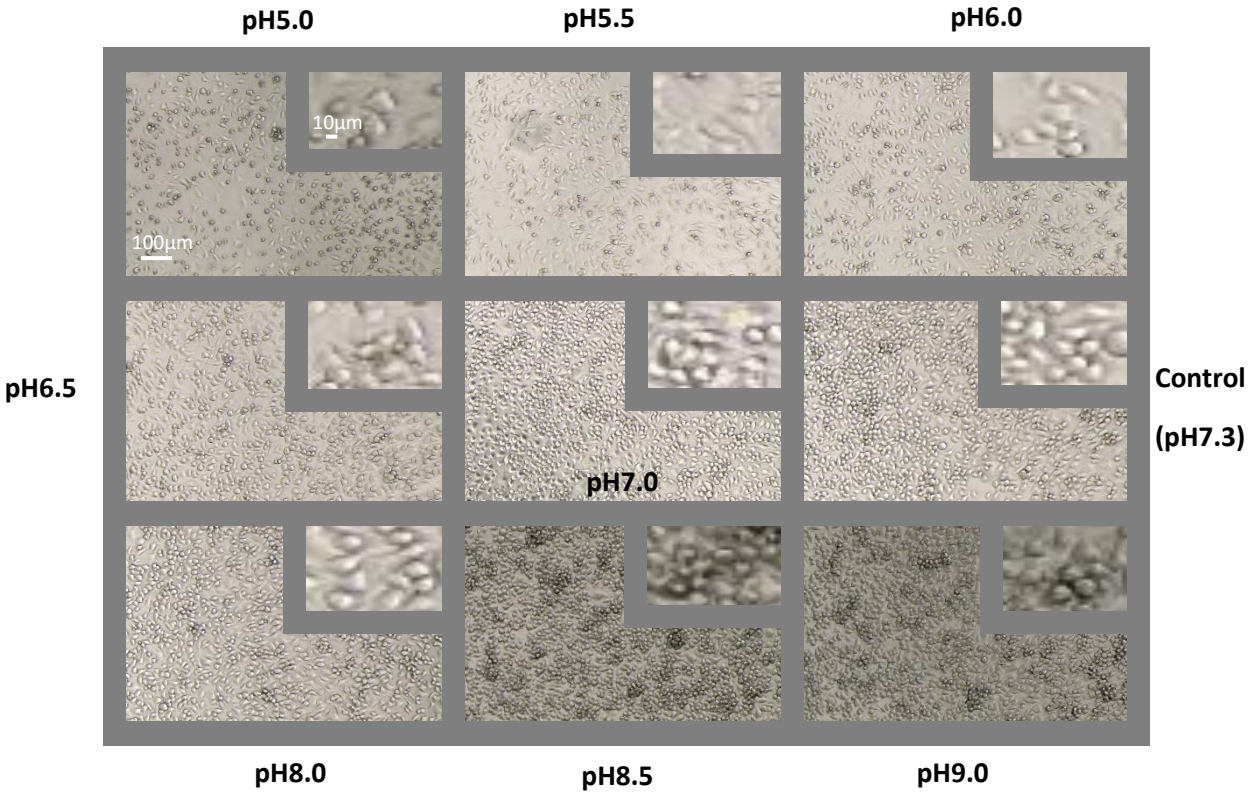

Figure 5.19 Acidic and alkali pH causes cell morphology changes in BV2 microglia
Effect of a range of pH values (5.0-9.0) on BV2 cells after 12 hours. Inset shows representative cell morphology at 12 hours (5x digital zoom)

5.2.5 Ischaemia causes cell death and morphological changes in BV2 Microglia

The final pathophysiological stress was ischaemic conditions. To simulate ischaemia the cells underwent oxygen-glucose deprivation (OGD). The cells were incubated for 12 hours in a glucose-free media in an atmosphere of 1% Oxygen and then the level of cell death was measured compared to cells in control conditions (Fig 5.20). Both P2X7K/O variant BV2 cells were used. The level of cell death for both the WT and the P2X7K/O variant BV2 cells that underwent OGD was much higher when compared to the relevant control, both reaching almost 100%. There was no difference between the levels of cell death when comparing between the WT and the P2X7K/O variant BV2 cells under OGD conditions.

For this model the viability assay (MTS) was not used as this assay uses the mitochondria to process the dye as proof of the cells viability but OGD makes this assay redundant as the cells metabolic health would be substantially changed by the lack of both glucose and oxygen.

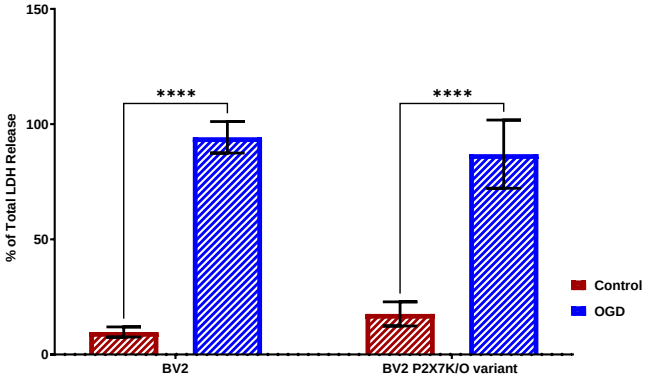

Figure 5.20 Ischaemia causes cell death in BV2 microglia Mean % LDH release after 12 Hours in BV2 and P2X7K/O BV2 microglial cells in response oxygen/glucose deprivation (n=3) * Indicates significance compared to control (P<0.05) using one-way ANOVA with Dunnett's post hoc test.

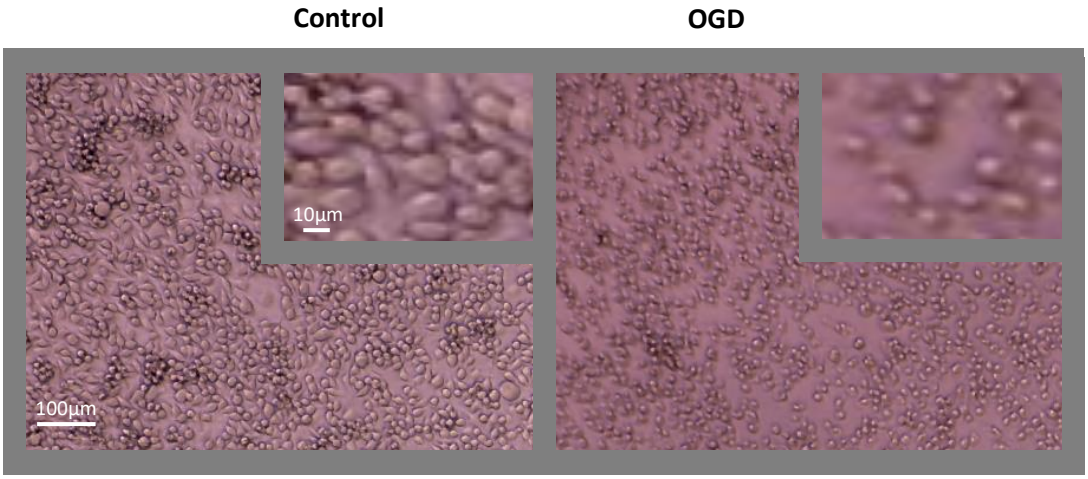

Figure 5.21 Ischaemia causes cell morphology changes in BV2 microglia Effect in response oxygen/glucose deprivation on BV2 cells after 12 hours. Inset shows representative cell morphology at 12 hours (5x digital zoom)

OGD treatment on the BV2 cells caused a significant reduction in cell number and the cell morphology changed, with the cells appearing to reduce in size (Fig 5.21). However, given the cell death data, it was surprising that any cells were present at all, indicating that there could be increased turnover, rather than simply lysis of all the cells.

In the presence of the various inhibitors linked to cell death (Fig 5.22), all the inhibitors used caused a slight drop in the level of cell death. A significant decrease of around 50% was seen when calpain was inhibited with CAT811.

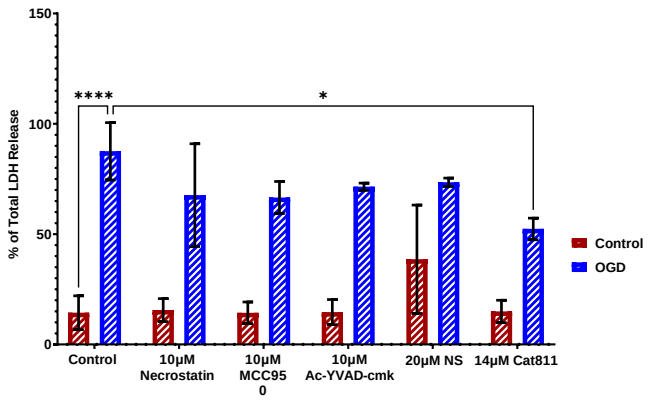

Figure 5.22 Ischaemia-induced cell death in BV2 microglia is altered by inhibition of calpain Mean % LDH release after 12 Hours in BV2 and P2X7K/O BV2 microglial cells in response oxygen/glucose deprivation ± Necrostatin 10µM, MCC950 10µM, Ac-YVAD-cmk 10µM, Necrosulfonamide 20µM and Cat811 14µM (n=3) * Indicates significance compared to control ($P<0.05$) using one-way ANOVA with Dunnett's post hoc test.

5.2.6 Pathophysiological Stressors cause a range of changes in gene expression in BV2 microglia

To further investigate the cell death process involved after BV2 cells were exposed to the pathophysiological insults (LPS, amyloid-β, oxidative stress, pH change, and ischaemia), the changes in mRNA expressions for different proteins of interest were measured. The proteins selected were the pyroptotically-linked NLRP3, caspase-1 and IL-1β, plus 3 members of the gasdermin family, gasdermin A3, D and E. Three members of the calpain family, calpain 1, 2 and 3 were also investigated, as was P2X7. These proteins were chosen as they are linked to inflammatory processes following LPS stimulation, so could be easily compared with the inflammatory actions of the other stressors. Cells were incubated for 4 hours with the different insults and RT-qPCR was performed.

The first of the insults investigated was 2μg/ml LPS (Fig 5.23). LPS is known to activate microglial cells and is also involved in processes connected to pyroptosis. One of the processes of pyroptosis that LPS is involved with is the upregulation of IL-1β, that fuels the inflammatory response created by LPS. As expected the mRNA level of IL-1β after LPS stimulation increases significantly (approx. x2500), NLRP3 expression also increased (x8), which again is to be expected. The level of gasdermin E mRNA expression has also increased but was not statistically significant. The mRNA levels of P2X7 and gasdermin D were both significantly reduced. Expression of the other genes remained unchanged. This gives a signature of gene expression changes which occur during "classic" activation of the BV2 cells.

When incubated in 50μM amyloid-β (Fig 5.24), the relative changes in mRNA expression were the same as was seen for the cells stimulated with LPS. Specifically, there was an increase for IL-1β (x10), NLRP3 (x3), gasdermins A3 (x5) and E (x8), and a reduction was seen for gasdermin D and P2X7. However, none of these changes were significant.

After incubation with 300μM H_2O_2 to act as a model of oxidative stress (Fig 5.25), there were increases in mRNA expression in IL-1β (x3), gasdermin E (x30), calpain 3 (x4), but these increases were not statistically significant. Only the reduction in P2X7 mRNA expression was significant.

When incubated in an acidic pH of 5.5 (Fig 5.26) the levels of mRNA expression were the same as the changes seen in LPS stimulated cells, with IL-1β (x50), NLRP3 (x5) gasdermins A3 (x45) and E (x100), although only the upregulation of gasdermin E being significant. Downregulation was seen in gasdermin D and P2X7 mRNA expression. A difference between LPS and pH 5.5 was that a significant reduction in caspase 1 was observed.

Finally, for cells that underwent OGD (Fig 5.27), increases were seen in P2X7 (x1.2 but significant), gasdermin E (x15) and gasdermin A3 (x10) and a decrease in caspase 1. The pattern seen here was very different to that of LPS treatment and the other pathophysiological stressors.

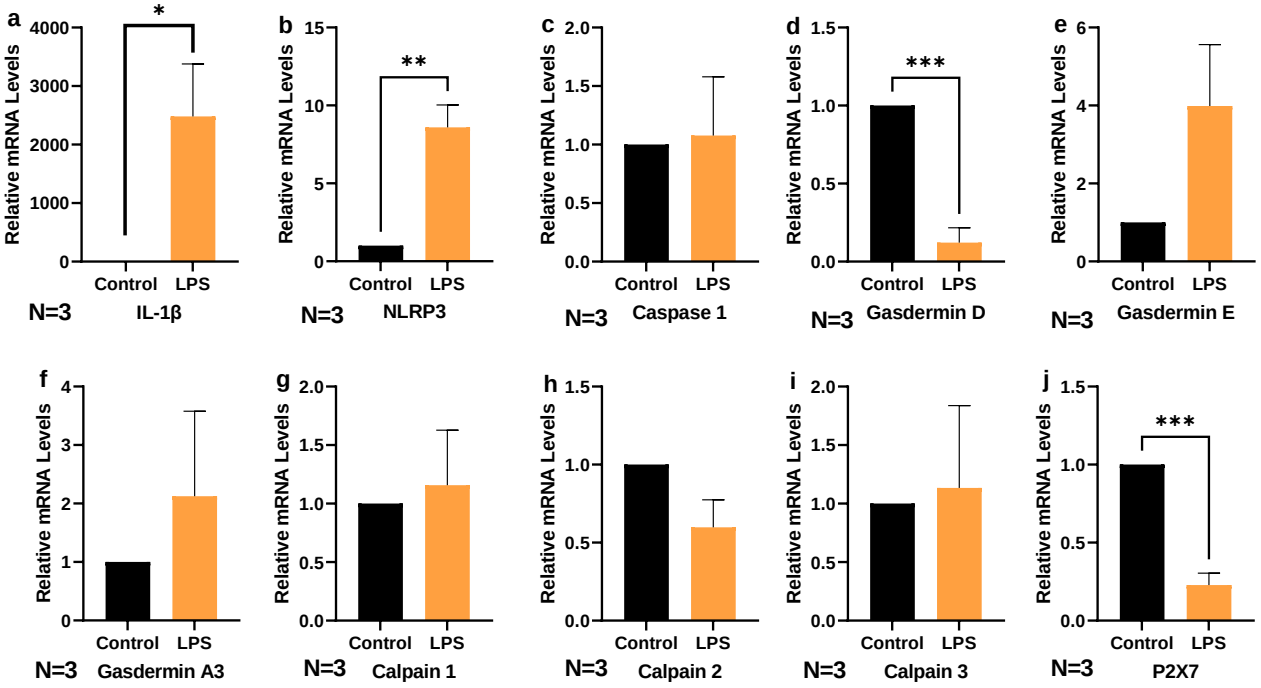

Figure 5.23 LPS causes changes in expression levels of mRNA in BV2 microglia Mean of the relative expression levels determined by qPCR on 10 selected genes following 4 hours of incubation in 2µg/ml LPS. Relative expression levels are calculated from Ct values according to the 2-ΔΔCt method. Actin was the reference gene for these qPCR experiments. * Indicates significance compared to control (P<0.05) using an unpaired t-test.

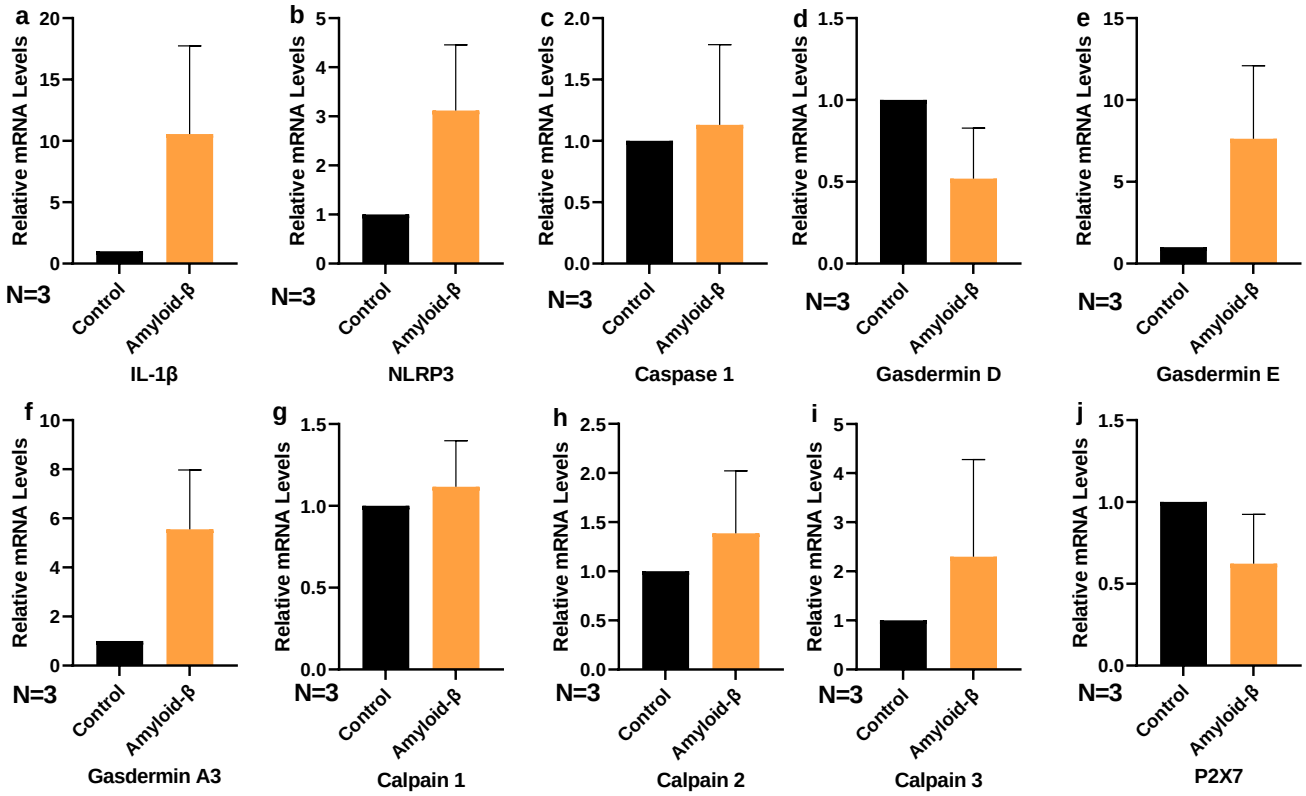

Figure 5.24 Amyloid-β causes changes in expression levels of mRNA in BV2 microglia Mean of the relative expression levels determined by qPCR on 10 selected genes following 4 hours of incubation in 50µM amyloid-β. Relative expression levels are calculated from Ct values according to the 2-ΔΔCt method. Actin was the reference gene for these qPCR experiments. * Indicates significance compared to control (P<0.05) using an unpaired t-test.

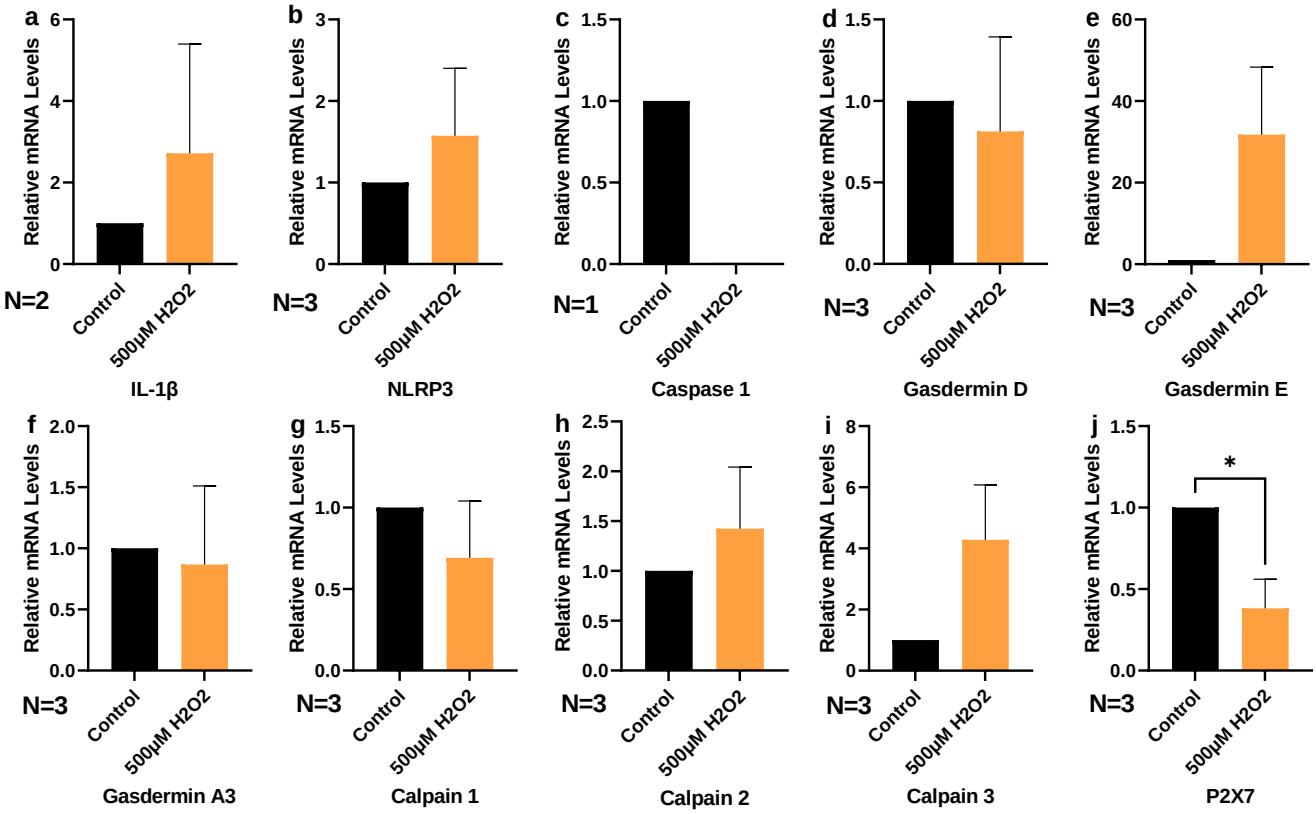

Figure 5.25 Oxidative Stress causes changes in expression levels of mRNA in BV2 microglia
Mean of the relative expression levels determined by qPCR on 10 selected genes following 4 hours of incubation in 500μM H_2O_2. Relative expression levels are calculated from Ct values according to the 2-ΔΔCt method. Actin was the reference gene for these qPCR experiments. * Indicates significance compared to control (P<0.05) using an unpaired t-test.

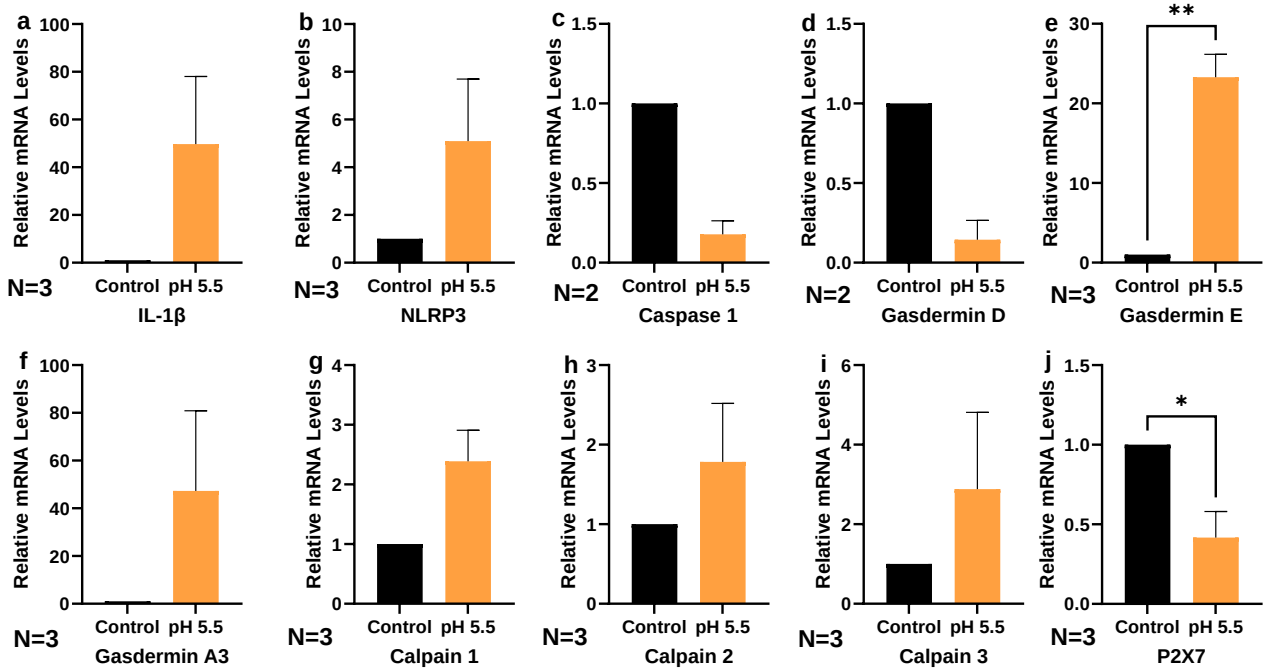

Figure 5.26 Acidic pH causes changes in expression levels of mRNA in BV2 microglia
Mean of the relative expression levels determined by qPCR on 10 selected genes following 4 hours of pH 5.5 conditions. Relative expression levels are calculated from Ct values according to the 2-ΔΔCt method. Actin was the reference gene for these qPCR experiments. * Indicates significance compared to control (P<0.05) using an unpaired t-test.

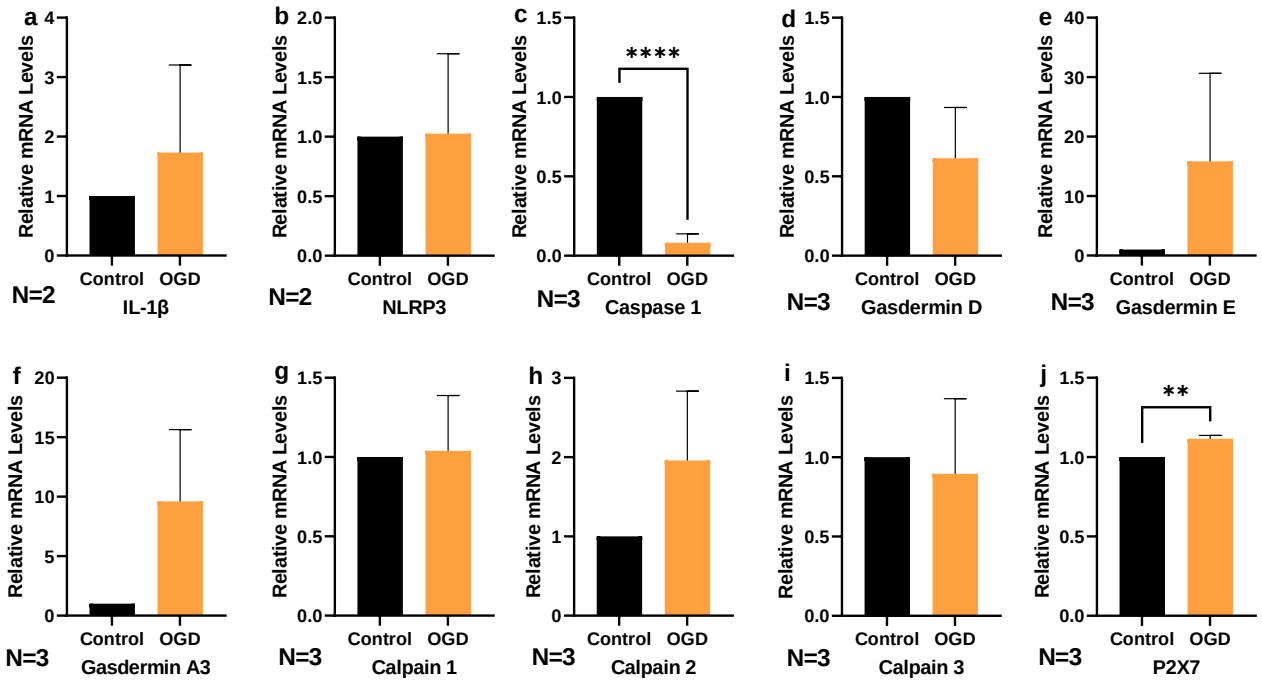

Figure 5.27 Ischaemia causes changes in expression levels of mRNA in BV2 microglia
Mean of the relative expression levels determined by qPCR on 10 selected genes following 4 hours of incubation in OGD conditions. Relative expression levels are calculated from Ct values according to the 2-ΔΔCt method. Actin was the reference gene for these qPCR experiments. * Indicates significance compared to control ($P<0.05$) using an unpaired t-test.

5.3 Discussion

As microglia are the resident macrophages of the CNS and CNS infections are relatively rare, the use of LPS and other bacterial proteins in research, although widespread, seems a little out of place for the normal obstacles these immune cells encounter. Other pathophysiological insults are frequently occurring in the brain and other parts of the CNS in various conditions ranging from Alzheimer's disease, glaucoma, stroke or other causes of ischaemia and even old age. These conditions have been shown to cause damage to cells in the local environment, specifically neuronal cells, which eventually leads to their deaths.

Following on from investigations described in previous chapters, the aim of the research described in this chapter was to investigate the effects of these stressors on cell death/viability and membrane permeability as well as any involvement of P2X7 in these processes and the effects of inhibitors of the various mechanisms involved in cell death. Activation of the BV2 cells by the various insults was also investigated using quantitative PCR to determine the expression of markers of microglial activation.

The use of LPS has been widespread throughout research for activation of immune cells as a model for bacterial infection (Rathkey et al., 2018), so LPS was used as the basis for comparison with the other pathophysiological insults investigated. The cell death assays (LDH and MTS) showed that there is no significant effect on BV2 cells exposed to LPS, although there was a trend of increasing cell death as the LPS concentration increases. No obvious changes in cell morphology were observed when compared to the control. However, the qPCR data shows that the LPS has a large impact on the cells, as there is a statistically significant increase in mRNA expression for IL-1β and NLRP3, while it also causes a statistically significant decrease in the mRNA expression of P2X7 and gasdermin D.

Looking at both the results from the previous chapter and the results here it can be seen that LPS stimulations does not cause cell death in the microglia, as cell death and viability are unaffected, but stimulation does add to the inflammatory environment via activation of the inflammasome and processing of interleukins. This is backed up by many other studies which show that incubating BV2 cells in LPS does cause an increase in IL-1β production. One study, using an array of detection techniques including qPCR and an ELISA, revealed a large increase in IL-1β mRNA and the protein itself (Roosen et al., 2021). Another study that used qPCR showed a large increase in IL-1β mRNA that could be blocked by a chemical product from the ginseng root (Lee et al., 2013). As discussed previously, bacterial infections are not something that microglia frequently encounter, so the use of LPS stimulation reveals little in terms of real-world situations. It does however, give a pattern of changes that are characteristic of classic activation, that would

therefore indicate microglial cells are entering a pro-inflammatory state. This gave a benchmark to investigate other stressors that are common in the CNS, including the retina.

The first of these stressors investigated was the Alzheimer's linked protein amyloid-β. Evidence has shown the importance of microglia in Alzheimer's disease (Cai et al., 2022). Fundamental to this understanding is that a previous Alzheimer's model in mice that genetically lack microglia led to the mice exhibiting increased brain calcification, haemorrhages, and premature lethality (Kiani Shabestari et al., 2022). This, therefore, indicates the essential protective role of microglia. However, as has already been discussed, overactivation can lead to neuroinflammation with detrimental effects on neuronal survival and, therefore, neurodegenerative disease progression.

Experimentally it has been shown that the neurotoxic section of amyloid-β is the 25-35 residues (Sato et al., 1995) which was used in all amyloid-β experiments in this chapter. The formation this polypeptide takes is not fully understood, although there is evidence that the conformation is that of a dimer or possible a trimer (Larini and Shea, 2012). Other studies have shown that there are multiple variations of structures that this form of amyloid-β takes, with any stock containing a mix of well organised dimers and unstructured dimers (Wei et al., 2010). Another study has shown that the conformation this form of amyloid-β adopts changes depending on different environments (Shanmugam and Polavarapu, 2004). Furthermore, this is dictated by the production, purification or isolation processes of the peptide, so confirmation is established before any experiment begins (Naldi et al., 2012). For the experiments performed in this chapter, the same stock of amyloid-β was used throughout and the same conditions maintained to reduce any variation that could be caused by these issues. It cannot be said, however, what conformation it is in, but experimental conditions were used to keep them to a minimum.

The cell death assays showed that the highest concentration used caused a significant increase in BV2 cells death and a significant decrease in cell viability, with a trend of increasing cell death and decreasing cell viability as the concentration of amyloid-β increased. The P2X7 receptor does not appear to be involved in this cell death as the P2X7K/O variant of BV2 vells showed similar changes in cell death and cell viability. The cell death assays in the presence of the cell death linked inhibitors revealed that none used were able to reduce the cell death or increase viability, with most of them having a similar result in both assays to the stimulated alone. However, the calpain inhibitor, CAT811, caused a statistically significant increase in cell death and a visible decrease in viability when cells were incubated in it together with amyloid-β. This suggests that calpains may play a protective role in microglia confronted with amyloid-β and thus blocking calpain leads to increased cell death. Studies have found a link between amyloid-β and calpains including one study that showed, in a mouse model of Alzheimer's disease that antagonists of the NMDA receptor reduced amyloid-β deposition by modulation of calpain-1 signalling and its role in

autophagy (Companys-Alemany et al., 2022). Another study showed that calpains play a role in the distribution of APP and inhibition of calpains led to an increase in the presence of both α- and β-amyloid cleavage (Mathews et al., 2002). Although these indicate a *in vivo* relationship between amyloid-β and calpain, they can't explain how calpain is involved in microglial responses to amyloid-β pathology. This requires further investigation.

Cell morphology tells an interesting story of the cells aggregating together as the concentration of amyloid-β increases. This could be caused by the microglia migrating to envelop the amyloid-β protein, and thus the higher the concentration of protein the more movement and aggregation. Evidence shows microglia gather around amyloid-β plaques to create a protective barrier, which is thought to compact the amyloid fibrils into a less toxic form, reducing axonal dystrophy (Condello et al., 2015). Other evidence shows that microglia promote the growth of plaques, specifically plaques with dense cores (Huang et al., 2021) and that this growth in plaque material is due to the microglia dying from uptake of amyloid-β (Baik et al., 2016). Again the actions of microglia are that of a double-edged sword, exhibiting both protective and destructive qualities.

When looking at the dye uptake experiments, the highest concentration (100μM amyloid-β) caused a rapid uptake of PI, which was less in the P2X7K/O variant BV2 cells. This is shown clearly in the AUC data, as the WT BV2 dye uptake is significantly different to control while the P2X7K/O variant BV2 cells uptake is not. Interestingly this difference is not seen in the YO-PRO uptake results with both cell types having similar dye uptake profiles. The P2X7 receptor may therefore be involved in increased cell permeability, as the large increase in PI uptake was reported, but further investigation is needed. For the dye uptake experiments in the presence of inhibitors, none caused any difference in the dye uptake profile or AUC, so it would appear that none of these targets play a role in the cell membrane disruption mechanism caused by amyloid-β. This includes calpain, as more cell death was seen with calpain inhibitor, increased cell permeability might have been expected.

The effects of amyloid-β on gene expression show increases to NLRP3, IL-1β, calpain 3 and both gasdermin A3 and E but decreases in P2X7 and gasdermin D. None of these changes were statistically significant, but the trends would suggest that an inflammatory phenotype occurs in the BV2 cells after incubation in the amyloid-β. The qPCR profile that was close to that seen in the cells stimulated with LPS. Studies have shown previously that amyloid-β may activate NLRP3 in microglia (Jung et al., 2022), while other studies have shown evidence for this activation and also the possible presence of IL-1β protein (Halle et al., 2008). A recent study that also used the BV2 cell line stimulated with amyloid-β showed evidence of activation of the NLRP3 inflammasome and also an increased secretion of IL-1β (Liu et al., 2020). These studies support the results found

in the qPCR data in this chapter as increases to NLRP3 and IL-1β could also point towards the activation of the inflammasome and the production and processing of IL-1β.

Oxidative stress plays a role in a range of conditions, whilst also being an issue that arises from simply aging (Liguori et al., 2018). To recreate an environment that was high in ROS, a model using H_2O_2 was utilised. The cell death assays showed that all concentrations of H_2O_2 caused a significant increase in the levels of cell death and a significant drop in viability. This is in keeping with experiments looking at H_2O_2-induced cell death (Singh et al., 2007). The dye uptake experiments suggested a dose dependent effect, as the higher concentration of H_2O_2 led to earlier and larger changes to dye uptake for both PI and YO-PRO. Investigations into the possible pathways involved in the H_2O_2 mediated cell death and cell membrane disruption started by comparing WT BV2 and the P2X7K/O variant BV2 cells to see if P2X7 played any part in the mechanism. There was no difference between the WT BV2 cells and the P2X7K/O variant BV2 cells across either the dye uptake, levels of cell death or cell viability results, so P2X7 appears to have no role to play in this mechanism. Inhibitors of various cell death linked proteins were used to investigate the role that they may play in this mechanism. Previous research has suggested an apoptotic mechanism (Singh et al., 2007). None of the inhibitors caused a significant change in cell death and cell viability. The NLRP3 inhibitor, MCC950, caused a visible reduction in cell death but this was not significant. H_2O_2-induced dye uptake was reduced by necrosulfonamide, and this was statistically significant, suggesting a possible role for gasdermin D. These results could point to a possible pyroptotic pathway rather than the apoptotic mechanism proposed previously.

The qPCR data for the microglia cells that were treated with 300µM H_2O_2 shows increases in mRNA expression of IL-1β, gasdermin E and calpain 3 and decreases in mRNA of P2X7 and caspase 1. which was comparable to the results seen in the LPS stimulated cells. This suggests a possible similar mechanism to the LPS, of inflammation and activation of the cells, giving extra evidence for a possible pyroptotic mechanism. However, as well as the Singh et al paper (Singh et al., 2007) described, other studies using the BV2 cell line have found apoptotic markers after stimulation with H_2O_2 and blocking the apoptotic pathway protected the BV2 cells from cell death (Hou et al., 2005, Ren et al., 2018). Two studies that exposed porcine retinal tissue to H_2O_2 saw an increase in apoptotic RGCs and an increased presence of microglia (Hurst et al., 2017, Mueller-Buehl et al., 2020), with one of these studies showing an increase in IL-1β mRNA expression, similar to the data found in qPCR experiments, and the other finding evidence of apoptosis. Another study that investigated the proteins effected by H_2O_2 exposure have shown that, again, apoptosis is the mechanism for cell death, but also that a Ca^{2+} influx and upregulation of calpains occurs, which is consistent with the increase in mRNA expression of calpain 3 (Ray et al., 2000). Finally another study found that a decrease in P2X7 expression was detected in astrocytes, thought to be caused by a H_2O_2 induced increase in intracellular zinc (Furuta et al., 2017), which again supports the

decrease in P2X7 mRNA expression seen in the qPCR data. In conclusion to this section the results suggest that H_2O_2 induces apoptosis, but there is also evidence around pro-inflammatory and a potential pyroptotic mechanism. It is not inconceivable that both are involved and could be concentration dependent.

The next pathophysiological insult that was tested was a change in pH. For the BV2 cells that were exposed to the alkaline conditions, no negative impacts could be seen, with cell viability potentially increasing slightly. The cell morphology revealed healthy cells that compare to that of the control and indicated that the cell number may have increased. This could also explain the slight increase in cell viability and cell death. The BV2 cells that were exposed to the acidic conditions clearly underwent cell death, shown by the increase in levels of cell death, the drop in viability and the severe changes in cell morphology and reduction in cell number. There was little difference between the WT BV2 cells and the P2X7K/O variant BV2 cells for cell viability. Although, the levels of cell death showed differences between the cells, suggested that P2X7 might have a protective capability in this mechanism as the P2X7K/O variant BV2 cells consistently had higher levels of cell death compared to the WT BV2. However, the results for gene expression showed a significant reduction in P2X7 expression, is not consistent and no firm conclusion can be drawn.

As the acidic conditions seem to cause the biggest insult to the cells and it has been suggested previously that in the brain following ischaemia during a stroke pH can drop to as low as pH6.5-6.0 (Gebert et al., 1971, Nedergaard et al., 1991). These levels of pH change were sufficient to cause cell death in these experiments. Acidic conditions also induced an increase in IL-1β, all 3 calpains and gasdermin A3 and E mRNA. Caspase 1 and P2X7 mRNA levels were both significantly reduced. This gives a mixed picture as the first 3 proteins are more linked to pyroptosis while the calpains would be more suggestive of necrosis.

In terms of the effects of pH on cell viability, previous research has shown that lowering of pH has a large impact in porcine nasal tissue, even when the conditions are only lowered to pH6.5. This had a more significant effect then when the same cells were incubated in IL-1β (Borrelli C, 2020). Other studies have also shown that a lower pH environment leads to an increased expression of IL-1β in human monocytes (Jancic et al., 2012). However in human macrophages, IL-1β production was negatively affected (Sušjan et al., 2020). A recent study that also used BV2 cells similarly found an increase in IL-1β after incubation in media that had an acidic pH (pH6.8) (Jang et al., 2022). Research into cell death when exposed to acidic conditions has returned a somewhat confused picture. One study that used Raji cells, a human lymphoblast-like cell line, proposed that the cells died via apoptosis due to the increased presence of Bax, cytochrome c and active caspase 3 (Sharma et al., 2015). Another study that used mouse microvascular endothelial cell line suggested that both apoptosis and necroptosis could be occurring at an acidic pH level (Zhang et

al., 2017). Finally, there have been 2 separate studies that have shown necrosis to be the main cause of cell death in cells that underwent acidic conditions. The first study using rat prostate and mammary carcinoma cells found that due to acidosis both cell lines displayed G1 arrest and an increase in necrotic cell death (Rauschner et al., 2021) and the other study, using human colon carcinoma cells, predominantly underwent necrosis under pH6.5 conditions (Sharma et al., 2005). Looking at all this in the context of the results shown here in BV2 cells, it is clear that acidic conditions are causing cell death in the BV2 cells, and due to the inability to use inhibitors, it is difficult to point to a proposed cell death mechanism. However, the results from the levels of mRNA would suggest possibly a necrotic or pyroptotic form of cell death. Future experiments could utilise the use of siRNA to block cell death associated proteins to investigate the pathway involved.

Lastly, a model for ischaemia (OGD) was used to replicate the loss of nutrients due to a lack of blood flow during events such as strokes and glaucoma. Starting with the cell death assays, a significant increase in cell death can be seen. There is no difference present between the WT BV2 and the P2X7K/O variant BV2 cells meaning its unlikely P2X7 plays a role in this increase in cell death. When testing the antagonists used previously to see what effect they can have on levels of cell death, the only inhibitor that had a significant effect on the cells was the calpain inhibitor, CAT811. The qPCR results for cells that underwent OGD, show that there was a significant drop in the mRNA levels of caspase 1, similar to that seen in the cells exposed to pH5.5. There were very small increases in mRNA production for IL-1β and calpain 2, but large increases for both gasdermin A3 and E. Interesting as this insult is the only one that leads to an increase in P2X7 expression although the fold change was very small. In fact all the others show a decrease in P2X7. These results would suggest a inflammatory pathway, but does not point to any specific form of cell death. The calpain inhibitor reducing cell death and a slight increase in calpain mRNA production would suggest a possible role of calpains in this process. Previous studies have shown a range of possible cell death mechanisms in different cell lines, but all have found a possible role for calpains. One study found that OGD in a RGC cell line was necroptotic in nature and there was an upregulation in calpain expression and a reduction in necroptosis could be seen when the calpains were inhibited (Chen et al., 2016). Another study found that astrocytes exposed to OGD induced two different cell death pathways, apoptosis or ischaemic necrosis, with the latter involving proteolysis of the cytoskeleton by calpains (Cao et al., 2010). A further study that looked at hippocampal slices that underwent OGD found that activation of calpains caused damage in the early stages (Grammer et al., 2008). Finally a study that used optic nerves and exposed them to OGD conditions, found that calpain inhibition was necessary but not sufficient to give protection to the cells (Stys and Jiang, 2002). This evidence, along with the results from this chapter, suggest

a key role for calpains in ischaemic cell death, which could be exploited as a possible therapeutic target following ischaemia.

Although the results here start to investigate how pathophysiological stressors might impact microglia cells survival and activation. The experiments have not yielded conclusive data. Investigating all pathophysiological stressors with other cell death assays, such as TUNEL assay or caspase 3/7 assay could help identify the cell death mechanisms. Further use of western blots could be used to see if protein expression changes are the same as the gene expression from the relevant qPCR data, to see if any mRNA expression change resulted in protein expression changes While the transcriptomics analysis of the cells, using the RNA-seq protocol, could identify an even wider array of cell death associated proteins screened, again to help clarify cell death mechanism.

It would also have been interesting to compare changes seen with the pathophysiological stressors with those seen with ATP. This would have allowed to tie the entire project together and would possibly help to add another piece of evidence into what form of cell death is occurring within the ATP stimulated microglia.

The pathophysiological stressors used in this chapter, all caused cell death in the BV2 cell line showing the damage that these stressors cause to microglia in the CNS. The overall results for each of the stressors did not identify any specific pathway for this cell death, however, when looking at the profile of genes expressed, and comparing to LPS, the stresses were certainly causing expression changes in genes associated with classic LPS-activation. Microglia could be therefore activated as a result of the pathophysiological changes. More research should be conducted looking at this and change the reliance on using LPS as a model to allow greater physiological relevance.

Chapter 6

General Discussion

The aims of this research were to firstly look at the effects of ATP stimulation on microglia, such as cell membrane disruption and cell death, and to see if the pathway behind these changes could be characterised using pharmacological inhibitors. The second aim of this research was to compare this cell death pathway with that of the cell death mechanism seen in macrophages. The final aim was to explore the effects of other pathophysiological stressors on microglia and to see if this could be characterised using pharmacological inhibitors. Over the course of this research all aims were met and the hypothesis, that BV2 microglia cell death would be pyroptotic in nature was disproved. As firstly the work carried out in this study has shown that pyroptosis is not the form of death activated within these BV2 microglia cells when the P2X7 receptor is stimulated by ATP. None of the inhibitors of proteins linked with pyroptosis caused any alteration in dye uptake, morphological changes or cell death. This was further reinforced by the results in J774 macrophages, which used the same techniques and inhibitors and showed that these cells, also of mouse origin, did undergo pyroptosis after P2X7 activation. The majority of research looking at pyroptosis in immune cells focuses on macrophage cells (Ma et al., 2021), with the assumption made that all immune cells are as readily able to perform this mechanism of cell death. However, the results shown here would suggest that this is not the case. Therefore the mechanism of death in microglia when stimulated with ATP is occurring through a different mechanism, that needs further study to clarify the exact pathway that is happening as this was not determined by the research presented here. Other results, in this research, revealed from work in the J774 macrophages, showed that LPS was not needed for the activation of the pyroptotic pathway, with ATP stimulation alone being enough. As most research looking at activation and pyroptosis uses LPS, this could be an important point for research on diseases that involve immune cell activation, but do not involve bacterial infection. The use of pathophysiological stressors showed that they all caused differing effects on the BV2 microglia, which can be classed as forms of activation with comparable phenotypic profiles.

A limitation of the work carried out in this study, and all research that uses non-human models, is mouse and human biology differs greatly. In the case of cell death proteins alone, humans have caspase 4/5, while caspase 11 is the mouse ortholog. Another example, is that in humans there is only one type of gasdermin A, where in mice there is gasdermin A1, A2 and A3. It isn't known how such differences would affect the processes but it seems unlikely that they will be identical and it should not be assumed that they are. A further study using animal models, may help to elucidate more details about this process in mice so the significance of the different isoforms can be investigated, but it will not be the full picture. A use of a human model may be a better option but

whether it is the use of an ex vivo intact human tissue model or isolation of microglia, this comes with challenges of its own including the ethical and legal complications of this option. There are also logistical problems, such as obtaining the tissue, which could lead to limited scalability of the experiments, transporting and storage of the tissue. Next to consider would be how representative the tissue is in practice, such as the heterogeneity of the tissue, the lack of full recapitulation of complex tissue architecture and microenvironment, and whether donor characteristics need to be considered, such as age, disease state and lifestyle factors. Techniques involving isolation and culture of the cells also require the use of serum to continue to maintain the cells during the experiments, which as mentioned previously creates its own problems, especially in immune cells.

It could be questioned as to whether blocking microglial cell death would be an effective treatment for neurodegenerative conditions including glaucoma. The cell death of RGCs is the cause of reduction in visual field and the progression of glaucoma (Weinreb et al., 2014). The main role of microglia in neurodegenerative conditions such as glaucoma and Alzheimer's disease is protective to begin with (Ahmad and Subramani, 2022, Long et al., 2022), such as clearing amyloid-β deposits or removing dying RGCs, however following excessive stimulation the microglia create the inflammatory environment that leads to the progression of these neurodegenerative conditions (Ahmad and Subramani, 2022, Long et al., 2022).

Therefore a better option may be to try and push the microglia into a "resolving" state (M2), releasing anti-inflammatory, wound healing and restorative cytokines such as IL-4 and IL-13, rather than pro-inflammatory cytokines seen in M1 (Colton, 2009, Ponomarev et al., 2007). Another option would be to change the cell death microglia undergo from one of the inflammatory pathways, such as pyroptosis or necroptosis, to an inflammatory silent pathway such as apoptosis (Pandian and Kanneganti, 2022).

With all the results discussed previously it is fair to say that cell death is extremely complicated. This is highlighted by the extensive cross talk seen between the different programmed cell death pathways, specifically apoptosis, necroptosis and pyroptosis (Kesavardhana et al., 2020). There have been shown to be many examples of this cross talk (Pandian and Kanneganti, 2022). Caspase 1 is thought to be able to cleave and activate caspase 7 after LPS and ATP treatment (Lamkanfi et al., 2008) and also initiate apoptosis through mitochondrial damage through the activation of gasdermin D (Rogers et al., 2019). Caspase 8, which has many roles in apoptosis, is required to be inhibited for the stabilisation of the necroptosome (Fritsch et al., 2019). It has also been found to be able to prime and activate the inflammasome and also cleave and activate caspase 1 (Gurung et al., 2014). Furthermore, following priming with LPS and nigericin stimulation in caspase 1 deficient cells, caspase 8 has been found to associate with ASC in the inflammasome to induce cell

death (Sagulenko et al., 2013) and multiple studies have found that under different infection conditions caspase 8 can cleave and activate gasdermin D (Demarco et al., 2020, Orning et al., 2018, Sarhan et al., 2018). Caspase 3 has been found to cleave gasdermin E in response to TNF-α, drugs used in chemotherapy and iron induced ROS (Rogers et al., 2017, Wang et al., 2017, Zhou et al., 2018) and the necroptosis linked protein MLKL has been found to activate the NLRP3 inflammasome, due to its ability to cause cell membrane disruption (Conos et al., 2017, Gutierrez et al., 2017).

The presence of this extensive cross talk and the studies into it, led to a new perspective on cell death pathways. This new concept of cell death was called PANoptosis (Pandian and Kanneganti, 2022). PANoptosis is a unique innate immune inflammatory cell death pathway regulated by the PANoptosome which is assembled by various components from a variety of cell death pathways (Pandian and Kanneganti, 2022). The PANoptosome, much like the inflammasome, is thought to consist of sensors, such as AIM2, NLRP3 or Z-confirmation nucleic acid binding protein 1 (ZBP1), adaptors such as ASC or FADD and effectors which include RIPK1, RIPK3, caspase 1, caspase 8 (Pandian and Kanneganti, 2022). It has been suggested that different PANoptosomes form in response to different insults (Pandian and Kanneganti, 2022). In a disease model for bone inflammation in mice, deletion of a single cell death associated protein was not sufficient to rescue the mice and needed the combined deletion of NLRP3 or caspase 1 along with caspase 8 and RIPK3 before protection was seen (Gurung et al., 2016, Lukens et al., 2014). A key investigation method for PANoptosis is the use of influenza A virus (IAV) DNA (Pandian and Kanneganti, 2022). IAV has been shown to activate pyroptotic, apoptotic and necroptotic proteins.

An important element of PANoptosis is thought to be ZBP1 (Hao et al., 2022). Deletion of cell death proteins individually did not protect the cell against IAV induced cell death but deletion of ZBP1 did, however, protect the cell (Christgen et al., 2020, Kuriakose et al., 2016, Zheng et al., 2020). ZBP1 was originally found to be an important innate immune sensor activated by pathogen responses such as NF-κB signalling (Rebsamen et al., 2009, Takaoka et al., 2007). However, later it was proposed to have an important role in the induction of PANoptosis (Upton et al., 2012). It has been shown previously that ZBP1 can also be activated by the presence of mitochondrial DNA (mtDNA) (Szczesny et al., 2018).

In the experiments presented in this thesis ATP mediated cell membrane disruption and cell death could not be blocked by any one inhibitor of cell death pathways. It could be possible that a PANoptotic pathway is occurring via the P2X7 receptor in BV2 cell upon stimulation with high levels of ATP. It is interesting that this is not true for every cell upon ATP stimulation, as shown in the J774 macrophage cells in Chapter 4, and the ability to block cell membrane disruption and cell death using pyroptotic inhibitors. However, it is difficult to say whether the J774s had undergone

cell death by looking at the cell morphology, also the LDH release showed that not all the pyroptotic inhibitors were able to stop this. It could be therefore that ATP-induced cell death involves multiple options for crosstalk within the cell death pathways. One possible mechanism though which this crosstalk could act involves the relationship between P2X7 and mitochondria.

The link between P2X7 stimulation and mitochondria has been suggested to be positive following basal ATP release (Di Virgilio et al., 2009). This leads to a tonically P2X7 stimulated intracellular Ca^{2+} concentration which allows higher levels of metabolism that facilitates cell survival and growth. Excessive stimulation, however, leads to an uncontrolled Ca^{2+} influx in both the cytoplasm and the mitochondria which causes cell death (Di Virgilio et al., 2009). Continued stimulation and activation of the P2X7 receptor has previously been found to increase mitochondrial Ca^{2+} concentration, disrupt the mitochondrial membrane potential and cause mitochondrial fragmentation (Adinolfi et al., 2005). It is interesting to speculate here that this could possibly provide a link between P2X7 and PANoptosis (Fig 6.1). Excessive P2X7 stimulation leads to an influx in Ca^{2+}, which overloads the mitochondria leading to mitochondrial fragmentation. This mitochondrial fragmentation then leads to mtDNA release into the cytoplasm. The mtDNA is detected by ZBP1 which becomes activated. Activated ZBP1 would then recruit the proteins needed for the PANoptosome, which would then lead to either a pyroptotic, necroptotic or apoptotic cell death pathway leading to cell death.

To investigate whether this mechanism is occurring, in the context of the research in this study, it would be interesting to look at the gene expression of ZBP1 to see if its expression was altered, to investigate this further the use of either an inhibitor or a siRNA to block ZBP1 activation could be performed. This could be done while measuring cell death or cell membrane disruption to see if any changes occur. Inspiration could be taken from the studies mentioned previously and block multiple cell death associated proteins all at once. Using inhibitors in this instance may not be beneficial as this may lead to cell toxicity, so again siRNA may be the better option. Another investigative avenue that could be looked at, are assays that involve mitochondrial mechanisms. Assays that could be used include measuring MitoSOX or dihydroethidium (DHE) fluorescent probes which measure mitochondrial ROS production, while another fluorescent based technique, such as MitoTracker, can be used to measure mitochondrial outer membrane permeability. Finally mitochondrial swelling could be assessed using techniques such as flow cytometry or electron microscopy to measure changes in mitochondrial size and morphology.

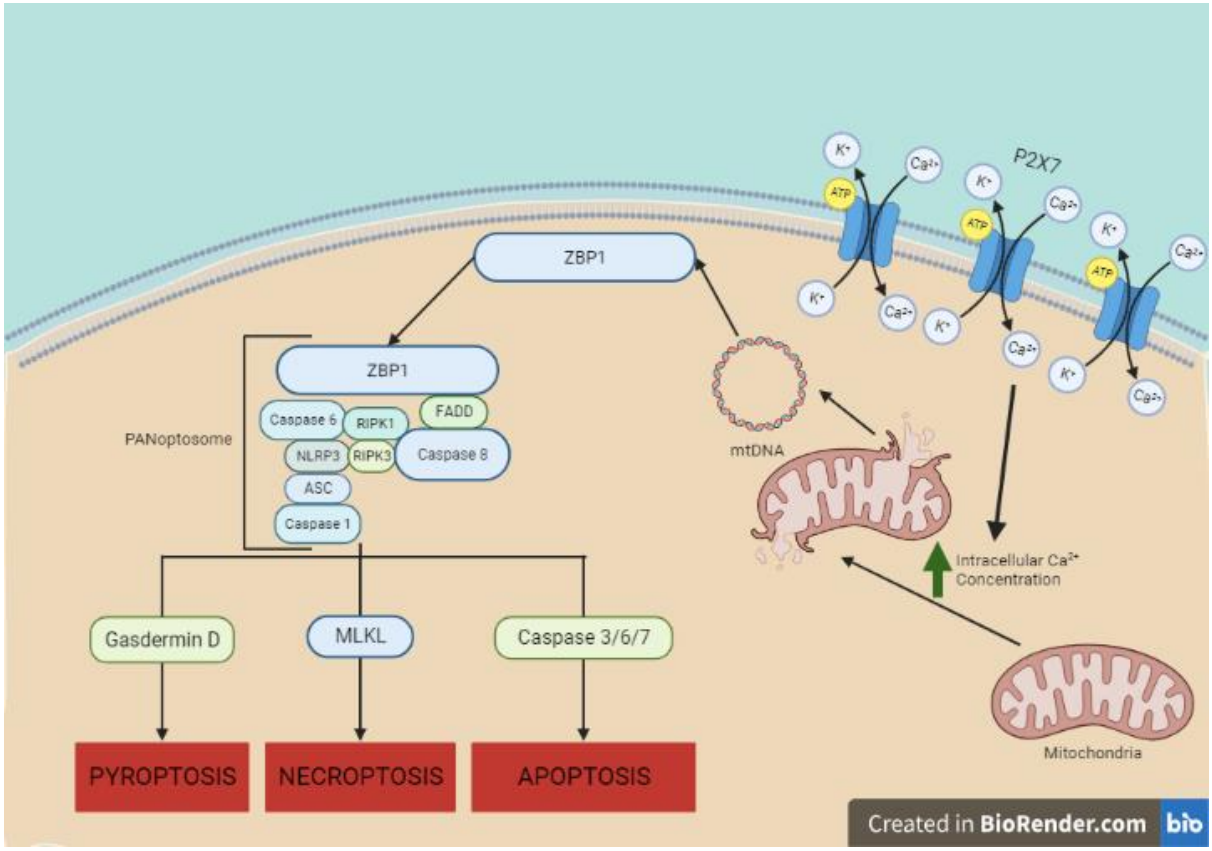

Figure 6.1 Proposed Mechanism for ATP Mediated PANoptosis P2X7 is activated by ATP, which causes an increase in intracellular Ca2+. This causes mitochondria disruption, leading to mitochondrial fragmentation and release of mtDNA into the cytoplasm. This is detected by ZBP1, which forms the PANoptosome which then activates either the pyroptosis, necroptosis or apoptosis pathways. Created with BioRender.com

It may be very difficult to block cell death totally, if a cell wants to die, it is going to die. Therefore, it may be the aim to try and move the pathway from an inflammatory mechanism of cell death, like pyroptosis and necroptosis, into a less inflammatory mechanism like apoptosis. This would help to avoid the inflammatory environment that leads to the progression of so many neurodegenerative conditions, which could either reduce the rate of decline or stop the decline altogether. More research to look at the option of guiding cells into a more peaceful cell death could help to find novel ways to treat neurodegenerative diseases. However, cells are still dying and defining the mechanisms and pathways involved in this complicated process is an important step to understanding these types of disease.

References

ABDAL DAYEM, A., HOSSAIN, M. K., LEE, S. B., KIM, K., SAHA, S. K., YANG, G. M., CHOI, H. Y. & CHO, S. G. 2017. The Role of Reactive Oxygen Species (ROS) in the Biological Activities of Metallic Nanoparticles. *Int J Mol Sci,* 18.

ABELL, A. D., JONES, M. A., COXON, J. M., MORTON, J. D., AITKEN, S. G., MCNABB, S. B., LEE, H. Y., MEHRTENS, J. M., ALEXANDER, N. A., STUART, B. G., NEFFE, A. T. & BICKERSTAFFE, R. 2009. Molecular modeling, synthesis, and biological evaluation of macrocyclic calpain inhibitors. *Angew Chem Int Ed Engl,* 48**,** 1455-8.

ADINOLFI, E., CALLEGARI, M. G., FERRARI, D., BOLOGNESI, C., MINELLI, M., WIECKOWSKI, M. R., PINTON, P., RIZZUTO, R. & DI VIRGILIO, F. 2005. Basal activation of the P2X7 ATP receptor elevates mitochondrial calcium and potential, increases cellular ATP levels, and promotes serum-independent growth. *Mol Biol Cell,* 16**,** 3260-72.

AGLIETTI, R. A., ESTEVEZ, A., GUPTA, A., RAMIREZ, M. G., LIU, P. S., KAYAGAKI, N., CIFERRI, C., DIXIT, V. M. & DUEBER, E. C. 2016. GsdmD p30 elicited by caspase-11 during pyroptosis forms pores in membranes. *Proc Natl Acad Sci U S A,* 113**,** 7858-63.

AHMAD, I. & SUBRAMANI, M. 2022. Microglia: Friends or Foes in Glaucoma? A Developmental Perspective. *Stem Cells Transl Med,* 11**,** 1210-1218.

AKHTER, A., GAVRILIN, M. A., FRANTZ, L., WASHINGTON, S., DITTY, C., LIMOLI, D., DAY, C., SARKAR, A., NEWLAND, C., BUTCHAR, J., MARSH, C. B., WEWERS, M. D., TRIDANDAPANI, S., KANNEGANTI, T. D. & AMER, A. O. 2009. Caspase-7 activation by the Nlrc4/Ipaf inflammasome restricts Legionella pneumophila infection. *PLoS Pathog,* 5**,** e1000361.

AKI, T., FUNAKOSHI, T., NORITAKE, K., UNUMA, K. & UEMURA, K. 2020. Extracellular glucose is crucially involved in the fate decision of LPS-stimulated RAW264.7 murine macrophage cells. *Sci Rep,* 10**,** 10581.

ALBERTO, A. V., FARIA, R. X., COUTO, C. G., FERREIRA, L. G., SOUZA, C. A., TEIXEIRA, P. C., FRÓES, M. M. & ALVES, L. A. 2013. Is pannexin the pore associated with the P2X7 receptor? *Naunyn Schmiedebergs Arch Pharmacol,* 386**,** 775-87.

ALLEN, I. C., SCULL, M. A., MOORE, C. B., HOLL, E. K., MCELVANIA-TEKIPPE, E., TAXMAN, D. J., GUTHRIE, E. H., PICKLES, R. J. & TING, J. P. 2009. The NLRP3 inflammasome mediates in vivo innate immunity to influenza A virus through recognition of viral RNA. *Immunity,* 30**,** 556-65.

ALMASIEH, M., WILSON, A. M., MORQUETTE, B., CUEVA VARGAS, J. L. & DI POLO, A. 2012. The molecular basis of retinal ganglion cell death in glaucoma. *Prog Retin Eye Res,* 31**,** 152-81.

ALVES, L. A., DE MELO REIS, R. A., DE SOUZA, C. A., DE FREITAS, M. S., TEIXEIRA, P. C., NETO MOREIRA FERREIRA, D. & XAVIER, R. F. 2014. The P2X7 receptor: shifting from a low- to a high-conductance channel - an enigmatic phenomenon? *Biochim Biophys Acta,* 1838**,** 2578-87.

AMER, A., FRANCHI, L., KANNEGANTI, T. D., BODY-MALAPEL, M., OZÖREN, N., BRADY, G., MESHINCHI, S., JAGIRDAR, R., GEWIRTZ, A., AKIRA, S. & NÚÑEZ, G. 2006. Regulation of Legionella phagosome maturation and infection through flagellin and host Ipaf. *J Biol Chem,* 281**,** 35217-23.

ANDREU, N., PHELAN, J., DE SESSIONS, P. F., CLIFF, J. M., CLARK, T. G. & HIBBERD, M. L. 2017. Primary macrophages and J774 cells respond differently to infection with Mycobacterium tuberculosis. *Sci Rep,* 7**,** 42225.

ANEIROS, E., CAO, L., PAPAKOSTA, M., STEVENS, E. B., PHILLIPS, S. & GRIMM, C. 2011. The biophysical and molecular basis of TRPV1 proton gating. *Embo j,* 30**,** 994-1002.

ANTONOPOULOS, C., EL SANADI, C., KAISER, W. J., MOCARSKI, E. S. & DUBYAK, G. R. 2013. Proapoptotic chemotherapeutic drugs induce noncanonical processing and release of IL-1β via caspase-8 in dendritic cells. *J Immunol,* 191**,** 4789-803.

ASADI, M., TAGHIZADEH, S., KAVIANI, E., VAKILI, O., TAHERI-ANGANEH, M., TAHAMTAN, M. & SAVARDASHTAKI, A. 2022. Caspase-3: Structure, function, and biotechnological aspects. *Biotechnol Appl Biochem,* 69**,** 1633-1645.

ASKEW, K., LI, K., OLMOS-ALONSO, A., GARCIA-MORENO, F., LIANG, Y., RICHARDSON, P., TIPTON, T., CHAPMAN, M. A., RIECKEN, K., BECCARI, S., SIERRA, A., MOLNÁR, Z., CRAGG, M. S.,

GARASCHUK, O., PERRY, V. H. & GOMEZ-NICOLA, D. 2017. Coupled Proliferation and Apoptosis Maintain the Rapid Turnover of Microglia in the Adult Brain. *Cell Rep,* 18**,** 391-405.

AZUMA, M., FUKIAGE, C., HIGASHINE, M., NAKAJIMA, T., MA, H. & SHEARER, T. R. 2000. Identification and characterization of a retina-specific calpain (Rt88) from rat. *Curr Eye Res,* 21**,** 710-20.

AZUMA, M., SAKAMOTO-MIZUTANI, K., NAKAJIMA, T., KANAAMI-DAIBO, S., TAMADA, Y. & SHEARER, T. R. 2004. Involvement of calpain isoforms in retinal degeneration in WBN/Kob rats. *Comp Med,* 54**,** 533-42.

BABU, S. R., BAO, F., ROBERTS, C. M., MARTIN, A. K., GOWAN, K., EISENBARTH, G. S. & FAIN, P. R. 2003. Caspase 7 is a positional candidate gene for IDDM 17 in a Bedouin Arab family. *Ann N Y Acad Sci,* 1005**,** 340-3.

BADIMON, A., STRASBURGER, H. J., AYATA, P., CHEN, X., NAIR, A., IKEGAMI, A., HWANG, P., CHAN, A. T., GRAVES, S. M., UWERU, J. O., LEDDEROSE, C., KUTLU, M. G., WHEELER, M. A., KAHAN, A., ISHIKAWA, M., WANG, Y. C., LOH, Y. E., JIANG, J. X., SURMEIER, D. J., ROBSON, S. C., JUNGER, W. G., SEBRA, R., CALIPARI, E. S., KENNY, P. J., EYO, U. B., COLONNA, M., QUINTANA, F. J., WAKE, H., GRADINARU, V. & SCHAEFER, A. 2020. Negative feedback control of neuronal activity by microglia. *Nature,* 586**,** 417-423.

BAI, R., GUO, J., YE, X. Y., XIE, Y. & XIE, T. 2022. Oxidative stress: The core pathogenesis and mechanism of Alzheimer's disease. *Ageing Res Rev,* 77**,** 101619.

BAIK, S. H., KANG, S., SON, S. M. & MOOK-JUNG, I. 2016. Microglia contributes to plaque growth by cell death due to uptake of amyloid β in the brain of Alzheimer's disease mouse model. *Glia,* 64**,** 2274-2290.

BAILEY, J. A., MALONEY, B., GE, Y. W. & LAHIRI, D. K. 2011. Functional activity of the novel Alzheimer's amyloid β-peptide interacting domain (AβID) in the APP and BACE1 promoter sequences and implications in activating apoptotic genes and in amyloidogenesis. *Gene,* 488**,** 13-22.

BAIN, C. C., BRAVO-BLAS, A., SCOTT, C. L., PERDIGUERO, E. G., GEISSMANN, F., HENRI, S., MALISSEN, B., OSBORNE, L. C., ARTIS, D. & MOWAT, A. M. 2014. Constant replenishment from circulating monocytes maintains the macrophage pool in the intestine of adult mice. *Nat Immunol,* 15**,** 929-937.

BAK, R. O., GOMEZ-OSPINA, N. & PORTEUS, M. H. 2018. Gene Editing on Center Stage. *Trends Genet,* 34**,** 600-611.

BARCIA, C., ROS, C. M., ANNESE, V., GÓMEZ, A., ROS-BERNAL, F., AGUADO-YERA, D., MARTÍNEZ-PAGÁN, M. E., DE PABLOS, V., FERNANDEZ-VILLALBA, E. & HERRERO, M. T. 2011. IFN-γ signaling, with the synergistic contribution of TNF-α, mediates cell specific microglial and astroglial activation in experimental models of Parkinson's disease. *Cell Death Dis,* 2**,** e142.

BARTLETT, R., YERBURY, J. J. & SLUYTER, R. 2013. P2X7 receptor activation induces reactive oxygen species formation and cell death in murine EOC13 microglia. *Mediators Inflamm,* 2013**,** 271813.

BARUCH-SUCHODOLSKY, R. & FISCHER, B. 2009. Abeta40, either soluble or aggregated, is a remarkably potent antioxidant in cell-free oxidative systems. *Biochemistry,* 48**,** 4354-70.

BAUDRY, M. & BI, X. 2013. Learning and memory: an emergent property of cell motility. *Neurobiol Learn Mem,* 104**,** 64-72.

BAUDRY, M. & BI, X. 2016. Calpain-1 and Calpain-2: The Yin and Yang of Synaptic Plasticity and Neurodegeneration. *Trends Neurosci,* 39**,** 235-245.

BAXTER, P. S., DANDO, O., EMELIANOVA, K., HE, X., MCKAY, S., HARDINGHAM, G. E. & QIU, J. 2021. Microglial identity and inflammatory responses are controlled by the combined effects of neurons and astrocytes. *Cell Rep,* 34**,** 108882.

BEN-DAVID, U., SIRANOSIAN, B., HA, G., TANG, H., OREN, Y., HINOHARA, K., STRATHDEE, C. A., DEMPSTER, J., LYONS, N. J., BURNS, R., NAG, A., KUGENER, G., CIMINI, B., TSVETKOV, P., MARUVKA, Y. E., O'ROURKE, R., GARRITY, A., TUBELLI, A. A., BANDOPADHAYAY, P., TSHERNIAK, A., VAZQUEZ, F., WONG, B., BIRGER, C., GHANDI, M., THORNER, A. R.,

BITTKER, J. A., MEYERSON, M., GETZ, G., BEROUKHIM, R. & GOLUB, T. R. 2018. Genetic and transcriptional evolution alters cancer cell line drug response. *Nature,* 560**,** 325-330.
BERGSBAKEN, T., FINK, S. L. & COOKSON, B. T. 2009. Pyroptosis: host cell death and inflammation. *Nat Rev Microbiol,* 7**,** 99-109.
BERGSBAKEN, T., FINK, S. L., DEN HARTIGH, A. B., LOOMIS, W. P. & COOKSON, B. T. 2011. Coordinated host responses during pyroptosis: caspase-1-dependent lysosome exocytosis and inflammatory cytokine maturation. *J Immunol,* 187**,** 2748-54.
BERRY, C., LA VECCHIA, C. & NICOTERA, P. 2010. Paraquat and Parkinson's disease. *Cell Death Differ,* 17**,** 1115-25.
BEYNON, S. B. & WALKER, F. R. 2012. Microglial activation in the injured and healthy brain: what are we really talking about? Practical and theoretical issues associated with the measurement of changes in microglial morphology. *Neuroscience,* 225**,** 162-71.
BIDULA, S., DHUNA, K., HELLIWELL, R. & STOKES, L. 2019. Positive allosteric modulation of P2X7 promotes apoptotic cell death over lytic cell death responses in macrophages. *Cell Death Dis,* 10**,** 882.
BISWAS, S., HARRIS, F., DENNISON, S., SINGH, J. & PHOENIX, D. A. 2004. Calpains: targets of cataract prevention? *Trends Mol Med,* 10**,** 78-84.
BJELOBABA, I., SAVIC, D. & LAVRNJA, I. 2017. Multiple Sclerosis and Neuroinflammation: The Overview of Current and Prospective Therapies. *Curr Pharm Des,* 23**,** 693-730.
BLASI, E., BARLUZZI, R., BOCCHINI, V., MAZZOLLA, R. & BISTONI, F. 1990. Immortalization of murine microglial cells by a v-raf/v-myc carrying retrovirus. *J Neuroimmunol,* 27**,** 229-37.
BOHLEN, C. J., BENNETT, F. C., TUCKER, A. F., COLLINS, H. Y., MULINYAWE, S. B. & BARRES, B. A. 2017. Diverse Requirements for Microglial Survival, Specification, and Function Revealed by Defined-Medium Cultures. *Neuron,* 94**,** 759-773.e8.
BOLAND, M. V., ERVIN, A. M., FRIEDMAN, D. S., JAMPEL, H. D., HAWKINS, B. S., VOLLENWEIDER, D., CHELLADURAI, Y., WARD, D., SUAREZ-CUERVO, C. & ROBINSON, K. A. 2013. Comparative effectiveness of treatments for open-angle glaucoma: a systematic review for the U.S. Preventive Services Task Force. *Ann Intern Med,* 158**,** 271-9.
BORRELLI C, B. C. 2020. Synergistic Effects of Acidic pH and Pro-Inflammatory Cytokines IL-1β and TNF-α for Cell-Based Intervertebral Disc Regeneration. *Applied Sciences,* 24**,** 9009.
BORST, K., DUMAS, A. A. & PRINZ, M. 2021. Microglia: Immune and non-immune functions. *Immunity,* 54**,** 2194-2208.
BRANDL, H. & LACHENMAYR, B. 1994. [Dependence of the sensitivity of the central visual field on hemoglobin-oxygen saturation]. *Ophthalmologe,* 91**,** 151-5.
BRÄNDLE, U., GUENTHER, E., IRRLE, C. & WHEELER-SCHILLING, T. H. 1998a. Gene expression of the P2X receptors in the rat retina. *Brain Res Mol Brain Res,* 59**,** 269-72.
BRÄNDLE, U., KOHLER, K. & WHEELER-SCHILLING, T. H. 1998b. Expression of the P2X7-receptor subunit in neurons of the rat retina. *Brain Res Mol Brain Res,* 62**,** 106-9.
BRIZ, V. & BAUDRY, M. 2017. Calpains: Master Regulators of Synaptic Plasticity. *Neuroscientist,* 23**,** 221-231.
BROUGH, D., LE FEUVRE, R. A., IWAKURA, Y. & ROTHWELL, N. J. 2002. Purinergic (P2X7) receptor activation of microglia induces cell death via an interleukin-1-independent mechanism. *Mol Cell Neurosci,* 19**,** 272-80.
BROUGH, D. & ROTHWELL, N. J. 2007. Caspase-1-dependent processing of pro-interleukin-1beta is cytosolic and precedes cell death. *J Cell Sci,* 120**,** 772-81.
BURNSTOCK, G. 2012. Purinergic signalling: Its unpopular beginning, its acceptance and its exciting future. *Bioessays,* 34**,** 218-25.
BUTOVSKY, O., JEDRYCHOWSKI, M. P., MOORE, C. S., CIALIC, R., LANSER, A. J., GABRIELY, G., KOEGLSPERGER, T., DAKE, B., WU, P. M., DOYKAN, C. E., FANEK, Z., LIU, L., CHEN, Z., ROTHSTEIN, J. D., RANSOHOFF, R. M., GYGI, S. P., ANTEL, J. P. & WEINER, H. L. 2014. Identification of a unique TGF-β-dependent molecular and functional signature in microglia. *Nat Neurosci,* 17**,** 131-43.
CAI, P., GAO, J. & ZHOU, Y. 2019. CRISPR-mediated genome editing in non-conventional yeasts for biotechnological applications. *Microb Cell Fact,* 18**,** 63.

CAI, Y., LIU, J., WANG, B., SUN, M. & YANG, H. 2022. Microglia in the Neuroinflammatory Pathogenesis of Alzheimer's Disease and Related Therapeutic Targets. *Front Immunol,* 13**,** 856376.

CAIN, K., INAYAT-HUSSAIN, S. H., COUET, C. & COHEN, G. M. 1996. A cleavage-site-directed inhibitor of interleukin-1 beta-converting enzyme-like proteases inhibits apoptosis in primary cultures of rat hepatocytes. *Biochem J,* 314 (Pt 1)**,** 27-32.

CAMP, D. A., YADAV, P., DALVIN, L. A. & SHIELDS, C. L. 2019. Glaucoma secondary to intraocular tumors: mechanisms and management. *Curr Opin Ophthalmol,* 30**,** 71-81.

CAO, X., ZHANG, Y., ZOU, L., XIAO, H., CHU, Y. & CHU, X. 2010. Persistent oxygen-glucose deprivation induces astrocytic death through two different pathways and calpain-mediated proteolysis of cytoskeletal proteins during astrocytic oncosis. *Neurosci Lett,* 479**,** 118-22.

CHAN, K. K. W., TANG, F., THAM, C. C. Y., YOUNG, A. L. & CHEUNG, C. Y. 2017. Retinal vasculature in glaucoma: a review. *BMJ Open Ophthalmol,* 1**,** e000032.

CHAN, P. H. 2001. Reactive oxygen radicals in signaling and damage in the ischemic brain. *J Cereb Blood Flow Metab,* 21**,** 2-14.

CHAO, K. L., KULAKOVA, L. & HERZBERG, O. 2017. Gene polymorphism linked to increased asthma and IBD risk alters gasdermin-B structure, a sulfatide and phosphoinositide binding protein. *Proc Natl Acad Sci U S A,* 114**,** E1128-e1137.

CHEN, S., YAN, J., DENG, H. X., LONG, L. L., HU, Y. J., WANG, M., SHANG, L., CHEN, D., HUANG, J. F. & XIONG, K. 2016. Inhibition of calpain on oxygen glucose deprivation-induced RGC-5 necroptosis. *J Huazhong Univ Sci Technolog Med Sci,* 36**,** 639-645.

CHEN, Z. & TRAPP, B. D. 2016. Microglia and neuroprotection. *J Neurochem,* 136 Suppl 1**,** 10-7.

CHESSELL, I. P., MICHEL, A. D. & HUMPHREY, P. P. 1997. Properties of the pore-forming P2X7 purinoceptor in mouse NTW8 microglial cells. *Br J Pharmacol,* 121**,** 1429-37.

CHESSELL, I. P., SIMON, J., HIBELL, A. D., MICHEL, A. D., BARNARD, E. A. & HUMPHREY, P. P. 1998. Cloning and functional characterisation of the mouse P2X7 receptor. *FEBS Lett,* 439**,** 26-30.

CHIDLOW, G., WOOD, J. P. M. & CASSON, R. J. 2017. Investigations into Hypoxia and Oxidative Stress at the Optic Nerve Head in a Rat Model of Glaucoma. *Front Neurosci,* 11**,** 478.

CHIOZZI, P., MURGIA, M., FALZONI, S., FERRARI, D. & DI VIRGILIO, F. 1996. Role of the purinergic P2Z receptor in spontaneous cell death in J774 macrophage cultures. *Biochem Biophys Res Commun,* 218**,** 176-81.

CHIZH, B. A. & ILLES, P. 2001. P2X receptors and nociception. *Pharmacol Rev,* 53**,** 553-68.

CHRISTGEN, S., ZHENG, M., KESAVARDHANA, S., KARKI, R., MALIREDDI, R. K. S., BANOTH, B., PLACE, D. E., BRIARD, B., SHARMA, B. R., TULADHAR, S., SAMIR, P., BURTON, A. & KANNEGANTI, T. D. 2020. Identification of the PANoptosome: A Molecular Platform Triggering Pyroptosis, Apoptosis, and Necroptosis (PANoptosis). *Front Cell Infect Microbiol,* 10**,** 237.

CHRYSOSTOMOU, V., REZANIA, F., TROUNCE, I. A. & CROWSTON, J. G. 2013. Oxidative stress and mitochondrial dysfunction in glaucoma. *Curr Opin Pharmacol,* 13**,** 12-5.

COCKCROFT, S. & GOMPERTS, B. D. 1980. The ATP4- receptor of rat mast cells. *Biochem J,* 188**,** 789-98.

COLL, R. C., ROBERTSON, A. A., CHAE, J. J., HIGGINS, S. C., MUÑOZ-PLANILLO, R., INSERRA, M. C., VETTER, I., DUNGAN, L. S., MONKS, B. G., STUTZ, A., CROKER, D. E., BUTLER, M. S., HANEKLAUS, M., SUTTON, C. E., NÚÑEZ, G., LATZ, E., KASTNER, D. L., MILLS, K. H., MASTERS, S. L., SCHRODER, K., COOPER, M. A. & O'NEILL, L. A. 2015. A small-molecule inhibitor of the NLRP3 inflammasome for the treatment of inflammatory diseases. *Nat Med,* 21**,** 248-55.

COLLO, G., NEIDHART, S., KAWASHIMA, E., KOSCO-VILBOIS, M., NORTH, R. A. & BUELL, G. 1997. Tissue distribution of the P2X7 receptor. *Neuropharmacology,* 36**,** 1277-83.

COLTON, C. & WILCOCK, D. M. 2010. Assessing activation states in microglia. *CNS Neurol Disord Drug Targets,* 9**,** 174-91.

COLTON, C. A. 2009. Heterogeneity of microglial activation in the innate immune response in the brain. *J Neuroimmune Pharmacol,* 4**,** 399-418.
COMITATO, A., SCHIROLI, D., MONTANARI, M. & MARIGO, V. 2020. Calpain Activation Is the Major Cause of Cell Death in Photoreceptors Expressing a Rhodopsin Misfolding Mutation. *Mol Neurobiol,* 57**,** 589-599.
COMPANYS-ALEMANY, J., TURCU, A. L., SCHNEIDER, M., MÜLLER, C. E., VÁZQUEZ, S., GRIÑÁN-FERRÉ, C. & PALLÀS, M. 2022. NMDA receptor antagonists reduce amyloid-β deposition by modulating calpain-1 signaling and autophagy, rescuing cognitive impairment in 5XFAD mice. *Cell Mol Life Sci,* 79**,** 408.
CONCHA, N. O. & ABDEL-MEGUID, S. S. 2002. Controlling apoptosis by inhibition of caspases. *Curr Med Chem,* 9**,** 713-26.
CONDELLO, C., YUAN, P., SCHAIN, A. & GRUTZENDLER, J. 2015. Microglia constitute a barrier that prevents neurotoxic protofibrillar Aβ42 hotspots around plaques. *Nat Commun,* 6**,** 6176.
CONOS, S. A., CHEN, K. W., DE NARDO, D., HARA, H., WHITEHEAD, L., NÚÑEZ, G., MASTERS, S. L., MURPHY, J. M., SCHRODER, K., VAUX, D. L., LAWLOR, K. E., LINDQVIST, L. M. & VINCE, J. E. 2017. Active MLKL triggers the NLRP3 inflammasome in a cell-intrinsic manner. *Proc Natl Acad Sci U S A,* 114**,** E961-e969.
CORDEIRO, M. F., GUO, L., COXON, K. M., DUGGAN, J., NIZARI, S., NORMANDO, E. M., SENSI, S. L., SILLITO, A. M., FITZKE, F. W., SALT, T. E. & MOSS, S. E. 2010. Imaging multiple phases of neurodegeneration: a novel approach to assessing cell death in vivo. *Cell Death Dis,* 1**,** e3.
CORNELL, J., SALINAS, S., HUANG, H. Y. & ZHOU, M. 2022. Microglia regulation of synaptic plasticity and learning and memory. *Neural Regen Res,* 17**,** 705-716.
CORTESIO, C. L., BOATENG, L. R., PIAZZA, T. M., BENNIN, D. A. & HUTTENLOCHER, A. 2011. Calpain-mediated proteolysis of paxillin negatively regulates focal adhesion dynamics and cell migration. *J Biol Chem,* 286**,** 9998-10006.
COUTINHO-SILVA, R., PERFETTINI, J. L., PERSECHINI, P. M., DAUTRY-VARSAT, A. & OJCIUS, D. M. 2001. Modulation of P2Z/P2X(7) receptor activity in macrophages infected with Chlamydia psittaci. *Am J Physiol Cell Physiol,* 280**,** C81-9.
COUTURIER, J., STANCU, I. C., SCHAKMAN, O., PIERROT, N., HUAUX, F., KIENLEN-CAMPARD, P., DEWACHTER, I. & OCTAVE, J. N. 2016. Activation of phagocytic activity in astrocytes by reduced expression of the inflammasome component ASC and its implication in a mouse model of Alzheimer disease. *J Neuroinflammation,* 13**,** 20.
CRAPSER, J. D., OCHABA, J., SONI, N., REIDLING, J. C., THOMPSON, L. M. & GREEN, K. N. 2020. Microglial depletion prevents extracellular matrix changes and striatal volume reduction in a model of Huntington's disease. *Brain,* 143**,** 266-288.
CREWS, F. T. & VETRENO, R. P. 2016. Mechanisms of neuroimmune gene induction in alcoholism. *Psychopharmacology (Berl),* 233**,** 1543-57.
CREWS, L., PATRICK, C., ADAME, A., ROCKENSTEIN, E. & MASLIAH, E. 2011. Modulation of aberrant CDK5 signaling rescues impaired neurogenesis in models of Alzheimer's disease. *Cell Death Dis,* 2**,** e120.
CSERÉP, C., PÓSFAI, B., LÉNÁRT, N., FEKETE, R., LÁSZLÓ, Z. I., LELE, Z., ORSOLITS, B., MOLNÁR, G., HEINDL, S., SCHWARCZ, A. D., UJVÁRI, K., KÖRNYEI, Z., TÓTH, K., SZABADITS, E., SPERLÁGH, B., BARANYI, M., CSIBA, L., HORTOBÁGYI, T., MAGLÓCZKY, Z., MARTINECZ, B., SZABÓ, G., ERDÉLYI, F., SZIPŐCS, R., TAMKUN, M. M., GESIERICH, B., DUERING, M., KATONA, I., LIESZ, A., TAMÁS, G. & DÉNES, Á. 2020. Microglia monitor and protect neuronal function through specialized somatic purinergic junctions. *Science,* 367**,** 528-537.
CZABOTAR, P. E. & MURPHY, J. M. 2015. A tale of two domains - a structural perspective of the pseudokinase, MLKL. *Febs j,* 282**,** 4268-78.
CZOGALLA, A. & SIKORSKI, A. F. 2005. Spectrin and calpain: a 'target' and a 'sniper' in the pathology of neuronal cells. *Cell Mol Life Sci,* 62**,** 1913-24.
D'ARCY, M. S. 2019. Cell death: a review of the major forms of apoptosis, necrosis and autophagy. *Cell Biol Int,* 43**,** 582-592.
DA COSTA, C. A. & CHECLER, F. 2010. A novel parkin-mediated transcriptional function links p53 to familial Parkinson's disease. *Cell Cycle,* 9**,** 16-7.

DAS, A., GUYTON, M. K., SMITH, A., WALLACE, G. T., MCDOWELL, M. L., MATZELLE, D. D., RAY, S. K. & BANIK, N. L. 2013. Calpain inhibitor attenuated optic nerve damage in acute optic neuritis in rats. *J Neurochem,* 124**,** 133-46.

DAVID, L. L. & SHEARER, T. R. 1986. Purification of calpain II from rat lens and determination of endogenous substrates. *Exp Eye Res,* 42**,** 227-38.

DEGTEREV, A., HUANG, Z., BOYCE, M., LI, Y., JAGTAP, P., MIZUSHIMA, N., CUNY, G. D., MITCHISON, T. J., MOSKOWITZ, M. A. & YUAN, J. 2005. Chemical inhibitor of nonapoptotic cell death with therapeutic potential for ischemic brain injury. *Nat Chem Biol,* 1**,** 112-9.

DEMARCO, B., GRAYCZYK, J. P., BJANES, E., LE ROY, D., TONNUS, W., ASSENMACHER, C. A., RADAELLI, E., FETTRELET, T., MACK, V., LINKERMANN, A., ROGER, T., BRODSKY, I. E., CHEN, K. W. & BROZ, P. 2020. Caspase-8-dependent gasdermin D cleavage promotes antimicrobial defense but confers susceptibility to TNF-induced lethality. *Sci Adv,* 6.

DENES, A., COUTTS, G., LÉNÁRT, N., CRUICKSHANK, S. M., PELEGRIN, P., SKINNER, J., ROTHWELL, N., ALLAN, S. M. & BROUGH, D. 2015. AIM2 and NLRC4 inflammasomes contribute with ASC to acute brain injury independently of NLRP3. *Proc Natl Acad Sci U S A,* 112**,** 4050-5.

DEUCHARS, S. A., ATKINSON, L., BROOKE, R. E., MUSA, H., MILLIGAN, C. J., BATTEN, T. F., BUCKLEY, N. J., PARSON, S. H. & DEUCHARS, J. 2001. Neuronal P2X7 receptors are targeted to presynaptic terminals in the central and peripheral nervous systems. *J Neurosci,* 21**,** 7143-52.

DHUNA, K., FELGATE, M., BIDULA, S. M., WALPOLE, S., BIBIC, L., CROMER, B. A., ANGULO, J., SANDERSON, J., STEBBING, M. J. & STOKES, L. 2019. Ginsenosides Act As Positive Modulators of P2X4 Receptors. *Mol Pharmacol,* 95**,** 210-221.

DI VIRGILIO, F., DAL BEN, D., SARTI, A. C., GIULIANI, A. L. & FALZONI, S. 2017. The P2X7 Receptor in Infection and Inflammation. *Immunity,* 47**,** 15-31.

DI VIRGILIO, F., FERRARI, D. & ADINOLFI, E. 2009. P2X(7): a growth-promoting receptor-implications for cancer. *Purinergic Signal,* 5**,** 251-6.

DIEPENBROEK, M., CASADEI, N., ESMER, H., SAIDO, T. C., TAKANO, J., KAHLE, P. J., NIXON, R. A., RAO, M. V., MELKI, R., PIERI, L., HELLING, S., MARCUS, K., KRUEGER, R., MASLIAH, E., RIESS, O. & NUBER, S. 2014. Overexpression of the calpain-specific inhibitor calpastatin reduces human alpha-Synuclein processing, aggregation and synaptic impairment in [A30P]αSyn transgenic mice. *Hum Mol Genet,* 23**,** 3975-89.

DING, J., WANG, K., LIU, W., SHE, Y., SUN, Q., SHI, J., SUN, H., WANG, D. C. & SHAO, F. 2016. Pore-forming activity and structural autoinhibition of the gasdermin family. *Nature,* 535**,** 111-6.

DISTELHORST, J. S. & HUGHES, G. M. 2003. Open-angle glaucoma. *Am Fam Physician,* 67**,** 1937-44.

DOITSH, G., GALLOWAY, N. L., GENG, X., YANG, Z., MONROE, K. M., ZEPEDA, O., HUNT, P. W., HATANO, H., SOWINSKI, S., MUÑOZ-ARIAS, I. & GREENE, W. C. 2014. Cell death by pyroptosis drives CD4 T-cell depletion in HIV-1 infection. *Nature,* 505**,** 509-14.

DONG, Y., SUN, Y., HUANG, Y., FANG, X., SUN, P., DWARAKANATH, B., KONG, L. & LU, J. J. 2019. Depletion of MLKL inhibits invasion of radioresistant nasopharyngeal carcinoma cells by suppressing epithelial-mesenchymal transition. *Ann Transl Med,* 7**,** 741.

DOS SANTOS, S. E., MEDEIROS, M., PORFIRIO, J., TAVARES, W., PESSÔA, L., GRINBERG, L., LEITE, R. E. P., FERRETTI-REBUSTINI, R. E. L., SUEMOTO, C. K., FILHO, W. J., NOCTOR, S. C., SHERWOOD, C. C., KAAS, J. H., MANGER, P. R. & HERCULANO-HOUZEL, S. 2020. Similar Microglial Cell Densities across Brain Structures and Mammalian Species: Implications for Brain Tissue Function. *J Neurosci,* 40**,** 4622-4643.

DRURY, A. N. & SZENT-GYÖRGYI, A. 1929. The physiological activity of adenine compounds with especial reference to their action upon the mammalian heart. *J Physiol,* 68**,** 213-37.

DUCE, J. A., TSATSANIS, A., CATER, M. A., JAMES, S. A., ROBB, E., WIKHE, K., LEONG, S. L., PEREZ, K., JOHANSSEN, T., GREENOUGH, M. A., CHO, H. H., GALATIS, D., MOIR, R. D., MASTERS, C. L., MCLEAN, C., TANZI, R. E., CAPPAI, R., BARNHAM, K. J., CICCOTOSTO, G. D., ROGERS, J. T. & BUSH, A. I. 2010. Iron-export ferroxidase activity of β-amyloid precursor protein is inhibited by zinc in Alzheimer's disease. *Cell,* 142**,** 857-67.

DUNCAN, J. A., GAO, X., HUANG, M. T., O'CONNOR, B. P., THOMAS, C. E., WILLINGHAM, S. B., BERGSTRALH, D. T., JARVIS, G. A., SPARLING, P. F. & TING, J. P. 2009. Neisseria

gonorrhoeae activates the proteinase cathepsin B to mediate the signaling activities of the NLRP3 and ASC-containing inflammasome. *J Immunol,* 182**,** 6460-9.
DUNNING, K., MARTZ, A., PERALTA, F. A., CEVOLI, F., BOUÉ-GRABOT, E., COMPAN, V., GAUTHERAT, F., WOLF, P., CHATAIGNEAU, T. & GRUTTER, T. 2021. P2X7 Receptors and TMEM16 Channels Are Functionally Coupled with Implications for Macropore Formation and Current Facilitation. *Int J Mol Sci,* 22.
DUPREZ, L., WIRAWAN, E., VANDEN BERGHE, T. & VANDENABEELE, P. 2009. Major cell death pathways at a glance. *Microbes Infect,* 11**,** 1050-62.
ECKHART, L., DECLERCQ, W., BAN, J., RENDL, M., LENGAUER, B., MAYER, C., LIPPENS, S., VANDENABEELE, P. & TSCHACHLER, E. 2000. Terminal differentiation of human keratinocytes and stratum corneum formation is associated with caspase-14 activation. *J Invest Dermatol,* 115**,** 1148-51.
ELALI, A. & RIVEST, S. 2016. Microglia Ontology and Signaling. *Front Cell Dev Biol,* 4**,** 72.
ELDRED, J. A., SANDERSON, J., WORMSTONE, M., REDDAN, J. R. & DUNCAN, G. 2003. Stress-induced ATP release from and growth modulation of human lens and retinal pigment epithelial cells. *Biochem Soc Trans,* 31**,** 1213-5.
ESKANDARI-SEDIGHI, G., JUNG, J. & MACAULEY, M. S. 2023. CD33 isoforms in microglia and Alzheimer's disease: Friend and foe. *Mol Aspects Med,* 90**,** 101111.
EVAVOLD, C. L., RUAN, J., TAN, Y., XIA, S., WU, H. & KAGAN, J. C. 2018. The Pore-Forming Protein Gasdermin D Regulates Interleukin-1 Secretion from Living Macrophages. *Immunity,* 48**,** 35-44.e6.
EYO, U. B., MINER, S. A., AHLERS, K. E., WU, L. J. & DAILEY, M. E. 2013. P2X7 receptor activation regulates microglial cell death during oxygen-glucose deprivation. *Neuropharmacology,* 73**,** 311-9.
FABBRIZIO, P., AMADIO, S., APOLLONI, S. & VOLONTÉ, C. 2017. P2X7 Receptor Activation Modulates Autophagy in SOD1-G93A Mouse Microglia. *Front Cell Neurosci,* 11**,** 249.
FAN, W., HUANG, W., CHEN, J., LI, N., MAO, L. & HOU, S. 2022. Retinal microglia: Functions and diseases. *Immunology,* 166**,** 268-286.
FAN, Z., BROOKS, D. J., OKELLO, A. & EDISON, P. 2017. An early and late peak in microglial activation in Alzheimer's disease trajectory. *Brain,* 140**,** 792-803.
FAVA, L. L., SCHULER, F., SLADKY, V., HASCHKA, M. D., SORATROI, C., EITERER, L., DEMETZ, E., WEISS, G., GELEY, S., NIGG, E. A. & VILLUNGER, A. 2017. The PIDDosome activates p53 in response to supernumerary centrosomes. *Genes Dev,* 31**,** 34-45.
FENG, S., YANG, Y., MEI, Y., MA, L., ZHU, D. E., HOTI, N., CASTANARES, M. & WU, M. 2007. Cleavage of RIP3 inactivates its caspase-independent apoptosis pathway by removal of kinase domain. *Cell Signal,* 19**,** 2056-67.
FERRARI, D., CHIOZZI, P., FALZONI, S., DAL SUSINO, M., COLLO, G., BUELL, G. & DI VIRGILIO, F. 1997a. ATP-mediated cytotoxicity in microglial cells. *Neuropharmacology,* 36**,** 1295-301.
FERRARI, D., CHIOZZI, P., FALZONI, S., HANAU, S. & DI VIRGILIO, F. 1997b. Purinergic modulation of interleukin-1 beta release from microglial cells stimulated with bacterial endotoxin. *J Exp Med,* 185**,** 579-82.
FERRARI, D., VILLALBA, M., CHIOZZI, P., FALZONI, S., RICCIARDI-CASTAGNOLI, P. & DI VIRGILIO, F. 1996. Mouse microglial cells express a plasma membrane pore gated by extracellular ATP. *J Immunol,* 156**,** 1531-9.
FINK, S. L. & COOKSON, B. T. 2006. Caspase-1-dependent pore formation during pyroptosis leads to osmotic lysis of infected host macrophages. *Cell Microbiol,* 8**,** 1812-25.
FINK, S. L. & COOKSON, B. T. 2007. Pyroptosis and host cell death responses during Salmonella infection. *Cell Microbiol,* 9**,** 2562-70.
FLAMMER, J., ORGÜL, S., COSTA, V. P., ORZALESI, N., KRIEGLSTEIN, G. K., SERRA, L. M., RENARD, J. P. & STEFÁNSSON, E. 2002. The impact of ocular blood flow in glaucoma. *Prog Retin Eye Res,* 21**,** 359-93.
FLEISCHHAUER, J. C., MITCHELL, C. H., STAMER, W. D., KARL, M. O., PETERSON-YANTORNO, K. & CIVAN, M. M. 2003. Common actions of adenosine receptor agonists in modulating human trabecular meshwork cell transport. *J Membr Biol,* 193**,** 121-36.

FLOWERS, S. A. & REBECK, G. W. 2020. APOE in the normal brain. *Neurobiol Dis,* 136**,** 104724.
FOWLER, C. J., GRIFFITHS, D. & DE GROAT, W. C. 2008. The neural control of micturition. *Nat Rev Neurosci,* 9**,** 453-66.
FRANK, D. & VINCE, J. E. 2019. Pyroptosis versus necroptosis: similarities, differences, and crosstalk. *Cell Death & Differentiation,* 26**,** 99-114.
FRANTZ, S., DUCHARME, A., SAWYER, D., ROHDE, L. E., KOBZIK, L., FUKAZAWA, R., TRACEY, D., ALLEN, H., LEE, R. T. & KELLY, R. A. 2003. Targeted deletion of caspase-1 reduces early mortality and left ventricular dilatation following myocardial infarction. *J Mol Cell Cardiol,* 35**,** 685-94.
FREDHOLM, B. B., ABBRACCHIO, M. P., BURNSTOCK, G., DALY, J. W., HARDEN, T. K., JACOBSON, K. A., LEFF, P. & WILLIAMS, M. 1994. Nomenclature and classification of purinoceptors. *Pharmacol Rev,* 46**,** 143-56.
FRITSCH, M., GÜNTHER, S. D., SCHWARZER, R., ALBERT, M. C., SCHORN, F., WERTHENBACH, J. P., SCHIFFMANN, L. M., STAIR, N., STOCKS, H., SEEGER, J. M., LAMKANFI, M., KRÖNKE, M., PASPARAKIS, M. & KASHKAR, H. 2019. Caspase-8 is the molecular switch for apoptosis, necroptosis and pyroptosis. *Nature,* 575**,** 683-687.
FROM, A. H., FONG, J. S. & GOOD, R. A. 1979. Polymyxin B sulfate modification of bacterial endotoxin: effects on the development of endotoxin shock in dogs. *Infect Immun,* 23**,** 660-4.
FUKIAGE, C., NAKAJIMA, E., MA, H., AZUMA, M. & SHEARER, T. R. 2002. Characterization and regulation of lens-specific calpain Lp82. *J Biol Chem,* 277**,** 20678-85.
FURUTA, T., MUKAI, A., OHISHI, A., NISHIDA, K. & NAGASAWA, K. 2017. Oxidative stress-induced increase of intracellular zinc in astrocytes decreases their functional expression of P2X7 receptors and engulfing activity. *Metallomics,* 9**,** 1839-1851.
GACHET, C. 2006. Regulation of platelet functions by P2 receptors. *Annu Rev Pharmacol Toxicol,* 46**,** 277-300.
GAFNI, J., HERMEL, E., YOUNG, J. E., WELLINGTON, C. L., HAYDEN, M. R. & ELLERBY, L. M. 2004. Inhibition of calpain cleavage of huntingtin reduces toxicity: accumulation of calpain/caspase fragments in the nucleus. *J Biol Chem,* 279**,** 20211-20.
GANESAN, S., RATHINAM, V. A. K., BOSSALLER, L., ARMY, K., KAISER, W. J., MOCARSKI, E. S., DILLON, C. P., GREEN, D. R., MAYADAS, T. N., LEVITZ, S. M., HISE, A. G., SILVERMAN, N. & FITZGERALD, K. A. 2014. Caspase-8 modulates dectin-1 and complement receptor 3-driven IL-1β production in response to β-glucans and the fungal pathogen, Candida albicans. *J Immunol,* 193**,** 2519-2530.
GAO, C., JIANG, J., TAN, Y. & CHEN, S. 2023. Microglia in neurodegenerative diseases: mechanism and potential therapeutic targets. *Signal Transduct Target Ther,* 8**,** 359.
GARWOOD, C., FAIZULLABHOY, A., WHARTON, S. B., INCE, P. G., HEATH, P. R., SHAW, P. J., BAXTER, L., GELSTHORPE, C., FORSTER, G., MATTHEWS, F. E., BRAYNE, C. & SIMPSON, J. E. 2013. Calcium dysregulation in relation to Alzheimer-type pathology in the ageing brain. *Neuropathol Appl Neurobiol,* 39**,** 788-99.
GATON, D. D., SAGARA, T., LINDSEY, J. D., GABELT, B. T., KAUFMAN, P. L. & WEINREB, R. N. 2001. Increased matrix metalloproteinases 1, 2, and 3 in the monkey uveoscleral outflow pathway after topical prostaglandin F(2 alpha)-isopropyl ester treatment. *Arch Ophthalmol,* 119**,** 1165-70.
GBD, A. 2021. Causes of blindness and vision impairment in 2020 and trends over 30 years, and prevalence of avoidable blindness in relation to VISION 2020: the Right to Sight: an analysis for the Global Burden of Disease Study. *Lancet Glob Health,* 9**,** e144-e160.
GBD, A. 2022. Estimation of the global prevalence of dementia in 2019 and forecasted prevalence in 2050: an analysis for the Global Burden of Disease Study 2019. *Lancet Public Health,* 7**,** e105-e125.
GEBERT, G., BENZING, H. & STROHM, M. 1971. Changes in the interstitial pH of dog myocardium in response to local ischemia, hypoxia, hyper- and hypocapnia, measured continuously by means of glass microelectrodes. *Pflugers Arch,* 329**,** 72-81.

GEBOREK, P., SAXNE, T., PETTERSSON, H. & WOLLHEIM, F. A. 1989. Synovial fluid acidosis correlates with radiological joint destruction in rheumatoid arthritis knee joints. *J Rheumatol,* 16**,** 468-72.

GINHOUX, F., GRETER, M., LEBOEUF, M., NANDI, S., SEE, P., GOKHAN, S., MEHLER, M. F., CONWAY, S. J., NG, L. G., STANLEY, E. R., SAMOKHVALOV, I. M. & MERAD, M. 2010. Fate mapping analysis reveals that adult microglia derive from primitive macrophages. *Science,* 330**,** 841-5.

GINHOUX, F. & GUILLIAMS, M. 2016. Tissue-Resident Macrophage Ontogeny and Homeostasis. *Immunity,* 44**,** 439-449.

GIRKIN, C. A., MCGWIN, G., JR., MORRIS, R. & KUHN, F. 2005. Glaucoma following penetrating ocular trauma: a cohort study of the United States Eye Injury Registry. *Am J Ophthalmol,* 139**,** 100-5.

GOEL, M., PICCIANI, R. G., LEE, R. K. & BHATTACHARYA, S. K. 2010. Aqueous humor dynamics: a review. *Open Ophthalmol J,* 4**,** 52-9.

GÓMEZ-GARCÍA, F., MARTÍNEZ-PULLEIRO, R., CARRERA, N., ALLEGUE, C. & GARCIA-GONZALEZ, M. A. 2022. Genetic Kidney Diseases (GKDs) Modeling Using Genome Editing Technologies. *Cells,* 11.

GOSSELIN, D., LINK, V. M., ROMANOSKI, C. E., FONSECA, G. J., EICHENFIELD, D. Z., SPANN, N. J., STENDER, J. D., CHUN, H. B., GARNER, H., GEISSMANN, F. & GLASS, C. K. 2014. Environment drives selection and function of enhancers controlling tissue-specific macrophage identities. *Cell,* 159**,** 1327-40.

GRAHAM, R. K., EHRNHOEFER, D. E. & HAYDEN, M. R. 2011. Caspase-6 and neurodegeneration. *Trends Neurosci,* 34**,** 646-56.

GRAMMER, M., LI, D., ARUNTHAVASOTHY, N. & LIPSKI, J. 2008. Contribution of calpain activation to early stages of hippocampal damage during oxygen-glucose deprivation. *Brain Res,* 1196**,** 121-30.

GRICIUC, A., PATEL, S., FEDERICO, A. N., CHOI, S. H., INNES, B. J., ORAM, M. K., CEREGHETTI, G., MCGINTY, D., ANSELMO, A., SADREYEV, R. I., HICKMAN, S. E., EL KHOURY, J., COLONNA, M. & TANZI, R. E. 2019. TREM2 Acts Downstream of CD33 in Modulating Microglial Pathology in Alzheimer's Disease. *Neuron,* 103**,** 820-835.e7.

GRINGHUIS, S. I., KAPTEIN, T. M., WEVERS, B. A., THEELEN, B., VAN DER VLIST, M., BOEKHOUT, T. & GEIJTENBEEK, T. B. 2012. Dectin-1 is an extracellular pathogen sensor for the induction and processing of IL-1β via a noncanonical caspase-8 inflammasome. *Nat Immunol,* 13**,** 246-54.

GUERREIRO, R., WOJTAS, A., BRAS, J., CARRASQUILLO, M., ROGAEVA, E., MAJOUNIE, E., CRUCHAGA, C., SASSI, C., KAUWE, J. S., YOUNKIN, S., HAZRATI, L., COLLINGE, J., POCOCK, J., LASHLEY, T., WILLIAMS, J., LAMBERT, J. C., AMOUYEL, P., GOATE, A., RADEMAKERS, R., MORGAN, K., POWELL, J., ST GEORGE-HYSLOP, P., SINGLETON, A. & HARDY, J. 2013. TREM2 variants in Alzheimer's disease. *N Engl J Med,* 368**,** 117-27.

GULLOTTA, G. S., COSTANTINO, G., SORTINO, M. A. & SPAMPINATO, S. F. 2023. Microglia and the Blood-Brain Barrier: An External Player in Acute and Chronic Neuroinflammatory Conditions. *Int J Mol Sci,* 24.

GUO, H., PÉTRIN, D., ZHANG, Y., BERGERON, C., GOODYER, C. G. & LEBLANC, A. C. 2006. Caspase-1 activation of caspase-6 in human apoptotic neurons. *Cell Death Differ,* 13**,** 285-92.

GUO, L., MOSS, S. E., ALEXANDER, R. A., ALI, R. R., FITZKE, F. W. & CORDEIRO, M. F. 2005. Retinal ganglion cell apoptosis in glaucoma is related to intraocular pressure and IOP-induced effects on extracellular matrix. *Invest Ophthalmol Vis Sci,* 46**,** 175-82.

GUO, L., SALT, T. E., LUONG, V., WOOD, N., CHEUNG, W., MAASS, A., FERRARI, G., RUSSO-MARIE, F., SILLITO, A. M., CHEETHAM, M. E., MOSS, S. E., FITZKE, F. W. & CORDEIRO, M. F. 2007. Targeting amyloid-beta in glaucoma treatment. *Proc Natl Acad Sci U S A,* 104**,** 13444-9.

GURUNG, P., ANAND, P. K., MALIREDDI, R. K., VANDE WALLE, L., VAN OPDENBOSCH, N., DILLON, C. P., WEINLICH, R., GREEN, D. R., LAMKANFI, M. & KANNEGANTI, T. D. 2014. FADD and caspase-8 mediate priming and activation of the canonical and noncanonical Nlrp3 inflammasomes. *J Immunol,* 192**,** 1835-46.

GURUNG, P., BURTON, A. & KANNEGANTI, T. D. 2016. NLRP3 inflammasome plays a redundant role with caspase 8 to promote IL-1β-mediated osteomyelitis. *Proc Natl Acad Sci U S A,* 113**,** 4452-7.

GUTIERREZ, K. D., DAVIS, M. A., DANIELS, B. P., OLSEN, T. M., RALLI-JAIN, P., TAIT, S. W., GALE, M., JR. & OBERST, A. 2017. MLKL Activation Triggers NLRP3-Mediated Processing and Release of IL-1β Independently of Gasdermin-D. *J Immunol,* 198**,** 2156-2164.

HALLE, A., HORNUNG, V., PETZOLD, G. C., STEWART, C. R., MONKS, B. G., REINHECKEL, T., FITZGERALD, K. A., LATZ, E., MOORE, K. J. & GOLENBOCK, D. T. 2008. The NALP3 inflammasome is involved in the innate immune response to amyloid-beta. *Nat Immunol,* 9**,** 857-65.

HAN, C., YANG, Y., YU, A., GUO, L., GUAN, Q., SHEN, H. & JIAO, Q. 2020. Investigation on the mechanism of mafenide in inhibiting pyroptosis and the release of inflammatory factors. *Eur J Pharm Sci,* 147**,** 105303.

HANLEY, P. J., KRONLAGE, M., KIRSCHNING, C., DEL REY, A., DI VIRGILIO, F., LEIPZIGER, J., CHESSELL, I. P., SARGIN, S., FILIPPOV, M. A., LINDEMANN, O., MOHR, S., KÖNIGS, V., SCHILLERS, H., BÄHLER, M. & SCHWAB, A. 2012. Transient P2X7 receptor activation triggers macrophage death independent of Toll-like receptors 2 and 4, caspase-1, and pannexin-1 proteins. *J Biol Chem,* 287**,** 10650-10663.

HAO, F., ZHANG, N. N., ZHANG, D. M., BAI, H. Y., PIAO, H., YUAN, B., ZHU, H. Y., YU, H., XIAO, C. S. & LI, A. P. 2013. Chemokine fractalkine attenuates overactivation and apoptosis of BV-2 microglial cells induced by extracellular ATP. *Neurochem Res,* 38**,** 1002-12.

HAO, Y., YANG, B., YANG, J., SHI, X., YANG, X., ZHANG, D., ZHAO, D., YAN, W., CHEN, L., ZHENG, H., ZHANG, K. & LIU, X. 2022. ZBP1: A Powerful Innate Immune Sensor and Double-Edged Sword in Host Immunity. *Int J Mol Sci,* 23.

HATTORI, M. & GOUAUX, E. 2012. Molecular mechanism of ATP binding and ion channel activation in P2X receptors. *Nature,* 485**,** 207-12.

HE, Y., TAYLOR, N., FOURGEAUD, L. & BHATTACHARYA, A. 2017. The role of microglial P2X7: modulation of cell death and cytokine release. *J Neuroinflammation,* 14**,** 135.

HEIDARI, A., YAZDANPANAH, N. & REZAEI, N. 2022. The role of Toll-like receptors and neuroinflammation in Parkinson's disease. *J Neuroinflammation,* 19**,** 135.

HEILIG, R., DICK, M. S., SBORGI, L., MEUNIER, E., HILLER, S. & BROZ, P. 2018. The Gasdermin-D pore acts as a conduit for IL-1β secretion in mice. *Eur J Immunol,* 48**,** 584-592.

HENN, A., LUND, S., HEDTJÄRN, M., SCHRATTENHOLZ, A., PÖRZGEN, P. & LEIST, M. 2009. The suitability of BV2 cells as alternative model system for primary microglia cultures or for animal experiments examining brain inflammation. *Altex,* 26**,** 83-94.

HERMEL, E., GAFNI, J., PROPP, S. S., LEAVITT, B. R., WELLINGTON, C. L., YOUNG, J. E., HACKAM, A. S., LOGVINOVA, A. V., PEEL, A. L., CHEN, S. F., HOOK, V., SINGARAJA, R., KRAJEWSKI, S., GOLDSMITH, P. C., ELLERBY, H. M., HAYDEN, M. R., BREDESEN, D. E. & ELLERBY, L. M. 2004. Specific caspase interactions and amplification are involved in selective neuronal vulnerability in Huntington's disease. *Cell Death Differ,* 11**,** 424-38.

HICKMAN, S. E., ALLISON, E. K. & EL KHOURY, J. 2008. Microglial dysfunction and defective beta-amyloid clearance pathways in aging Alzheimer's disease mice. *J Neurosci,* 28**,** 8354-60.

HIRATA, M., SHEARER, T. R. & AZUMA, M. 2015. Hypoxia Activates Calpains in the Nerve Fiber Layer of Monkey Retinal Explants. *Invest Ophthalmol Vis Sci,* 56**,** 6049-57.

HOFFMANN, E. K., LAMBERT, I. H. & PEDERSEN, S. F. 2009. Physiology of cell volume regulation in vertebrates. *Physiol Rev,* 89**,** 193-277.

HOLTON, P. 1959. The liberation of adenosine triphosphate on antidromic stimulation of sensory nerves. *J Physiol,* 145**,** 494-504.

HORN, S., HUGHES, M. A., SCHILLING, R., STICHT, C., TENEV, T., PLOESSER, M., MEIER, P., SPRICK, M. R., MACFARLANE, M. & LEVERKUS, M. 2017. Caspase-10 Negatively Regulates Caspase-8-Mediated Cell Death, Switching the Response to CD95L in Favor of NF-κB Activation and Cell Survival. *Cell Rep,* 19**,** 785-797.

HOSSEINI, M., NAJMABADI, H. & KAHRIZI, K. 2018. Calpains: Diverse Functions but Enigmatic. *Arch Iran Med,* 21**,** 170-179.

HOTCHKISS, R. S. & NICHOLSON, D. W. 2006. Apoptosis and caspases regulate death and inflammation in sepsis. *Nat Rev Immunol,* 6**,** 813-22.
HOTCHKISS, R. S., STRASSER, A., MCDUNN, J. E. & SWANSON, P. E. 2009. Cell death. *N Engl J Med,* 361**,** 1570-83.
HOU, R. C., WU, C. C., HUANG, J. R., CHEN, Y. S. & JENG, K. C. 2005. Oxidative toxicity in BV-2 microglia cells: sesamolin neuroprotection of H2O2 injury involving activation of p38 mitogen-activated protein kinase. *Ann N Y Acad Sci,* 1042**,** 279-85.
HSIEH, H. L. & YANG, C. M. 2013. Role of redox signaling in neuroinflammation and neurodegenerative diseases. *Biomed Res Int,* 2013**,** 484613.
HU, B., ELINAV, E., HUBER, S., BOOTH, C. J., STROWIG, T., JIN, C., EISENBARTH, S. C. & FLAVELL, R. A. 2010a. Inflammation-induced tumorigenesis in the colon is regulated by caspase-1 and NLRC4. *Proc Natl Acad Sci U S A,* 107**,** 21635-40.
HU, H., LU, W., ZHANG, M., ZHANG, X., ARGALL, A. J., PATEL, S., LEE, G. E., KIM, Y. C., JACOBSON, K. A., LATIES, A. M. & MITCHELL, C. H. 2010b. Stimulation of the P2X7 receptor kills rat retinal ganglion cells in vivo. *Exp Eye Res,* 91**,** 425-32.
HU, X., ZHAO, G. L., XU, M. X., ZHOU, H., LI, F., MIAO, Y., LEI, B., YANG, X. L. & WANG, Z. 2021. Interplay between Müller cells and microglia aggravates retinal inflammatory response in experimental glaucoma. *J Neuroinflammation,* 18**,** 303.
HU, Z., MURAKAMI, T., SUZUKI, K., TAMURA, H., KUWAHARA-ARAI, K., IBA, T. & NAGAOKA, I. 2014. Antimicrobial cathelicidin peptide LL-37 inhibits the LPS/ATP-induced pyroptosis of macrophages by dual mechanism. *PLoS One,* 9**,** e85765.
HUANG, W., FILETA, J., RAWE, I., QU, J. & GROSSKREUTZ, C. L. 2010. Calpain activation in experimental glaucoma. *Invest Ophthalmol Vis Sci,* 51**,** 3049-54.
HUANG, Y., HAPPONEN, K. E., BURROLA, P. G., O'CONNOR, C., HAH, N., HUANG, L., NIMMERJAHN, A. & LEMKE, G. 2021. Microglia use TAM receptors to detect and engulf amyloid β plaques. *Nat Immunol,* 22**,** 586-594.
HUANG, Z., ZHOU, T., SUN, X., ZHENG, Y., CHENG, B., LI, M., LIU, X. & HE, C. 2018. Necroptosis in microglia contributes to neuroinflammation and retinal degeneration through TLR4 activation. *Cell Death Differ,* 25**,** 180-189.
HURST, J., KUEHN, S., JASHARI, A., TSAI, T., BARTZ-SCHMIDT, K. U., SCHNICHELS, S. & JOACHIM, S. C. 2017. A novel porcine ex vivo retina culture model for oxidative stress induced by H_2O_2. *Altern Lab Anim,* 45**,** 11-25.
IPPAGUNTA, S. K., BRAND, D. D., LUO, J., BOYD, K. L., CALABRESE, C., STIENSTRA, R., VAN DE VEERDONK, F. L., NETEA, M. G., JOOSTEN, L. A., LAMKANFI, M. & KANNEGANTI, T. D. 2010. Inflammasome-independent role of apoptosis-associated speck-like protein containing a CARD (ASC) in T cell priming is critical for collagen-induced arthritis. *J Biol Chem,* 285**,** 12454-62.
ISHII, K., KANEDA, M., LI, H., ROCKLAND, K. S. & HASHIKAWA, T. 2003. Neuron-specific distribution of P2X7 purinergic receptors in the monkey retina. *J Comp Neurol,* 459**,** 267-77.
ISHII, S., KIHARA, Y. & SHIMIZU, T. 2005. Identification of T cell death-associated gene 8 (TDAG8) as a novel acid sensing G-protein-coupled receptor. *J Biol Chem,* 280**,** 9083-7.
ITO, Y., SHIMAZAWA, M., TSURUMA, K., MAYAMA, C., ISHII, K., ONOE, H., AIHARA, M., ARAIE, M. & HARA, H. 2012. Induction of amyloid-β(1-42) in the retina and optic nerve head of chronic ocular hypertensive monkeys. *Mol Vis,* 18**,** 2647-57.
IVACKO, J. A., SUN, R. & SILVERSTEIN, F. S. 1996. Hypoxic-ischemic brain injury induces an acute microglial reaction in perinatal rats. *Pediatr Res,* 39**,** 39-47.
JANCIC, C. C., CABRINI, M., GABELLONI, M. L., RODRÍGUEZ RODRIGUES, C., SALAMONE, G., TREVANI, A. S. & GEFFNER, J. 2012. Low extracellular pH stimulates the production of IL-1β by human monocytes. *Cytokine,* 57**,** 258-68.
JANG, K. B., YOU, M. J., YANG, B., RIM, C., KIM, H. J. & KWON, M. S. 2022. Persistent Acidic Environment Induces Impaired Phagocytosis via ERK in Microglia. *Neurochem Res,* 47**,** 1341-1353.
JIANG, S., ZHANG, Y., ZHENG, J. H., LI, X., YAO, Y. L., WU, Y. L., SONG, S. Z., SUN, P., NAN, J. X. & LIAN, L. H. 2017. Potentiation of hepatic stellate cell activation by extracellular ATP is

dependent on P2X7R-mediated NLRP3 inflammasome activation. *Pharmacol Res,* 117**,** 82-93.

JIN, Y., LI, H., XIE, G., CHEN, S., WU, S. & FANG, X. 2013. Sevoflurane combined with ATP activates caspase-1 and triggers caspase-1-dependent pyroptosis in murine J774 macrophages. *Inflammation,* 36**,** 330-6.

JULIEN, O. & WELLS, J. A. 2017. Caspases and their substrates. *Cell Death Differ,* 24**,** 1380-1389.

JUNG, E. S., SUH, K., HAN, J., KIM, H., KANG, H. S., CHOI, W. S. & MOOK-JUNG, I. 2022. Amyloid-β activates NLRP3 inflammasomes by affecting microglial immunometabolism through the Syk-AMPK pathway. *Aging Cell,* 21**,** e13623.

KACHAPATI, K., O'BRIEN, T. R., BERGERON, J., ZHANG, M. & DEAN, M. 2006. Population distribution of the functional caspase-12 allele. *Hum Mutat,* 27**,** 975.

KACZMAREK-HAJEK, K., ZHANG, J., KOPP, R., GROSCHE, A., RISSIEK, B., SAUL, A., BRUZZONE, S., ENGEL, T., JOOSS, T., KRAUTLOHER, A., SCHUSTER, S., MAGNUS, T., STADELMANN, C., SIRKO, S., KOCH-NOLTE, F., EULENBURG, V. & NICKE, A. 2018. Re-evaluation of neuronal P2X7 expression using novel mouse models and a P2X7-specific nanobody. *Elife,* 7.

KACZMAREK, A., VANDENABEELE, P. & KRYSKO, D. V. 2013. Necroptosis: the release of damage-associated molecular patterns and its physiological relevance. *Immunity,* 38**,** 209-23.

KARASAWA, A. & KAWATE, T. 2016. Structural basis for subtype-specific inhibition of the P2X7 receptor. *Elife,* 5.

KARCH, C. M., JENG, A. T., NOWOTNY, P., CADY, J., CRUCHAGA, C. & GOATE, A. M. 2012. Expression of novel Alzheimer's disease risk genes in control and Alzheimer's disease brains. *PLoS One,* 7**,** e50976.

KAWAMURA, H., SUGIYAMA, T., WU, D. M., KOBAYASHI, M., YAMANISHI, S., KATSUMURA, K. & PURO, D. G. 2003. ATP: a vasoactive signal in the pericyte-containing microvasculature of the rat retina. *J Physiol,* 551**,** 787-99.

KAWANO, A., TSUKIMOTO, M., NOGUCHI, T., HOTTA, N., HARADA, H., TAKENOUCHI, T., KITANI, H. & KOJIMA, S. 2012. Involvement of P2X4 receptor in P2X7 receptor-dependent cell death of mouse macrophages. *Biochem Biophys Res Commun,* 419**,** 374-80.

KAYAGAKI, N., STOWE, I. B., LEE, B. L., O'ROURKE, K., ANDERSON, K., WARMING, S., CUELLAR, T., HALEY, B., ROOSE-GIRMA, M., PHUNG, Q. T., LIU, P. S., LILL, J. R., LI, H., WU, J., KUMMERFELD, S., ZHANG, J., LEE, W. P., SNIPAS, S. J., SALVESEN, G. S., MORRIS, L. X., FITZGERALD, L., ZHANG, Y., BERTRAM, E. M., GOODNOW, C. C. & DIXIT, V. M. 2015. Caspase-11 cleaves gasdermin D for non-canonical inflammasome signalling. *Nature,* 526**,** 666-71.

KELLEY, N., JELTEMA, D., DUAN, Y. & HE, Y. 2019. The NLRP3 Inflammasome: An Overview of Mechanisms of Activation and Regulation. *Int J Mol Sci,* 20.

KELLIHER, M. A., GRIMM, S., ISHIDA, Y., KUO, F., STANGER, B. Z. & LEDER, P. 1998. The death domain kinase RIP mediates the TNF-induced NF-kappaB signal. *Immunity,* 8**,** 297-303.

KESAVARDHANA, S., MALIREDDI, R. K. S. & KANNEGANTI, T. D. 2020. Caspases in Cell Death, Inflammation, and Pyroptosis. *Annu Rev Immunol,* 38**,** 567-595.

KIANI SHABESTARI, S., MORABITO, S., DANHASH, E. P., MCQUADE, A., SANCHEZ, J. R., MIYOSHI, E., CHADAREVIAN, J. P., CLAES, C., COBURN, M. A., HASSELMANN, J., HIDALGO, J., TRAN, K. N., MARTINI, A. C., CHANG ROTHERMICH, W., PASCUAL, J., HEAD, E., HUME, D. A., PRIDANS, C., DAVTYAN, H., SWARUP, V. & BLURTON-JONES, M. 2022. Absence of microglia promotes diverse pathologies and early lethality in Alzheimer's disease mice. *Cell Rep,* 39**,** 110961.

KIECHLE, T., DEDEOGLU, A., KUBILUS, J., KOWALL, N. W., BEAL, M. F., FRIEDLANDER, R. M., HERSCH, S. M. & FERRANTE, R. J. 2002. Cytochrome C and caspase-9 expression in Huntington's disease. *Neuromolecular Med,* 1**,** 183-95.

KIERDORF, K., ERNY, D., GOLDMANN, T., SANDER, V., SCHULZ, C., PERDIGUERO, E. G., WIEGHOFER, P., HEINRICH, A., RIEMKE, P., HÖLSCHER, C., MÜLLER, D. N., LUCKOW, B., BROCKER, T., DEBOWSKI, K., FRITZ, G., OPDENAKKER, G., DIEFENBACH, A., BIBER, K., HEIKENWALDER, M., GEISSMANN, F., ROSENBAUER, F. & PRINZ, M. 2013. Microglia

emerge from erythromyeloid precursors via Pu.1- and Irf8-dependent pathways. *Nat Neurosci,* 16**,** 273-80.

KIM, J. W., JOE, C. O. & CHOI, E. J. 2001a. Role of receptor-interacting protein in tumor necrosis factor-alpha -dependent MEKK1 activation. *J Biol Chem,* 276**,** 27064-70.

KIM, M., JIANG, L. H., WILSON, H. L., NORTH, R. A. & SURPRENANT, A. 2001b. Proteomic and functional evidence for a P2X7 receptor signalling complex. *Embo j,* 20**,** 6347-58.

KIM, Y. J., YI, Y., SAPP, E., WANG, Y., CUIFFO, B., KEGEL, K. B., QIN, Z. H., ARONIN, N. & DIFIGLIA, M. 2001c. Caspase 3-cleaved N-terminal fragments of wild-type and mutant huntingtin are present in normal and Huntington's disease brains, associate with membranes, and undergo calpain-dependent proteolysis. *Proc Natl Acad Sci U S A,* 98**,** 12784-9.

KISCHKEL, F. C., HELLBARDT, S., BEHRMANN, I., GERMER, M., PAWLITA, M., KRAMMER, P. H. & PETER, M. E. 1995. Cytotoxicity-dependent APO-1 (Fas/CD95)-associated proteins form a death-inducing signaling complex (DISC) with the receptor. *Embo j,* 14**,** 5579-88.

KO, M. L., HU, D. N., RITCH, R. & SHARMA, S. C. 2000. The combined effect of brain-derived neurotrophic factor and a free radical scavenger in experimental glaucoma. *Invest Ophthalmol Vis Sci,* 41**,** 2967-71.

KO, M. L., PENG, P. H., MA, M. C., RITCH, R. & CHEN, C. F. 2005. Dynamic changes in reactive oxygen species and antioxidant levels in retinas in experimental glaucoma. *Free Radic Biol Med,* 39**,** 365-73.

KOVACS, S. B. & MIAO, E. A. 2017. Gasdermins: Effectors of Pyroptosis. *Trends Cell Biol,* 27**,** 673-684.

KRAMEROVA, I., ERMOLOVA, N., ESKIN, A., HEVENER, A., QUEHENBERGER, O., ARMANDO, A. M., HALLER, R., ROMAIN, N., NELSON, S. F. & SPENCER, M. J. 2016. Failure to up-regulate transcription of genes necessary for muscle adaptation underlies limb girdle muscular dystrophy 2A (calpainopathy). *Hum Mol Genet,* 25**,** 2194-2207.

KRASEMANN, S., MADORE, C., CIALIC, R., BAUFELD, C., CALCAGNO, N., EL FATIMY, R., BECKERS, L., O'LOUGHLIN, E., XU, Y., FANEK, Z., GRECO, D. J., SMITH, S. T., TWEET, G., HUMULOCK, Z., ZRZAVY, T., CONDE-SANROMAN, P., GACIAS, M., WENG, Z., CHEN, H., TJON, E., MAZAHERI, F., HARTMANN, K., MADI, A., ULRICH, J. D., GLATZEL, M., WORTHMANN, A., HEEREN, J., BUDNIK, B., LEMERE, C., IKEZU, T., HEPPNER, F. L., LITVAK, V., HOLTZMAN, D. M., LASSMANN, H., WEINER, H. L., OCHANDO, J., HAASS, C. & BUTOVSKY, O. 2017. The TREM2-APOE Pathway Drives the Transcriptional Phenotype of Dysfunctional Microglia in Neurodegenerative Diseases. *Immunity,* 47**,** 566-581.e9.

KUIDA, K., LIPPKE, J. A., KU, G., HARDING, M. W., LIVINGSTON, D. J., SU, M. S. & FLAVELL, R. A. 1995. Altered cytokine export and apoptosis in mice deficient in interleukin-1 beta converting enzyme. *Science,* 267**,** 2000-3.

KUIDA, K., ZHENG, T. S., NA, S., KUAN, C., YANG, D., KARASUYAMA, H., RAKIC, P. & FLAVELL, R. A. 1996. Decreased apoptosis in the brain and premature lethality in CPP32-deficient mice. *Nature,* 384**,** 368-72.

KURASHIMA, Y. & KIYONO, H. 2014. New era for mucosal mast cells: their roles in inflammation, allergic immune responses and adjuvant development. *Exp Mol Med,* 46**,** e83.

KURBATSKAYA, K., PHILLIPS, E. C., CROFT, C. L., DENTONI, G., HUGHES, M. M., WADE, M. A., AL-SARRAJ, S., TROAKES, C., O'NEILL, M. J., PEREZ-NIEVAS, B. G., HANGER, D. P. & NOBLE, W. 2016. Upregulation of calpain activity precedes tau phosphorylation and loss of synaptic proteins in Alzheimer's disease brain. *Acta Neuropathol Commun,* 4**,** 34.

KURIAKOSE, T., MAN, S. M., MALIREDDI, R. K., KARKI, R., KESAVARDHANA, S., PLACE, D. E., NEALE, G., VOGEL, P. & KANNEGANTI, T. D. 2016. ZBP1/DAI is an innate sensor of influenza virus triggering the NLRP3 inflammasome and programmed cell death pathways. *Sci Immunol,* 1.

LAKHANI, S. A., MASUD, A., KUIDA, K., PORTER, G. A., JR., BOOTH, C. J., MEHAL, W. Z., INAYAT, I. & FLAVELL, R. A. 2006. Caspases 3 and 7: key mediators of mitochondrial events of apoptosis. *Science,* 311**,** 847-51.

LAMKANFI, M. & KANNEGANTI, T. D. 2010. Caspase-7: a protease involved in apoptosis and inflammation. *Int J Biochem Cell Biol,* 42**,** 21-4.

LAMKANFI, M., KANNEGANTI, T. D., VAN DAMME, P., VANDEN BERGHE, T., VANOVERBERGHE, I., VANDEKERCKHOVE, J., VANDENABEELE, P., GEVAERT, K. & NÚÑEZ, G. 2008. Targeted peptidecentric proteomics reveals caspase-7 as a substrate of the caspase-1 inflammasomes. *Mol Cell Proteomics,* 7**,** 2350-63.

LAMKANFI, M., MOREIRA, L. O., MAKENA, P., SPIERINGS, D. C., BOYD, K., MURRAY, P. J., GREEN, D. R. & KANNEGANTI, T. D. 2009. Caspase-7 deficiency protects from endotoxin-induced lymphocyte apoptosis and improves survival. *Blood,* 113**,** 2742-5.

LANE, C. A., HARDY, J. & SCHOTT, J. M. 2018. Alzheimer's disease. *Eur J Neurol,* 25**,** 59-70.

LANGMANN, T. 2007. Microglia activation in retinal degeneration. *J Leukoc Biol,* 81**,** 1345-51.

LARINI, L. & SHEA, J. E. 2012. Role of β-hairpin formation in aggregation: the self-assembly of the amyloid-β(25-35) peptide. *Biophys J,* 103**,** 576-586.

LAVIN, Y., WINTER, D., BLECHER-GONEN, R., DAVID, E., KEREN-SHAUL, H., MERAD, M., JUNG, S. & AMIT, I. 2014. Tissue-resident macrophage enhancer landscapes are shaped by the local microenvironment. *Cell,* 159**,** 1312-26.

LAWSON, L. J., PERRY, V. H. & GORDON, S. 1992. Turnover of resident microglia in the normal adult mouse brain. *Neuroscience,* 48**,** 405-15.

LE RHUN, A., ESCALERA-MAURER, A., BRATOVIČ, M. & CHARPENTIER, E. 2019. CRISPR-Cas in Streptococcus pyogenes. *RNA Biol,* 16**,** 380-389.

LEE, J. W., LEE, Y. K., YUK, D. Y., CHOI, D. Y., BAN, S. B., OH, K. W. & HONG, J. T. 2008. Neuro-inflammation induced by lipopolysaccharide causes cognitive impairment through enhancement of beta-amyloid generation. *J Neuroinflammation,* 5**,** 37.

LEE, M. H., LIN, S. R., CHANG, J. Y., SCHULTZ, L., HEATH, J., HSU, L. J., KUO, Y. M., HONG, Q., CHIANG, M. F., GONG, C. X., SZE, C. I. & CHANG, N. S. 2010. TGF-β induces TIAF1 self-aggregation via type II receptor-independent signaling that leads to generation of amyloid β plaques in Alzheimer's disease. *Cell Death Dis,* 1**,** e110.

LEE, Y. Y., PARK, J. S., JUNG, J. S., KIM, D. H. & KIM, H. S. 2013. Anti-inflammatory effect of ginsenoside Rg5 in lipopolysaccharide-stimulated BV2 microglial cells. *Int J Mol Sci,* 14**,** 9820-33.

LEHLE, A. S., FARIN, H. F., MARQUARDT, B., MICHELS, B. E., MAGG, T., LI, Y., LIU, Y., GHALANDARY, M., LAMMENS, K., HOLLIZECK, S., ROHLFS, M., HAUCK, F., CONCA, R., WALZ, C., WEISS, B., LEV, A., SIMON, A. J., GROß, O., GAIDT, M. M., HORNUNG, V., CLEVERS, H., YAZBECK, N., HANNA-WAKIM, R., SHOUVAL, D. S., WARNER, N., SOMECH, R., MUISE, A. M., SNAPPER, S. B., BUFLER, P., KOLETZKO, S., KLEIN, C. & KOTLARZ, D. 2019. Intestinal Inflammation and Dysregulated Immunity in Patients With Inherited Caspase-8 Deficiency. *Gastroenterology,* 156**,** 275-278.

LEITNER, G. R., WENZEL, T. J., MARSHALL, N., GATES, E. J. & KLEGERIS, A. 2019. Targeting toll-like receptor 4 to modulate neuroinflammation in central nervous system disorders. *Expert Opin Ther Targets,* 23**,** 865-882.

LEONARD, J. R., KLOCKE, B. J., D'SA, C., FLAVELL, R. A. & ROTH, K. A. 2002. Strain-dependent neurodevelopmental abnormalities in caspase-3-deficient mice. *J Neuropathol Exp Neurol,* 61**,** 673-7.

LI, C. G., YAN, L., JING, Y. Y., XU, L. H., LIANG, Y. D., WEI, H. X., HU, B., PAN, H., ZHA, Q. B., OUYANG, D. Y. & HE, X. H. 2017. Berberine augments ATP-induced inflammasome activation in macrophages by enhancing AMPK signaling. *Oncotarget,* 8**,** 95-109.

LI, H., ZHU, H., XU, C. J. & YUAN, J. 1998. Cleavage of BID by caspase 8 mediates the mitochondrial damage in the Fas pathway of apoptosis. *Cell,* 94**,** 491-501.

LI, P., ALLEN, H., BANERJEE, S., FRANKLIN, S., HERZOG, L., JOHNSTON, C., MCDOWELL, J., PASKIND, M., RODMAN, L., SALFELD, J. & ET AL. 1995. Mice deficient in IL-1 beta-converting enzyme are defective in production of mature IL-1 beta and resistant to endotoxic shock. *Cell,* 80**,** 401-11.

LI, T., CHIOU, B., GILMAN, C. K., LUO, R., KOSHI, T., YU, D., OAK, H. C., GIERA, S., JOHNSON-VENKATESH, E., MUTHUKUMAR, A. K., STEVENS, B., UMEMORI, H. & PIAO, X. 2020. A splicing isoform of GPR56 mediates microglial synaptic refinement via phosphatidylserine binding. *Embo j,* 39**,** e104136.

LIAO, X. X., DAI, Y. Z., ZHAO, Y. Z. & NIE, K. 2022. Gasdermin E: A Prospective Target for Therapy of Diseases. *Front Pharmacol,* 13**,** 855828.

LIEBERMAN, J., WU, H. & KAGAN, J. C. 2019. Gasdermin D activity in inflammation and host defense. *Sci Immunol,* 4.

LIGUORI, I., RUSSO, G., CURCIO, F., BULLI, G., ARAN, L., DELLA-MORTE, D., GARGIULO, G., TESTA, G., CACCIATORE, F., BONADUCE, D. & ABETE, P. 2018. Oxidative stress, aging, and diseases. *Clin Interv Aging,* 13**,** 757-772.

LIN, Y., DEVIN, A., RODRIGUEZ, Y. & LIU, Z. G. 1999. Cleavage of the death domain kinase RIP by caspase-8 prompts TNF-induced apoptosis. *Genes Dev,* 13**,** 2514-26.

LITOSH, V. A., ROCHMAN, M., RYMER, J. K., POROLLO, A., KOTTYAN, L. C. & ROTHENBERG, M. E. 2017. Calpain-14 and its association with eosinophilic esophagitis. *J Allergy Clin Immunol,* 139**,** 1762-1771.e7.

LIU, J., CAO, C., JIN, Y., WANG, Y., MA, X., LI, J., GUO, S., YANG, J., NIU, J. & LIANG, X. 2023a. Induced neural stem cells suppressed neuroinflammation by inhibiting the microglial pyroptotic pathway in intracerebral hemorrhage rats. *iScience,* 26**,** 107022.

LIU, J. P., NAKAKURA, T., TOMURA, H., TOBO, M., MOGI, C., WANG, J. Q., HE, X. D., TAKANO, M., DAMIRIN, A., KOMACHI, M., SATO, K. & OKAJIMA, F. 2010. Each one of certain histidine residues in G-protein-coupled receptor GPR4 is critical for extracellular proton-induced stimulation of multiple G-protein-signaling pathways. *Pharmacol Res,* 61**,** 499-505.

LIU, S., LIU, H., JOHNSTON, A., HANNA-ADDAMS, S., REYNOSO, E., XIANG, Y. & WANG, Z. 2017. MLKL forms disulfide bond-dependent amyloid-like polymers to induce necroptosis. *Proc Natl Acad Sci U S A,* 114**,** E7450-e7459.

LIU, S., YANG, W., LI, Y. & SUN, C. 2023b. Fetal bovine serum, an important factor affecting the reproducibility of cell experiments. *Sci Rep,* 13**,** 1942.

LIU, X., ZHANG, Z., RUAN, J., PAN, Y., MAGUPALLI, V. G., WU, H. & LIEBERMAN, J. 2016. Inflammasome-activated gasdermin D causes pyroptosis by forming membrane pores. *Nature,* 535**,** 153-8.

LIU, Y., DAI, Y., LI, Q., CHEN, C., CHEN, H., SONG, Y., HUA, F. & ZHANG, Z. 2020. Beta-amyloid activates NLRP3 inflammasome via TLR4 in mouse microglia. *Neurosci Lett,* 736**,** 135279.

LIU, Y., MI, Y., MUELLER, T., KREIBICH, S., WILLIAMS, E. G., VAN DROGEN, A., BOREL, C., FRANK, M., GERMAIN, P. L., BLUDAU, I., MEHNERT, M., SEIFERT, M., EMMENLAUER, M., SORG, I., BEZRUKOV, F., BENA, F. S., ZHOU, H., DEHIO, C., TESTA, G., SAEZ-RODRIGUEZ, J., ANTONARAKIS, S. E., HARDT, W. D. & AEBERSOLD, R. 2019. Multi-omic measurements of heterogeneity in HeLa cells across laboratories. *Nat Biotechnol,* 37**,** 314-322.

LONG, H. Z., ZHOU, Z. W., CHENG, Y., LUO, H. Y., LI, F. J., XU, S. G. & GAO, L. C. 2022. The Role of Microglia in Alzheimer's Disease From the Perspective of Immune Inflammation and Iron Metabolism. *Front Aging Neurosci,* 14**,** 888989.

LORD, B., AMERIKS, M. K., WANG, Q., FOURGEAUD, L., VLIEGEN, M., VERLUYTEN, W., HASPESLAGH, P., CARRUTHERS, N. I., LOVENBERG, T. W., BONAVENTURE, P., LETAVIC, M. A. & BHATTACHARYA, A. 2015. A novel radioligand for the ATP-gated ion channel P2X7: [3H] JNJ-54232334. *Eur J Pharmacol,* 765**,** 551-9.

LOW, K. E., KARUNAN PARTHA, S., DAVIES, P. L. & CAMPBELL, R. L. 2014. Allosteric inhibitors of calpains: Reevaluating inhibition by PD150606 and LSEAL. *Biochim Biophys Acta,* 1840**,** 3367-73.

LU, D. W., CHANG, C. J. & WU, J. N. 2001. The changes of vitreous pH values in an acute glaucoma rabbit model. *J Ocul Pharmacol Ther,* 17**,** 343-50.

LU, Y. C., YEH, W. C. & OHASHI, P. S. 2008. LPS/TLR4 signal transduction pathway. *Cytokine,* 42**,** 145-151.

LUKENS, J. R., GURUNG, P., VOGEL, P., JOHNSON, G. R., CARTER, R. A., MCGOLDRICK, D. J., BANDI, S. R., CALABRESE, C. R., VANDE WALLE, L., LAMKANFI, M. & KANNEGANTI, T. D. 2014. Dietary modulation of the microbiome affects autoinflammatory disease. *Nature,* 516**,** 246-9.

MA, D., YANG, B., GUAN, B., SONG, L., LIU, Q., FAN, Y., ZHAO, L., WANG, T., ZHANG, Z., GAO, Z., LI, S. & XU, H. 2021. A Bibliometric Analysis of Pyroptosis From 2001 to 2021. *Front Immunol,* 12**,** 731933.

MAEDLER, K., DHARMADHIKARI, G., SCHUMANN, D. M. & STØRLING, J. 2009. Interleukin-1 beta targeted therapy for type 2 diabetes. *Expert Opin Biol Ther,* 9**,** 1177-88.

MAELFAIT, J., VERCAMMEN, E., JANSSENS, S., SCHOTTE, P., HAEGMAN, M., MAGEZ, S. & BEYAERT, R. 2008. Stimulation of Toll-like receptor 3 and 4 induces interleukin-1beta maturation by caspase-8. *J Exp Med,* 205**,** 1967-73.

MAGI, S., CASTALDO, P., MACRÌ, M. L., MAIOLINO, M., MATTEUCCI, A., BASTIOLI, G., GRATTERI, S., AMOROSO, S. & LARICCIA, V. 2016. Intracellular Calcium Dysregulation: Implications for Alzheimer's Disease. *Biomed Res Int,* 2016**,** 6701324.

MAHAJAN, V. B. & LIN, J. H. 2013. Lymphocyte infiltration in CAPN5 autosomal dominant neovascular inflammatory vitreoretinopathy. *Clin Ophthalmol,* 7**,** 1339-45.

MALONEY, B. & LAHIRI, D. K. 2011. The Alzheimer's amyloid β-peptide (Aβ) binds a specific DNA Aβ-interacting domain (AβID) in the APP, BACE1, and APOE promoters in a sequence-specific manner: characterizing a new regulatory motif. *Gene,* 488**,** 1-12.

MÅNSSON, B., GEBOREK, P., SAXNE, T. & BJÖRNSSON, S. 1990. Cytidine deaminase activity in synovial fluid of patients with rheumatoid arthritis: relation to lactoferrin, acidosis, and cartilage proteoglycan release. *Ann Rheum Dis,* 49**,** 594-7.

MARIATHASAN, S., WEISS, D. S., NEWTON, K., MCBRIDE, J., O'ROURKE, K., ROOSE-GIRMA, M., LEE, W. P., WEINRAUCH, Y., MONACK, D. M. & DIXIT, V. M. 2006. Cryopyrin activates the inflammasome in response to toxins and ATP. *Nature,* 440**,** 228-32.

MARTÍN-SÁNCHEZ, F., DIAMOND, C., ZEITLER, M., GOMEZ, A. I., BAROJA-MAZO, A., BAGNALL, J., SPILLER, D., WHITE, M., DANIELS, M. J., MORTELLARO, A., PEÑALVER, M., PASZEK, P., STERINGER, J. P., NICKEL, W., BROUGH, D. & PELEGRÍN, P. 2016. Inflammasome-dependent IL-1β release depends upon membrane permeabilisation. *Cell Death Differ,* 23**,** 1219-31.

MARTIN, B. N., WANG, C., ZHANG, C. J., KANG, Z., GULEN, M. F., ZEPP, J. A., ZHAO, J., BIAN, G., DO, J. S., MIN, B., PAVICIC, P. G., JR., EL-SANADI, C., FOX, P. L., AKITSU, A., IWAKURA, Y., SARKAR, A., WEWERS, M. D., KAISER, W. J., MOCARSKI, E. S., ROTHENBERG, M. E., HISE, A. G., DUBYAK, G. R., RANSOHOFF, R. M. & LI, X. 2016. T cell-intrinsic ASC critically promotes T(H)17-mediated experimental autoimmune encephalomyelitis. *Nat Immunol,* 17**,** 583-92.

MARTINON, F., PÉTRILLI, V., MAYOR, A., TARDIVEL, A. & TSCHOPP, J. 2006. Gout-associated uric acid crystals activate the NALP3 inflammasome. *Nature,* 440**,** 237-41.

MASS, E., BALLESTEROS, I., FARLIK, M., HALBRITTER, F., GÜNTHER, P., CROZET, L., JACOME-GALARZA, C. E., HÄNDLER, K., KLUGHAMMER, J., KOBAYASHI, Y., GOMEZ-PERDIGUERO, E., SCHULTZE, J. L., BEYER, M., BOCK, C. & GEISSMANN, F. 2016. Specification of tissue-resident macrophages during organogenesis. *Science,* 353.

MASUDA, T., SANKOWSKI, R., STASZEWSKI, O., BÖTTCHER, C., AMANN, L., SAGAR, SCHEIWE, C., NESSLER, S., KUNZ, P., VAN LOO, G., COENEN, V. A., REINACHER, P. C., MICHEL, A., SURE, U., GOLD, R., GRÜN, D., PRILLER, J., STADELMANN, C. & PRINZ, M. 2019. Spatial and temporal heterogeneity of mouse and human microglia at single-cell resolution. *Nature,* 566**,** 388-392.

MASUDA, Y., NAKAYA, M., NAKAJO, S. & NAKAYA, K. 1997. Geranylgeraniol potently induces caspase-3-like activity during apoptosis in human leukemia U937 cells. *Biochem Biophys Res Commun,* 234**,** 641-5.

MASUMOTO, J., TANIGUCHI, S., AYUKAWA, K., SARVOTHAM, H., KISHINO, T., NIIKAWA, N., HIDAKA, E., KATSUYAMA, T., HIGUCHI, T. & SAGARA, J. 1999. ASC, a novel 22-kDa protein, aggregates during apoptosis of human promyelocytic leukemia HL-60 cells. *J Biol Chem,* 274**,** 33835-8.

MATCOVITCH-NATAN, O., WINTER, D. R., GILADI, A., VARGAS AGUILAR, S., SPINRAD, A., SARRAZIN, S., BEN-YEHUDA, H., DAVID, E., ZELADA GONZÁLEZ, F., PERRIN, P., KEREN-SHAUL, H., GURY, M., LARA-ASTAISO, D., THAISS, C. A., COHEN, M., BAHAR HALPERN, K., BARUCH, K., DECZKOWSKA, A., LORENZO-VIVAS, E., ITZKOVITZ, S., ELINAV, E., SIEWEKE, M.

H., SCHWARTZ, M. & AMIT, I. 2016. Microglia development follows a stepwise program to regulate brain homeostasis. *Science,* 353**,** aad8670.
MATHEWS, P. M., JIANG, Y., SCHMIDT, S. D., GRBOVIC, O. M., MERCKEN, M. & NIXON, R. A. 2002. Calpain activity regulates the cell surface distribution of amyloid precursor protein. Inhibition of calpains enhances endosomal generation of beta-cleaved C-terminal APP fragments. *J Biol Chem,* 277**,** 36415-24.
MAWUENYEGA, K. G., SIGURDSON, W., OVOD, V., MUNSELL, L., KASTEN, T., MORRIS, J. C., YARASHESKI, K. E. & BATEMAN, R. J. 2010. Decreased clearance of CNS beta-amyloid in Alzheimer's disease. *Science,* 330**,** 1774.
MCCOMB, S., CHEUNG, H. H., KORNELUK, R. G., WANG, S., KRISHNAN, L. & SAD, S. 2012. cIAP1 and cIAP2 limit macrophage necroptosis by inhibiting Rip1 and Rip3 activation. *Cell Death Differ,* 19**,** 1791-801.
MCKENZIE, B. A., FERNANDES, J. P., DOAN, M. A. L., SCHMITT, L. M., BRANTON, W. G. & POWER, C. 2020. Activation of the executioner caspases-3 and -7 promotes microglial pyroptosis in models of multiple sclerosis. *J Neuroinflammation,* 17**,** 253.
MCQUEEN, C. A. 2010. Comprehensive toxicology. 2nd ed. / ed. Oxford: Elsevier.
MENDES, M. S. & MAJEWSKA, A. K. 2021. An overview of microglia ontogeny and maturation in the homeostatic and pathological brain. *Eur J Neurosci,* 53**,** 3525-3547.
MENKIN, V. & WARNER, C. R. 1937. Studies on Inflammation: XIII. Carbohydrate Metabolism, Local Acidosis, and the Cytological Picture in Inflammation. *Am J Pathol,* 13**,** 25-44.1.
MENU, P. & VINCE, J. E. 2011. The NLRP3 inflammasome in health and disease: the good, the bad and the ugly. *Clin Exp Immunol,* 166**,** 1-15.
MERLINI, M., RAFALSKI, V. A., MA, K., KIM, K. Y., BUSHONG, E. A., RIOS CORONADO, P. E., YAN, Z., MENDIOLA, A. S., SOZMEN, E. G., RYU, J. K., HABERL, M. G., MADANY, M., SAMPSON, D. N., PETERSEN, M. A., BARDEHLE, S., TOGNATTA, R., DEAN, T., JR., ACEVEDO, R. M., CABRIGA, B., THOMAS, R., COUGHLIN, S. R., ELLISMAN, M. H., PALOP, J. J. & AKASSOGLOU, K. 2021. Microglial G(i)-dependent dynamics regulate brain network hyperexcitability. *Nat Neurosci,* 24**,** 19-23.
MIAO, J., MA, H., YANG, Y., LIAO, Y., LIN, C., ZHENG, J., YU, M. & LAN, J. 2023. Microglia in Alzheimer's disease: pathogenesis, mechanisms, and therapeutic potentials. *Front Aging Neurosci,* 15**,** 1201982.
MICHEL, A. D., CHAMBERS, L. J., CLAY, W. C., CONDREAY, J. P., WALTER, D. S. & CHESSELL, I. P. 2007. Direct labelling of the human P2X7 receptor and identification of positive and negative cooperativity of binding. *Br J Pharmacol,* 151**,** 103-14.
MILIARAKI, M., BRIASSOULIS, P., ILIA, S., POLONIFI, A., MANTZOURANI, M., BRIASSOULI, E., VARDAS, K., NANAS, S., PISTIKI, A., THEODORAKOPOULOU, M., TAVLADAKI, T., SPANAKI, A. M., KONDILI, E., DIMITRIOU, H., TSIODRAS, S., GEORGOPOULOS, D., ARMAGANIDIS, A., DAIKOS, G. & BRIASSOULIS, G. 2021. Survivin and caspases serum protein levels and survivin variants mRNA expression in sepsis. *Sci Rep,* 11**,** 1049.
MILLS, C. D., KINCAID, K., ALT, J. M., HEILMAN, M. J. & HILL, A. M. 2000. M-1/M-2 macrophages and the Th1/Th2 paradigm. *J Immunol,* 164**,** 6166-73.
MILNE, M. D. 1965. Influence of acid-base balance on efficacy and toxicity of drugs. *Proc R Soc Med,* 58**,** 961-3.
MIRAS-PORTUGAL, M. T., SEBASTIÁN-SERRANO, Á., DE DIEGO GARCÍA, L. & DÍAZ-HERNÁNDEZ, M. 2017. Neuronal P2X7 Receptor: Involvement in Neuronal Physiology and Pathology. *J Neurosci,* 37**,** 7063-7072.
MISHRA D, B. P. A. S., MK 2018. *Essentials in Ophthalmology,* New Delhi, RELX India Pvt. ltd.
MITCHELL, C. H. 2001. Release of ATP by a human retinal pigment epithelial cell line: potential for autocrine stimulation through subretinal space. *J Physiol,* 534**,** 193-202.
MITTLER, R. 2017. ROS Are Good. *Trends Plant Sci,* 22**,** 11-19.
MOFFATT, M. F., GUT, I. G., DEMENAIS, F., STRACHAN, D. P., BOUZIGON, E., HEATH, S., VON MUTIUS, E., FARRALL, M., LATHROP, M. & COOKSON, W. 2010. A large-scale, consortium-based genomewide association study of asthma. *N Engl J Med,* 363**,** 1211-1221.

MOFFATT, M. F., KABESCH, M., LIANG, L., DIXON, A. L., STRACHAN, D., HEATH, S., DEPNER, M., VON BERG, A., BUFE, A., RIETSCHEL, E., HEINZMANN, A., SIMMA, B., FRISCHER, T., WILLIS-OWEN, S. A., WONG, K. C., ILLIG, T., VOGELBERG, C., WEILAND, S. K., VON MUTIUS, E., ABECASIS, G. R., FARRALL, M., GUT, I. G., LATHROP, G. M. & COOKSON, W. O. 2007. Genetic variants regulating ORMDL3 expression contribute to the risk of childhood asthma. *Nature,* 448**,** 470-3.

MOIR, R. D., LATHE, R. & TANZI, R. E. 2018. The antimicrobial protection hypothesis of Alzheimer's disease. *Alzheimers Dement,* 14**,** 1602-1614.

MONIF, M., BURNSTOCK, G. & WILLIAMS, D. A. 2010. Microglia: proliferation and activation driven by the P2X7 receptor. *Int J Biochem Cell Biol,* 42**,** 1753-6.

MONROE, K. M., YANG, Z., JOHNSON, J. R., GENG, X., DOITSH, G., KROGAN, N. J. & GREENE, W. C. 2014. IFI16 DNA sensor is required for death of lymphoid CD4 T cells abortively infected with HIV. *Science,* 343**,** 428-32.

MONTEITH, A. J., VINCENT, H. A., KANG, S., LI, P., CLAIBORNE, T. M., RAJFUR, Z., JACOBSON, K., MOORMAN, N. J. & VILEN, B. J. 2018. mTORC2 Activity Disrupts Lysosome Acidification in Systemic Lupus Erythematosus by Impairing Caspase-1 Cleavage of Rab39a. *J Immunol,* 201**,** 371-382.

MORIWAKI, K., BALAJI, S., MCQUADE, T., MALHOTRA, N., KANG, J. & CHAN, F. K. 2014. The necroptosis adaptor RIPK3 promotes injury-induced cytokine expression and tissue repair. *Immunity,* 41**,** 567-78.

MOZAFFARIEH, M., GRIESHABER, M. C. & FLAMMER, J. 2008. Oxygen and blood flow: players in the pathogenesis of glaucoma. *Mol Vis,* 14**,** 224-33.

MUELLER-BUEHL, A. M., DOEPPER, H., GRAUTHOFF, S., KIEBLER, T., PETERS, L., HURST, J., KUEHN, S., BARTZ-SCHMIDT, K. U., DICK, H. B., JOACHIM, S. C. & SCHNICHELS, S. 2020. Oxidative stress-induced retinal damage is prevented by mild hypothermia in an ex vivo model of cultivated porcine retinas. *Clin Exp Ophthalmol,* 48**,** 666-681.

MULRYAN, K., GITTERMAN, D. P., LEWIS, C. J., VIAL, C., LECKIE, B. J., COBB, A. L., BROWN, J. E., CONLEY, E. C., BUELL, G., PRITCHARD, C. A. & EVANS, R. J. 2000. Reduced vas deferens contraction and male infertility in mice lacking P2X1 receptors. *Nature,* 403**,** 86-9.

MURPHY, J. M., CZABOTAR, P. E., HILDEBRAND, J. M., LUCET, I. S., ZHANG, J. G., ALVAREZ-DIAZ, S., LEWIS, R., LALAOUI, N., METCALF, D., WEBB, A. I., YOUNG, S. N., VARGHESE, L. N., TANNAHILL, G. M., HATCHELL, E. C., MAJEWSKI, I. J., OKAMOTO, T., DOBSON, R. C., HILTON, D. J., BABON, J. J., NICOLA, N. A., STRASSER, A., SILKE, J. & ALEXANDER, W. S. 2013. The pseudokinase MLKL mediates necroptosis via a molecular switch mechanism. *Immunity,* 39**,** 443-53.

MURRAY, P. J., ALLEN, J. E., BISWAS, S. K., FISHER, E. A., GILROY, D. W., GOERDT, S., GORDON, S., HAMILTON, J. A., IVASHKIV, L. B., LAWRENCE, T., LOCATI, M., MANTOVANI, A., MARTINEZ, F. O., MEGE, J. L., MOSSER, D. M., NATOLI, G., SAEIJ, J. P., SCHULTZE, J. L., SHIREY, K. A., SICA, A., SUTTLES, J., UDALOVA, I., VAN GINDERACHTER, J. A., VOGEL, S. N. & WYNN, T. A. 2014. Macrophage activation and polarization: nomenclature and experimental guidelines. *Immunity,* 41**,** 14-20.

MUZIO, L., VIOTTI, A. & MARTINO, G. 2021. Microglia in Neuroinflammation and Neurodegeneration: From Understanding to Therapy. *Front Neurosci,* 15**,** 742065.

NAHRENDORF, M. & SWIRSKI, F. K. 2016. Abandoning M1/M2 for a Network Model of Macrophage Function. *Circ Res,* 119**,** 414-7.

NALDI, M., FIORI, J., PISTOLOZZI, M., DRAKE, A. F., BERTUCCI, C., WU, R., MLYNARCZYK, K., FILIPEK, S., DE SIMONE, A. & ANDRISANO, V. 2012. Amyloid β-peptide 25-35 self-assembly and its inhibition: a model undecapeptide system to gain atomistic and secondary structure details of the Alzheimer's disease process and treatment. *ACS Chem Neurosci,* 3**,** 952-62.

NEDERGAARD, M., KRAIG, R. P., TANABE, J. & PULSINELLI, W. A. 1991. Dynamics of interstitial and intracellular pH in evolving brain infarct. *Am J Physiol,* 260**,** R581-8.

NEWMAN, E. A. 2001. Propagation of intercellular calcium waves in retinal astrocytes and Müller cells. *J Neurosci,* 21**,** 2215-23.

NEWMAN, E. A. 2003. Glial cell inhibition of neurons by release of ATP. *J Neurosci,* 23**,** 1659-66.

NEWTON, K., WICKLIFFE, K. E., DUGGER, D. L., MALTZMAN, A., ROOSE-GIRMA, M., DOHSE, M., KŐMŰVES, L., WEBSTER, J. D. & DIXIT, V. M. 2019. Cleavage of RIPK1 by caspase-8 is crucial for limiting apoptosis and necroptosis. *Nature,* 574**,** 428-431.

NICKE, A., BÄUMERT, H. G., RETTINGER, J., EICHELE, A., LAMBRECHT, G., MUTSCHLER, E. & SCHMALZING, G. 1998. P2X1 and P2X3 receptors form stable trimers: a novel structural motif of ligand-gated ion channels. *Embo j,* 17**,** 3016-28.

NICKELLS, R. W. 1999. Apoptosis of retinal ganglion cells in glaucoma: an update of the molecular pathways involved in cell death. *Surv Ophthalmol,* 43 Suppl 1**,** S151-61.

NIKOLAEV, A., MCLAUGHLIN, T., O'LEARY, D. D. & TESSIER-LAVIGNE, M. 2009. APP binds DR6 to trigger axon pruning and neuron death via distinct caspases. *Nature,* 457**,** 981-9.

NING, A., CUI, J., TO, E., ASHE, K. H. & MATSUBARA, J. 2008. Amyloid-beta deposits lead to retinal degeneration in a mouse model of Alzheimer disease. *Invest Ophthalmol Vis Sci,* 49**,** 5136-43.

NISHIOKU, T., TAKAI, N., MIYAMOTO, K., MURAO, K., HARA, C., YAMAMOTO, K. & NAKANISHI, H. 2000. Involvement of caspase 3-like protease in methylmercury-induced apoptosis of primary cultured rat cerebral microglia. *Brain Res,* 871**,** 160-4.

NIYADURUPOLA, N., SIDAWAY, P., MA, N., RHODES, J. D., BROADWAY, D. C. & SANDERSON, J. 2013. P2X7 receptor activation mediates retinal ganglion cell death in a human retina model of ischemic neurodegeneration. *Invest Ophthalmol Vis Sci,* 54**,** 2163-70.

NORTH, R. A. 2002. Molecular physiology of P2X receptors. *Physiol Rev,* 82**,** 1013-67.

OBERST, A., DILLON, C. P., WEINLICH, R., MCCORMICK, L. L., FITZGERALD, P., POP, C., HAKEM, R., SALVESEN, G. S. & GREEN, D. R. 2011. Catalytic activity of the caspase-8-FLIP(L) complex inhibits RIPK3-dependent necrosis. *Nature,* 471**,** 363-7.

OFENGEIM, D., MAZZITELLI, S., ITO, Y., DEWITT, J. P., MIFFLIN, L., ZOU, C., DAS, S., ADICONIS, X., CHEN, H., ZHU, H., KELLIHER, M. A., LEVIN, J. Z. & YUAN, J. 2017. RIPK1 mediates a disease-associated microglial response in Alzheimer's disease. *Proc Natl Acad Sci U S A,* 114**,** E8788-e8797.

OLIVEIRA, M. B., DE VASCONCELLOS, J. P. C., ANANINA, G., COSTA, V. P. & DE MELO, M. B. 2018. Association between IL1A and IL1B polymorphisms and primary open angle glaucoma in a Brazilian population. *Exp Biol Med (Maywood),* 243**,** 1083-1091.

ONA, V. O., LI, M., VONSATTEL, J. P., ANDREWS, L. J., KHAN, S. Q., CHUNG, W. M., FREY, A. S., MENON, A. S., LI, X. J., STIEG, P. E., YUAN, J., PENNEY, J. B., YOUNG, A. B., CHA, J. H. & FRIEDLANDER, R. M. 1999. Inhibition of caspase-1 slows disease progression in a mouse model of Huntington's disease. *Nature,* 399**,** 263-7.

ONO, Y., OJIMA, K., SHINKAI-OUCHI, F., HATA, S. & SORIMACHI, H. 2016a. An eccentric calpain, CAPN3/p94/calpain-3. *Biochimie,* 122**,** 169-87.

ONO, Y., SAIDO, T. C. & SORIMACHI, H. 2016b. Calpain research for drug discovery: challenges and potential. *Nat Rev Drug Discov,* 15**,** 854-876.

ONO, Y. & SORIMACHI, H. 2012. Calpains: an elaborate proteolytic system. *Biochim Biophys Acta,* 1824**,** 224-36.

ORNING, P. & LIEN, E. 2021. Multiple roles of caspase-8 in cell death, inflammation, and innate immunity. *J Leukoc Biol,* 109**,** 121-141.

ORNING, P., WENG, D., STARHEIM, K., RATNER, D., BEST, Z., LEE, B., BROOKS, A., XIA, S., WU, H., KELLIHER, M. A., BERGER, S. B., GOUGH, P. J., BERTIN, J., PROULX, M. M., GOGUEN, J. D., KAYAGAKI, N., FITZGERALD, K. A. & LIEN, E. 2018. Pathogen blockade of TAK1 triggers caspase-8-dependent cleavage of gasdermin D and cell death. *Science,* 362**,** 1064-1069.

OSBORNE, N. N., LASCARATOS, G., BRON, A. J., CHIDLOW, G. & WOOD, J. P. 2006. A hypothesis to suggest that light is a risk factor in glaucoma and the mitochondrial optic neuropathies. *Br J Ophthalmol,* 90**,** 237-41.

PANDIAN, N. & KANNEGANTI, T. D. 2022. PANoptosis: A Unique Innate Immune Inflammatory Cell Death Modality. *J Immunol,* 209**,** 1625-1633.

PANDURANGAN, M., HWANG, I., ORHIRBAT, C., JIEUN, Y. & CHO, S. H. 2014. The calpain system and diabetes. *Pathophysiology,* 21**,** 161-7.

PANEK, W. C., HOLLAND, G. N., LEE, D. A. & CHRISTENSEN, R. E. 1990. Glaucoma in patients with uveitis. *Br J Ophthalmol,* 74**,** 223-7.

PÁNICO, P., SALAZAR, A. M., BURNS, A. L. & OSTROSKY-WEGMAN, P. 2014. Role of calpain-10 in the development of diabetes mellitus and its complications. *Arch Med Res,* 45**,** 103-15.

PANNICKE, T., FISCHER, W., BIEDERMANN, B., SCHÄDLICH, H., GROSCHE, J., FAUDE, F., WIEDEMANN, P., ALLGAIER, C., ILLES, P., BURNSTOCK, G. & REICHENBACH, A. 2000. P2X7 receptors in Müller glial cells from the human retina. *J Neurosci,* 20**,** 5965-72.

PAOLICELLI, R. C., SIERRA, A., STEVENS, B., TREMBLAY, M. E., AGUZZI, A., AJAMI, B., AMIT, I., AUDINAT, E., BECHMANN, I., BENNETT, M., BENNETT, F., BESSIS, A., BIBER, K., BILBO, S., BLURTON-JONES, M., BODDEKE, E., BRITES, D., BRÔNE, B., BROWN, G. C., BUTOVSKY, O., CARSON, M. J., CASTELLANO, B., COLONNA, M., COWLEY, S. A., CUNNINGHAM, C., DAVALOS, D., DE JAGER, P. L., DE STROOPER, B., DENES, A., EGGEN, B. J. L., EYO, U., GALEA, E., GAREL, S., GINHOUX, F., GLASS, C. K., GOKCE, O., GOMEZ-NICOLA, D., GONZÁLEZ, B., GORDON, S., GRAEBER, M. B., GREENHALGH, A. D., GRESSENS, P., GRETER, M., GUTMANN, D. H., HAASS, C., HENEKA, M. T., HEPPNER, F. L., HONG, S., HUME, D. A., JUNG, S., KETTENMANN, H., KIPNIS, J., KOYAMA, R., LEMKE, G., LYNCH, M., MAJEWSKA, A., MALCANGIO, M., MALM, T., MANCUSO, R., MASUDA, T., MATTEOLI, M., MCCOLL, B. W., MIRON, V. E., MOLOFSKY, A. V., MONJE, M., MRACSKO, E., NADJAR, A., NEHER, J. J., NENISKYTE, U., NEUMANN, H., NODA, M., PENG, B., PERI, F., PERRY, V. H., POPOVICH, P. G., PRIDANS, C., PRILLER, J., PRINZ, M., RAGOZZINO, D., RANSOHOFF, R. M., SALTER, M. W., SCHAEFER, A., SCHAFER, D. P., SCHWARTZ, M., SIMONS, M., SMITH, C. J., STREIT, W. J., TAY, T. L., TSAI, L. H., VERKHRATSKY, A., VON BERNHARDI, R., WAKE, H., WITTAMER, V., WOLF, S. A., WU, L. J. & WYSS-CORAY, T. 2022. Microglia states and nomenclature: A field at its crossroads. *Neuron,* 110**,** 3458-3483.

PAPPOLLA, M. A., OMAR, R. A., KIM, K. S. & ROBAKIS, N. K. 1992. Immunohistochemical evidence of oxidative [corrected] stress in Alzheimer's disease. *Am J Pathol,* 140**,** 621-8.

PAWATE, S., SHEN, Q., FAN, F. & BHAT, N. R. 2004. Redox regulation of glial inflammatory response to lipopolysaccharide and interferongamma. *J Neurosci Res,* 77**,** 540-51.

PELEGRIN, P. & SURPRENANT, A. 2006. Pannexin-1 mediates large pore formation and interleukin-1beta release by the ATP-gated P2X7 receptor. *Embo j,* 25**,** 5071-82.

PETRIE, E. J., SANDOW, J. J., JACOBSEN, A. V., SMITH, B. J., GRIFFIN, M. D. W., LUCET, I. S., DAI, W., YOUNG, S. N., TANZER, M. C., WARDAK, A., LIANG, L. Y., COWAN, A. D., HILDEBRAND, J. M., KERSTEN, W. J. A., LESSENE, G., SILKE, J., CZABOTAR, P. E., WEBB, A. I. & MURPHY, J. M. 2018. Conformational switching of the pseudokinase domain promotes human MLKL tetramerization and cell death by necroptosis. *Nat Commun,* 9**,** 2422.

PHILIP, N. H., DILLON, C. P., SNYDER, A. G., FITZGERALD, P., WYNOSKY-DOLFI, M. A., ZWACK, E. E., HU, B., FITZGERALD, L., MAULDIN, E. A., COPENHAVER, A. M., SHIN, S., WEI, L., PARKER, M., ZHANG, J., OBERST, A., GREEN, D. R. & BRODSKY, I. E. 2014. Caspase-8 mediates caspase-1 processing and innate immune defense in response to bacterial blockade of NF-κB and MAPK signaling. *Proc Natl Acad Sci U S A,* 111**,** 7385-90.

PIANCONE, F., LA ROSA, F., MARVENTANO, I., SARESELLA, M. & CLERICI, M. 2021. The Role of the Inflammasome in Neurodegenerative Diseases. *Molecules,* 26.

PIATKOV, K. I., OH, J. H., LIU, Y. & VARSHAVSKY, A. 2014. Calpain-generated natural protein fragments as short-lived substrates of the N-end rule pathway. *Proc Natl Acad Sci U S A,* 111**,** E817-26.

PIRCHL, M., MARKSTEINER, J. & HUMPEL, C. 2006. Effects of acidosis on brain capillary endothelial cells and cholinergic neurons: relevance to vascular dementia and Alzheimer's disease. *Neurol Res,* 28**,** 657-64.

PIZZO, P., MURGIA, M., ZAMBON, A., ZANOVELLO, P., BRONTE, V., PIETROBON, D. & DI VIRGILIO, F. 1992. Role of P2z purinergic receptors in ATP-mediated killing of tumor necrosis factor (TNF)-sensitive and TNF-resistant L929 fibroblasts. *J Immunol,* 149**,** 3372-8.

PLUTA, R. 2022. Alzheimer's Disease Connected Genes in the Post-Ischemic Hippocampus and Temporal Cortex. *Genes (Basel),* 13.

POLLACK, M. & YOUNG, L. S. 1979. Protective activity of antibodies to exotoxin A and lipopolysaccharide at the onset of Pseudomonas aeruginosa septicemia in man. *J Clin Invest,* 63**,** 276-86.

PONOMAREV, E. D., MARESZ, K., TAN, Y. & DITTEL, B. N. 2007. CNS-derived interleukin-4 is essential for the regulation of autoimmune inflammation and induces a state of alternative activation in microglial cells. *J Neurosci,* 27**,** 10714-21.

PRILLER, C., BAUER, T., MITTEREGGER, G., KREBS, B., KRETZSCHMAR, H. A. & HERMS, J. 2006. Synapse formation and function is modulated by the amyloid precursor protein. *J Neurosci,* 26**,** 7212-21.

PRINZ, M., JUNG, S. & PRILLER, J. 2019. Microglia Biology: One Century of Evolving Concepts. *Cell,* 179**,** 292-311.

PRONIN, A., PHAM, D., AN, W., DVORIANTCHIKOVA, G., RESHETNIKOVA, G., QIAO, J., KOZHEKBAEVA, Z., REISER, A. E., SLEPAK, V. Z. & SHESTOPALOV, V. I. 2019. Inflammasome Activation Induces Pyroptosis in the Retina Exposed to Ocular Hypertension Injury. *Front Mol Neurosci,* 12**,** 36.

PUTHUSSERY, T. & FLETCHER, E. L. 2004. Synaptic localization of P2X7 receptors in the rat retina. *J Comp Neurol,* 472**,** 13-23.

QU, Y. & DUBYAK, G. R. 2009. P2X7 receptors regulate multiple types of membrane trafficking responses and non-classical secretion pathways. *Purinergic Signal,* 5**,** 163-73.

RADU, C. G., NIJAGAL, A., MCLAUGHLIN, J., WANG, L. & WITTE, O. N. 2005. Differential proton sensitivity of related G protein-coupled receptors T cell death-associated gene 8 and G2A expressed in immune cells. *Proc Natl Acad Sci U S A,* 102**,** 1632-7.

RAHMAN, M. Q., BEARD, S. M., DISCOMBE, R., SHARMA, R. & MONTGOMERY, D. M. 2013. Direct healthcare costs of glaucoma treatment. *Br J Ophthalmol,* 97**,** 720-4.

RALEVIC, V. & BURNSTOCK, G. 1998. Receptors for purines and pyrimidines. *Pharmacol Rev,* 50**,** 413-92.

RAMASAMY, K., SISY SAM, S. & CHANDRASEKARAN, A. 2006. Allele and genotype frequency of MDR1 C3435T in Tamilian population. *Drug Metab Pharmacokinet,* 21**,** 506-8.

RAMI, A., AGARWAL, R., BOTEZ, G. & WINCKLER, J. 2000. mu-Calpain activation, DNA fragmentation, and synergistic effects of caspase and calpain inhibitors in protecting hippocampal neurons from ischemic damage. *Brain Res,* 866**,** 299-312.

RANSOHOFF, R. M. 2016. A polarizing question: do M1 and M2 microglia exist? *Nat Neurosci,* 19**,** 987-91.

RATHKEY, J. K., ZHAO, J., LIU, Z., CHEN, Y., YANG, J., KONDOLF, H. C., BENSON, B. L., CHIRIELEISON, S. M., HUANG, A. Y., DUBYAK, G. R., XIAO, T. S., LI, X. & ABBOTT, D. W. 2018. Chemical disruption of the pyroptotic pore-forming protein gasdermin D inhibits inflammatory cell death and sepsis. *Sci Immunol,* 3.

RAUSCHNER, M., LANGE, L., HÜSING, T., REIME, S., NOLZE, A., MASCHEK, M., THEWS, O. & RIEMANN, A. 2021. Impact of the acidic environment on gene expression and functional parameters of tumors in vitro and in vivo. *J Exp Clin Cancer Res,* 40**,** 10.

RAY, S. K., FIDAN, M., NOWAK, M. W., WILFORD, G. G., HOGAN, E. L. & BANIK, N. L. 2000. Oxidative stress and Ca2+ influx upregulate calpain and induce apoptosis in PC12 cells. *Brain Res,* 852**,** 326-34.

REBSAMEN, M., HEINZ, L. X., MEYLAN, E., MICHALLET, M. C., SCHRODER, K., HOFMANN, K., VAZQUEZ, J., BENEDICT, C. A. & TSCHOPP, J. 2009. DAI/ZBP1 recruits RIP1 and RIP3 through RIP homotypic interaction motifs to activate NF-kappaB. *EMBO Rep,* 10**,** 916-22.

REIGADA, D., LU, W., ZHANG, M. & MITCHELL, C. H. 2008. Elevated pressure triggers a physiological release of ATP from the retina: Possible role for pannexin hemichannels. *Neuroscience,* 157**,** 396-404.

REIGADA, D., LU, W., ZHANG, X., FRIEDMAN, C., PENDRAK, K., MCGLINN, A., STONE, R. A., LATIES, A. M. & MITCHELL, C. H. 2005. Degradation of extracellular ATP by the retinal pigment epithelium. *Am J Physiol Cell Physiol,* 289**,** C617-24.

REIGADA, D. & MITCHELL, C. H. 2005. Release of ATP from retinal pigment epithelial cells involves both CFTR and vesicular transport. *Am J Physiol Cell Physiol,* 288**,** C132-40.

REN, R., CHEN, S. D., FAN, J., ZHANG, G. & LI, J. B. 2018. miRNA-138 regulates MLK3/JNK/MAPK pathway to protect BV-2 cells from H2O2-induced apoptosis. *Bratisl Lek Listy,* 119**,** 284-288.

RENATUS, M., STENNICKE, H. R., SCOTT, F. L., LIDDINGTON, R. C. & SALVESEN, G. S. 2001. Dimer formation drives the activation of the cell death protease caspase 9. *Proc Natl Acad Sci U S A,* 98**,** 14250-5.

RESTA, V., NOVELLI, E., VOZZI, G., SCARPA, C., CALEO, M., AHLUWALIA, A., SOLINI, A., SANTINI, E., PARISI, V., DI VIRGILIO, F. & GALLI-RESTA, L. 2007. Acute retinal ganglion cell injury caused by intraocular pressure spikes is mediated by endogenous extracellular ATP. *Eur J Neurosci,* 25**,** 2741-54.

RICHARDS, P., DIDSZUN, C., CAMPESAN, S., SIMPSON, A., HORLEY, B., YOUNG, K. W., GLYNN, P., CAIN, K., KYRIACOU, C. P., GIORGINI, F. & NICOTERA, P. 2011. Dendritic spine loss and neurodegeneration is rescued by Rab11 in models of Huntington's disease. *Cell Death Differ,* 18**,** 191-200.

RÍO-HORTEGA, P. 1919. El “tercer elemento” de los centros nerviosos [The “third element” of the nerve centers]. *Boletín de la Sociedad Española de Biología,* 9**,** 68-166.

ROBERTSON, F. C., LEPARD, J. R., MEKARY, R. A., DAVIS, M. C., YUNUSA, I., GORMLEY, W. B., BATICULON, R. E., MAHMUD, M. R., MISRA, B. K., RATTANI, A., DEWAN, M. C. & PARK, K. B. 2018. Epidemiology of central nervous system infectious diseases: a meta-analysis and systematic review with implications for neurosurgeons worldwide. *J Neurosurg,* 130**,** 1107-1126.

ROBINSON, N., GANESAN, R., HEGEDŰS, C., KOVÁCS, K., KUFER, T. A. & VIRÁG, L. 2019. Programmed necrotic cell death of macrophages: Focus on pyroptosis, necroptosis, and parthanatos. *Redox Biol,* 26**,** 101239.

ROGERS, C., ERKES, D. A., NARDONE, A., APLIN, A. E., FERNANDES-ALNEMRI, T. & ALNEMRI, E. S. 2019. Gasdermin pores permeabilize mitochondria to augment caspase-3 activation during apoptosis and inflammasome activation. *Nat Commun,* 10**,** 1689.

ROGERS, C., FERNANDES-ALNEMRI, T., MAYES, L., ALNEMRI, D., CINGOLANI, G. & ALNEMRI, E. S. 2017. Cleavage of DFNA5 by caspase-3 during apoptosis mediates progression to secondary necrotic/pyroptotic cell death. *Nat Commun,* 8**,** 14128.

ROMANO, G. L., AMATO, R., LAZZARA, F., PORCIATTI, V., CHOU, T. H., DRAGO, F. & BUCOLO, C. 2020. P2X7 receptor antagonism preserves retinal ganglion cells in glaucomatous mice. *Biochem Pharmacol,* 180**,** 114199.

ROOSEN, K., SCHELD, M., MANDZHALOVA, M., CLARNER, T., BEYER, C. & ZENDEDEL, A. 2021. CXCL12 inhibits inflammasome activation in LPS-stimulated BV2 cells. *Brain Res,* 1763**,** 147446.

ROS, U., PEÑA-BLANCO, A., HÄNGGI, K., KUNZENDORF, U., KRAUTWALD, S., WONG, W. W. & GARCÍA-SÁEZ, A. J. 2017. Necroptosis Execution Is Mediated by Plasma Membrane Nanopores Independent of Calcium. *Cell Rep,* 19**,** 175-187.

ROST, N. S., BRODTMANN, A., PASE, M. P., VAN VELUW, S. J., BIFFI, A., DUERING, M., HINMAN, J. D. & DICHGANS, M. 2022. Post-Stroke Cognitive Impairment and Dementia. *Circ Res,* 130**,** 1252-1271.

ROTSTEIN, O. D., NASMITH, P. E. & GRINSTEIN, S. 1987. The Bacteroides by-product succinic acid inhibits neutrophil respiratory burst by reducing intracellular pH. *Infect Immun,* 55**,** 864-70.

ROTSTEIN, O. D., VITTORINI, T., KAO, J., MCBURNEY, M. I., NASMITH, P. E. & GRINSTEIN, S. 1989. A soluble Bacteroides by-product impairs phagocytic killing of Escherichia coli by neutrophils. *Infect Immun,* 57**,** 745-53.

ROZENGURT, E., HEPPEL, L. A. & FRIEDBERG, I. 1977. Effect of exogenous ATP on the permeability properties of transformed cultures of mouse cell lines. *J Biol Chem,* 252**,** 4584-90.

RUSSO, H. M., RATHKEY, J., BOYD-TRESSLER, A., KATSNELSON, M. A., ABBOTT, D. W. & DUBYAK, G. R. 2016. Active Caspase-1 Induces Plasma Membrane Pores That Precede Pyroptotic Lysis and Are Blocked by Lanthanides. *J Immunol,* 197**,** 1353-67.

RUSSO, M. V. & MCGAVERN, D. B. 2015. Immune Surveillance of the CNS following Infection and Injury. *Trends Immunol,* 36**,** 637-650.

SACCÀ, S. C., PASCOTTO, A., CAMICIONE, P., CAPRIS, P. & IZZOTTI, A. 2005. Oxidative DNA damage in the human trabecular meshwork: clinical correlation in patients with primary open-angle glaucoma. *Arch Ophthalmol,* 123**,** 458-63.

SAEKI, N., USUI, T., AOYAGI, K., KIM, D. H., SATO, M., MABUCHI, T., YANAGIHARA, K., OGAWA, K., SAKAMOTO, H., YOSHIDA, T. & SASAKI, H. 2009. Distinctive expression and function of four GSDM family genes (GSDMA-D) in normal and malignant upper gastrointestinal epithelium. *Genes Chromosomes Cancer,* 48**,** 261-71.

SÁEZ, M. E., GONZÁLEZ-SÁNCHEZ, J. L., RAMÍREZ-LORCA, R., MARTÍNEZ-LARRAD, M. T., ZABENA, C., GONZÁLEZ, A., MORÓN, F. J., RUIZ, A. & SERRANO-RÍOS, M. 2008. The CAPN10 gene is associated with insulin resistance phenotypes in the Spanish population. *PLoS One,* 3**,** e2953.

SAGULENKO, V., THYGESEN, S. J., SESTER, D. P., IDRIS, A., CRIDLAND, J. A., VAJJHALA, P. R., ROBERTS, T. L., SCHRODER, K., VINCE, J. E., HILL, J. M., SILKE, J. & STACEY, K. J. 2013. AIM2 and NLRP3 inflammasomes activate both apoptotic and pyroptotic death pathways via ASC. *Cell Death Differ,* 20**,** 1149-60.

SAHILLIOGLU, A. C., SUMBUL, F., OZOREN, N. & HALILOGLU, T. 2014. Structural and dynamics aspects of ASC speck assembly. *Structure,* 22**,** 1722-1734.

SARHAN, J., LIU, B. C., MUENDLEIN, H. I., LI, P., NILSON, R., TANG, A. Y., RONGVAUX, A., BUNNELL, S. C., SHAO, F., GREEN, D. R. & POLTORAK, A. 2018. Caspase-8 induces cleavage of gasdermin D to elicit pyroptosis during Yersinia infection. *Proc Natl Acad Sci U S A,* 115**,** E10888-e10897.

SASSONE, J., COLCIAGO, C., MARCHI, P., ASCARDI, C., ALBERTI, L., DI PARDO, A., ZIPPEL, R., SIPIONE, S., SILANI, V. & CIAMMOLA, A. 2010. Mutant Huntingtin induces activation of the Bcl-2/adenovirus E1B 19-kDa interacting protein (BNip3). *Cell Death Dis,* 1**,** e7.

SATO, K., WAKAMIYA, A., MAEDA, T., NOGUCHI, K., TAKASHIMA, A. & IMAHORI, K. 1995. Correlation among secondary structure, amyloid precursor protein accumulation, and neurotoxicity of amyloid beta(25-35) peptide as analyzed by single alanine substitution. *J Biochem,* 118**,** 1108-11.

SAWADA, M., SUZUMURA, A., HOSOYA, H., MARUNOUCHI, T. & NAGATSU, T. 1999. Interleukin-10 inhibits both production of cytokines and expression of cytokine receptors in microglia. *J Neurochem,* 72**,** 1466-71.

SBORGI, L., RÜHL, S., MULVIHILL, E., PIPERCEVIC, J., HEILIG, R., STAHLBERG, H., FARADY, C. J., MÜLLER, D. J., BROZ, P. & HILLER, S. 2016. GSDMD membrane pore formation constitutes the mechanism of pyroptotic cell death. *Embo j,* 35**,** 1766-78.

SCHIELKE, G. P., YANG, G. Y., SHIVERS, B. D. & BETZ, A. L. 1998. Reduced ischemic brain injury in interleukin-1 beta converting enzyme-deficient mice. *J Cereb Blood Flow Metab,* 18**,** 180-5.

SCHULZ, C., GOMEZ PERDIGUERO, E., CHORRO, L., SZABO-ROGERS, H., CAGNARD, N., KIERDORF, K., PRINZ, M., WU, B., JACOBSEN, S. E., POLLARD, J. W., FRAMPTON, J., LIU, K. J. & GEISSMANN, F. 2012. A lineage of myeloid cells independent of Myb and hematopoietic stem cells. *Science,* 336**,** 86-90.

SCOTT-HEWITT, N., PERRUCCI, F., MORINI, R., ERRENI, M., MAHONEY, M., WITKOWSKA, A., CAREY, A., FAGGIANI, E., SCHUETZ, L. T., MASON, S., TAMBORINI, M., BIZZOTTO, M., PASSONI, L., FILIPELLO, F., JAHN, R., STEVENS, B. & MATTEOLI, M. 2020. Local externalization of phosphatidylserine mediates developmental synaptic pruning by microglia. *Embo j,* 39**,** e105380.

SEINFELD, J., BAUDRY, N., XU, X., BI, X. & BAUDRY, M. 2016. Differential Activation of Calpain-1 and Calpain-2 following Kainate-Induced Seizure Activity in Rats and Mice. *eNeuro,* 3.

SEKAR, P., HSIAO, G., CHEN, Y. S., LIN, W. W. & CHAN, C. M. 2023. P2X7 Is Involved in the Mouse Retinal Degeneration via the Coordinated Actions in Different Retinal Cell Types. *Antioxidants (Basel),* 12.

SHANMUGAM, G. & POLAVARAPU, P. L. 2004. Structure of A beta(25-35) peptide in different environments. *Biophys J,* 87**,** 622-30.
SHARMA, M. & DE ALBA, E. 2021. Structure, Activation and Regulation of NLRP3 and AIM2 Inflammasomes. *Int J Mol Sci,* 22.
SHARMA, M., SAHU, K., DUBE, A. & GUPTA, P. K. 2005. Extracellular pH influences the mode of cell death in human colon adenocarcinoma cells subjected to photodynamic treatment with chlorin p6. *J Photochem Photobiol B,* 81**,** 107-13.
SHARMA, V., KAUR, R., BHATNAGAR, A. & KAUR, J. 2015. Low-pH-induced apoptosis: role of endoplasmic reticulum stress-induced calcium permeability and mitochondria-dependent signaling. *Cell Stress Chaperones,* 20**,** 431-40.
SHAVIT, N., DILLEY, R. A. & SAN PIETRO, A. 1968. Ion translocation in isolated chloroplasts. Uncoupling of photophosphorylation and translocation of K+ and H+ ions induced by Nigericin. *Biochemistry,* 7**,** 2356-63.
SHAW, P. J., LUKENS, J. R., BURNS, S., CHI, H., MCGARGILL, M. A. & KANNEGANTI, T. D. 2010. Cutting edge: critical role for PYCARD/ASC in the development of experimental autoimmune encephalomyelitis. *J Immunol,* 184**,** 4610-4.
SHEN, R., YIN, P., YAO, H., CHEN, L., CHANG, X., LI, H. & HOU, X. 2021. Punicalin Ameliorates Cell Pyroptosis Induced by LPS/ATP Through Suppression of ROS/NLRP3 Pathway. *J Inflamm Res,* 14**,** 711-718.
SHEN, W., LI, T., HU, Y., LIU, H. & SONG, M. 2013. Calpain-10 genetic polymorphisms and polycystic ovary syndrome risk: a meta-analysis and meta-regression. *Gene,* 531**,** 426-34.
SHI, P., TANG, A., XIAN, L., HOU, S., ZOU, D., LV, Y., HUANG, Z., WANG, Q., SONG, A., LIN, Z. & GAO, X. 2015. Loss of conserved Gsdma3 self-regulation causes autophagy and cell death. *Biochem J,* 468**,** 325-36.
SHIELDS, D. C., SCHAECHER, K. E., HOGAN, E. L. & BANIK, N. L. 2000. Calpain activity and expression increased in activated glial and inflammatory cells in penumbra of spinal cord injury lesion. *J Neurosci Res,* 61**,** 146-50.
SHIELDS, D. C., TYOR, W. R., DEIBLER, G. E., HOGAN, E. L. & BANIK, N. L. 1998. Increased calpain expression in activated glial and inflammatory cells in experimental allergic encephalomyelitis. *Proc Natl Acad Sci U S A,* 95**,** 5768-72.
SIEGMUND, B., LEHR, H. A., FANTUZZI, G. & DINARELLO, C. A. 2001. IL-1 beta -converting enzyme (caspase-1) in intestinal inflammation. *Proc Natl Acad Sci U S A,* 98**,** 13249-54.
SIKLOS, M., BENAISSA, M. & THATCHER, G. R. 2015. Cysteine proteases as therapeutic targets: does selectivity matter? A systematic review of calpain and cathepsin inhibitors. *Acta Pharm Sin B,* 5**,** 506-19.
SIMMEN, H. P., BATTAGLIA, H., GIOVANOLI, P. & BLASER, J. 1994. Analysis of pH, pO2 and pCO2 in drainage fluid allows for rapid detection of infectious complications during the follow-up period after abdominal surgery. *Infection,* 22**,** 386-9.
SIMMEN, H. P. & BLASER, J. 1993. Analysis of pH and pO2 in abscesses, peritoneal fluid, and drainage fluid in the presence or absence of bacterial infection during and after abdominal surgery. *Am J Surg,* 166**,** 24-7.
SIMS, R., HILL, M. & WILLIAMS, J. 2020. The multiplex model of the genetics of Alzheimer's disease. *Nat Neurosci,* 23**,** 311-322.
SINGH, A., KUKRETI, R., SASO, L. & KUKRETI, S. 2019. Oxidative Stress: A Key Modulator in Neurodegenerative Diseases. *Molecules,* 24.
SINGH, M., SHARMA, H. & SINGH, N. 2007. Hydrogen peroxide induces apoptosis in HeLa cells through mitochondrial pathway. *Mitochondrion,* 7**,** 367-73.
SIVAKUMAR, V., FOULDS, W. S., LUU, C. D., LING, E. A. & KAUR, C. 2011. Retinal ganglion cell death is induced by microglia derived pro-inflammatory cytokines in the hypoxic neonatal retina. *J Pathol,* 224**,** 245-60.
SKRZYPCZAK-WIERCIOCH, A. & SAŁAT, K. 2022. Lipopolysaccharide-Induced Model of Neuroinflammation: Mechanisms of Action, Research Application and Future Directions for Its Use. *Molecules,* 27.
SLUYTER, R. 2017. The P2X7 Receptor. *Adv Exp Med Biol,* 1051**,** 17-53.

SNYDERMAN, R., PIKE, M. C., FISCHER, D. G. & KOREN, H. S. 1977. Biologic and biochemical activities of continuous macrophage cell lines P388D1 and J774.1. *J Immunol,* 119**,** 2060-6.
SOKOLOVSKA, A., BECKER, C. E., IP, W. K., RATHINAM, V. A., BRUDNER, M., PAQUETTE, N., TANNE, A., VANAJA, S. K., MOORE, K. J., FITZGERALD, K. A., LACY-HULBERT, A. & STUART, L. M. 2013. Activation of caspase-1 by the NLRP3 inflammasome regulates the NADPH oxidase NOX2 to control phagosome function. *Nat Immunol,* 14**,** 543-53.
SOLLEIRO-VILLAVICENCIO, H. & RIVAS-ARANCIBIA, S. 2018. Effect of Chronic Oxidative Stress on Neuroinflammatory Response Mediated by CD4(+)T Cells in Neurodegenerative Diseases. *Front Cell Neurosci,* 12**,** 114.
SOLTOFF, S. P., MCMILLIAN, M. K., LECHLEITER, J. D., CANTLEY, L. C. & TALAMO, B. R. 1990. Elevation of [Ca2+]i and the activation of ion channels and fluxes by extracellular ATP and phospholipase C-linked agonists in rat parotid acinar cells. *Ann N Y Acad Sci,* 603**,** 76-90; discussion 91-2.
SONG, B., DAVIS, K., LIU, X. S., LEE, H. G., SMITH, M. & LIU, X. 2011. Inhibition of Polo-like kinase 1 reduces beta-amyloid-induced neuronal cell death in Alzheimer's disease. *Aging (Albany NY),* 3**,** 846-51.
SONG, W., HOOLI, B., MULLIN, K., JIN, S. C., CELLA, M., ULLAND, T. K., WANG, Y., TANZI, R. E. & COLONNA, M. 2017. Alzheimer's disease-associated TREM2 variants exhibit either decreased or increased ligand-dependent activation. *Alzheimers Dement,* 13**,** 381-387.
SOREQ, L., ROSE, J., SOREQ, E., HARDY, J., TRABZUNI, D., COOKSON, M. R., SMITH, C., RYTEN, M., PATANI, R. & ULE, J. 2017. Major Shifts in Glial Regional Identity Are a Transcriptional Hallmark of Human Brain Aging. *Cell Rep,* 18**,** 557-570.
SORIMACHI, H., HATA, S. & ONO, Y. 2011a. Calpain chronicle--an enzyme family under multidisciplinary characterization. *Proc Jpn Acad Ser B Phys Biol Sci,* 87**,** 287-327.
SORIMACHI, H., HATA, S. & ONO, Y. 2011b. Impact of genetic insights into calpain biology. *J Biochem,* 150**,** 23-37.
SPRANGER, J., KROKE, A., MÖHLIG, M., HOFFMANN, K., BERGMANN, M. M., RISTOW, M., BOEING, H. & PFEIFFER, A. F. 2003. Inflammatory cytokines and the risk to develop type 2 diabetes: results of the prospective population-based European Prospective Investigation into Cancer and Nutrition (EPIC)-Potsdam Study. *Diabetes,* 52**,** 812-7.
SRINIVASULA, S. M., POYET, J. L., RAZMARA, M., DATTA, P., ZHANG, Z. & ALNEMRI, E. S. 2002. The PYRIN-CARD protein ASC is an activating adaptor for caspase-1. *J Biol Chem,* 277**,** 21119-22.
STANGA, S., LANNI, C., GOVONI, S., UBERTI, D., D'ORAZI, G. & RACCHI, M. 2010. Unfolded p53 in the pathogenesis of Alzheimer's disease: is HIPK2 the link? *Aging (Albany NY),* 2**,** 545-54.
STANGER, B. Z., LEDER, P., LEE, T. H., KIM, E. & SEED, B. 1995. RIP: a novel protein containing a death domain that interacts with Fas/APO-1 (CD95) in yeast and causes cell death. *Cell,* 81**,** 513-23.
STANSLEY, B., POST, J. & HENSLEY, K. 2012. A comparative review of cell culture systems for the study of microglial biology in Alzheimer's disease. *J Neuroinflammation,* 9**,** 115.
STEHLIK, C., LEE, S. H., DORFLEUTNER, A., STASSINOPOULOS, A., SAGARA, J. & REED, J. C. 2003. Apoptosis-associated speck-like protein containing a caspase recruitment domain is a regulator of procaspase-1 activation. *J Immunol,* 171**,** 6154-63.
STEINBERG, T. H., NEWMAN, A. S., SWANSON, J. A. & SILVERSTEIN, S. C. 1987. ATP4-permeabilizes the plasma membrane of mouse macrophages to fluorescent dyes. *J Biol Chem,* 262**,** 8884-8.
STOKES, L. 2021. Type to NEWMAN, J.
STYS, P. K. & JIANG, Q. 2002. Calpain-dependent neurofilament breakdown in anoxic and ischemic rat central axons. *Neurosci Lett,* 328**,** 150-4.
SU, L., QUADE, B., WANG, H., SUN, L., WANG, X. & RIZO, J. 2014. A plug release mechanism for membrane permeation by MLKL. *Structure,* 22**,** 1489-500.
SUBHRAMANYAM, C. S., WANG, C., HU, Q. & DHEEN, S. T. 2019. Microglia-mediated neuroinflammation in neurodegenerative diseases. *Semin Cell Dev Biol,* 94**,** 112-120.

SUGIYAMA, T., OKU, H., SHIBATA, M., FUKUHARA, M., YOSHIDA, H. & IKEDA, T. 2010. Involvement of P2X7 receptors in the hypoxia-induced death of rat retinal neurons. *Invest Ophthalmol Vis Sci,* 51**,** 3236-43.

SUN, L., WANG, H., WANG, Z., HE, S., CHEN, S., LIAO, D., WANG, L., YAN, J., LIU, W., LEI, X. & WANG, X. 2012. Mixed lineage kinase domain-like protein mediates necrosis signaling downstream of RIP3 kinase. *Cell,* 148**,** 213-27.

SUN, Q., GAO, W., LOUGHRAN, P., SHAPIRO, R., FAN, J., BILLIAR, T. R. & SCOTT, M. J. 2013. Caspase 1 activation is protective against hepatocyte cell death by up-regulating beclin 1 protein and mitochondrial autophagy in the setting of redox stress. *J Biol Chem,* 288**,** 15947-58.

SUN, X., LEE, J., NAVAS, T., BALDWIN, D. T., STEWART, T. A. & DIXIT, V. M. 1999. RIP3, a novel apoptosis-inducing kinase. *J Biol Chem,* 274**,** 16871-5.

SURPRENANT, A., RASSENDREN, F., KAWASHIMA, E., NORTH, R. A. & BUELL, G. 1996. The cytolytic P2Z receptor for extracellular ATP identified as a P2X receptor (P2X7). *Science,* 272**,** 735-8.

SUŠJAN, P., BENČINA, M. & HAFNER-BRATKOVIČ, I. 2020. Differential Effect of Extracellular Acidic Environment on IL-1β Released from Human and Mouse Phagocytes. *Int J Mol Sci,* 21.

SUZUKI-KERR, H., WALKER, K. L., HAN, M. H., LIM, J. C. & DONALDSON, P. J. 2022. Hyposmotic stress causes ATP release in a discrete zone within the outer cortex of rat lens. *Mol Vis,* 28**,** 245-256.

SUZUKI, K., HATA, S., KAWABATA, Y. & SORIMACHI, H. 2004. Structure, activation, and biology of calpain. *Diabetes,* 53 Suppl 1**,** S12-8.

SUZUKI, R., OKA, T., TAMADA, Y., SHEARER, T. R. & AZUMA, M. 2014. Degeneration and dysfunction of retinal neurons in acute ocular hypertensive rats: involvement of calpains. *J Ocul Pharmacol Ther,* 30**,** 419-28.

SWANSON, K. V., DENG, M. & TING, J. P. 2019. The NLRP3 inflammasome: molecular activation and regulation to therapeutics. *Nat Rev Immunol,* 19**,** 477-489.

SZCZESNY, B., MARCATTI, M., AHMAD, A., MONTALBANO, M., BRUNYÁNSZKI, A., BIBLI, S. I., PAPAPETROPOULOS, A. & SZABO, C. 2018. Mitochondrial DNA damage and subsequent activation of Z-DNA binding protein 1 links oxidative stress to inflammation in epithelial cells. *Sci Rep,* 8**,** 914.

TAABAZUING, C. Y., OKONDO, M. C. & BACHOVCHIN, D. A. 2017. Pyroptosis and Apoptosis Pathways Engage in Bidirectional Crosstalk in Monocytes and Macrophages. *Cell Chem Biol,* 24**,** 507-514.e4.

TAKAOKA, A., WANG, Z., CHOI, M. K., YANAI, H., NEGISHI, H., BAN, T., LU, Y., MIYAGISHI, M., KODAMA, T., HONDA, K., OHBA, Y. & TANIGUCHI, T. 2007. DAI (DLM-1/ZBP1) is a cytosolic DNA sensor and an activator of innate immune response. *Nature,* 448**,** 501-5.

TAMOUTOUNOUR, S., GUILLIAMS, M., MONTANANA SANCHIS, F., LIU, H., TERHORST, D., MALOSSE, C., POLLET, E., ARDOUIN, L., LUCHE, H., SANCHEZ, C., DALOD, M., MALISSEN, B. & HENRI, S. 2013. Origins and functional specialization of macrophages and of conventional and monocyte-derived dendritic cells in mouse skin. *Immunity,* 39**,** 925-38.

TANAKA, S., MIZUSHINA, Y., KATO, Y., TAMURA, M. & SHIROISHI, T. 2013. Functional conservation of Gsdma cluster genes specifically duplicated in the mouse genome. *G3 (Bethesda),* 3**,** 1843-50.

TANG, Y. & LE, W. 2016. Differential Roles of M1 and M2 Microglia in Neurodegenerative Diseases. *Mol Neurobiol,* 53**,** 1181-1194.

TANZER, M. C., MATTI, I., HILDEBRAND, J. M., YOUNG, S. N., WARDAK, A., TRIPAYDONIS, A., PETRIE, E. J., MILDENHALL, A. L., VAUX, D. L., VINCE, J. E., CZABOTAR, P. E., SILKE, J. & MURPHY, J. M. 2016. Evolutionary divergence of the necroptosis effector MLKL. *Cell Death Differ,* 23**,** 1185-97.

TAO, T., CHEN, X., ZHOU, Y., ZHENG, Q., GAO, S., WANG, J., DING, P., LI, X., PENG, Z., LU, Y., GAO, Y., ZHUANG, Z., HANG, C. H. & LI, W. 2022. Continued P2X7 activation leads to mitochondrial fission and compromising microglial phagocytosis after subarachnoid haemorrhage. *J Neurochem,* 163**,** 419-437.

TAY, T. L., MAI, D., DAUTZENBERG, J., FERNÁNDEZ-KLETT, F., LIN, G., SAGAR, DATTA, M., DROUGARD, A., STEMPFL, T., ARDURA-FABREGAT, A., STASZEWSKI, O., MARGINEANU, A., SPORBERT, A., STEINMETZ, L. M., POSPISILIK, J. A., JUNG, S., PRILLER, J., GRÜN, D., RONNEBERGER, O. & PRINZ, M. 2017. A new fate mapping system reveals context-dependent random or clonal expansion of microglia. *Nat Neurosci,* 20**,** 793-803.

TEIXEIRA, V. H., JACQ, L., LASBLEIZ, S., HILLIQUIN, P., OLIVEIRA, C. R., CORNELIS, F. & PETIT-TEIXEIRA, E. 2008. Genetic and expression analysis of CASP7 gene in a European Caucasian population with rheumatoid arthritis. *J Rheumatol,* 35**,** 1912-8.

THAKUR, S., DHAPOLA, R., SARMA, P., MEDHI, B. & REDDY, D. H. 2023. Neuroinflammation in Alzheimer's Disease: Current Progress in Molecular Signaling and Therapeutics. *Inflammation,* 46**,** 1-17.

THAM, Y. C., LI, X., WONG, T. Y., QUIGLEY, H. A., AUNG, T. & CHENG, C. Y. 2014. Global prevalence of glaucoma and projections of glaucoma burden through 2040: a systematic review and meta-analysis. *Ophthalmology,* 121**,** 2081-90.

THOMAS, P. G., DASH, P., ALDRIDGE, J. R., JR., ELLEBEDY, A. H., REYNOLDS, C., FUNK, A. J., MARTIN, W. J., LAMKANFI, M., WEBBY, R. J., BOYD, K. L., DOHERTY, P. C. & KANNEGANTI, T. D. 2009. The intracellular sensor NLRP3 mediates key innate and healing responses to influenza A virus via the regulation of caspase-1. *Immunity,* 30**,** 566-75.

THORNBERRY, N. A., RANO, T. A., PETERSON, E. P., RASPER, D. M., TIMKEY, T., GARCIA-CALVO, M., HOUTZAGER, V. M., NORDSTROM, P. A., ROY, S., VAILLANCOURT, J. P., CHAPMAN, K. T. & NICHOLSON, D. W. 1997. A combinatorial approach defines specificities of members of the caspase family and granzyme B. Functional relationships established for key mediators of apoptosis. *J Biol Chem,* 272**,** 17907-11.

TIAN, D., XING, Y., GAO, W., ZHANG, H., SONG, Y., TIAN, Y. & DAI, Z. 2021. Sevoflurane Aggravates the Progress of Alzheimer's Disease Through NLRP3/Caspase-1/Gasdermin D Pathway. *Front Cell Dev Biol,* 9**,** 801422.

TOLDI, J. P. & THOMAS, J. L. 2020. Evaluation and Management of Sports-Related Eye Injuries. *Curr Sports Med Rep,* 19**,** 29-34.

UGUR, M. & UGUR, Ö. 2019. A Mechanism-Based Approach to P2X7 Receptor Action. *Mol Pharmacol,* 95**,** 442-450.

UPTON, J. W., KAISER, W. J. & MOCARSKI, E. S. 2012. DAI/ZBP1/DLM-1 complexes with RIP3 to mediate virus-induced programmed necrosis that is targeted by murine cytomegalovirus vIRA. *Cell Host Microbe,* 11**,** 290-7.

VAJJHALA, P. R., LU, A., BROWN, D. L., PANG, S. W., SAGULENKO, V., SESTER, D. P., CRIDLAND, S. O., HILL, J. M., SCHRODER, K., STOW, J. L., WU, H. & STACEY, K. J. 2015. The Inflammasome Adaptor ASC Induces Procaspase-8 Death Effector Domain Filaments. *J Biol Chem,* 290**,** 29217-30.

VÄLIMÄKI, E., CYPRYK, W., VIRKANEN, J., NURMI, K., TURUNEN, P. M., EKLUND, K. K., ÅKERMAN, K. E., NYMAN, T. A. & MATIKAINEN, S. 2016. Calpain Activity Is Essential for ATP-Driven Unconventional Vesicle-Mediated Protein Secretion and Inflammasome Activation in Human Macrophages. *J Immunol,* 197**,** 3315-3325.

VAN OPDENBOSCH, N. & LAMKANFI, M. 2019. Caspases in Cell Death, Inflammation, and Disease. *Immunity,* 50**,** 1352-1364.

VARFOLOMEEV, E. E., SCHUCHMANN, M., LURIA, V., CHIANNILKULCHAI, N., BECKMANN, J. S., METT, I. L., REBRIKOV, D., BRODIANSKI, V. M., KEMPER, O. C., KOLLET, O., LAPIDOT, T., SOFFER, D., SOBE, T., AVRAHAM, K. B., GONCHAROV, T., HOLTMANN, H., LONAI, P. & WALLACH, D. 1998. Targeted disruption of the mouse Caspase 8 gene ablates cell death induction by the TNF receptors, Fas/Apo1, and DR3 and is lethal prenatally. *Immunity,* 9**,** 267-76.

VAROL, D., MILDNER, A., BLANK, T., SHEMER, A., BARASHI, N., YONA, S., DAVID, E., BOURA-HALFON, S., SEGAL-HAYOUN, Y., CHAPPELL-MAOR, L., KEREN-SHAUL, H., LESHKOWITZ, D., HORNSTEIN, E., FUHRMANN, M., AMIT, I., MAGGIO, N., PRINZ, M. & JUNG, S. 2017. Dicer Deficiency Differentially Impacts Microglia of the Developing and Adult Brain. *Immunity,* 46**,** 1030-1044.e8.

VECINO, E., RODRIGUEZ, F. D., RUZAFA, N., PEREIRO, X. & SHARMA, S. C. 2016. Glia-neuron interactions in the mammalian retina. *Prog Retin Eye Res,* 51**,** 1-40.

VESSEY, K. A. & FLETCHER, E. L. 2012. Rod and cone pathway signalling is altered in the P2X7 receptor knock out mouse. *PLoS One,* 7**,** e29990.

VIAL, C. & EVANS, R. J. 2000. P2X receptor expression in mouse urinary bladder and the requirement of P2X(1) receptors for functional P2X receptor responses in the mouse urinary bladder smooth muscle. *Br J Pharmacol,* 131**,** 1489-95.

VIDAL-ITRIAGO, A., RADFORD, R. A. W., ARAMIDEH, J. A., MAUREL, C., SCHERER, N. M., DON, E. K., LEE, A., CHUNG, R. S., GRAEBER, M. B. & MORSCH, M. 2022. Microglia morphophysiological diversity and its implications for the CNS. *Front Immunol,* 13**,** 997786.

VILLA, P. G., HENZEL, W. J., SENSENBRENNER, M., HENDERSON, C. E. & PETTMANN, B. 1998. Calpain inhibitors, but not caspase inhibitors, prevent actin proteolysis and DNA fragmentation during apoptosis. *J Cell Sci,* 111 (Pt 6)**,** 713-22.

VINCE, J. E., WONG, W. W., GENTLE, I., LAWLOR, K. E., ALLAM, R., O'REILLY, L., MASON, K., GROSS, O., MA, S., GUARDA, G., ANDERTON, H., CASTILLO, R., HÄCKER, G., SILKE, J. & TSCHOPP, J. 2012. Inhibitor of apoptosis proteins limit RIP3 kinase-dependent interleukin-1 activation. *Immunity,* 36**,** 215-27.

VIRGINIO, C., CHURCH, D., NORTH, R. A. & SURPRENANT, A. 1997. Effects of divalent cations, protons and calmidazolium at the rat P2X7 receptor. *Neuropharmacology,* 36**,** 1285-94.

VUONO, R., KOULI, A., LEGAULT, E. M., CHAGNON, L., ALLINSON, K. S., LA SPADA, A., BIUNNO, I., BARKER, R. A. & DROUIN-OUELLET, J. 2020. Association Between Toll-Like Receptor 4 (TLR4) and Triggering Receptor Expressed on Myeloid Cells 2 (TREM2) Genetic Variants and Clinical Progression of Huntington's Disease. *Mov Disord,* 35**,** 401-408.

WALSH, J. G., CULLEN, S. P., SHERIDAN, C., LÜTHI, A. U., GERNER, C. & MARTIN, S. J. 2008. Executioner caspase-3 and caspase-7 are functionally distinct proteases. *Proc Natl Acad Sci U S A,* 105**,** 12815-9.

WANG, J., ZHENG, L., LOBITO, A., CHAN, F. K., DALE, J., SNELLER, M., YAO, X., PUCK, J. M., STRAUS, S. E. & LENARDO, M. J. 1999. Inherited human Caspase 10 mutations underlie defective lymphocyte and dendritic cell apoptosis in autoimmune lymphoproliferative syndrome type II. *Cell,* 98**,** 47-58.

WANG, J. W., CHEN, S. D., ZHANG, X. L. & JONAS, J. B. 2016. Retinal Microglia in Glaucoma. *J Glaucoma,* 25**,** 459-65.

WANG, M., PAN, W., XU, Y., ZHANG, J., WAN, J. & JIANG, H. 2022. Microglia-Mediated Neuroinflammation: A Potential Target for the Treatment of Cardiovascular Diseases. *J Inflamm Res,* 15**,** 3083-3094.

WANG, M. & WONG, W. T. 2014. Microglia-Müller cell interactions in the retina. *Adv Exp Med Biol,* 801**,** 333-8.

WANG, R., REN, H., KAZNACHEYEVA, E., LU, X. & WANG, G. 2023. Association of Glial Activation and α-Synuclein Pathology in Parkinson's Disease. *Neurosci Bull,* 39**,** 479-490.

WANG, W., HE, M., LI, Z. & HUANG, W. 2019a. Epidemiological variations and trends in health burden of glaucoma worldwide. *Acta Ophthalmol,* 97**,** e349-e355.

WANG, X., JIANG, W., YAN, Y., GONG, T., HAN, J., TIAN, Z. & ZHOU, R. 2014. RNA viruses promote activation of the NLRP3 inflammasome through a RIP1-RIP3-DRP1 signaling pathway. *Nat Immunol,* 15**,** 1126-33.

WANG, X. J., CAO, Q., LIU, X., WANG, K. T., MI, W., ZHANG, Y., LI, L. F., LEBLANC, A. C. & SU, X. D. 2010. Crystal structures of human caspase 6 reveal a new mechanism for intramolecular cleavage self-activation. *EMBO reports,* 11**,** 841-847.

WANG, Y., GAO, W., SHI, X., DING, J., LIU, W., HE, H., WANG, K. & SHAO, F. 2017. Chemotherapy drugs induce pyroptosis through caspase-3 cleavage of a gasdermin. *Nature,* 547**,** 99-103.

WANG, Y., SHI, P., CHEN, Q., HUANG, Z., ZOU, D., ZHANG, J., GAO, X. & LIN, Z. 2019b. Mitochondrial ROS promote macrophage pyroptosis by inducing GSDMD oxidation. *J Mol Cell Biol,* 11**,** 1069-1082.

WARD, M. M., PUTHUSSERY, T., VESSEY, K. A. & FLETCHER, E. L. 2010. The role of purinergic receptors in retinal function and disease. *Adv Exp Med Biol,* 664**,** 385-91.
WARD, T. T. & STEIGBIGEL, R. T. 1978. Acidosis of synovial fluid correlates with synovial fluid leukocytosis. *Am J Med,* 64**,** 933-6.
WAREHAM, K. J. & SEWARD, E. P. 2016. P2X7 receptors induce degranulation in human mast cells. *Purinergic Signal,* 12**,** 235-46.
WATABE, K., ITO, A., ASADA, H., ENDO, Y., KOBAYASHI, T., NAKAMOTO, K., ITAMI, S., TAKAO, S., SHINOMURA, Y., AIKOU, T., YOSHIKAWA, K., MATSUZAWA, Y., KITAMURA, Y. & NOJIMA, H. 2001. Structure, expression and chromosome mapping of MLZE, a novel gene which is preferentially expressed in metastatic melanoma cells. *Jpn J Cancer Res,* 92**,** 140-51.
WATSON, A. B. 2014. A formula for human retinal ganglion cell receptive field density as a function of visual field location. *J Vis,* 14.
WEBER, J. J., ORTIZ RIOS, M. M., RIESS, O., CLEMENS, L. E. & NGUYEN, H. P. 2016. The calpain-suppressing effects of olesoxime in Huntington's disease. *Rare Dis,* 4**,** e1153778.
WEI, G., JEWETT, A. I. & SHEA, J. E. 2010. Structural diversity of dimers of the Alzheimer amyloid-beta(25-35) peptide and polymorphism of the resulting fibrils. *Phys Chem Chem Phys,* 12**,** 3622-9.
WEI, X., CHO, K. S., THEE, E. F., JAGER, M. J. & CHEN, D. F. 2019. Neuroinflammation and microglia in glaucoma: time for a paradigm shift. *J Neurosci Res,* 97**,** 70-76.
WEINREB, R. N., AUNG, T. & MEDEIROS, F. A. 2014. The pathophysiology and treatment of glaucoma: a review. *Jama,* 311**,** 1901-11.
WELLINGTON, M., KOSELNY, K., SUTTERWALA, F. S. & KRYSAN, D. J. 2014. Candida albicans triggers NLRP3-mediated pyroptosis in macrophages. *Eukaryot Cell,* 13**,** 329-40.
WEMMIE, J. A., TAUGHER, R. J. & KREPLE, C. J. 2013. Acid-sensing ion channels in pain and disease. *Nat Rev Neurosci,* 14**,** 461-71.
WEWERS, M. D. & SARKAR, A. 2009. P2X(7) receptor and macrophage function. *Purinergic Signal,* 5**,** 189-95.
WILDSMITH, K. R., HOLLEY, M., SAVAGE, J. C., SKERRETT, R. & LANDRETH, G. E. 2013. Evidence for impaired amyloid β clearance in Alzheimer's disease. *Alzheimers Res Ther,* 5**,** 33.
WILLIAMS, P. A., MARSH-ARMSTRONG, N. & HOWELL, G. R. 2017. Neuroinflammation in glaucoma: A new opportunity. *Exp Eye Res,* 157**,** 20-27.
WONG, W. W., VINCE, J. E., LALAOUI, N., LAWLOR, K. E., CHAU, D., BANKOVACKI, A., ANDERTON, H., METCALF, D., O'REILLY, L., JOST, P. J., MURPHY, J. M., ALEXANDER, W. S., STRASSER, A., VAUX, D. L. & SILKE, J. 2014. cIAPs and XIAP regulate myelopoiesis through cytokine production in an RIPK1- and RIPK3-dependent manner. *Blood,* 123**,** 2562-72.
WOODBURN, S. C., BOLLINGER, J. L. & WOHLEB, E. S. 2021. The semantics of microglia activation: neuroinflammation, homeostasis, and stress. *J Neuroinflammation,* 18**,** 258.
WU, H., ROMIEU, I., SIENRA-MONGE, J. J., LI, H., DEL RIO-NAVARRO, B. E. & LONDON, S. J. 2009. Genetic variation in ORM1-like 3 (ORMDL3) and gasdermin-like (GSDML) and childhood asthma. *Allergy,* 64**,** 629-35.
XU, H., DU, X., LIU, G., HUANG, S., DU, W., ZOU, S., TANG, D., FAN, C., XIE, Y., WEI, Y., TIAN, Y. & FU, X. 2019. The pseudokinase MLKL regulates hepatic insulin sensitivity independently of inflammation. *Mol Metab,* 23**,** 14-23.
XU, S., WANG, J., ZHONG, J., SHAO, M., JIANG, J., SONG, J., ZHU, W., ZHANG, F., XU, H., XU, G., ZHANG, Y., MA, X. & LYU, F. 2021. CD73 alleviates GSDMD-mediated microglia pyroptosis in spinal cord injury through PI3K/AKT/Foxo1 signaling. *Clin Transl Med,* 11**,** e269.
YANG, D., HE, Y., MUÑOZ-PLANILLO, R., LIU, Q. & NÚÑEZ, G. 2015. Caspase-11 Requires the Pannexin-1 Channel and the Purinergic P2X7 Pore to Mediate Pyroptosis and Endotoxic Shock. *Immunity,* 43**,** 923-32.
YANG, J., LIN, Y., GUO, Z., CHENG, J., HUANG, J., DENG, L., LIAO, W., CHEN, Z., LIU, Z. & SU, B. 2001. The essential role of MEKK3 in TNF-induced NF-kappaB activation. *Nat Immunol,* 2**,** 620-4.
YANG, J., WISE, L. & FUKUCHI, K. I. 2020. TLR4 Cross-Talk With NLRP3 Inflammasome and Complement Signaling Pathways in Alzheimer's Disease. *Front Immunol,* 11**,** 724.

YAO, Y., LI, C., QIAN, F., ZHAO, Y., SHI, X., HONG, D., AI, Q. & ZHONG, L. 2021. Ginsenoside Rg1 Inhibits Microglia Pyroptosis Induced by Lipopolysaccharide Through Regulating STAT3 Signaling. *J Inflamm Res,* 14**,** 6619-6632.

YONEDA, S., HARA, H., HIRATA, A., FUKUSHIMA, M., INOMATA, Y. & TANIHARA, H. 2005. Vitreous fluid levels of beta-amyloid((1-42)) and tau in patients with retinal diseases. *Jpn J Ophthalmol,* 49**,** 106-8.

YU, J., KANG, M. J., KIM, B. J., KWON, J. W., SONG, Y. H., CHOI, W. A., SHIN, Y. J. & HONG, S. J. 2011. Polymorphisms in GSDMA and GSDMB are associated with asthma susceptibility, atopy and BHR. *Pediatr Pulmonol,* 46**,** 701-8.

YU, P. W., HUANG, B. C., SHEN, M., QUAST, J., CHAN, E., XU, X., NOLAN, G. P., PAYAN, D. G. & LUO, Y. 1999. Identification of RIP3, a RIP-like kinase that activates apoptosis and NFkappaB. *Curr Biol,* 9**,** 539-42.

ZAKARIA, A., RADY, M., MAHRAN, L. & ABOU-AISHA, K. 2019. Pioglitazone Attenuates Lipopolysaccharide-Induced Oxidative Stress, Dopaminergic Neuronal Loss and Neurobehavioral Impairment by Activating Nrf2/ARE/HO-1. *Neurochem Res*.

ZANDY, A. J., LAKHANI, S., ZHENG, T., FLAVELL, R. A. & BASSNETT, S. 2005. Role of the executioner caspases during lens development. *J Biol Chem,* 280**,** 30263-72.

ZENG, C. Y., LI, C. G., SHU, J. X., XU, L. H., OUYANG, D. Y., MAI, F. Y., ZENG, Q. Z., ZHANG, C. C., LI, R. M. & HE, X. H. 2019. ATP induces caspase-3/gasdermin E-mediated pyroptosis in NLRP3 pathway-blocked murine macrophages. *Apoptosis,* 24**,** 703-717.

ZEPPIERI, M. & GURNANI, B. 2023. Applanation Tonometry. *StatPearls.* Treasure Island (FL): StatPearls Publishing

ZHA, X. M., XIONG, Z. G. & SIMON, R. P. 2022. pH and proton-sensitive receptors in brain ischemia. *J Cereb Blood Flow Metab,* 42**,** 1349-1363.

ZHANG, C., SONG, J. W., HUANG, H. H., FAN, X., HUANG, L., DENG, J. N., TU, B., WANG, K., LI, J., ZHOU, M. J., YANG, C. X., ZHAO, Q. W., YANG, T., WANG, L. F., ZHANG, J. Y., XU, R. N., JIAO, Y. M., SHI, M., SHAO, F., SÉKALY, R. P. & WANG, F. S. 2021. NLRP3 inflammasome induces CD4+ T cell loss in chronically HIV-1-infected patients. *J Clin Invest,* 131.

ZHANG, D., LIN, J. & HAN, J. 2010. Receptor-interacting protein (RIP) kinase family. *Cell Mol Immunol,* 7**,** 243-9.

ZHANG, J., ZHANG, L., YI, S., JIANG, X., QIAO, Y., ZHANG, Y., XIAO, C. & ZHOU, T. 2020. Mouse Astrocytes Promote Microglial Ramification by Releasing TGF-β and Forming Glial Fibers. *Front Cell Neurosci,* 14**,** 195.

ZHANG, W. H., WANG, X., NARAYANAN, M., ZHANG, Y., HUO, C., REED, J. C. & FRIEDLANDER, R. M. 2003. Fundamental role of the Rip2/caspase-1 pathway in hypoxia and ischemia-induced neuronal cell death. *Proc Natl Acad Sci U S A,* 100**,** 16012-7.

ZHANG, X., LI, A., GE, J., REIGADA, D., LATIES, A. M. & MITCHELL, C. H. 2007. Acute increase of intraocular pressure releases ATP into the anterior chamber. *Exp Eye Res,* 85**,** 637-43.

ZHANG, X., ZHANG, M., LATIES, A. M. & MITCHELL, C. H. 2005. Stimulation of P2X7 receptors elevates Ca2+ and kills retinal ganglion cells. *Invest Ophthalmol Vis Sci,* 46**,** 2183-91.

ZHANG, Z. X., GAN, I., PAVLOSKY, A., HUANG, X., FUHRMANN, B. & JEVNIKAR, A. M. 2017. Intracellular pH Regulates TRAIL-Induced Apoptosis and Necroptosis in Endothelial Cells. *J Immunol Res,* 2017**,** 1503960.

ZHAO, P., YUE, Z., NIE, L., ZHAO, Z., WANG, Q., CHEN, J. & WANG, Q. 2021. Hyperglycaemia-associated macrophage pyroptosis accelerates periodontal inflamm-aging. *J Clin Periodontol,* 48**,** 1379-1392.

ZHAO, S., ZHAO, J., ZHANG, T. & GUO, C. 2016. Increased apoptosis in the platelets of patients with Alzheimer's disease and amnestic mild cognitive impairment. *Clin Neurol Neurosurg,* 143**,** 46-50.

ZHAO, Y., QI, Y., LI, Q., QUAN, H., LIU, D. & ZHOU, H. 2022. Connexin43 inhibition attenuated dopaminergic neuronal loss in the lipopolysaccharide-induced mice model of Parkinson's disease. *Neurosci Lett,* 771**,** 136471.

ZHENG, M., KARKI, R., VOGEL, P. & KANNEGANTI, T. D. 2020. Caspase-6 Is a Key Regulator of Innate Immunity, Inflammasome Activation, and Host Defense. *Cell,* 181**,** 674-687.e13.
ZHENG, Z., WANG, T., CHEN, J., QIU, H., ZHANG, C., LIU, W., QIN, S., TIAN, J. & GUO, J. 2021. Inflammasome-Induced Osmotic Pressure and the Mechanical Mechanisms Underlying Astrocytic Swelling and Membrane Blebbing in Pyroptosis. *Front Immunol,* 12**,** 688674.
ZHOU, B., ZHANG, J. Y., LIU, X. S., CHEN, H. Z., AI, Y. L., CHENG, K., SUN, R. Y., ZHOU, D., HAN, J. & WU, Q. 2018. Tom20 senses iron-activated ROS signaling to promote melanoma cell pyroptosis. *Cell Res,* 28**,** 1171-1185.
ZHU, W., CAO, F. S., FENG, J., CHEN, H. W., WAN, J. R., LU, Q. & WANG, J. 2017. NLRP3 inflammasome activation contributes to long-term behavioral alterations in mice injected with lipopolysaccharide. *Neuroscience,* 343**,** 77-84.
ZOU, K., GONG, J. S., YANAGISAWA, K. & MICHIKAWA, M. 2002. A novel function of monomeric amyloid beta-protein serving as an antioxidant molecule against metal-induced oxidative damage. *J Neurosci,* 22**,** 4833-41.